INFLUENCE OF ERROR SENSOR AND CONTROL SOURCE CONFIGURATION AND TYPE UPON THE PERFORMANCE OF ACTIVE NOISE CONTROL SYSTEMS

Anthony C. Zander

Department of Mechanical Engineering
The University of Adelaide
South Australia 5005

Submitted for the degree of Doctor of Philosophy, 16th February 1994;
awarded 16th June 1994.

Awarded 1994

INFLUENCE OF ERROR SENSOR AND CONTROL SOURCE CONFIGURATION AND TYPE UPON THE PERFORMANCE OF ACTIVE NOISE CONTROL SYSTEMS

CONTENTS

INFLUENCE OF ERROR SENSOR AND CONTROL SOURCE CONFIGURATION AND TYPE UPON THE PERFORMANCE OF ACTIVE NOISE CONTROL SYSTEMS

ABSTRACT

An investigation is made of the influence of error sensor and control source configuration and type upon the performance of active noise control systems. The research is applied to two different cases: a discrete modal system and a continuous modal system.

i) Discrete modal system

For this case a rigid-walled duct of rectangular cross-section is examined. The number of propagating acoustic modes is determined by the duct geometry and the excitation frequency. Hence, for a given frequency, a finite number of modes are able to propagate and the system is thus modally discrete. A theoretical model is developed for ducts of arbitrary length and termination impedance, such that various duct end conditions can be examined, including rigid, infinite, open, and baffled. The model also accounts for finite size acoustic sources and sensors. The influence of the number and location of acoustic control sources is investigated, together with a variety of error sensor strategies, for the control of both plane waves and higher order modes. The system is not treated as an enclosure inside which the sound field is ideally minimised globally, but as an acoustic

transmission path, with the objective of minimising the components of the sound field propagating along the duct. For this reason, it has been found more effective to minimise the power transmission downstream of the control sources, as measured by a modal decomposition technique, rather than to minimise a measure of the acoustic potential energy, as would be appropriate for an enclosure. The modal decomposition technique also enables the effect of evanescent modes to be eliminated from the error signal. This is particularly important at excitation frequencies around the cut-on frequency of each acoustic mode.

ii) Continuous modal system

The system under investigation for this case is a simplified model of a light aircraft fuselage, and consists of a finite length cylinder with an integral floor structure. This is modelled theoretically using modal coupling theory between the structure and the interior acoustic field. The structural mode shapes are determined using component mode synthesis, which combines the mode shape basis functions for the plain cylinder and the floor to obtain a mode shape function for the total structure. The two-dimensional acoustic mode shape functions are found using a finite difference implementation of the Helmholtz equation, while the axial acoustic mode shape function is equal to that of a rigid-walled one-dimensional enclosure. For the system modelled, all structural and acoustic modes contribute to the interior sound field to varying degrees, with a finite number of dominant modes contributing most to the enclosed sound field at any particular frequency. Hence, this system is modally continuous, with the objective generally being to control the

dominant modes. The error sensor criteria under investigation include minimisation of the acoustic pressure at a number of microphones located within the enclosed acoustic field, which provides a practically achievable measure of the acoustic response, and theoretical minimisation of the acoustic potential energy in the enclosure. Vibrational point sources applied to the structure are used as control sources.

Statement of originality

STATEMENT OF ORIGINALITY

To the best of my knowledge and belief all of the material presented in this thesis, except where otherwise referenced, is my own original work, and has not been presented previously for the award of any other degree or diploma in any University. If accepted for the award of the degree of Doctor of Philosophy, I consent that this thesis be made available for loan and photocopying.

Anthony C. Zander

ACKNOWLEDGMENTS

I would like to acknowledge the efforts of the other people who have made a contribution towards this thesis. Many thanks to my parents, Irene and Arnold Zander, who encouraged my mathematical and scientific interests from an early age, and made many sacrifices to provide me with a good education.

My thanks to Professor R.E. (Sam) Luxton and all the staff in the Mechanical Engineering Department who helped in some way towards the preparation of this work. In particular, the consistently excellent technical support from the Instrumentation, Electronics and Engineering Workshops deserves recognition. I am also grateful for the assistance given by other students in the early days, especially Scott Snyder for his helpful comments and advice.

Thanks to Dr Colin Hansen for his supervision, and the guidance and encouragement which enabled me to perform the work within the great research environment he has established.

Support for this research from the Australian Research Council and the Sir Ross and Sir Keith Smith fund is also gratefully acknowledged.

Finally, I would like to thank Danielle for her endless encouragement and positive outlook in all aspects of our lives during the preparation of this thesis.

CHAPTER 1. INTRODUCTION

In this thesis, the influence of error sensor and control source configuration and type upon the performance of active noise control systems is investigated with reference to two different physical systems. The first is a rigid walled duct of rectangular cross-section, which is a discrete modal system; and the second is a simplified model of a light aircraft fuselage, consisting of a finite length cylinder with a structurally integral longitudinal floor partition, with the acoustic space enclosed by the structure, forming a system which is modally continuous. The thesis is thus presented in two parts, each corresponding to the respective physical system examined. For clarity, the literature review pertaining to each system will be presented in the introduction section of the respective parts of the thesis.

The rigid walled duct of rectangular cross-section is first examined in Chapter 2, for the simple case of a semi-infinite duct. A single error sensor criterion of minimisation of the total acoustic power output of the primary and control sources is used. The influence of geometric variables, such as source size and location, on the levels of reduction for this simple physical system are examined. The active control of higher order acoustic modes within the semi-infinite hard-walled rectangular duct is examined analytically for harmonic constant volume velocity sound sources. The effect of source location, size, strength and relative phase upon the total mean acoustic power transmission is investigated for both single and dual control source configurations, at a number of excitation frequencies. For the analysis, the primary source is mounted in the plane of the duct cross section, which may be a uniform surface of arbitrary finite impedance. It is shown that the reduction in

total acoustic power is dependent upon the relative location of the primary and control sources, both laterally across the wall of the duct and axially along the duct. The reduction in total acoustic power is a maximum at axial source separation distances corresponding to multiples of half-wavelengths of the propagating modes, and at relative lateral locations such that the primary and control source mode shape function values are equivalent.

In a practical situation, finite impedance terminations will be encountered at both ends of the rigid-walled duct. Thus, the semi-infinite duct model is extended in Chapter 3 to include higher order mode reflection from both of the duct terminations, which are modelled as having arbitrary impedance. A generalised solution is obtained for a duct of arbitrary length which allows the calculation of infinite, semi-infinite, finite and impedance boundary terminated duct cases through the use of specific termination impedance values. Determination of appropriate termination impedance values is outlined and demonstrated for the case of a flanged duct radiating into free space. The theory is applicable for both plane wave and higher order mode propagation. Finite size acoustic source configurations are modelled in addition to simple point sources. Experimental results are presented with the theory and indicate good agreement.

Having developed a suitable model for describing the acoustic response in ducts of arbitrary length and termination conditions, comparison of a number of different error sensor strategies for the active control of duct noise is undertaken in Chapter 4. Error sensor strategies investigated include minimisation of the acoustic pressure at a point, minimisation of the total real acoustic power output, and minimisation of an estimate of

the acoustic potential energy. A new error sensor strategy is also proposed and investigated. The strategy is based upon minimisation of the downstream acoustic power transmission determined by a modal decomposition of the duct sound field. Error sensor strategies are analysed for both plane wave and multi-mode sound fields, and for a range of duct termination conditions. The criterion used to assess the error sensor strategies is the minimisation of the sound field downstream of the control sources. The model is also utilised in Chapter 4 to determine the influence of various error sensor/control source configurations and duct termination conditions upon the acoustic field, and the resultant effect on the levels of noise reduction achieved using acoustic sources in an active noise control system. Theoretical and experimental results are presented for a range of error sensor, control source and duct configurations, and for both plane wave and higher order mode propagation. A sensor/source strategy is proposed which is applicable to any number of rigid walled duct acoustic modes, and enables the effect of evanescent modes to be eliminated from the error sensor signal.

The second part of the thesis is concerned with a physical system consisting of a finite length cylinder with a structurally integral longitudinal floor partition, with the acoustic space enclosed by the structure. A model describing the response of this system to harmonic point force excitation is presented in Chapter 5, where the system is modelled theoretically using modal coupling theory between the structure and the interior acoustic field. The structural mode shapes are determined using component mode synthesis, which combines the mode shape basis functions for the plain cylinder and the floor to obtain a mode shape function for the total structure. The two-dimensional acoustic mode shape

functions are found using a finite difference implementation of the Helmholtz equation, while the axial acoustic mode shape function is equal to that of a rigid-walled one-dimensional enclosure. Experimental work on a test structure is presented and the results compared with a number of theoretical predictions.

In the latter part of Chapter 5, a formulation for the optimal control forces required to achieve minimisation of a number of error sensor criteria is given for the modelled structure. Experimental and theoretical results are presented for the application of active noise control to the coupled structural/acoustic system.

The formulation for active control of the cylinder with an integral floor is utilised in Chapter 6 to investigate the influence of error sensor and control source configuration and type upon the effectiveness of active noise control applied to the structure via vibrational point forces. Simulations are performed for various numbers of control sources and error sensors, and different locations of each of these active control system elements. Two different frequencies are examined: one corresponding to resonant acoustic excitation; and the other to non-resonant excitation. The distinction between resonant and non-resonant structural excitation has not been made in this thesis because of the high modal density of the structural modes for the test structure examined. A summary of the major factors influencing the performance of the active control system, applied to the simple aircraft fuselage model, is presented.

A comparison of the results from the two cases examined, the modally discrete and

modally continuous, is given in Chapter 7, which contains the conclusions of the thesis. Comments relating to the effectiveness of active noise control on each of the systems are presented. The similarities and differences between the two cases are outlined, in terms of the error sensor criteria and the variables which have a major influence on the effectiveness of active noise control. Recommendations for future work are also presented in Chapter 7.

Some of the work described in detail in this thesis has also been published by the author in condensed form in International Journals and Conference Proceedings. The relevant articles are listed below.

Zander, A.C., and Hansen, C.H. (1990) "Active control of higher order acoustic modes in ducts," *Journal of the Acoustical Society of America*, Supplement 1, Vol. 88, 120th Meeting of the Acoustical Society of America.

Zander, A.C., Snyder, S.D., and Hansen, C.H. (1991) "Active control of interior noise levels in a cylinder with an in-built floor : effect of actuator and sensor location," *Proceedings of Inter-Noise 91*, 1237-1240.

Zander, A.C., and Hansen, C.H. (1992) "Higher order acoustic modes in ducts : propagation properties and active control," *Acoustics Australia*, Vol. 20, No. 1, 21-23.

Zander, A.C., and Hansen, C.H. (1992) "Active control of higher order acoustic modes in ducts," *Journal of the Acoustical Society of America*, Vol. 92, No. 1, 244-257.

Hansen, C.H., and Zander, A.C. (1993) "Active control of sound in rigid walled ducts of arbitrary length and termination conditions," *Proceedings of Noise-Con 1993*, 273-278.

Zander, A.C., and Hansen, C.H. (1993) "A comparison of error sensor strategies for the active control of duct noise," *Journal of the Acoustical Society of America*, Vol. 94, No. 2, 841-848.

CHAPTER 2. ACTIVE CONTROL OF HIGHER ORDER ACOUSTIC MODES IN SEMI-INFINITE RIGID WALLED DUCTS

2.1 INTRODUCTION

Active control of plane wave sound propagation in ducts has been shown to be feasible and commercial systems are now available. However, little headway has been made in controlling noise propagating at frequencies above the cut-on frequency of the first higher order mode. For large air conditioning ducts this frequency could be as low as 100 Hz. Thus, in many cases involving higher frequency noise, control of plane wave propagation only will not solve the problem. One solution is to partition the duct to reduce its effective cross-sectional size and apply active control in each partition. However, this is not always practical and a number of researchers are currently investigating alternative means to control higher order mode propagation.

The majority of previous work on the active control of noise propagation in ducts has concentrated on control of the plane wave, or fundamental acoustic mode, with various mechanisms for control being proposed. Much of the early work describes the acoustic mechanism as cancellation, with the pressure fields produced by the primary disturbance and the control sources superimposing, resulting in reduced noise levels (Ffowcs-Williams, 1984; Tichy et al., 1984; Mazanikov and Tyutekin, 1976). The reflection of the primary source wave by the control source has also been proposed as a control mechanism (Trinder and Nelson, 1983), which is implemented by driving the instantaneous plane wave pressure to zero at a specific duct cross-section, with the result that the downstream

travelling plane wave is reflected back upstream. Absorption of the incident energy from the primary source by a suitable arrangement of control sources has also been investigated (Leitch and Tokhi, 1987; Swinbanks, 1973). Much of this previous work has resulted in analytical expressions for the strength and phasing of the control sources for optimum attenuation of the noise, but relatively little analysis has been presented for the cases when the control sources are not ideally adjusted.

Generally, the analysis to date has been concerned with the interaction between a propagating wave or pressure field and the control sources and, as a consequence, only a few researchers have examined the mechanism of control in terms of the acoustic impedance seen by the primary and control sources, and the effect that each source has on the other's impedance (Berengier and Roure, 1980; Snyder and Hansen, 1989). An analytical model has been developed previously to describe the active control of the plane wave mode based upon these impedances and has also been verified experimentally (Snyder and Hansen, 1989).

Much of the early work published on duct noise has concentrated upon modelling relatively simple cases, the majority being plane wave propagation within hard-walled ducts of infinite length (Swinbanks, 1973; Tichy et al., 1984). However, to accurately model realistic systems, models of more general applicability are required which incorporate the effect of duct termination conditions and frequencies for which higher order modes are propagated. A thorough examination of the sound fields produced by both simple and finite size sources in hard-walled ducts of infinite (Doak, 1973a) and finite

length (Doak, 1973b) has been conducted, and portions of this work have been applied by other researchers to aspects of active noise control (Tichy et al, 1984; Trinder and Nelson, 1983; Berengier and Roure, 1980). For the case of plane wave propagation, the acoustic response of a finite length hard-walled duct having one rigid termination and a partially absorptive termination has been modelled in state space form (Hull et al., 1990).

The acoustic response of hard-walled ducts with impedance boundary conditions at both terminations has been theoretically modelled for plane wave propagation (Elliott and Nelson, 1984; Banks et al., 1990) and higher order mode propagation (Doak, 1973b; Stell and Bernhard, 1991), however only results relating to the active control of propagation of higher order modes in semi-infinite or infinite ducts have been presented. Hence, part of this thesis is devoted to deriving a formulation for the acoustic pressure within a rigid-walled duct having arbitrary termination impedances, for both plane wave and higher order mode propagation.

Earlier models used for describing active control in ducts considered the acoustic response for completely rigid or anechoic terminations. In a practical situation arbitrary termination impedances will be encountered. The termination impedances will determine the form of the acoustic response and will thus be a factor influencing the application of active control to the duct. Theoretical methods for determining the acoustic radiation impedance, and hence termination impedances, of specific termination conditions have been presented; plane wave propagation in a circular pipe with an infinite flange has been examined theoretically (Norris and Sheng, 1989), and the reflection coefficients determined; the

reflection coefficients for an unflanged pipe have been examined theoretically (Levine and Schwinger, 1948) and experimentally (Davies et al., 1980) for the case of plane wave propagation in the pipe; the radiation efficiency of higher order modes in a baffled annular opening have been examined (Morfey, 1969), however, it should be noted that only the real part of the radiation efficiency is presented, and this is insufficient to calculate the termination impedance. Experimental techniques have been employed to determine the reflection coefficients of duct terminations for multi-modal sound fields (Åbom, 1989).

For the case of higher order acoustic modes, theoretical results have been presented for systems to actively control an arbitrary number of propagating modes (Fedoryuk, 1975). A system to actively control N propagating acoustic modes by using $2N$ error sensors and $2N$ control sources has also been proposed (Mazanikov et al., 1977) and experimentally investigated. For particular point measurement locations and excitation frequencies, up to 20 dB reduction in sound pressure levels was reported. However, as superposition of the source sound fields is considered to be the control mechanism, relatively little consideration has been given to the effects of control source location, size and strength.

Experiments have been conducted using a system in which the control sources, namely two loudspeakers, were positioned in the cutoff of a centrifugal fan casing (Neise and Koopmann, 1991). The aim was to attenuate the unwanted acoustic signal near, or at best in the source region to reduce the sound level for several or even all transmission paths simultaneously. Despite previous success (Koopmann et al., 1988) for excitation frequencies in the range where only plane waves could propagate, it was found that the

results were unsatisfactory when attempting to actively control higher frequencies in the range where higher order modes could propagate. It was believed that the acoustic pressure distribution generated by the centrifugal fan was too complex to be adequately controlled by the simple arrangement of control sources used in the experiments. A more sophisticated control source arrangement consisting of a larger number of individually driven loudspeakers is intended to be used for future research (Neise and Koopmann, 1991).

Implementation issues associated with placement of the sensor and actuator components of a practical active noise control system have also been addressed for the case of an infinite duct (Stell and Bernhard, 1991) and a finite duct (Stell and Bernhard, 1990a), with particular reference to the effects of evanescent acoustic modes.

Research has also been undertaken into the active control of random noise for frequencies below the first higher order mode cut-on frequency (La Fontaine and Shepherd, 1985), and for propagation of higher order modes (Silcox and Elliott, 1990); however a detailed analysis of the influence of geometric parameters upon system performance has not been presented. For the particular case of random noise excitation, the noise incident to, and that reflected from, a duct termination are assumed to be uncorrelated and thus the total noise level is obtained from addition of the amplitudes of the two components. A more complex interaction occurs between the components incident to, and those reflected from, a duct termination for periodic noise, because both the amplitude and relative phase of the components affect the resultant noise level.

A number of error sensor strategies have been proposed for systems which actively control duct noise. Generally, each strategy has been associated with a particular duct configuration and a particular objective for minimising the sound field. This work will be discussed here with the idea of providing the background necessary for the development of the new error sensor strategy presented in Chapter 4. It has been suggested that the total time-averaged acoustic potential energy is a relevant single measure of the amplitude of the sound field in an enclosure (Nelson et al., 1985). A practical approach to the minimisation of the acoustic potential energy within a finite length duct has been presented (Curtis et al.,1987), using the sum of the squares of the sound pressures at a number of evenly distributed locations throughout the enclosure to approximate the acoustic potential energy. Results were presented for plane waves in a reverberant duct having rigid walls and terminations. Minimisation of the acoustic potential energy within a region downstream of the control sources has been investigated (Stell and Bernhard, 1990) as a strategy for active control of higher order acoustic modes in a semi-infinite duct; this criterion being especially suitable for cases when the contribution of evanescent modes is significant.

Investigations, in which minimisation of the total real power output of the primary and control sources has been used as the error criterion, have been conducted for plane wave propagation in infinite and semi-infinite ducts (Snyder and Hansen, 1989).

Minimisation of the pressure at a point close to the control source face to create an "acoustical virtual earth" has been investigated (Trinder and Nelson, 1983) for plane waves

in finite length ducts, in addition to a number of studies of the minimisation of the sound pressure at a point (Jessel and Mangiante, 1972; Swinbanks, 1973; Tichy et al., 1984) for plane wave propagation.

Formulation of the controller modal transfer functions, between the error sensor and the control source, for minimising the pressure at a point in a multi-mode sound field within an infinite duct has been investigated (Stell and Bernhard, 1991) for the idealised case of modally independent reference sensors, control sources and error sensors; however, techniques for the practical implementation of such elements have not been proposed.

An experimental system (Eriksson et al., 1989) which utilises multiple adaptive systems has been presented for actively controlling one higher order acoustic mode in a duct. In this system, a separate adaptive filter model is used for each positive and negative portion of the non-uniform pressure distribution associated with the higher order mode. Each filter model obtains information from a separate error transducer and outputs a signal to a separate loudspeaker. An independent random noise source is used with each adaptive filter to model the transfer functions between the loudspeakers and the error microphones. The advantages of using multiple adaptive control systems rather than a single multi-channel system have not been indicated. The active control system was reported to reduce tonal noise by 20-25 dB at a single measurement location, and broadband noise, above the cut-on frequency of the higher order acoustic mode, by about 10-25 dB; however, the response at locations other than the error microphone locations has not been presented. System stability and convergence were found to be problematic and future research is

focussed on improving these characteristics. No indication was given of a suitable system configuration to attenuate duct noise when more than one higher order acoustic mode propagates. Two recursively-coupled multi-channel adaptive control systems have been developed (Rubenstein et al., 1992) to cancel the plane wave and the first higher order mode; however, no indication of the advantage of using multiple adaptive control systems, or a suitable configuration for attenuating more than one higher order mode, has been given. Minimisation of the sound pressure at two error sensor locations has also been used (Silcox and Elliott, 1990) as a strategy to minimise a multi-modal sound field excited by random noise within the frequency range for propagation of plane waves and a single higher order mode.

Additional processing of the sound pressure measured at a number of microphones has been used to form an error signal proportional to the complex reflection coefficient for plane wave propagation (Guicking and Karcher, 1984), in a system to actively change the impedance of a duct termination in which a source is located. This concept has been extended to an adaptive system to actively change the acoustical impedance presented by a source located in the duct termination (Orduña-Bustamante and Nelson, 1992), using an error signal indicating the difference between the actual and desired impedance, which is obtained by processing the signals from a two-microphone probe.

Other researchers have used error measures such as intensity or energy density (Nashif and Sommerfeldt, 1992) for frequencies at which only plane waves are propagated; however, at frequencies for which higher order modes may propagate, the intensity and energy

density are non-uniformly distributed over the duct cross-section and hence a point measurement of these variables is not proportional to the downstream acoustic power, making this sensor criterion inappropriate for cases other than plane wave propagation.

The number of error microphones required for multi-modal attenuation has been theoretically investigated (Baumann and Greiner, 1992a), independently from the number of control sources (Baumann and Greiner, 1992b). An analytical investigation of instances in which minimisation of pressure closely approximates minimisation of potential energy and propagating power has been undertaken (Stell, 1991), and criteria for placement of error sensors in such instances have been proposed. For cases with significant evanescent mode response, placing the sensors and sources on the nodal lines of the dominant evanescent modes has been suggested (Stell, 1991); however, for certain duct geometries and excitation frequencies the nodal lines of one evanescent mode may correspond to the anti-nodal line of another mode.

The work outlined in this chapter extends previous research (Snyder and Hansen, 1989) by developing an analytical model, based upon the acoustic impedance of each source, to describe the active control of higher order acoustic modes. The model enables calculation of the acoustic power output for the individual sources and the effect of source variables such as size, location, strength and relative phase to be taken into account. Results are presented which show the influence of these source variables on the level of reduction in total mean acoustic power output, for the semi-infinite hard-walled rectangular duct considered.

2.2 THEORY

2.2.1 Single control source

The model used in the following analysis is a semi-infinite hard-walled rectangular duct of uniform cross-sectional area, terminated in the plane of the duct cross-section at $z = 0$ by a uniform surface of arbitrary acoustic impedance. A uniform acoustic impedance surface is used for simplicity in this analysis because the modes will not "mix" upon reflection from such a surface. However, if the surface has an acoustic impedance which is a function of position, the modes will tend to couple, and a single incident mode will be reflected as several different modes. In practice, an anechoic termination is used to achieve an infinitely extending duct in the positive z-direction. The fluid contained within the duct is assumed to be at rest with constant and uniform ambient temperature and density. Excitation of the fluid by finite size, harmonic rectangular sources is assumed. The excitation frequency is unconstrained, as the propagation of higher order acoustic modes within the duct is accounted for in the analysis. The model assumes that both the primary and control sources are constant volume velocity sources, which is equivalent to assuming infinite internal impedance sources. Although infinite internal impedance sources are not practically achievable, models based upon such sources have been found sufficiently accurate (Snyder and Hansen, 1989), as loudspeakers backed by a small air-tight cavity may be approximately modelled in this manner at low frequencies.

In the following analysis, the positive time-dependence term $e^{j\omega t}$ is omitted with the assumption that the volume velocities, particle velocities and acoustic pressures used are amplitudes, unless otherwise stated.

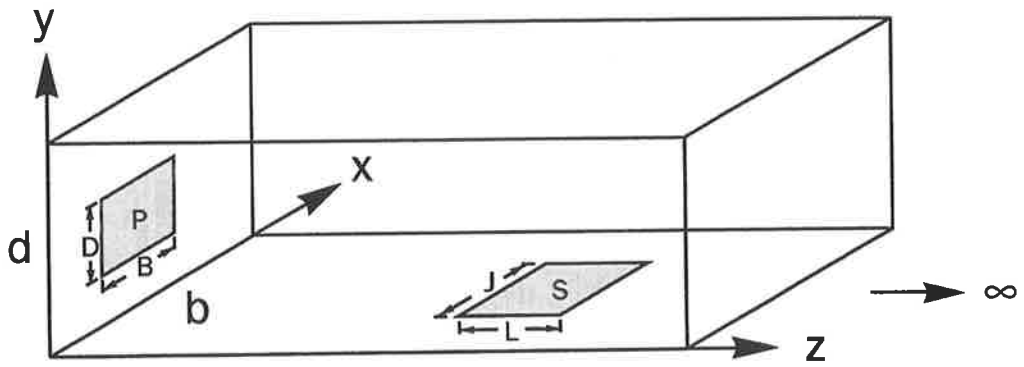

Figure 2.1 Single control source system and duct coordinate axes.

The source arrangement and coordinate axes are shown in Figure 2.1, where the finite size primary source is shown mounted in the termination plane of the duct cross section at z = 0, while the finite size control sources may be mounted in any of the four duct walls. Only positive values of z are allowed by this arrangement.

The total power flow along the duct is the sum of the powers from the primary and control sources. The reduction due to active control is the difference in total power with and without the control source operating. If the sources are speakers, the acoustic particle velocity across the face of each source will be essentially uniform and the acoustic power, for a single control source, will be given by

$$W = \frac{1}{2}Re\left[Q_p p_p^*\right] + \frac{1}{2}Re\left[Q_c p_c^*\right] \tag{2.1}$$

where Q and p are, respectively the complex source volume velocity amplitude and complex acoustic pressure amplitude at the surface of the source. The subscripts p and c denote primary and control source respectively. If the acoustic particle velocity were not uniform across the face of the primary source, then the product of acoustic particle velocity and the complex conjugate of the acoustic pressure would have to be integrated

over the source surface.

The purpose of the following analysis is to determine the optimum value of Q_c which will minimise W. This firstly requires that expressions for p_p and p_c be found for the case of both sources operating.

We begin with the expression for the Green's function for an infinite duct (Morse and Ingard, 1968; modified to account for $e^{+j\omega t}$ time dependence used here) which effectively relates the acoustic pressure and particle velocity at any location in the duct. Thus

$$G(\vec{x},\vec{x}_o,\omega) = \frac{-j}{S}\sum_{mn}\frac{\Psi_{mn}(x,y)\Psi_{mn}(x_o,y_o)}{\Lambda_{mn}k_{mn}}e^{-jk_{mn}|z-z_o|} \tag{2.2}$$

where ω is the angular frequency of the excitation, $\vec{x}_o = (x_o,y_o,z_o)$ are the coordinates describing the location of the source and $\vec{x} = (x,y,z)$ is an arbitrary point within the duct. S is the cross-sectional area of the duct, k_{mn} is the modal wavenumber, Ψ_{mn} is the characteristic or mode shape function of the duct and Λ_{mn} is the modal normalisation factor. For a rectangular duct

$$\Psi_{mn}(x,y) = \cos\left(\frac{m\pi x}{b}\right)\cos\left(\frac{n\pi y}{d}\right) \tag{2.3}$$

where m, n are the modal indices and b and d the duct cross-section dimensions. Note that if plane waves only are considered $m = n = 0$.

$$\Lambda_{mn} = \frac{1}{S}\int_S \Psi_{mn}^2\, dS \tag{2.4}$$

and

$$k_{mn} = \sqrt{\left(\frac{\omega}{c_o}\right)^2 - \left(\frac{\pi m}{b}\right)^2 - \left(\frac{\pi n}{d}\right)^2} \tag{2.5}$$

where ω is the excitation frequency and c_o the speed of sound in free space.

The pressure at a point $\vec{x} = (x,y,z)$ in a semi-infinite duct due to a finite size, plane primary source located at $\vec{x}_o = (x_o,y_o,0)$ at the finite end of the duct in a plane normal to the duct axis is given by (Fahy, 1985)

$$p_p(x,y,z) = j\rho\omega \int_0^D \int_0^B q_p G(\vec{x},\vec{x}_o,\omega)\, dx_o dy_o \tag{2.6}$$

where q_p is the particle velocity on the face of the primary source of width B and height D which has a surface area A_p. Note that if p is an amplitude, then q must also be an amplitude.

Expressing Equation (2.6) in terms of the primary source volume velocity amplitude Q_p, the pressure amplitude at an arbitrary point (x,y,z) due to a simple point primary source located at $(x_o,y_o,0)$ is given by

$$p_p(x,y,z) = \frac{\rho\omega Q_p}{S} \sum_{mn} \frac{\Psi_{mn}(x,y)\Psi_{mn}(x_o,y_o)}{\Lambda_{mn} k_{mn}} e^{-jk_{mn}z} \tag{2.7}$$

The corresponding pressure at point (x,y,z) due to a finite size primary source is given by

$$p_p(x,y,z) = \frac{\rho\omega}{S}\sum_{mn}\int_0^D\int_0^B q_p \frac{\Psi_{mn}(x,y)\Psi_{mn}(x_o,y_o)}{\Lambda_{mn}k_{mn}} e^{-jk_{mn}z}\,dx_o dy_o \tag{2.8}$$

Solving the integral for the rectangular duct case and a rectangular primary source, as illustrated in Figure 2.1, yields

$$p_p(x,y,z) = \frac{\rho\omega Q_p}{SA_p}\sum_{mn}\frac{\Psi_{mn}(x,y)F_{pm}F_{pn}}{\Lambda_{mn}k_{mn}} e^{-jk_{mn}z} \tag{2.9a}$$

where Q_p is the complex volume velocity amplitude of the primary source. If only plane wave propagation is considered ($m = n = 0$), $\Psi_{00} = 1$, $\Lambda_{00} = 1$ and $k_{00} = k_o = \omega/c_o$; thus Equation (2.9a) can be written as

$$p_p(x,y,z) = \frac{\rho c_o}{S} Q_p e^{-jk_o z} \tag{2.9b}$$

F_{pm} and F_{pn} are the primary source finite source factors given by

$$F_{pm} = \begin{cases} \dfrac{2b}{m\pi}\sin\left(\dfrac{m\pi B}{2b}\right)\cos\left(\dfrac{m\pi x_o}{b}\right) & m \neq 0 \\ B & m = 0 \end{cases} \tag{2.10}$$

$$F_{pn} = \begin{cases} \dfrac{2d}{n\pi}\sin\left(\dfrac{n\pi D}{2d}\right)\cos\left(\dfrac{n\pi y_o}{d}\right) & n \neq 0 \\ D & n = 0 \end{cases} \tag{2.11}$$

The mean pressure over the face of the primary source is (Berengier and Roure, 1980)

$$p_{p/p} = \frac{1}{A_p} \int_0^D \int_0^B p_p(x,y,0)\, dxdy \tag{2.12}$$

The subscript p/p refers to a quantity at the primary source due to the primary source. Similarly p/c refers to a quantity at the primary source due to the control source. This notation will be used throughout the analysis. Solving for the case considered yields

$$p_{p/p} = \frac{\rho \omega Q_p}{A_p^2 S} \sum_{mn} \frac{F_{pm}^2 F_{pn}^2}{\Lambda_{mn} k_{mn}} \tag{2.13a}$$

Again for plane wave propagation, this expression becomes

$$p_{p/p} = \frac{\rho c_o}{S} Q_p \tag{2.13b}$$

Equation (2.12) can be rewritten for the pressure at the control source located in the z, x plane of a duct wall at $y = 0$ due to the primary source as

$$p_{c/p} = \frac{1}{A_c} \int_0^L \int_0^J p_p(x,0,z)\, dxdz \tag{2.14}$$

where A_c is the surface area of the control source of length L in the axial direction and lateral length J. Substituting the expression for the pressure at a point due to the primary source, given in Equation (2.9), into Equation (2.14) yields the mean pressure over the face of the finite size control source due to the primary source, namely

$$p_{c/p} = \frac{\rho \omega Q_p}{A_p A_c S} \sum_{mn} \frac{F_{pm} F_{pn} F_{cm} F_{cn} F_{cL}}{\Lambda_{mn} k_{mn}} e^{-jk_{mn} z_c} \tag{2.15a}$$

For plane waves only

$$p_{c/p} = \frac{\rho c_o}{S} Q_p e^{-jk_o z_c} \frac{2}{k_o L} \sin\left(\frac{k_o L}{2}\right) \tag{2.15b}$$

where z_c is the axial distance from the primary source face to the centre of the control source. F_{cm}, F_{cn} and F_{cL} are the control source finite source factors. For a control source mounted in the $y = d$ plane of the duct these are given by

$$F_{cm} = \begin{cases} \frac{2b}{m\pi} \sin\left(\frac{m\pi J}{2b}\right) \cos\left(\frac{m\pi x_c}{b}\right) & m \neq 0 \\ J & m = 0 \end{cases} \tag{2.16}$$

$$F_{cn} = (-1)^n \tag{2.17}$$

$$F_{cL} = \begin{cases} \frac{2}{k_n} \sin\left(\frac{k_n L}{2}\right) & k_n \neq 0 \\ L & k_n = 0 \end{cases} \tag{2.18}$$

The acoustic pressure at any point in the semi-infinite duct due to a source mounted part way along the duct in one of the duct walls consists of the sum of the direct pressure p_{c_d} from the source and the pressure p_{c_r} reflected from the finite end.

The contribution to the pressure coming directly from a simple point control source is given by

$$p_{c_d}(x,y,z) = \frac{\rho\omega Q_c}{2S}\sum_{mn}\frac{\Psi_{mn}(x,y)\Psi_{mn}(x_c,y_c)}{\Lambda_{mn}k_{mn}}e^{-jk_{mn}|z-z_c|} \tag{2.19}$$

Assuming a rigid termination, the pressure at point (x,y,z) due to the component reflected from the primary source end is given by

$$p_{c_r}(x,y,z) = \frac{\rho\omega Q_c}{2S}\sum_{mn}\frac{\Psi_{mn}(x,y)\Psi_{mn}(x_c,y_c)}{\Lambda_{mn}k_{mn}}e^{-jk_{mn}(z+z_c)} \tag{2.20}$$

The total pressure at a point is equal to the sum of the direct and reflected pressure components, namely

$$p_c(x,y,z) = p_{c_d}(x,y,z)+p_{c_r}(x,y,z) \tag{2.21}$$

For a point (x,y,z) downstream of the control source, that is for $z \geq z_c$

$$p_c(x,y,z) = \frac{\rho\omega Q_c}{S}\sum_{mn}\frac{\Psi_{mn}(x,y)\Psi_{mn}(x_c,y_c)}{\Lambda_{mn}k_{mn}}e^{-jk_{mn}z} \times\left[\frac{e^{jk_{mn}z_c}+e^{-jk_{mn}z_c}}{2}\right] \tag{2.22}$$

or

$$p_c(x,y,z) = \frac{\rho\omega Q_c}{S}\sum_{mn}\frac{\Psi_{mn}(x,y)\Psi_{mn}(x_c,y_c)}{\Lambda_{mn}k_{mn}}e^{-jk_{mn}z}\cosh(jk_{mn}z_c) \tag{2.23}$$

Thus for $z \geq z_c$

$$p_c(x,y,z) = \frac{\rho\omega Q_c}{S}\sum_{mn}\frac{\Psi_{mn}(x,y)\Psi_{mn}(x_c,y_c)}{\Lambda_{mn}k_{mn}}e^{-jk_{mn}z}\cos(k_{mn}z_c) \tag{2.24a}$$

For plane waves only we have

$$p_c(z) = \frac{\rho c_o}{S} Q_c e^{-jk_o z} \cos(k_o z_c) \tag{2.24b}$$

A similar approach can be used to derive the total pressure, due to the control source only, at a point (x,y,z) located between the primary source and the control source, to give for $0 \leq z \leq z_c$

$$p_c(x,y,z) = \frac{\rho \omega Q_c}{S} \sum_{mn} \frac{\Psi_{mn}(x,y)\Psi_{mn}(x_c,y_c)}{\Lambda_{mn} k_{mn}} e^{-jk_{mn} z_c} \cos(k_{mn} z) \tag{2.25a}$$

where (x_c,y_c,z_c) is the coordinate of the control source. For plane waves only

$$p_c(z) = \frac{\rho c_o}{S} Q_c e^{-jk_o z_c} \cos(k_o z) \tag{2.25b}$$

Using a similar approach to that used for the primary source, the mean pressure over the face of the control source, due to the sound field produced by the control source, is found to be

$$p_{c/c} = \frac{\rho \omega Q_c}{A_c^2 S} \sum_{mn} \frac{F_{cm}^2 F_{cn}^2 F_{cL}^2}{\Lambda_{mn} k_{mn}} e^{-jk_{mn} z_c} \cos(k_{mn} z_c) \tag{2.26a}$$

For plane waves only, Equation (2.26a) becomes

$$p_{c/c} = \frac{\rho c_o}{S} Q_c e^{-jk_o z_c} \cos(k_o z_c) \left(\frac{2}{k_o L} \right)^2 \sin^2 \left(\frac{k_o L}{2} \right) \tag{2.26b}$$

The pressure over the face of the primary source due to the control source is

$$p_{p/c} = \frac{\rho \omega Q_c}{A_c A_p S} \sum_{mn} \frac{F_{cm} F_{cn} F_{pm} F_{pn} F_{cL}}{\Lambda_{mn} k_{mn}} e^{-jk_{mn} z_c} \tag{2.27a}$$

For plane waves only

$$p_{p/c} = \frac{\rho c_o}{S} Q_c e^{-jk_o z_c} \frac{2}{k_o L} \sin\left(\frac{k_o L}{2}\right) \tag{2.27b}$$

The total acoustic pressure amplitude at the face of the primary source is equal to the sum of the pressure at the source location due to the primary source itself and the pressure contribution from the control source, and is given by

$$p_p = p_{p/p} + p_{p/c} \tag{2.28}$$

which is found by adding together Equations (2.13) and (2.27).

The total pressure at the face of the control source is

$$p_c = p_{c/p} + p_{c/c} \tag{2.29}$$

which is found by adding together Equations (2.15) and (2.26). The total power radiated down the duct is then found by substituting Equations (2.28) and (2.29) into (2.1).

Previously the acoustic pressure at a point has been expressed as the sum of modal contributions, with m and n extending from zero to infinity. The acoustic pressure may be otherwise expressed in terms of its real and imaginary components by considering that for an excitation frequency ω, there are a finite number of modes which are "cut-on", and hence contribute to the propagating part of the pressure, while those modes with a cut-on frequency greater than the excitation frequency contribute only to the non-propagating component of the pressure. This may be written as

$$\begin{aligned} \omega &\geq \kappa_{mn} c_o \quad \textit{mode cut-on} \\ \omega &< \kappa_{mn} c_o \quad \textit{mode cut-off} \end{aligned} \tag{2.30}$$

where κ_{mn} is the modal eigenvalue given by

$$\kappa_{mn} = \sqrt{\left(\frac{\pi m}{b}\right)^2 + \left(\frac{\pi n}{d}\right)^2} \tag{2.31}$$

Hence the propagating part of the pressure may be written as the sum of contributions from the N+1 cut-on modes extending from zero to N, as the plane wave or fundamental mode is cut-on for all frequencies of excitation, where

$$\kappa_N < \frac{\omega}{c_o} < \kappa_{N+1} \tag{2.32}$$

Acoustic modes having modal eigenvalues greater than ω / c_o do not propagate along the duct as waves, but decay in an exponential manner with axial distance from the source, in contrast to the cut-on modes which, for the rigid walled case considered here, are not attenuated and propagate along the duct. As found previously, for these cut-off modes the pressure and axial particle velocity are exactly out of phase, and hence the modes transport no mean energy. A more detailed examination of the relationship between cut-off modes and the total mean acoustic power flow is presented by Doak (1973a).

In this chapter, the sources are assumed to be in each other's far-field and hence the pressure at one source's face due to the other is found by considering only the propagating part of the pressure produced by each source. A more detailed analysis of the near-field produced by a finite size source is presented by Tichy et al. (1984) and Doak (1973a).

2.2.2 Multiple control sources

The purpose of the following section is to extend the analysis presented in the previous section for the acoustic pressure at a single primary and a single control source, in a rigidly-terminated semi-infinite duct, to the case of multiple control sources.

We will begin by considering two control sources, and in the analysis the subscript 1 will refer to the control source S_1, and the subscript 2 will refer to the control source S_2. A source arrangement for two control sources is shown in Figure 2.2. Using a procedure similar to that used for the single control source case, the additional acoustic pressure terms are derived in the following manner.

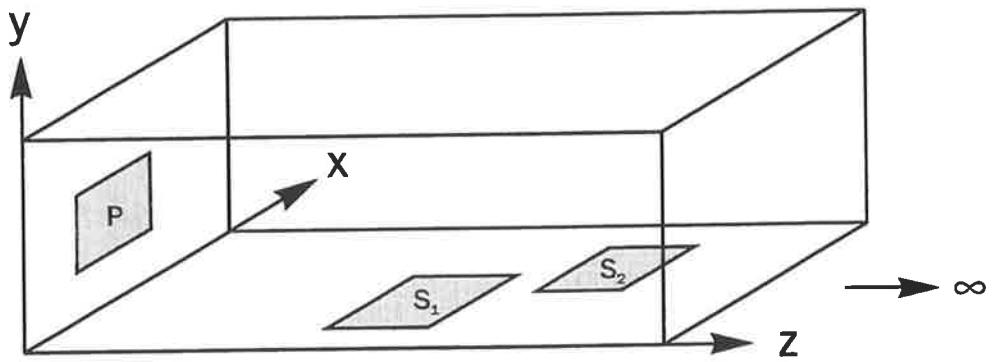

Figure 2.2 Dual control source system.

Assuming the control source S_2 to be located at a greater axial distance from the primary source than control source S_1, that is for $z_{S2} \geq z_{S1}$, the mean pressure over the face of S_2 due to S_1 is

$$p_{s_2/s_1} = \frac{\rho \omega Q_{s_1}}{A_{s_1} A_{s_2} S} \sum_{mn} \frac{F_{s_2 m} F_{s_2 n} F_{s_1 m} F_{s_1 n} F_{s_1 L} F_{s_2 L}}{\Lambda_{mn} k_{mn}} \times \cos(k_{mn} z_{s_1}) \, e^{-jk_{mn} z_{s_2}} \tag{2.33a}$$

For plane waves only

$$p_{s2/s1} = \frac{\rho c_o}{S} Q_{s1} e^{-jk_o z_{s2}} \cos(k_o z_{s1}) \frac{4}{k_o^2 L_1 L_2} \sin\left(\frac{k_o L_1}{2}\right) \sin\left(\frac{k_o L_2}{2}\right) \quad (2.33b)$$

Similar expressions hold for $p_{s1/s2}$ and the total pressure at source S_1 is now

$$p_{s1} = p_{s1/p} + p_{s1/s1} + p_{s1/s2} \quad (2.34)$$

where $p_{s1/p}$ is equivalent to $p_{c/p}$ of Equation (2.15) and $p_{s1/s1}$ is equivalent to $p_{c/c}$ of Equation (2.26). Similar expressions hold for p_{s2} and p_p.

The total acoustic power radiated down the duct for the dual control source system is

$$W = \frac{1}{2} Re\left[Q_p p_p^* + Q_{s1} p_{s1}^* + Q_{s2} p_{s2}^* \right] \quad (2.35)$$

The analysis required for more than two control sources follows similar reasoning as that just outlined for two control sources. Equations (2.34) and (2.35) will have C+1 terms where C is the number of control sources.

2.2.3 Uniform impedance termination

The purpose of the following section is to present expressions for the pressure at the primary and control source locations, for a semi-infinite duct which is rigidly terminated by a uniform, finite impedance surface. Alteration of the termination plane at $z = 0$ from a rigid termination to a uniform, finite impedance surface allows greater flexibility in the model, and enables a more accurate prediction of a real system's performance. Again the pressure at a point in the duct will be equal to the sum of the contribution directly from the source and the contribution of waves reflected from the termination plane at $z = 0$. A

plane wall of uniform impedance will not couple modes or reflect a multiple number of modes from a single incident mode. Hence an n^{th} order mode incident upon the termination will be reflected from the surface as an n^{th} order mode. The alteration of the incident wave due to the impedance surface can be expressed in exponential form as

$$e^{-2\Phi_{mn}} \tag{2.36}$$

where

$$\Phi_{mn} = \pi\alpha_{mn} + j\pi\beta_{mn} \tag{2.37}$$

The ratio of the amplitudes of the reflected and incident waves at $z = 0$ is given by (Morse and Ingard, 1968)

$$\frac{|p_r|}{|p_i|} = e^{-2Re(\Phi_{mn})} = e^{-2\pi\alpha_{mn}} \tag{2.38}$$

where p_r is the reflected wave amplitude and p_i the incident wave amplitude, and the phase change on reflection from the impedance surface is

$$-2Im(\Phi_{mn}) = -2\pi\beta_{mn} \tag{2.39}$$

The pressure, due to the control source only, at a point (x,y,z) positioned between the primary and control source, that is for $0 \le z \le z_c$, is given for a simple point control source by

$$p_c(x,y,z) = \frac{\rho\omega Q_c}{S}\sum_{mn}\frac{\Psi_{mn}(x,y)\Psi_{mn}(x_c,y_c)}{\Lambda_{mn}k_{mn}}e^{-\Phi_{mn}-jk_{mn}z_c} \times \cosh(\Phi_{mn}+jk_{mn}z) \tag{2.40}$$

Similarly for an axial location $z \ge z_c$

$$p_c(x,y,z) = \frac{\rho\omega Q_c}{S}\sum_{mn}\frac{\Psi_{mn}(x,y)\Psi_{mn}(x_c,y_c)}{\Lambda_{mn}k_{mn}}e^{-\Phi_{mn}-jk_{mn}z} \times\cosh(\Phi_{mn}+jk_{mn}z_c) \tag{2.41a}$$

For plane waves only, we have

$$p_c(z) = \frac{\rho c_o}{S}Q_c e^{-(\Phi_o+jk_oz)}\cosh(\Phi_o+jk_oz_c) \tag{2.41b}$$

Expressions for p_p, $p_{p/p}$ and $p_{c/p}$ corresponding to finite size sources are identical to expressions (2.28), (2.13) and (2.15) respectively for a rigid termination at the primary source. However expressions for $p_{p/c}$ and $p_{c/c}$ are different to those for a rigid termination and may be written as follows

$$p_{p/c} = \frac{\rho\omega Q_c}{A_cA_pS}\sum_{mn}\frac{F_{cm}F_{cn}F_{pm}F_{pn}F_{cL}}{\Lambda_{mn}k_{mn}}e^{-(jk_{mn}z_c+\Phi_{mn})}\cosh(\Phi_{mn}) \tag{2.42}$$

$$p_{c/c} = \frac{\rho\omega Q_c}{A_c^2S}\sum_{mn}\frac{F_{cm}^2F_{cn}^2F_{cL}^2}{\Lambda_{mn}k_{mn}}e^{-(jk_{mn}z_c+\Phi_{mn})}\cosh(\Phi_{mn}+jk_{mn}z_c) \tag{2.43}$$

The total radiated power may be calculated as before by using Equations (2.1), (2.28), (2.29), (2.13), (2.15), (2.26) and (2.27).

2.2.4 Optimum control source volume velocity

The objective of this section is to determine the optimum control source volume velocity for a rigidly-terminated semi-infinite duct, and also for a semi-infinite duct terminated by a uniform, finite impedance surface. For the case of a rigid duct termination plane at $z = 0$ it is possible to express the total acoustic power output of the system as a quadratic

function of the complex control source volume velocity amplitude Q_c, where

$$Q_c = \bar{Q}_c e^{-j\beta_c} \tag{2.44}$$

The quantity $\bar{Q}_c$ is the scalar volume velocity amplitude of the control source and β_c is its phase relative to some reference source. For a system consisting of a finite size primary source and a single control source the total acoustic power output is given by

$$W = Q_c^* \hat{a} Q_c + Q_c^* \hat{b} + \hat{b}^* Q_c + \hat{c} \tag{2.45}$$

where

$$\hat{a} = \frac{1}{2}\frac{\rho\omega}{A_c^2 S}\sum_{n=0}^{N}\frac{F_{cm}^2 F_{cn}^2 F_{cL}^2}{\Lambda_{mn} k_{mn}}\cos^2(k_{mn} z_c) \tag{2.46}$$

$$\hat{b} = \frac{1}{2}\frac{\rho\omega Q_p}{A_c A_p S}\sum_{n=0}^{N}\frac{F_{cm} F_{cn} F_{pm} F_{pn} F_{cL}}{\Lambda_{mn} k_{mn}}\cos(k_{mn} z_c) \tag{2.47}$$

and

$$\hat{c} = \frac{1}{2}\frac{\rho\omega}{A_p^2 S}|Q_p|^2\sum_{n=0}^{N}\frac{F_{pm}^2 F_{pn}^2}{\Lambda_{mn} k_{mn}} \tag{2.48}$$

In the preceding equations, the solution for plane waves is found by setting $m = n = 0$, $F_{c0}^2 F_{c0}^2 / A_c^2 = 1$ and $\Lambda_{00} = 1$.

Although this quadratic is not differentiable with respect to the complex volume velocity Q_c, it is possible to differentiate the total acoustic power W with respect to the real and

imaginary parts of the control source volume velocity, Q_R and Q_I. Equating each of these gradients to zero, $\partial W/\partial Q_R = 0$ and $\partial W/\partial Q_I = 0$, yields the complex control source volume velocity which minimises the total acoustic power. This optimum volume velocity amplitude is given by (Pan and Hansen, 1990)

$$Q_{c_{opt}} = -\hat{a}^{-1}\,\hat{b} \tag{2.49}$$

For a duct with a uniform impedance surface termination plane, the total acoustic power for a system comprising one primary source and a single control source is

$$W = Q_c^* Re\{\hat{a}\} Q_c + Re\{\hat{b}_1 Q_c\} + Re\{\hat{b}_2 Q_c^*\} + \hat{c} \tag{2.50}$$

where

$$\hat{a} = \frac{1}{2} Re\left\{ \frac{\rho\omega}{A_c^2 S} \sum_{n=0}^{N} \frac{F_{cm}^2 F_{cn}^2 F_{cL}^2}{\Lambda_{mn} k_{mn}} e^{-jk_{mn}z_c} e^{-\Phi_{mn}} \cosh(jk_{mn}z_c + \Phi_{mn}) \right\} \tag{2.51}$$

$$\hat{b}_1 = \frac{1}{2} \frac{\rho\omega Q_p^*}{A_c A_p S} Re\left\{ \sum_{n=0}^{N} \frac{F_{cm}F_{cn}F_{pm}F_{pn}F_{cL}}{\Lambda_{mn} k_{mn}} e^{-jk_{mn}z_c} \right\} \tag{2.52}$$

$$\hat{b}_2 = \frac{1}{2} \frac{\rho\omega Q_p}{A_c A_p S} Re\left\{ \sum_{n=0}^{N} \frac{F_{cm}F_{cn}F_{pm}F_{pn}F_{cL}}{\Lambda_{mn} k_{mn}} e^{-jk_{mn}z_c} e^{-\Phi_{mn}} \cosh(\Phi_{mn}) \right\} \tag{2.53}$$

$$\hat{c} = \frac{1}{2} \frac{\rho\omega}{A_p^2 S} |Q_p|^2 \sum_{n=0}^{N} \frac{F_{pm}^2 F_{pn}^2}{\Lambda_{mn} k_{mn}} \tag{2.54}$$

Differentiating the total power expression with respect to the real and imaginary components of the complex control source volume velocity yields the optimum control source volume velocity which is given by

$$Q_{c_{opt}} = -\frac{1}{2} Re\{\hat{a}\}^{-1} (\hat{b}_1^* + \hat{b}_2) \tag{2.55}$$

2.2.5 Residual power flow measurement

Active systems for the control of noise propagated as a plane wave, or fundamental mode, have traditionally utilised microphones as error sensors (Mazanikov and Tyutekin, 1976; Trinder and Nelson, 1983; Eriksson et al., 1989). Inherent in the use of such sensors has been the assumption that the minimisation of the total acoustic pressure at the sensor location is directly related to the minimisation of the total acoustic power flow. Although the propagating portion of the pressure is uniform over a plane of the duct cross-section for the fundamental mode, the non-propagating component of the pressure is non-uniformly distributed, and this results in the mean square pressure also being non-uniformly distributed across the duct cross-section at locations close to a source. Because the non-propagating component of the pressure decays in an exponential manner with axial distance from the source, it is generally assumed that at large distances from the source the pressure distribution is uniform, and hence a point measurement of the pressure is proportional to the total acoustic power flow. As has been noted previously (Doak, 1973a), when the excitation frequency approaches the cut-on frequency of a higher order acoustic mode, the rate of decay of the non-propagating component of the pressure for the fundamental mode may be small, and hence this component makes a considerable

contribution to the mean square pressure at relatively large distances from the source.

For the case of higher order modes the propagating part of the acoustic pressure is non-uniformly distributed over a plane of the duct cross-section in addition to the non-propagating portion. Hence neither a point measurement of the propagating portion of the acoustic pressure or the mean square pressure at a point are proportional to the total acoustic power flow.

The instantaneous acoustic intensity in the z-direction is given by

$$I_z = p u_z \tag{2.56}$$

where p is the instantaneous pressure and u_z the instantaneous acoustic particle velocity component in the z-direction. For simple harmonic excitation the mean acoustic intensity in the z-direction is

$$\bar{I}_z = \overline{p u_z} = \frac{1}{2} Re(\bar{p}\bar{u}_z^*) \tag{2.57}$$

where * denotes the complex conjugate and

$$p = \bar{p}\, e^{j\omega t} \tag{2.58}$$

$$u = \bar{u}\, e^{j\omega t} \tag{2.59}$$

For a simple source located in the plane of the duct cross-section at one end of a semi-infinite rectangular duct this becomes (Doak, 1973a)

$$\bar{I}_z(x,y) = \frac{1}{2}Re\left\{\left[\frac{\rho\omega Q}{S}\sum_{mn}\frac{\Psi_{mn}(x,y)\Psi_{mn}(x_o,y_o)}{\Lambda_{mn}k_{mn}}e^{-jk_{mn}z}\right]\times\left[\frac{Q^*}{S}\sum_{\mu\nu}\frac{\Psi_{\mu\nu}(x,y)\Psi_{\mu\nu}(x_o,y_o)}{\Lambda_{\mu\nu}}e^{jk^*_{mn}z}\right]\right\} \tag{2.60a}$$

where Q is the source volume velocity amplitude. For plane waves only this equation becomes

$$\bar{I}_z = \frac{\rho c_o Q^2}{2S^2} \tag{2.60b}$$

Note that at each point on the duct cross-section, the mean acoustic intensity includes cross-term contributions from products of the acoustic pressure in one mode with the acoustic particle velocity in another, or vice versa. This implies that the mean acoustic intensity in the z-direction is also non-uniformly distributed over a plane of the duct cross-section and hence a point measurement of this quantity is not proportional to the total acoustic power flow either. Because of the orthogonality of the modes, these cross-terms do not contribute to the total mean acoustic power given by

$$W = \int_S \bar{I}_z(x,y)\,dS \tag{2.61}$$

which for a simple source mounted in the termination plane of a semi-infinite rectangular duct is

$$W = \frac{\rho\omega Q^2}{2S}\sum_{n=0}^{N}\frac{\Psi^2_{mn}(x_o,y_o)}{\Lambda_{mn}k_{mn}} \tag{2.62a}$$

For plane waves only

$$W = \frac{\rho c_o Q^2}{2S} \tag{2.62b}$$

For the case modelled in this study the error sensor criterion used was the minimisation of the total mean acoustic power output, which is equivalent to minimisation of the total mean downstream acoustic power transmission for a semi-infinite duct. Other error sensor criteria such as minimisation of mean acoustic pressure at a point, minimisation of mean acoustic intensity at a point, or minimisation of the acoustic pressure or intensity averaged over a number of points were not investigated for the reasons mentioned above. Hence the results obtained relate to the potential performance of active control for this particular error sensor criterion. The performance achievable in practice will depend upon the accuracy with which a particular sensor configuration can sense the acoustic power transmission.

2.3 RESULTS

A series of cases have been studied using the analytical model to determine the effect of geometric variables upon the total acoustic power output reduction achievable using active control. Results are presented for a number of duct geometries and source locations because, in contrast to the plane wave or fundamental mode case, the duct aspect ratio and the relative positioning of the primary source within the duct cross-section have a great influence on the pressure field produced in the duct. The three primary source and duct aspect configurations for which results were obtained are shown in Figure 2.3. For all of the cases examined in this thesis the primary source is located within the duct cross-section at the axial location $z = 0$.

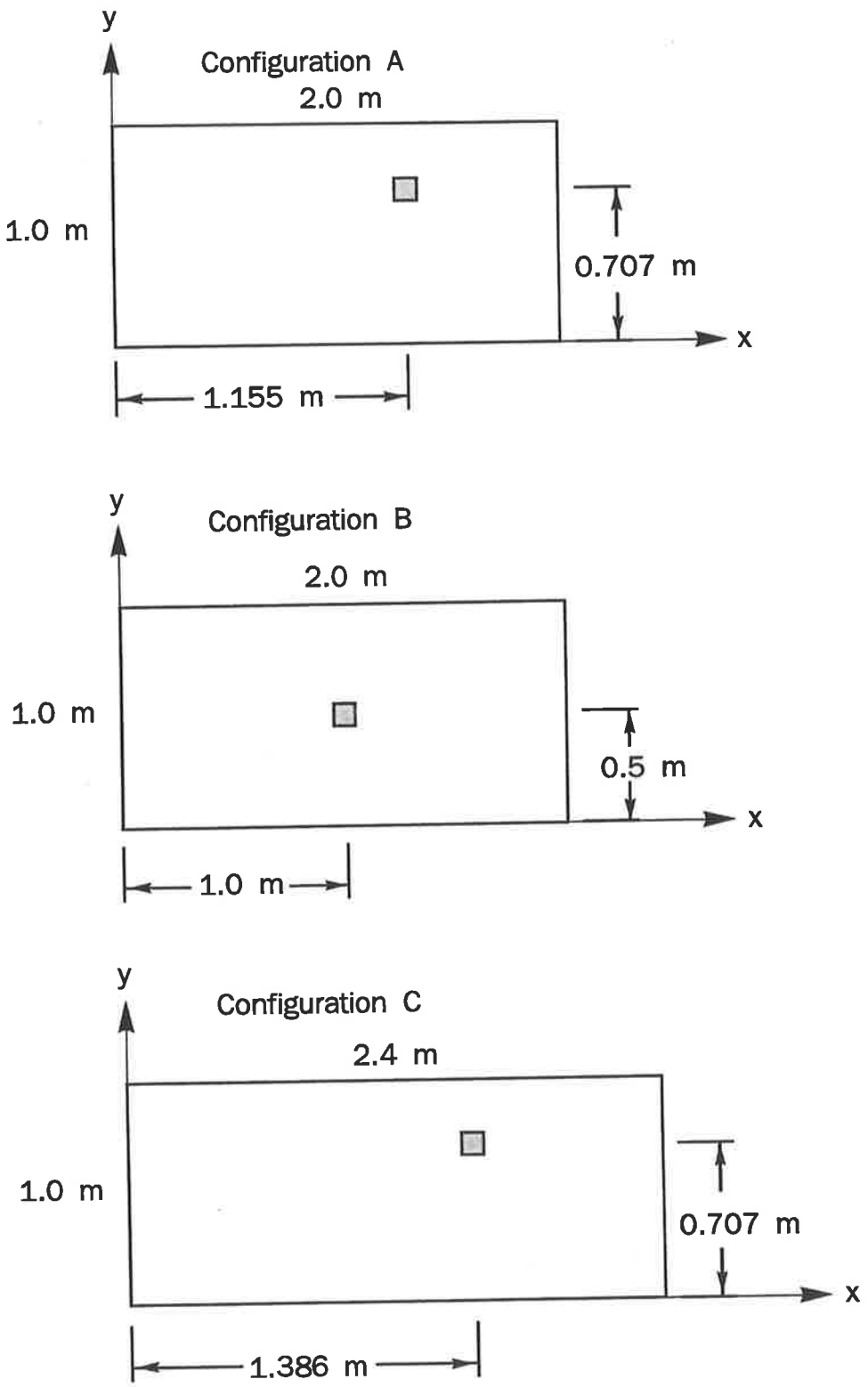

Figure 2.3 Primary source and duct aspect configurations for primary source located within the duct cross-section at $z = 0$.

Considering firstly excitation of the plane wave by a finite size source mounted in the plane of the duct cross-section, it can be shown that the real part of the pressure at a point within the duct is not influenced by the duct aspect ratio because the modal eigenvalue κ is equal to zero and the mode shape function Ψ_{mn} is equal to unity for all source and measurement locations. Hence, the pressure field produced when only the plane wave is propagated is proportional only to the frequency of excitation ω and the source volume velocity Q_p, for a constant duct cross-sectional area. Similarly the fundamental mode wavelength λ is only dependent upon the frequency of excitation. Referring to Equation (2.9), which provides the pressure at a point for a finite size primary source, it can be seen that the active pressure component is independent of both the relative location of the source and the source size.

Examination of Equation (2.27), an expression for the mean pressure at the primary source due to a finite size control source, reveals that for the plane wave case, the pressure at the primary source is proportional to the finite size source factor, F_{cL}, which accounts for the length of the control source along the duct axis. F_{cL} is given by

$$F_{cL} = \frac{2}{k_{mn}} \sin\left(\frac{k_{mn}L}{2}\right) \tag{2.63}$$

and approaches zero for increasing L. Although this term is inversely proportional to the length of the control source L, a constant pressure value may be maintained at the primary source for variable L by altering the control source volume velocity Q_c. Hence it is theoretically possible to completely control the total acoustic power output for a plane wave with a single control source, for all control source locations and sizes in a semi-

infinite duct with a rigid termination plane at $z = 0$. Constraining the control source volume velocity to be below a finite value causes the total power reduction to be a function of the axial distance separating the primary and control sources, and the control source size. For the case of a finite control source volume velocity the total acoustic power reduction is maximised for a primary source and control source separation distance corresponding to an integer multiple of half-wavelengths, and is a minimum for source separation distances equal to odd quarter wavelengths. This case is shown in Figure 2.4 for an excitation frequency of 50 Hz which is below the cut-on frequency of the first higher order mode (86 Hz) in the 2 m × 1 m duct, with the control source volume velocity constrained to below ten times the primary source volume velocity. Similarly, replacing the rigid termination at $z = 0$ with a surface of uniform impedance results in equivalently positioned maxima and minima of total power reduction with respect to the separation distance between the primary and control sources. This case is illustrated in Figure 2.5, with the control source volume velocity constrained to below ten times the primary source volume velocity. The two plane wave cases presented here correspond to results derived previously (Hansen and Snyder, 1990).

Increasing the excitation frequency above 86 Hz to an arbitrary value of 100 Hz causes propagation of the (1,0) acoustic mode in addition to the fundamental mode. The cut-on frequencies of the first five acoustic modes of a 2 m × 1 m rectangular duct are given in Table 2.1. Note that the control source volume velocity is unconstrained for all of the following cases examined.

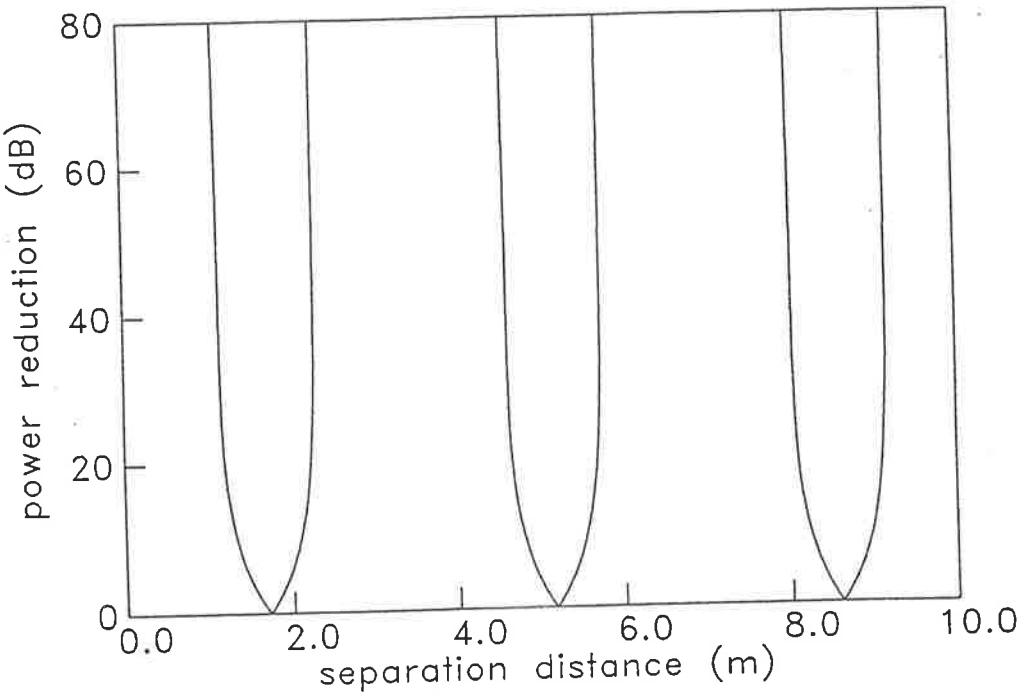

Figure 2.4 Acoustic power reduction using single control source at 50 Hz for semi-infinite duct with rigid duct termination at $z = 0$ as a function of separation between the primary and control sources.

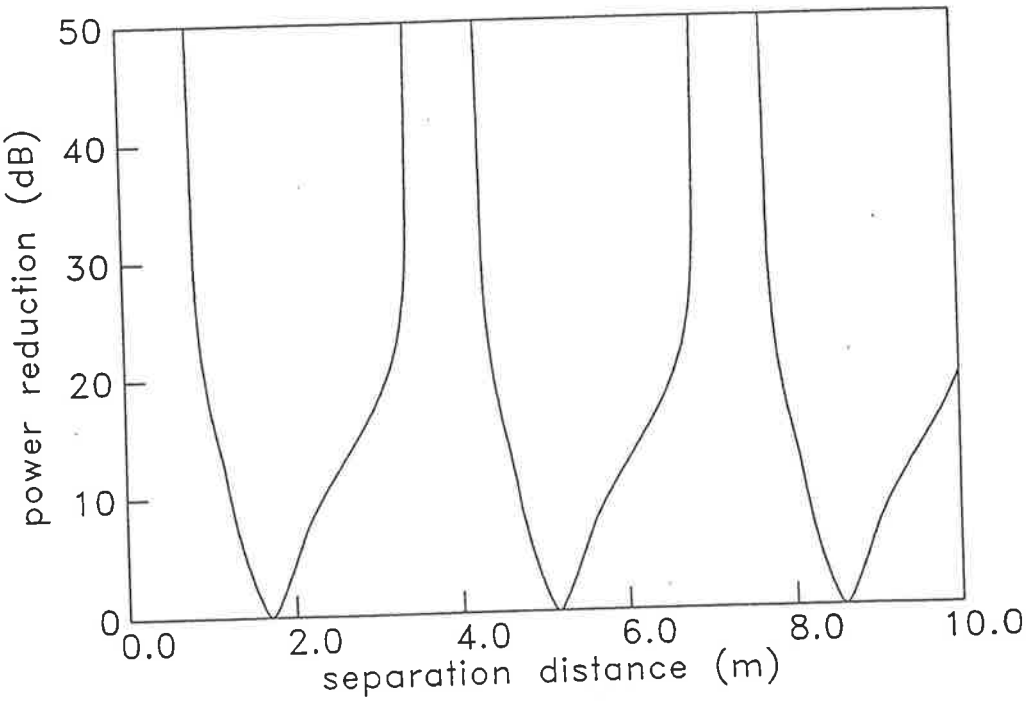

Figure 2.5 Acoustic power reduction using single control source at 50 Hz for semi-infinite duct with uniform impedance surface duct termination at $z = 0$ as a function of separation between the primary and control sources.

Table 2.1

Acoustic Mode Cut-On Frequencies for 2 m × 1 m Duct

Acoustic Mode	Cut-On Frequency Hz
(0,0)	0.0
(1,0)	86.0
(2,0)	172.0
(0,1)	172.0
(1,1)	192.3

The first test case, Configuration A, in which the primary disturbance is generated, at an excitation frequency of 100 Hz, by a 0.1 m × 0.1 m rectangular constant volume velocity source mounted in the $z = 0$ termination plane of the duct cross-section, with its centre located at a non-symmetric location, $x_o = b/\sqrt{3}$ and $y_o = d/\sqrt{2}$, is shown in Figure 2.3. A single constant volume velocity control source is located in the $y = 0$ plane of the duct at an axial distance z_c from the primary source and in line with the primary source at $x_c = b/\sqrt{3}$. Examining the total acoustic power reduction achievable with an effectively simple control source for the case of a rigid termination at $z = 0$, the solid line in Figure 2.6, illustrates that regions of local minima and maxima in power reduction occur when varying the separation distance between the primary and control sources. The total acoustic power reduction in dB is given by

$$\Delta W = -10 \log_{10} \left(\frac{W_{controlled}}{W_{uncontrolled}} \right) \tag{2.64}$$

The attenuation minima are located approximately at odd quarter wavelengths of the

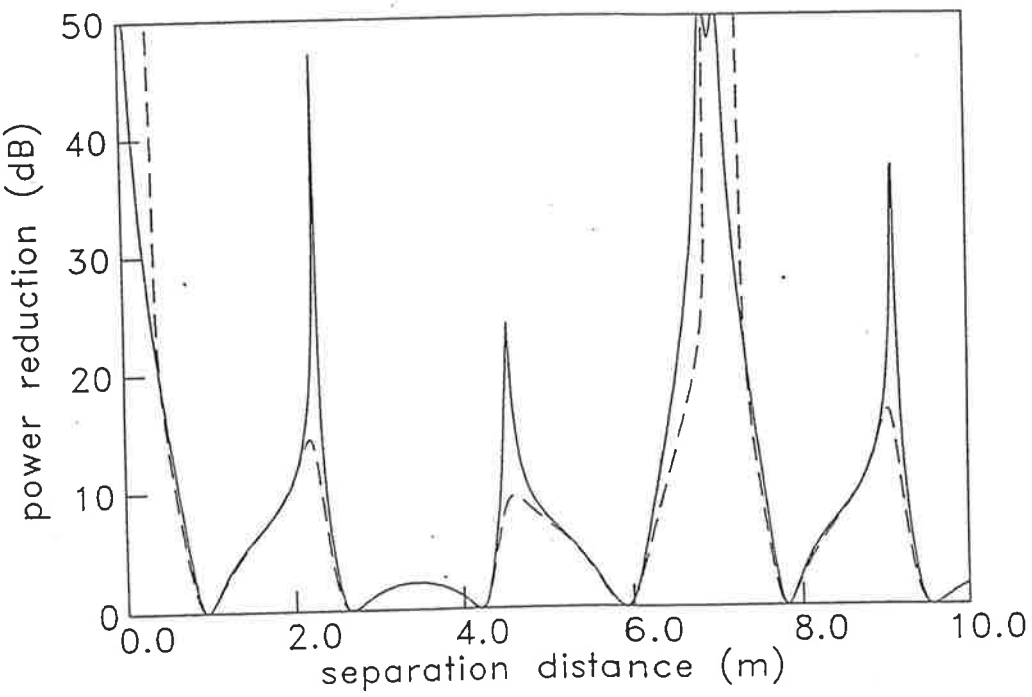

Figure 2.6 Acoustic power reduction using single control source in-line with the primary source at 100 Hz as a function of separation between the primary and control sources. —— = rigid termination, — — = uniform impedance surface termination. Primary source located at (x_o, y_o, z_o) = (1.155, 0.707, 0.0) m.

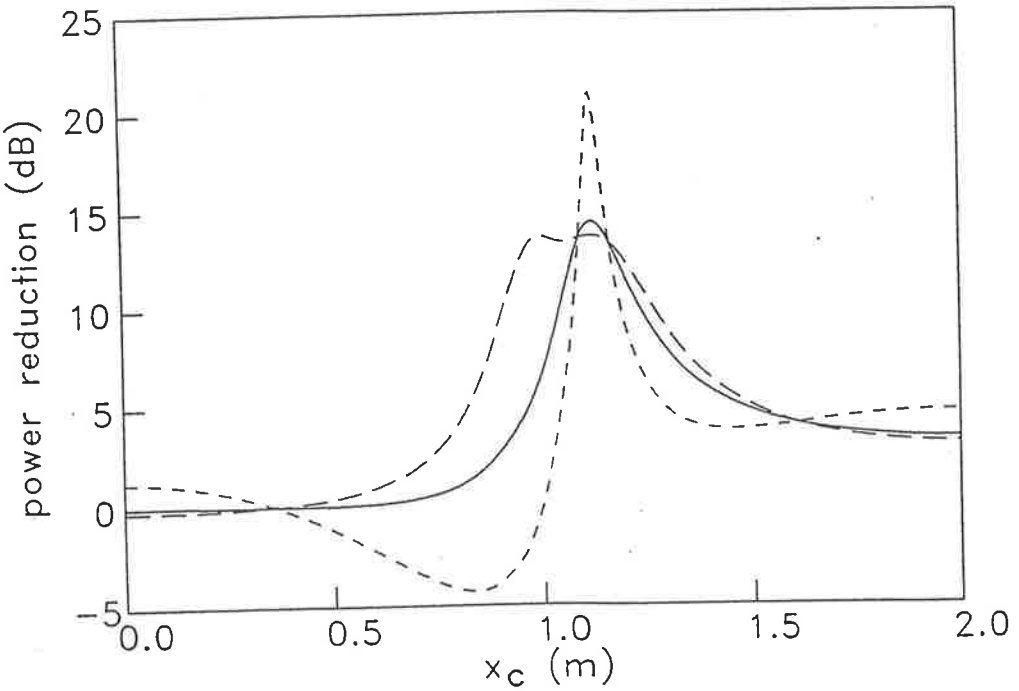

Figure 2.7 Acoustic power reduction at 100 Hz using single control source at z_c = 6.5 m as a function of control source location x_c across the duct. —— = total, — — = (0,0) mode, - - - = (1,0) mode. Primary source located at (x_o, y_o, z_o) = (1.155,0.707,0.0) m.

fundamental mode, the fundamental mode wavelength being given by

$$\lambda_{00} = \frac{2\pi c_o}{\omega} \tag{2.65}$$

with the modal wavelength λ_{mn}, for rectangular duct higher order acoustic modes, given by (Morse and Ingard, 1968)

$$\lambda_{mn} = \frac{2\pi}{\sqrt{\left(\frac{\omega}{c_o}\right)^2 - \left(\frac{\pi m}{b}\right)^2 - \left(\frac{\pi n}{d}\right)^2}} \tag{2.66}$$

The modal wavelengths for a 2 m × 1 m duct are given in Table 2.2 for a range of excitation frequencies. Referring to Figure 2.6 it can be seen that an attenuation maximum occurs at a source separation distance of 6.8 m. This distance corresponds to approximately twice the fundamental mode wavelength, that is $2\lambda_{00}$, and a single (1,0) mode wavelength λ_{10}. A similar result is achievable for a uniform impedance surface termination plane at $z = 0$. This case is represented by the broken line in Figure 2.6, with the values of $\alpha_{mn} = 0.01$ and $\beta_{mn} = 0.01$ assumed to be constant for all modes. The relative location of the power reduction minima and maxima is approximately the same as for the rigidly terminated case corresponding to $\alpha_{mn} = 0$ and $\beta_{mn} = 0$, but the levels of reduction are slightly decreased for the non-rigid termination case. The results presented henceforth assume a uniform impedance termination surface at $z = 0$.

To gain an understanding of the physical aspects of the active process for controlling the total acoustic power output, an examination of the acoustic radiation impedance values for each source is beneficial. Choosing an arbitrary control source location at $x_c = 1.155$ m

and z_c = 6.5 m, the acoustic impedance components for optimum attenuation of total acoustic power are given in Table 2.3 for an excitation frequency of 100 Hz, corresponding to propagation of the (0,0) and (1,0) acoustic modes.

Table 2.2

Modal Wavelengths (m) for 2 m × 1 m Duct

Frequency Hz	(0,0) Mode	(1,0) Mode	(2,0) Mode	(0,1) Mode
50	6.880	...	...	...
100	3.440	6.741	...	...
150	2.293	2.799	...	...
180	1.911	2.175	6.482	6.482

Table 2.3

Source Acoustic Impedances and Power

	Acoustic Impedance $kgm^{-4}s^{-1}$	Acoustic Power μW
$Z_{p/p}$	255.25	255.25
$Z_{p/S1}$	-238.62	-238.62
Z_{ptotal}	16.63	16.63
$Z_{S1/p}$	-175.88	-252.00
$Z_{S1/S1}$	171.96	244.21
$Z_{S1total}$	-3.92	-5.57
$W_{uncontrolled}$	...	255.25
$W_{controlled}$	...	11.06

The total mean acoustic power radiated by the primary source operating alone is calculated by

$$W_{uncontrolled} = Q_p^2 R_{p/p} \tag{2.67}$$

and in this case is 255.25 μW for a primary source of volume velocity Q_p of 1×10^{-3} m^3/s. Introduction of the control source, with its volume velocity Q_c and phase β_c adjusted so that the total acoustic power is minimised, results in an alteration in the acoustic impedance presented to the primary source of -238.62 $kgm^{-4}s^{-1}$, corresponding to $R_{p/S1}$. Hence the total acoustic impedance presented to the primary source is reduced to 16.63 $kgm^{-4}s^{-1}$ because of the pressure field produced by the control source and its effect upon the primary source face. The control source S_1 has a self-impedance, or impedance presented to it by the duct alone, $R_{S1/S1}$ of 171.96 $kgm^{-4}s^{-1}$, and the acoustic impedance alteration of the control source by the primary source $R_{S1/p}$ is -175.88 $kgm^{-4}s^{-1}$, resulting in a total control source acoustic impedance of -3.92 $kgm^{-4}s^{-1}$. This corresponds to an acoustic power value of -5.57 μW. The negative value of power output for the control source indicates that it is acting as an absorber. The control source is thus seen to have a dual effect, altering the acoustic radiation impedance of the primary source, and absorbing a portion of the total acoustic power generated by the two sources. The total acoustic power under active control is equal to 11.06 μW, a reduction from the uncontrolled value of 255.25 μW, which corresponds to a reduction of 13.6 dB.

Returning to consideration of the effect of control source location upon the acoustic power reduction, variation of the control source position across the duct cross-section reveals that

there is a related variation in the level of power reduction achievable. This is shown in Figure 2.7 for a control source located at an axial distance of 6.5 m from the primary source and for an excitation frequency of 100 Hz which enables propagation of the (0,0) and (1,0) acoustic modes. The total power reduction is represented by the solid line while the modal components of the power reduction are shown as broken lines. The optimum location for a control source, at this particular distance from the primary source, is directly in-line with the primary source at x_c = 1.155 m. Interestingly, the greatest reduction in acoustic power occurs for a control source positioned such that the duct mode shape function at its location is equal to the same value as at the primary source location, rather than being greatest at the edges of the duct where the control source mode shape function is maximised, and equal to unity. This can again be explained in terms of the alteration in the sources' acoustic impedance. For a control source positioned such that the duct mode shape function at its location is equal to that at the primary source location, the acoustic impedance terms are well 'matched', but for a control source positioned otherwise, the total acoustic power output is being increased by the control source for an equivalent alteration in the primary source acoustic impedance.

For a source mounted in the $x = b$ plane, the levels of reduction in acoustic power for a simple control source will be equivalent to a source mounted at the edge of the duct in the $y = 0$ plane. Hence the level of reduction for a control source mounted in the $x = b$ plane is less than that possible for a source mounted in the $y = 0$ plane for this particular case because the modal index in the y-direction is equal to zero.

Figure 2.8 displays the acoustic power reduction contours in dB corresponding to variation of the lateral location of the control source across the duct and the separation distance between the primary and control sources along the duct. The primary source is located at x_c = 1.155 m (Figure 2.3, configuration A) and the excitation frequency is 100 Hz. As mentioned previously, the control source location in the x-direction across the duct corresponding to attenuation maxima is the same as the primary source. The attenuation maxima along the duct are separated by a distance corresponding to multiples of the fundamental mode wavelength, λ_{00}, and the (1,0) mode wavelength, λ_{10}. Attenuation maxima are also achievable at a control source lateral location of $x_c = b - x_o$, where x_o is the lateral primary source location. The mode shape function values for the fundamental and (1,0) modes at this control source position are equal to the mode shape function values at the primary source location. The attenuation maxima are also separated, for a control source positioned at this lateral location, by an axial distance corresponding to locations where a multiple of the fundamental mode wavelength is equal to a multiple of the (1,0) mode wavelength.

As the modal wavelength λ_{mn} is a function of the excitation frequency, the optimum location for a control source is also frequency dependent. Hence the possibility exists that a control source positioned at an optimum location for a particular excitation frequency will provide relatively poor acoustic power reduction at other frequencies. The introduction of an additional control source provides a means of increasing the total power reduction for an original control source positioned at a non-optimum location, and can hence make the overall system more robust in terms of achievable power reduction over a range of

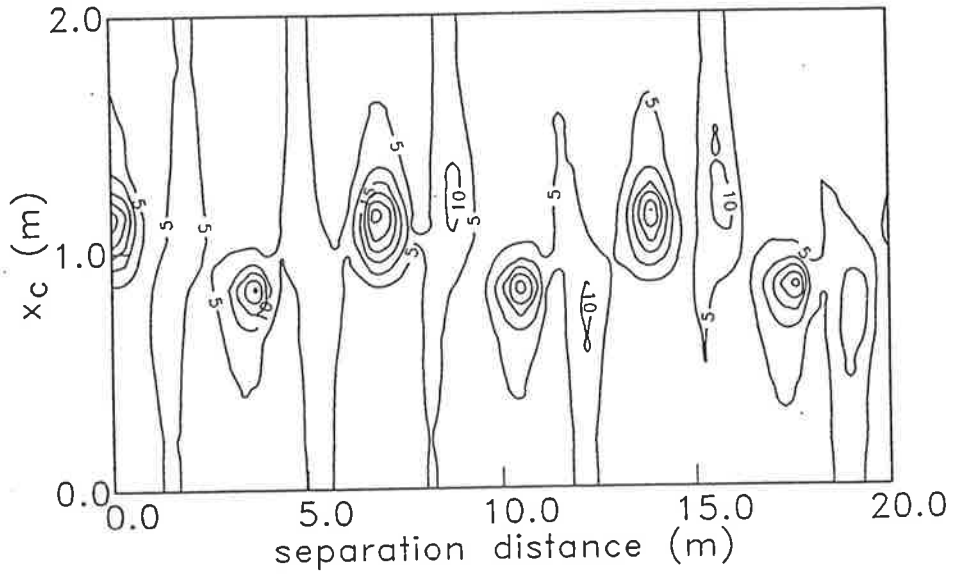

Figure 2.8 Acoustic power reduction in dB using single control source at 100 Hz as a function of separation between the primary and control sources. Primary source located at (x_o, y_o, z_o) = (1.155, 0.707, 0.0) m.

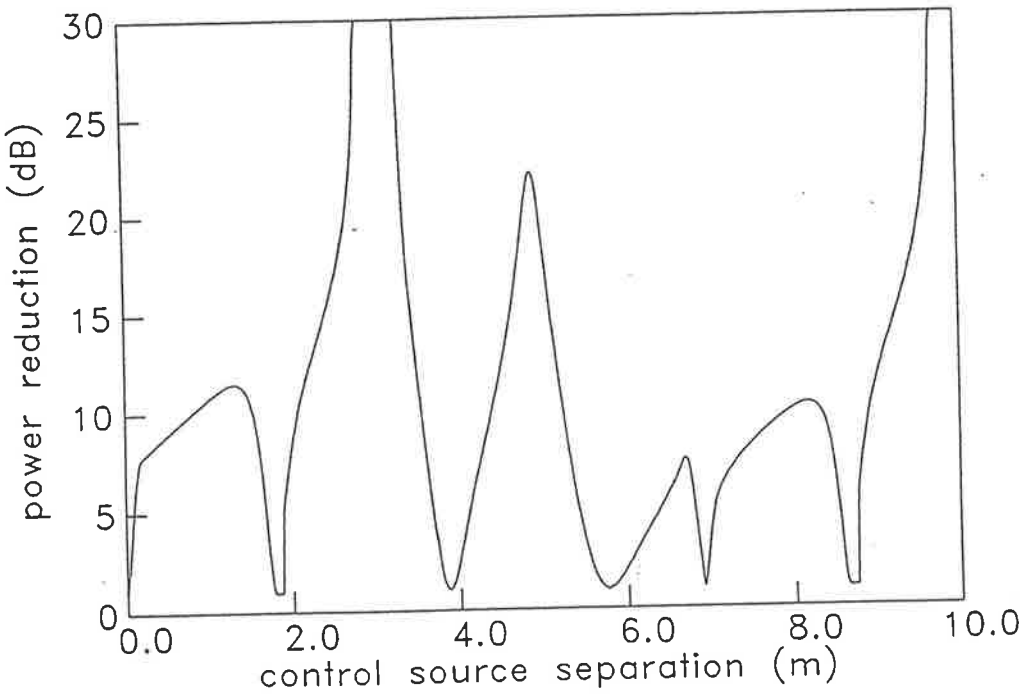

Figure 2.9 Acoustic power reduction using dual control source system at 100 Hz as a function of separation between control sources S_1 and S_2. Control source S_1 located at z_{S1} = 4.0 m. Control source S_2 located downstream of S_1.

excitation frequencies. For the dual control source cases examined, the phase and volume velocity of both control sources were optimised at the same time, and hence in an equivalent real system, the controller would be required to optimise the two channels concurrently. Figure 2.9 shows the acoustic power reduction at 100 Hz for a dual control source system, with the control source S_1 positioned at x_{S1} = 1.155 m and z_{S1} = 4.0 m, and the other control source S_2 positioned at x_{S2} = 1.155 m, with the axial distance from S_1 varied. With only a single control source S_1 operating, the reduction in total acoustic power is equal to 1.0 dB. With both control sources operating, the reduction in acoustic power is increased to above 30 dB at the optimum control source separation distance, and above 1.0 dB for the majority of control source separation distances. The optimum control source separation distance for this case is approximately 2.8 m. This distance corresponds to an overall axial distance of approximately $2\lambda_{00}$ or λ_{10} between the primary source and control source S_2. It should be noted that the total power reduction achievable at any particular frequency using dual control sources, positioned as stated, is greater than the reduction achievable for a single control source positioned at an equivalent location as control source S_2. The use of two control sources provides greater flexibility in source location for a substantial noise reduction at a given frequency and also increases the bandwidth corresponding to substantial noise reduction for given, fixed control source locations.

To examine the influence of control source size upon the reduction of the total acoustic power output, the control source was arbitrarily positioned at x_c = 1.155 m and z_c = 6.5 m, and the model was used to determine the power reduction for various source sizes at an

excitation frequency of 100 Hz. The relationship between source size and the reduction of power output is quite complex, as the source size factors, which account for size of the sources and the degree to which an acoustic mode is excited by the source, have different values for each acoustic mode and for each excitation frequency, and in addition, any reduction in acoustic power output from a source caused by a decreased value of source size factor may be compensated for by an increase in the source volume velocity. This can be seen by examination of Equation (2.27), where the impedance presented to the primary source by the control source is proportional to the control source size factors, F_{cm}, F_{cn}, and F_{cL}, and the control source volume velocity, Q_c. Figure 2.10 shows the acoustic power reduction as a function of the control source length across the duct cross-section, J, with the source length, L, along the duct axis constant and sufficiently small that the source is effectively a simple source. The solid line represents the total power reduction and the modal components of power reduction are shown as broken lines. As shown in Figure 2.10, the reduction of acoustic power output is approximately constant over the range of control source lengths considered, although the control source volume velocity to achieve the reduction increases with control source size. The optimal control source volume velocity varied from 1.19 times the primary source volume velocity, for a source of small dimension, to 1.27 times the primary source volume velocity for the largest source considered of length J = 1.69 m. Figure 2.11 shows the results for variation of the control source length in the axial direction L, for J constant. The reduction of acoustic power is seen to be greatest for a source of relatively small dimensions. The modal component of power reduction for the (1,0) mode is a maximum for a control source length L = 3.44 m, which corresponds to the modal wavelength λ_{00} of the fundamental

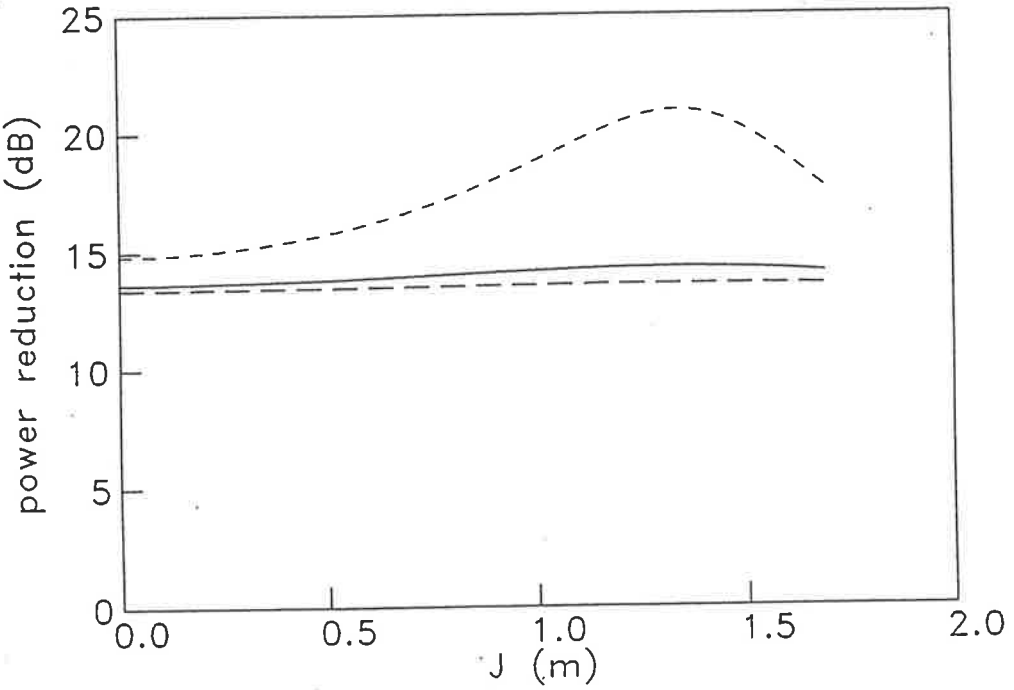

Figure 2.10 Acoustic power reduction at 100 Hz using single control source at z_c = 6.5 m and in-line with the primary source as a function of control source width. —— = total, — — = (0,0) mode, - - - = (1,0) mode.

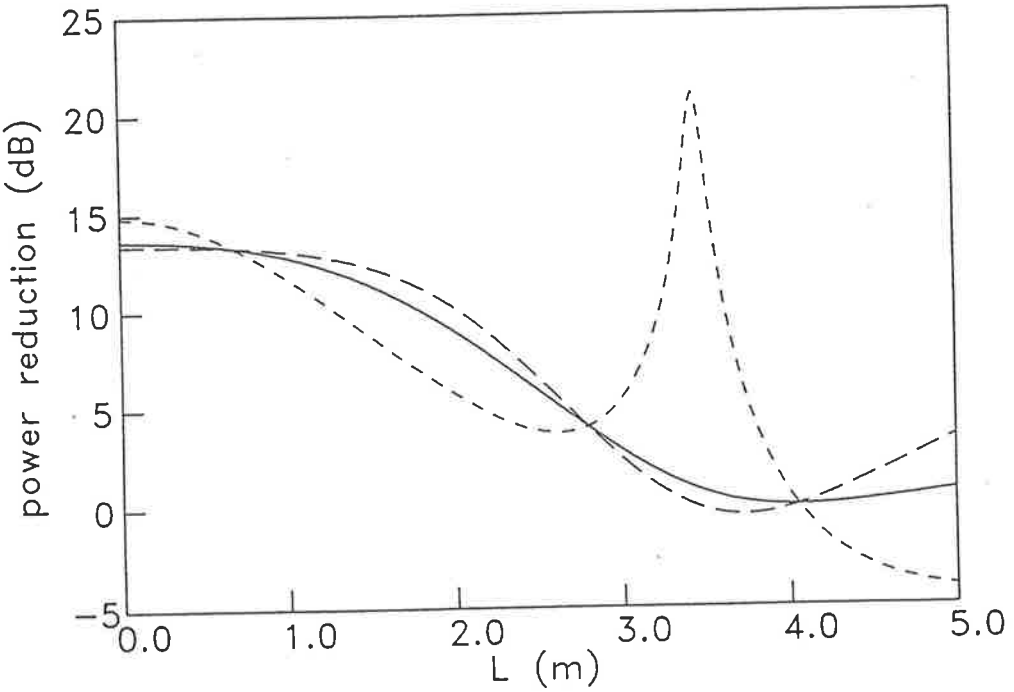

Figure 2.11 Acoustic power reduction at 100 Hz using single control source at z_c = 6.5 m and in-line with the primary source as a function of control source length. —— = total, — — = (0,0) mode, - - - = (1,0) mode.

mode. Also the power reduction of the fundamental mode is equal to zero for this control source length. This illustrates the fact that a control source of equivalent length to a modal wavelength is unable to effectively control that acoustic mode because the modal component of the mean pressure produced at the primary source is equal to zero, independent of control source location, and hence the alteration in the primary source radiation impedance is also zero. A 3.44 m long control source is not, however, likely to be realisable in practice. As most commonly used loudspeaker sources are either circular or rectangular, the effect of source size on the acoustic power reduction for a square source is shown in Figure 2.12, and reveals that the reduction in acoustic power is approximately constant for the range of control source sizes considered, for this particular excitation frequency, duct geometry, and source arrangement, although, as mentioned previously, the required control source volume velocity to achieve this reduction increases with increased control source size.

Altering the excitation frequency from 100 Hz for the same primary source size and location, given by configuration A, results in the optimum primary to control source separation distance for a single simple control source being altered from that for the cases considered thus far. The same is true for finite size control sources, although simple control sources are used in the following cases.

Figure 2.13 shows the power reduction achievable over a range of source separation distances for an excitation frequency of 150 Hz, which still enables only the fundamental and (1,0) modes to propagate in the duct. At an excitation frequency of 150 Hz the

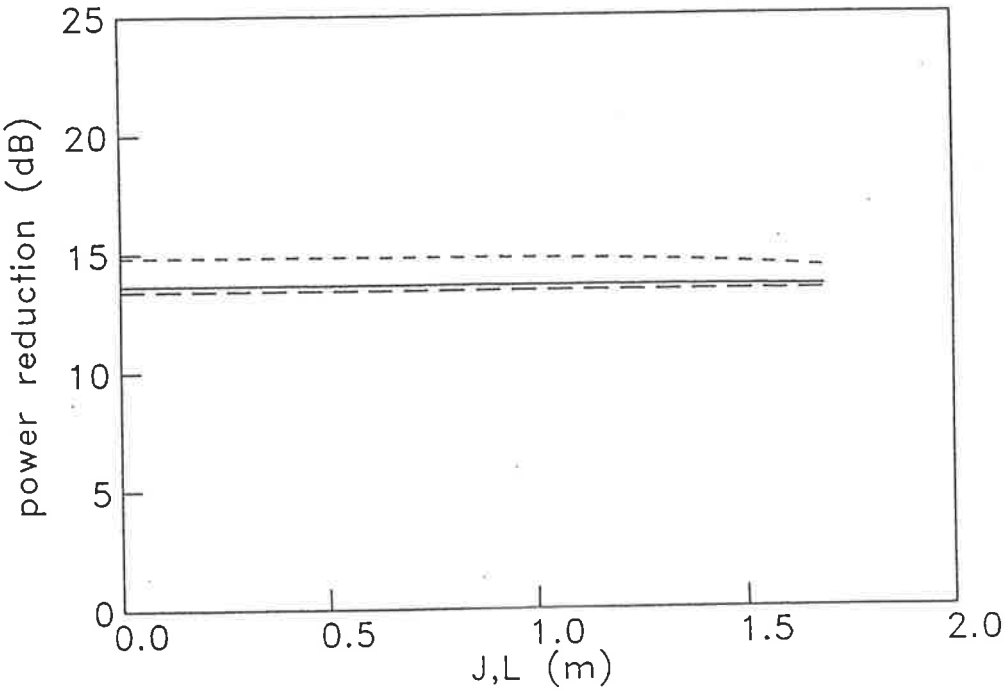

Figure 2.12 Acoustic power reduction at 100 Hz using single control source at z_c = 6.5 m and in-line with the primary source as a function of control source size. —— = total, — — = (0,0) mode, - - - = (1,0) mode.

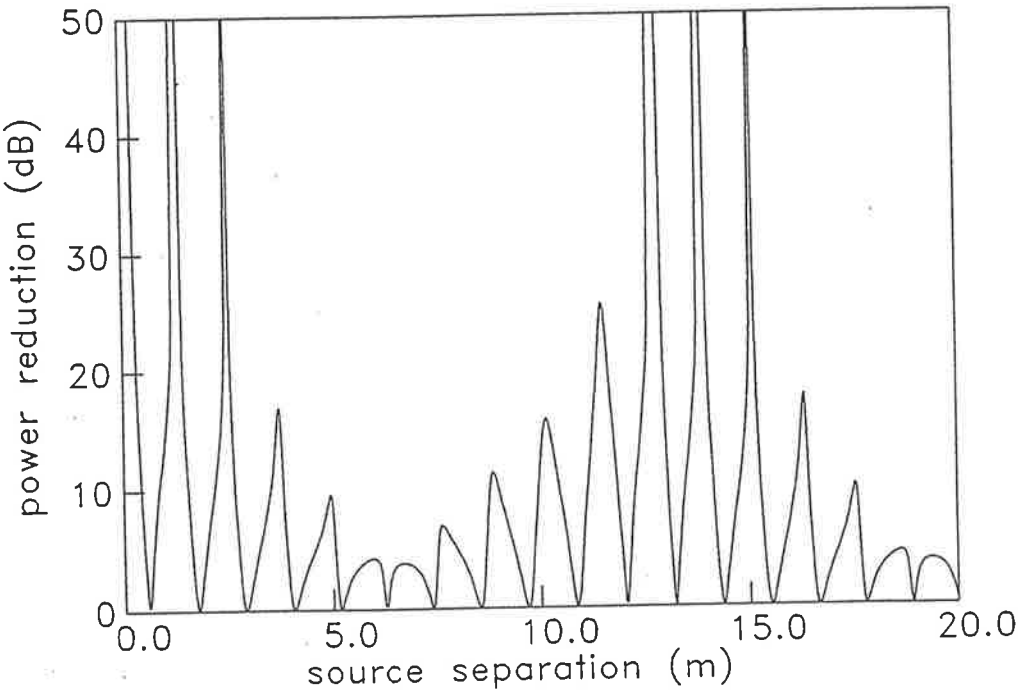

Figure 2.13 Acoustic power reduction using single control source in-line with the primary source at 150 Hz as a function of separation between the primary and control sources. Primary source located at (x_o, y_o, z_o) = (1.155, 0.707, 0.0) m.

correspondence between multiples of the two modal wavelengths is not as close as in the previous case of 100 Hz, and as a result the optimum axial source separation distance is increased. An axial source separation distance of 14 m results in a reduction of the total acoustic power by greater than 50 dB, this distance being approximately equal to six times the fundamental mode wavelength and five times the (1,0) mode wavelength. The result of increasing the excitation frequency to 180 Hz, such that the (0,0), (1,0), (2,0), and (0,1) acoustic modes can propagate, is shown in Figure 2.14. The poor correspondence of the modal wavelengths for this particular excitation frequency has resulted in acoustic power reduction values of less than 1 dB for a single control source located within 20 m of the primary source. This result indicates that a greater number of control sources may be required to achieve higher levels of power reduction at certain excitation frequencies.

Consider a primary source such as that shown in Figure 2.3 as Configuration B, in which a primary source of dimensions 0.1 m × 0.1 m is centrally located within a 2 m × 1 m duct. At an excitation frequency of 100 Hz only the plane wave propagates along the duct, as the primary source is positioned at a node of the (1,0) acoustic mode. Contours of power reduction in dB are shown in Figure 2.15 for a range of values of x_c and z_c for a single control source. As also shown in Figure 2.10 for primary source configuration B, the control source location in the x-direction corresponding to attenuation maxima is the same as the primary source location in this direction, namely x_c = 1.0 m, and the axial source separation distances between the control and primary sources corresponding to attenuation maxima are multiples of the fundamental mode half-wavelength $\lambda_{00}/2$. The location of these power reduction maxima can be explained by considering that a control

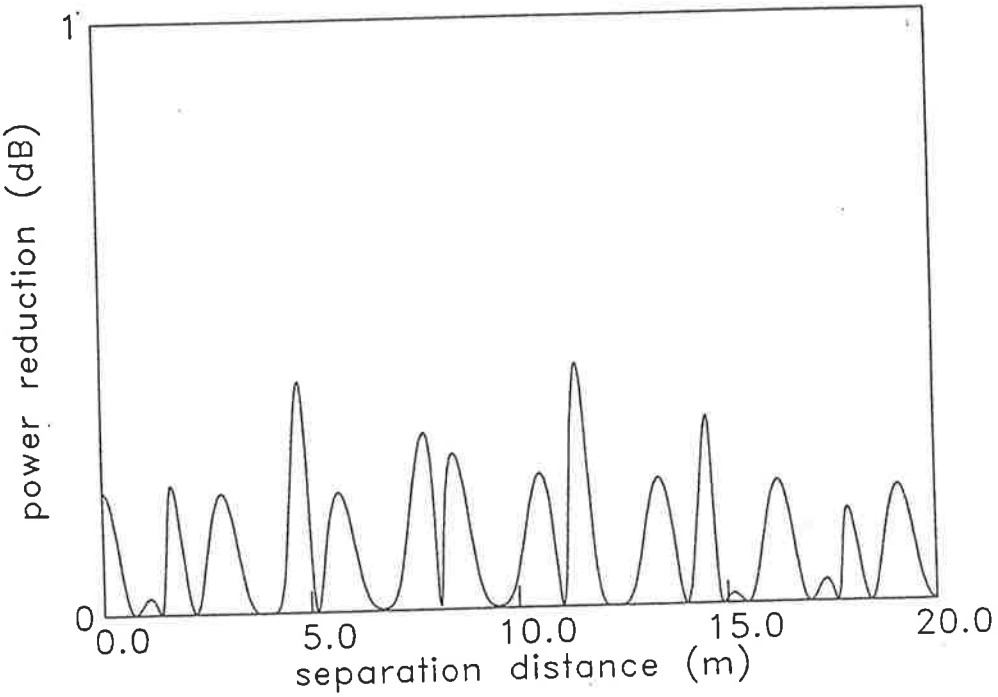

Figure 2.14 Acoustic power reduction using single control source in-line with the primary source at 180 Hz as a function of separation between the primary and control sources. Primary source located at (x_o, y_o, z_o) = (1.155, 0.707, 0.0) m.

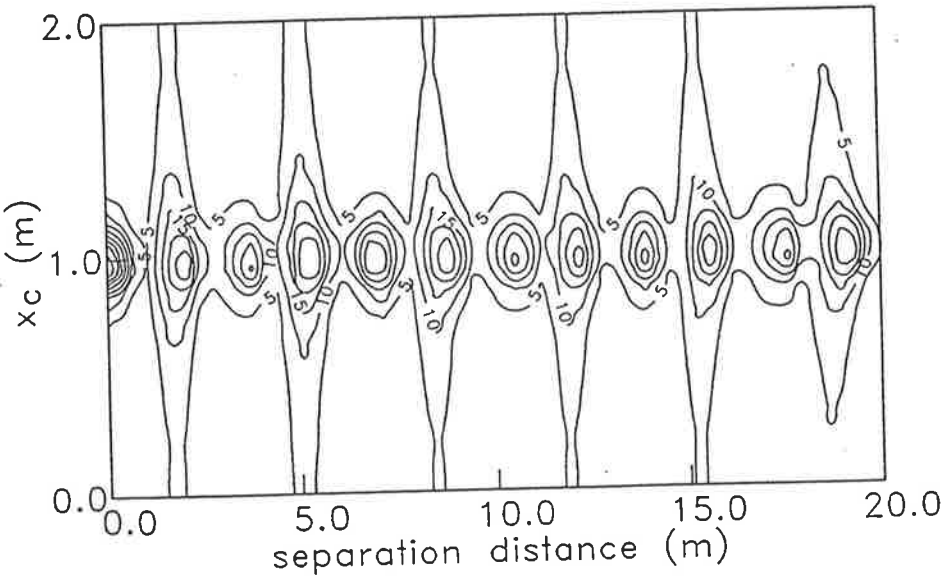

Figure 2.15 Acoustic power reduction in dB for a single control source at 100 Hz as a function of separation between the primary and control sources : configuration B. Primary source located at (x_o, y_o, z_o) = (1.0, 0.5, 0.0) m.

source not positioned in-line with the primary source will generate a (1,0) mode and hence contribute to the total power output associated with this mode, while having the same effect upon the acoustic impedance of the primary source as would a control source positioned in-line with the primary source, which does not contribute to the power output of the (1,0) mode. In other words, as found for primary source configuration A, maxima in the power output reduction occur at control source locations where the mode shape function values are the same as at the primary source location.

Alteration of the duct aspect ratio will also change the modal wavelength correspondence. In Configuration C, shown in Figure 2.3, a finite size primary source of dimensions 0.1 m × 0.1 m is located at $x_o = b/\sqrt{3}$ and $y_o = d/\sqrt{2}$, within a 2.4 m × 1 m duct. The cut-on frequencies for the first five acoustic modes are presented in Table 2.4, and the modal wavelengths for a range of excitation frequencies are given in Table 2.5.

Table 2.4

Acoustic Mode Cut-On Frequencies for 2.4 m × 1 m Duct

Acoustic Mode	Cut-On Frequency Hz
(0,0)	0.0
(1,0)	71.7
(2,0)	143.3
(0,1)	172.0
(1,1)	186.3

Table 2.5

Modal Wavelengths (m) for 2.4 m × 1 m Duct

Frequency Hz	(0,0) Mode	(1,0) Mode	(2,0) Mode
100	3.440	4.932	...
150	2.293	2.611	7.779

For an excitation frequency of 100 Hz the modal wavelength of the plane wave mode is 3.44 m and the wavelength of the (1,0) acoustic mode is 4.93 m for configuration C. Figure 2.16 shows that the optimum primary to control source separation distance for a simple control source positioned at the same lateral location as the primary source is approximately 12 m, which corresponds to three and a half times the fundamental mode wavelength and two and a half times the (1,0) mode wavelength. Figure 2.17 reveals that the location of the attenuation maxima follows a similar trend to that shown in Figure 2.8 for the duct aspect ratio *d/b* equal to 0.5, except that the axial source separation distances between the primary and control sources corresponding to attenuation maxima are increased because of the decreased correspondence between the modal wavelengths in this case.

Increasing the excitation frequency to 150 Hz, such that the (0,0), (1,0) and (2,0) acoustic modes propagate, results in the axial source separation distance between the primary and control sources corresponding to maximum acoustic power reduction being increased to 15.9 m, for a single control source positioned at the same lateral location as the primary source. The importance of the correspondence in modal wavelengths is again evident when

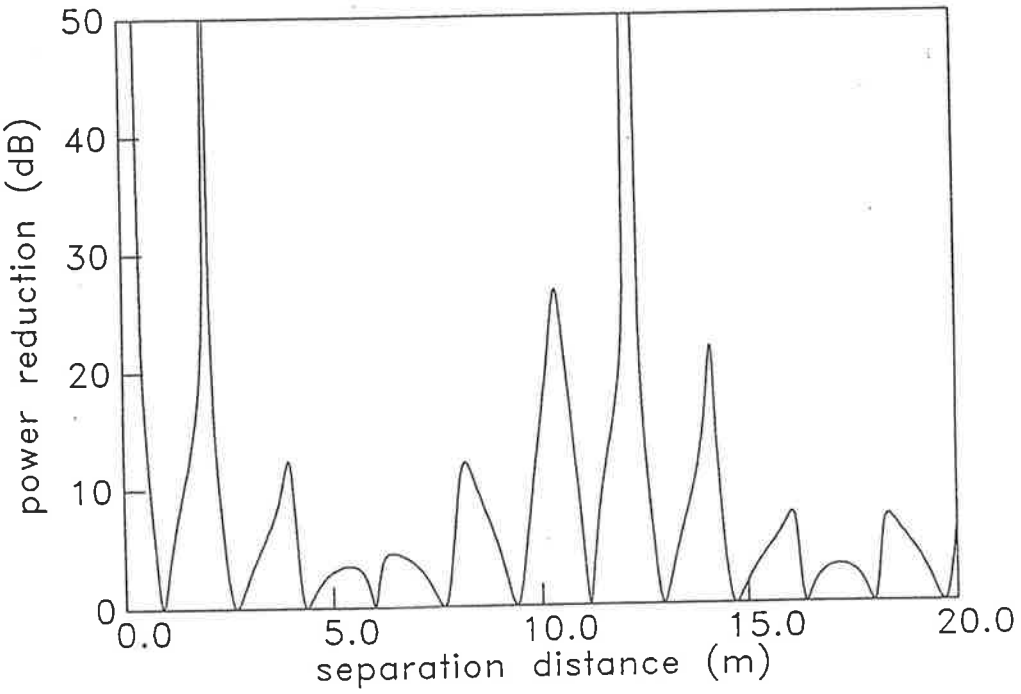

Figure 2.16 Acoustic power reduction using single control source in-line with the primary source at 100 Hz as a function of separation between primary and control sources : configuration C. Primary source located at (x_o, y_o, z_o) = (1.386, 0.707, 0.0) m.

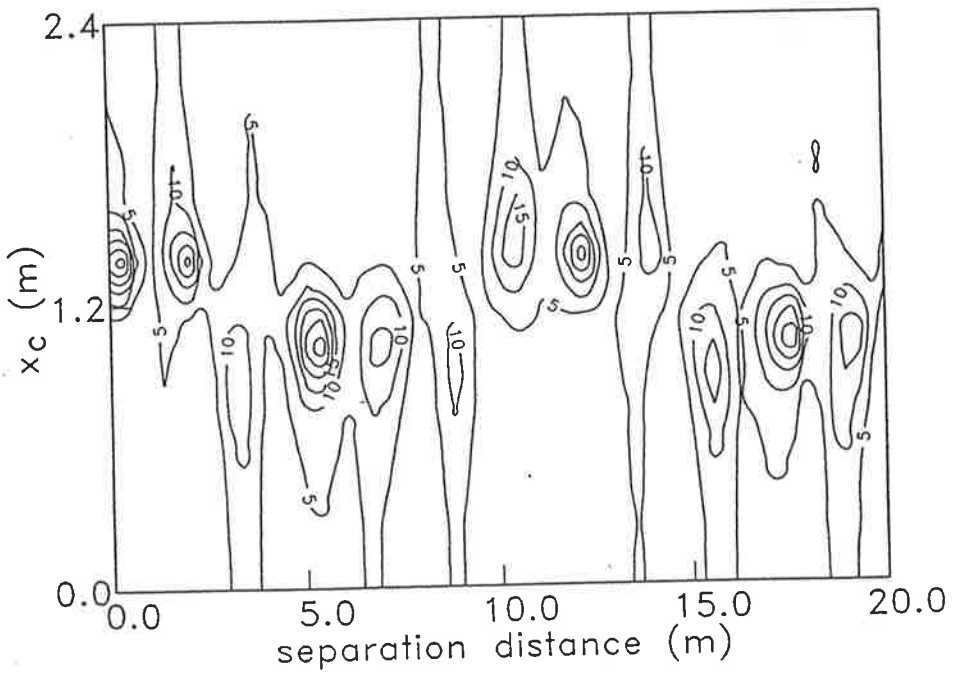

Figure 2.17 Acoustic power reduction in dB at 100 Hz for a single control source as a function of separation between primary and control sources : configuration C. Primary source located at (x_o, y_o, z_o) = (1.386, 0.707, 0.0) m.

one examines the number of modal wavelengths corresponding to a distance of 15.9 m, which is found to be approximately equal to seven times the fundamental mode wavelength, six times the (1,0) mode wavelength and twice the (2,0) mode wavelength. This case is shown in Figure 2.18.

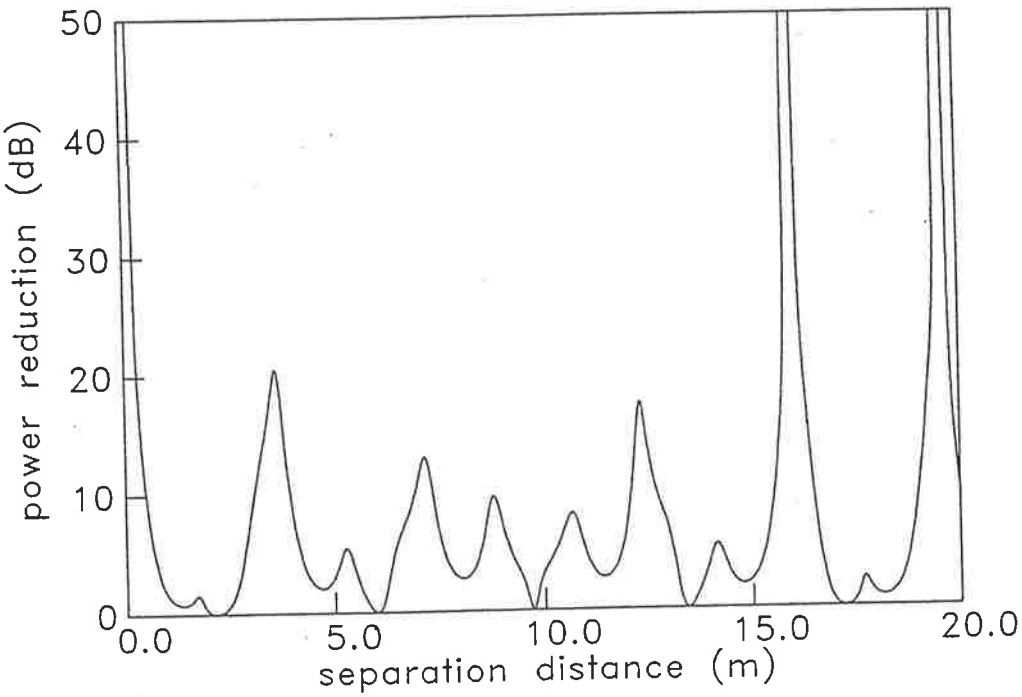

Figure 2.18 Acoustic power reduction at 150 Hz for a single control source as a function of separation between primary and control sources : configuration C.

2.4 CONCLUSIONS

An analytical model has been developed to describe the active control of higher order acoustic modes in ducts. The model allows calculation of the individual source power outputs for a given source location, size, strength and relative phase. Both single and dual control source configurations are examined.

It is shown that a reduction in the total acoustic power output is achievable by two mechanisms - alteration of the acoustic radiation impedance of the primary source by the control sources and absorption of the primary source acoustic power by the control sources. The degree to which each mechanism contributes to the reduction in total acoustic power output is a complex function of the duct geometry, excitation frequency and the source location, size and number. Determining which mechanism is dominant thus requires calculation of the acoustic power output of the sources for each particular duct configuration.

The duct geometry, source location and excitation frequency were shown as the major factors in determining the levels of acoustic power output reduction achievable. Control source size was shown to have a minor influence on the levels of acoustic power reduction over the range of source sizes examined, although increasing the source size resulted in an increase in the source volume velocity required for the same level of control. In addition, a control source of equivalent length to a modal wavelength is unable to effectively control that acoustic mode because the modal component of the mean pressure produced at the primary source is equal to zero, independent of control source location, and hence the alteration in the primary source radiation impedance is also zero.

It was found that the optimum location of the control source to reduce the total acoustic power output is at a lateral location such that the primary source and control source are in locations characterised by equal values of the mode shape function Ψ_{mn}, and at an axial source separation distance which corresponds to a multiple of half-wavelengths for each of

the modes propagating within the duct. Introduction of an additional control source increases the levels of power attenuation that are achievable, and increases the effective frequency range of operation for the active control system, for both higher order and plane wave only propagation. For plane wave only propagation, constraining the control source volume velocity to be below a finite value causes the total power reduction to be a function of the axial distance separating the primary and control sources, and the control source size. For the case of a finite control source volume velocity the total acoustic power reduction is maximised for a primary source and control source separation distance corresponding to an integer multiple of half-wavelengths, and is a minimum for source separation distances equal to odd quarter wavelengths.

The results yielded by this analysis indicate that, for excitation frequencies which result in propagation of acoustic modes other than the fundamental or plane wave mode, accurate characterisation of the primary source properties is of major importance in establishing an effective configuration of control sources to reduce the total acoustic power output.

CHAPTER 3. ACOUSTIC RESPONSE IN DUCTS OF ARBITRARY LENGTH AND TERMINATION CONDITIONS

3.1 INTRODUCTION

In a practical situation, finite impedance terminations will be encountered at both ends of the rigid-walled duct. Thus, the semi-infinite duct model examined in Chapter 2 is extended in this chapter to include higher order mode reflection from both of the duct terminations, which are modelled as having arbitrary impedance. A generalised solution is obtained for a duct of arbitrary length which allows the calculation of infinite, semi-infinite, finite and impedance boundary terminated duct cases through the use of specific termination impedance values. Theoretical and experimental determination of appropriate termination impedance values is outlined and demonstrated for the case of a flanged duct radiating into free space. The theory is applicable for both plane wave and higher order mode propagation. Finite size acoustic source configurations are modelled in addition to simple point sources. Experimental results are presented with the theory and indicate good agreement.

3.2 ACOUSTIC RESPONSE FOR ARBITRARY TERMINATION CONDITIONS

The system under consideration in the following analysis, shown in Figure 3.1, is a hard-walled duct of uniform cross-sectional area S and length L, having arbitrary termination impedances at both ends, represented by Φ_1 and Φ_2. The fluid contained within the duct is assumed to be at rest with constant and uniform ambient temperature and density, ρ.

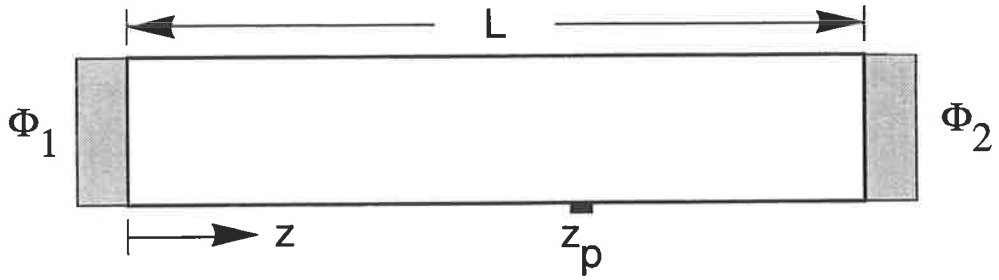

Figure 3.1 Modelled arrangement for duct of arbitrary length, L, and terminations Φ_1 and Φ_2.

For a simple point source located at a point $\vec{x}_p = (x_p, y_p, z_p)$, the pressure at an arbitrary point $\vec{x} = (x, y, z)$ in the duct is equal to the superposition of the pressure components coming directly from the source and those arising from reflections from the duct terminations. The pressure due to the wave coming directly from the source is (Doak, 1973a; Morse and Ingard, 1968)

$$p_p(\vec{x}) = \frac{\rho \omega Q_p}{2S} \sum_{mn} \frac{\Psi_{mn}(\vec{x}) \Psi_{mn}(\vec{x}_p)}{\Lambda_{mn} k_{mn}} e^{-jk_{mn}|z_p - z|} \tag{3.1}$$

where the time dependent term $e^{j\omega t}$ has been omitted for convenience. The negative time dependence used by Morse and Ingard has been compensated for by reversing the sign of their axial dependence term $e^{jk_{mn}|z_p - z|}$. Ψ_{mn} is the characteristic or mode shape function of the duct, k_{mn} is the complex modal wavenumber, Λ_{mn} is the modal normalisation factor and Q_p the source volume velocity. For the rectangular duct case considered here

$$\Psi_{mn}(\vec{x}) = \cos\left(\frac{m\pi x}{b}\right)\cos\left(\frac{n\pi y}{d}\right) \tag{3.2}$$

and

$$k_{mn} = \sqrt{\left(\frac{\omega}{c_o}\right)^2 - \left(\frac{\pi m}{b}\right)^2 - \left(\frac{\pi n}{d}\right)^2} \tag{3.3}$$

$$\Lambda_{mn} = \frac{1}{S}\int_S \Psi_{mn}^2 dS \tag{3.4}$$

where m and n are the modal indices, ω is the excitation frequency and c_o the speed of sound in free space.

A wave which has undergone a single reflection from the impedance termination represented by Φ_1 will produce a pressure at point $\vec{x}$

$$p_p(\vec{x}) = \sum_{mn} A_{mn}(\vec{x},\vec{x}_p) e^{-jk_{mn}(z_p+z)} e^{-2\Phi_1} \tag{3.5}$$

where $A_{mn}(\vec{x},\vec{x}_p)$ is the modal amplitude given by

$$A_{mn}(\vec{x},\vec{x}_p) = \frac{\rho\omega Q_p}{2S} \frac{\Psi_{mn}(\vec{x})\Psi_{mn}(\vec{x}_p)}{\Lambda_{mn} k_{mn}} \tag{3.6}$$

Similarly, a wave having undergone a single reflection from the impedance termination represented by Φ_2 will yield

$$p_p(\vec{x}) = \sum_{mn} A_{mn}(\vec{x},\vec{x}_p) e^{jk_{mn}(z_p+z)} e^{-2\Phi_2} e^{-j2k_{mn}L} \tag{3.7}$$

while a wave which has been reflected from both duct terminations gives

$$p_p(\vec{x}) = \sum_{mn} A_{mn}(\vec{x},\vec{x}_p) e^{jk_{mn}|z_p-z|} e^{-2\Phi_2} e^{-2\Phi_1} e^{-j2k_{mn}L} \tag{3.8}$$

Superposition of these four terms, together with consideration of the additional reflections

from the duct terminations, the number depending upon the termination impedances, gives the total pressure at point $\vec{x}$ as

$$\begin{aligned} p_p(\vec{x}) = \sum_{mn} A_{mn}(\vec{x},\vec{x}_p)\Big[& e^{-jk_{mn}|z_p - z|} + e^{-jk_{mn}(z_p+z)} e^{-2\Phi_1} \\ & + e^{jk_{mn}(z_p+z)} e^{-j2k_{mn}L} e^{-2\Phi_2} \\ & + e^{jk_{mn}|z_p - z|} e^{-2\Phi_2} e^{-2\Phi_1} e^{-j2k_{mn}L} \Big] T_{mn} \end{aligned} \tag{3.9}$$

where T_{mn} is the modal reverberation factor for the duct and is given by

$$\begin{aligned} T_{mn} &= \sum_{i=0}^{\infty} \left\{ e^{-j2k_{mn}L} e^{-2\Phi_1} e^{-2\Phi_2} \right\}^i \\ &= \frac{1}{1 - e^{-j2k_{mn}L} e^{-2\Phi_1} e^{-2\Phi_2}} \end{aligned} \tag{3.10}$$

The above expressions for an arbitrary impedance terminated duct agree with those found previously for the plane wave case (Elliott and Nelson, 1984) and for higher order mode propagation (Stell, 1991).

For finite size sources, the pressure at a point in the duct, $\vec{x}$, can be expressed as the pressure due to a simple point source multiplied by a source size factor. Hence the modal amplitude $A_{mn}(\vec{x},\vec{x}_p)$ becomes

$$A_{mn}(\vec{x},\vec{x}_p) = \frac{\rho \omega Q_p}{2S} \frac{F_{tmn}(\vec{x}_p)\Psi_{mn}(\vec{x})\Psi_{mn}(\vec{x}_p)}{\Lambda_{mn} k_{mn}} \tag{3.11}$$

where $F_{tmn}(\vec{x}_p)$ is the total modal source size factor, which approaches unity for decreasing source size. Expressions for the modal source size factor are contained in the previous chapter. The individual source size factor expressions given in the previous

chapter have been combined with the source area, A_p, to produce a total modal source size factor, as used in Equation (3.11). For a source arbitrarily located at $\vec{x}_p$ the individual source size factors are combined by

$$F_{tmn}(\vec{x}_p) = \frac{F_{pm}F_{pn}F_{pL}}{A_p} \tag{3.12}$$

3.3 DERIVATION OF TERMINATION IMPEDANCES

In the above analysis, the termination impedance parameters have been represented as Φ_1 and Φ_2, although these impedances are generally frequency dependent and will differ for each mode. Hence the notation $\Phi_{1_{mn}}$ and $\Phi_{2_{mn}}$ is more appropriate and will be used. Φ_{mn} is defined as (Morse, 1948)

$$\Phi_{mn} = \pi\alpha_{mn} - j\pi\beta_{mn} \tag{3.13}$$

Substitution of appropriate values for α_{mn} and β_{mn} yields specific termination conditions. A rigid, totally reflective termination is achieved for $\alpha_{mn} = \beta_{mn} = 0$, while an anechoic termination is characterised by $\alpha_{mn} = \infty$. By substitution of these appropriate values, Equation (3.9) reduces to the expressions presented previously for rigidly terminated (Curtis et al., 1987), infinite (Doak, 1973a) and semi-infinite (Snyder and Hansen, 1991) ducts. Values of α_{mn} and β_{mn} for other termination conditions can be derived both theoretically and experimentally. The specific case of a flanged duct radiating into free space will be examined in detail as an example of the methodology.

3.3.1 Theoretical determination of termination impedance

The first stage in determining appropriate α_{mn} and β_{mn} to represent a flanged duct

radiating into free space is to calculate the specific acoustic impedance presented to the exit plane of the duct by free space. The specific acoustic impedance is frequency dependent and is also different for each duct mode because of the different velocity distributions at the exit plane for each mode.

The normal velocity at a point on the duct exit plane $\vec{x}_s = (x_s, y_s)$ is given by

$$v_{mn}(\vec{x}_s) = \bar{v}_{mn}\Psi_{mn}(\vec{x}_s) \tag{3.14}$$

where $\bar{v}_{mn}$ is the velocity amplitude of the acoustic mode at the exit plane. The pressure at a point $\vec{x} = (x, y)$ on the exit plane due to each modal distribution is given by (Fahy, 1985)

$$p_{mn}(\vec{x}) = \frac{j\rho\omega}{2\pi}\int_S \frac{\bar{v}_{mn}\Psi_{mn}(\vec{x}_s)e^{-jkr}}{r}d\vec{x}_s \tag{3.15}$$

where $r = |\vec{x}_s - \vec{x}|$ and k is the wavenumber in free space.

The modal specific acoustic impedance at the exit plane, $Z_{s_{mn}}$, is defined as

$$Z_{s_{mn}} = \frac{1}{S}\int_S \frac{p_{mn}(\vec{x})}{v_{mn}(\vec{x})}d\vec{x} \tag{3.16}$$

which becomes

$$Z_{s_{mn}} = \frac{j\rho\omega}{2\pi S}\int_S \Psi_{mn}(\vec{x})^{-1}\left[\int_S \frac{\Psi_{mn}(\vec{x}_s)e^{-jkr}}{r}d\vec{x}_s\right]d\vec{x} \tag{3.17}$$

and reduces to

$$Z_{s_{00}} = \frac{j\rho\omega}{2\pi S}\int_S\int_S \frac{e^{-jkr}}{r} d\vec{x}_s d\vec{x} \tag{3.18}$$

for the case of plane wave propagation.

In a similar problem, Morse (1948) has calculated the (0,0) mode (plane wave) radiation impedance for a circular opening, and resolved the pressure distribution over the opening into higher order modes to determine the direct and coupling impedances for the (0,0) mode. The graphs presented indicate that when the impedance is uniform over the duct exit plane, the coupling impedances are small except near the cut-on frequencies of the higher order modes. Hence in this analysis it will be assumed that the coupling impedances are negligible, and that the modal specific acoustic impedance, $Z_{s_{mn}}$, can be used to calculate α_{mn} and β_{mn} directly. This assumption implies that a mode incident upon the duct termination will be reflected as the same mode and will not be coupled into other modes.

The modal specific acoustic impedance is related to the termination impedance parameter values by (Morse and Ingard, 1968)

$$\begin{aligned} Z_{s_{mn}} &= \rho c_o \tanh(\pi\alpha_{mn} - j\pi(\beta_{mn} - \frac{1}{2})) \\ &= \rho c_o \coth(\Phi_{mn}) \end{aligned} \tag{3.19}$$

Note that the real and imaginary components of the modal specific acoustic impedance, $Z_{s_{mn}}$, are not independently related to the real and imaginary components of the termination impedance function, α_{mn} and β_{mn}, but are related by the tanh function as

stated in Equation (3.19). See Plate 1, Morse and Ingard (1968) for a graphical representation of the relationship between the modal specific acoustic impedance and the termination impedance functions. The complex modal reflection coefficient, R_{mn}, can alternatively be used to describe the termination where

$$R_{mn} = e^{-2\Phi_{mn}} \tag{3.20}$$

and can be related to the modal specific acoustic impedance by

$$Z_{s_{mn}} = \rho c_o \left(\frac{1 + R_{mn}}{1 - R_{mn}} \right) \tag{3.21}$$

The complex radiation efficiency, or radiation resistance ratio, σ,is defined by (Hansen and Bies, 1979)

$$\sigma_{mn} = \frac{W_{mn}}{\langle v_{mn}^2 \rangle_{st} S \rho c_o} = \frac{Z_{s_{mn}}}{\rho c_o} \tag{3.22}$$

where W is the complex power radiated at the opening, the real part of which is associated with energy propagating to the far field and the imaginary part of which is associated with storage of potential energy in the near field, and $\langle v^2 \rangle_{st}$ is the space-time average mean square normal velocity at the duct exit; the subscript mn indicating modal components of these variables. Substitution of Equations (3.19) and (3.21) into (3.22) relates the complex radiation efficiency and the complex reflection coefficient as

$$\sigma_{mn} = \tanh(\pi \alpha_{mn} - j\pi(\beta_{mn} - \frac{1}{2})) = \frac{1 + R_{mn}}{1 - R_{mn}} \tag{3.23}$$

The preceding analysis can be used to determine the duct termination impedance,

reflection coefficient and radiation efficiency once the specific acoustic impedance at the exit plane is known. Many such specific acoustic impedances have been calculated previously, for example an unflanged pipe radiating into free space (Levine and Schwinger, 1948).

3.3.2 Experimental determination of termination impedance

Impedance tube measurements have been used extensively to determine the acoustical properties of various materials for plane wave propagation. For instances in which higher order modes are also propagated it is necessary to determine the impedance characteristics of the materials for each mode. This is accomplished by performing a modal decomposition on the multi-modal sound field in the duct to determine the relative amplitudes of the modal component propagating towards and away from the duct terminations, and hence the termination impedances. The modal decomposition technique used here is similar to that described previously (Åbom, 1989) and involves taking acoustic pressure measurements at two cross-sectional planes in the duct at a minimum of N locations for each plane, where N is the number of cut-on modes. To determine the termination impedance values for both ends of the duct, it is necessary to perform a modal decomposition between the source and each duct termination. Separate modal decompositions are required to determine the termination impedances at each end of the duct because the upstream and downstream travelling components of the acoustic response are not continuous along the whole length of the duct. A component reflected from one of the duct terminations is modified by the source prior to its arrival at the other termination, and hence a single decomposition is unable to determine the amplitudes of the component

before and after its modification by the source. The method also enables calculation of the acoustic power transmission for each mode.

For the simplest case, when the modes are uncoupled, the termination impedance is proportional to the ratio of the amplitudes corresponding to each direction of propagation. Expressing Equation (3.9) in terms of waves incident on and reflected from the termination represented by Φ_2 gives the termination impedance parameter at $z = L$ as

$$e^{-2\Phi_{mn}} = \frac{A_{mnr}}{A_{mni}} e^{j2k_{mn}(L-z_1)} \tag{3.24}$$

where A_{mnr} is the complex modal amplitude at $z = z_1$ of the wave reflected from the termination, and A_{mni} is the complex modal amplitude at $z = z_1$ of the wave travelling towards the termination. $(L-z_1)$ is the distance from the duct termination to the measurement plane further from the termination. The ratio A_{mnr}/A_{mni} when $z_1 = L$ is the complex modal amplitude reflection coefficient, R_{mn}. Calculation of the termination impedance at $z = 0$, using Equation (3.24), is achieved by taking at least $2N$ pressure measurements in cross-sectional planes located between the source and the termination at $z = 0$, and transforming the duct origin to the location $z = L$ and reversing the orientation of the z axis.

The modal decomposition technique determines the modal amplitudes of N propagating modes from $2N$ measurements of acoustic pressure in the duct. The measurements are taken at N independent locations in two cross-sectional planes of the duct. The pressure at the measurement locations can be expressed as

$$[p] = [\Omega][A] \tag{3.25}$$

where $[p]$ is a $2N \times 1$ matrix containing the complex acoustic pressure measurements such that

$$[p]^T = \begin{bmatrix} p_1 & .. & p_{2N} \end{bmatrix} \tag{3.26}$$

where the measurement locations are numbered 1 to N for the first measurement plane, and $N + 1$ to $2N$ for the second measurement plane, which is closer to the duct termination of interest. The complex pressures are obtained by converting amplitude and phase to complex format. Each element represents the pressure amplitude at the point, and a phase, relative to a reference location. The reference is an arbitrary point in the duct, and can include one of the measurement points. $[\Omega]$ is a $2N \times 2N$ matrix which represents the transfer functions between the two measurement planes. Each row corresponds to the modal contributions to the pressure at the m^{th} measurement location, with each element representing the contribution from each modal component. Hence row m of the matrix would have the form

$$\begin{bmatrix} \Psi_0(\vec{x}_m)e^{-jk_0 z_m} & \Psi_0(\vec{x}_m)e^{jk_0 z_m} & .. & .. \\ .. & .. & \Psi_{N-1}(\vec{x}_m)e^{-jk_{N-1} z_m} & \Psi_{N-1}(\vec{x}_m)e^{jk_{N-1} z_m} \end{bmatrix} \tag{3.27}$$

where z_m is the distance between the measurement point and the first measurement plane. $[A]$, a $2N \times 1$ matrix, contains the modal amplitude components for each direction of propagation such that

$$[A]^T = \left[(A_{0i}, A_{0r})^T \;\; .. \;\; (A_{(N-1)i}, A_{(N-1)r})^T \right] \tag{3.28}$$

where A_{ni} and A_{nr} are the modal components propagating towards, and away from, the termination, respectively.

Rearrangement of Equation (3.25) provides a solution for the modal amplitudes as

$$[A] = [\Omega]^{-1}[p] \tag{3.29}$$

3.4 EXPERIMENTAL RESULTS

The experimental apparatus consisted of a duct of cross-sectional dimensions 215 × 215 mm, and length approximately 3.2 m, the exact value depending on the type of terminations used. The source used was a 145 mm diameter circular speaker, modelled in the analysis as a square piston of equivalent area, with the rear portion enclosed in a small hard-walled box. As shown previously (Snyder and Hansen, 1989), a measurement of the pressure, p_b, at a point inside the speaker box, of known volume V, enables calculation of the source volume velocity Q_p. Hence

$$Q_p = \frac{-p_b}{Z_v} = \frac{-jV\omega p_b}{\rho c_o^2} \tag{3.30}$$

where Z_v is the acoustic impedance of the speaker box. A small microphone mounted on a traverse was used to measure the acoustic response in the duct, and to perform the modal decomposition on both sides of the source to determine the termination impedances. The theoretical curves used for comparison with experimental data were calculated using

the values for volume velocity and termination impedances found from experiment. This enabled testing of both the validity of the theoretical model and the accuracy with which the required variables could be experimentally determined.

Evanescent modes were also incorporated into the theoretical calculations to account for the near-field of the source, with 20 modes being used to approximate the infinite sum. All experimental measurements were taken relative to the input signal to the source speaker, which acted as a reference. Hence the pressure amplitude was obtained from the autospectrum of the measurement microphone, and the relative phase was given by the cross-spectrum phase between the speaker terminals and the measurement location. This enabled the same microphone to be used for all of the measurements, thus eliminating the problem of phase mismatch between microphone pairs. The use of a single microphone to measure all of the locations involves the implicit assumption that the acoustic response is time invariant.

The first series of tests were conducted at an excitation frequency of 600 Hz which is below the first cut-on frequency (800 Hz) of the rectangular duct used in all of the experiments presented here. The first case, results for which are shown in Figure 3.2, corresponds to a duct rigidly terminated at $z = 0$ by 18 mm thick chipboard, and semi-anechoically terminated at $z = L$. The duct length is 3.2 m, with the source centrally located in the xz plane at $z_p = 1.960$ m, such that $z_p/L = 0.61$. From modal decomposition of the acoustic field at both ends of the duct, the impedance functions at $z = 0$ were found to be $(\alpha_{00}, \beta_{00}) = 0.0128, 0.0304$ which compares favourably with

the ideal values for a totally reflective surface of $(\alpha_{00},\beta_{00}) = 0.0, 0.0$. At $z = L$ it was found that $(\alpha_{00},\beta_{00}) = 0.4517, 0.0328$ which implies that the termination used was actually partially reflective, in comparison to an ideal anechoic termination for which α_{00} values above 0.5 yield an approximately anechoic termination. As shown in Figure 3.2, the theoretical curve, calculated using measured values of source volume velocity and impedance functions, agrees well with the experimental data, for both amplitude and phase of the acoustic response.

In the next configuration, the results for which are shown in Figure 3.3, the termination at $z = L$ consisted of two 18 mm thick layers of fibreglass insulation material backed by the semi-anechoic termination, the front face of the material being at $z = 3.215$ m. The measured values of impedance functions at $z = L$ were $(\alpha_{00},\beta_{00}) = 0.1954, 0.0082$, indicating a partially absorptive termination. The relative source location was $z_p/L = 0.61$. Again, it can be seen from the figure that the experimental and theoretical values agree well.

For the next test, a partially absorptive termination was installed at $z = 0$, consisting of two layers of 18 mm thick fibreglass insulation, backed by the rigid termination described above, in addition to the partially absorptive termination at $z = L$. The measured termination impedance parameters for the surface at $z = 0$ were $(\alpha_{00},\beta_{00}) = 0.2066, 0.7030$. The results for this case are shown in Figure 3.4, and reveal that the agreement between theory and experiment is good, especially for the relative phase of the response. It should be noted that the experimental amplitudes decrease with distance from the source,

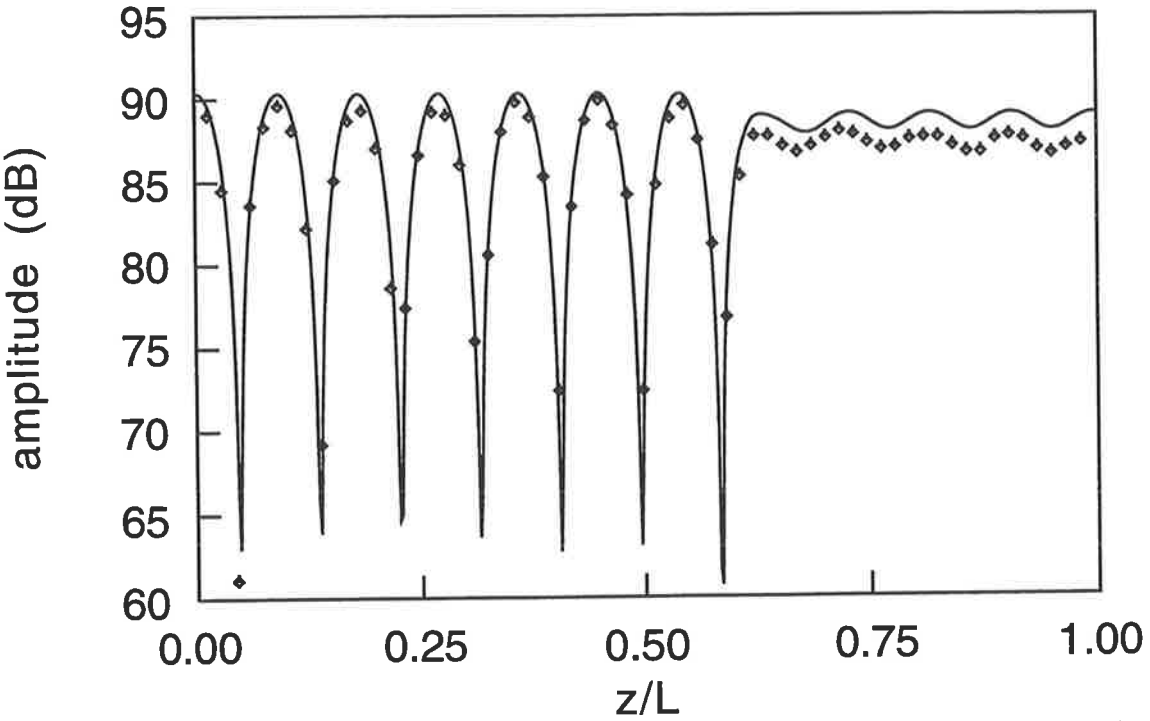

Figure 3.2a Response pressure amplitude for semi-infinite duct at 600 Hz with a source located at $z/L = 0.61$. ♦ = experiment, – = theory.

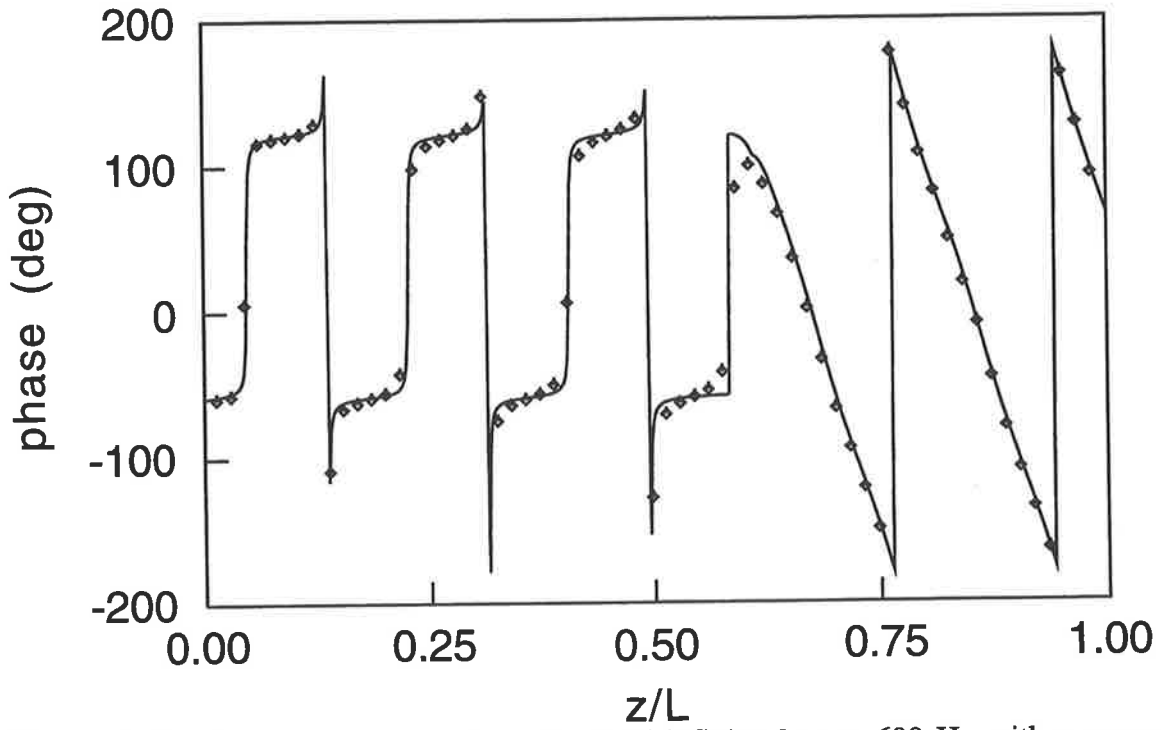

Figure 3.2b Response pressure phase for semi-infinite duct at 600 Hz with a source located at $z/L = 0.61$. ♦ = experiment, – = theory.

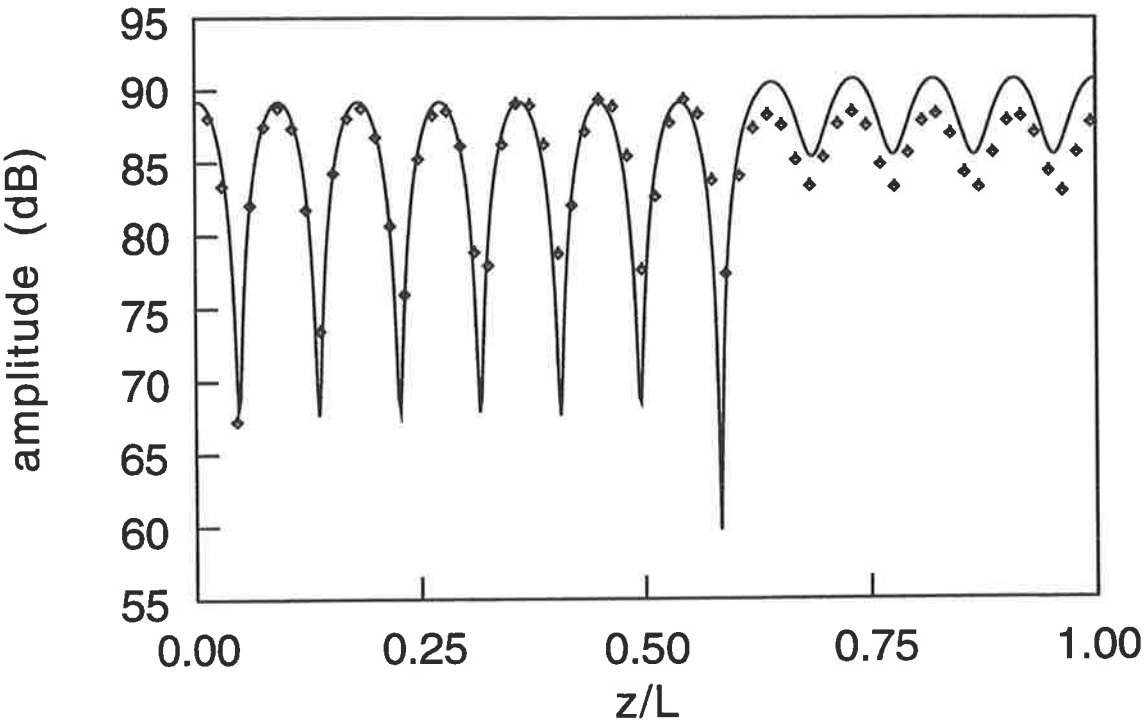

Figure 3.3a Response pressure amplitude for rigid-finite impedance duct at 600 Hz with a source located at $z/L = 0.61$. ♦ = experiment, – = theory.

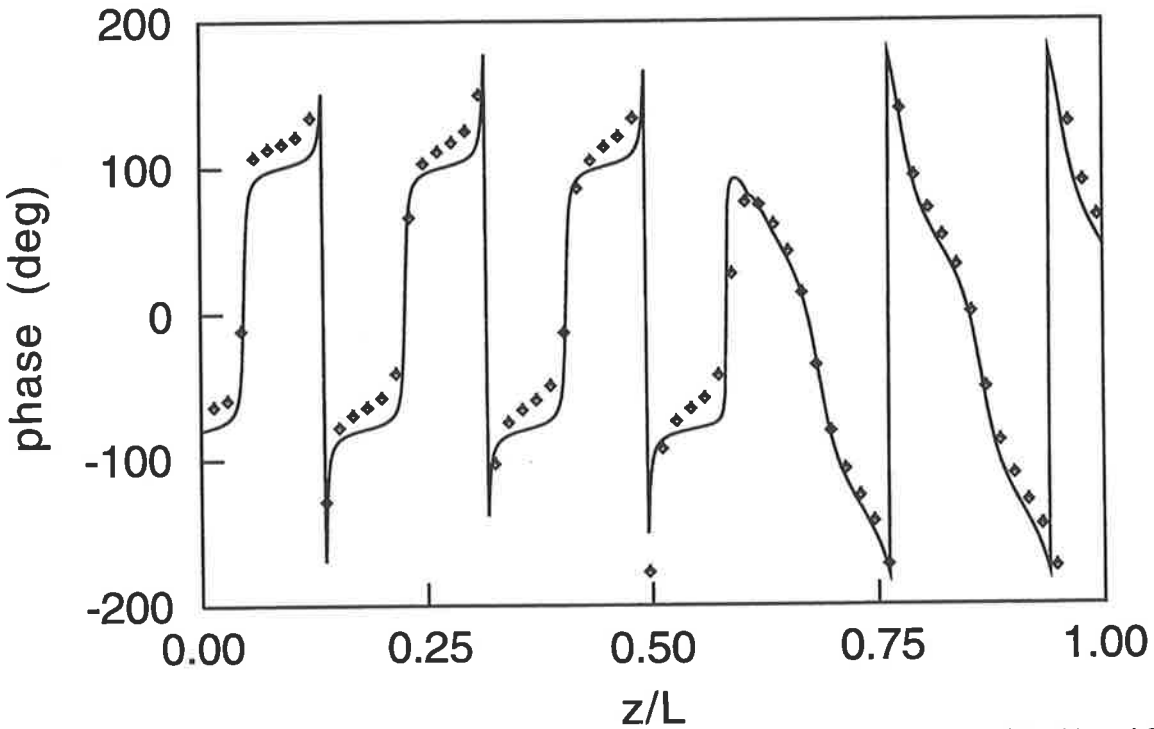

Figure 3.3b Response pressure phase for rigid-finite impedance duct at 600 Hz with a source located at $z/L = 0.61$. ♦ = experiment, – = theory.

indicating that the duct walls are not behaving as the ideal totally rigid case which is modelled. A better agreement between theory and experiment may be achieved by incorporating a damping factor into the complex modal wavenumber k_n, to represent the non-ideal behaviour of the experimental rig and similar non-rigid wall cases.

For the remainder of the tests a shorter length duct was used, of length around 2.3 m, depending on the termination conditions. The source location to duct length ratio was hence also altered to $z_p/L = 0.86$. The first six cut-on frequencies for the experimental duct, under ambient conditions, are given in Table 3.1. For an excitation frequency of 900 Hz the (1,0) and (0,1) modes are able to propagate, in addition to the fundamental, or (0,0) mode, and hence the pressure distribution over the duct cross-section is non-uniform. Propagation of these modes thus necessitated the measurement of acoustic pressure in at least six locations, three in each of two cross-sectional planes, to enable determination of the impedance of a termination. This process was repeated at a location between the source and the duct termination for each end of the duct, to determine the impedance corresponding to each termination. Results for the case of a duct rigidly terminated at both ends, as described previously, for excitation at 900 Hz, are shown in Figure 3.5. This figure represents the acoustic response measured by a microphone traversed along the duct at a constant cross-sectional location given by $(x,y) = 0.70b,\ 0.26d$. The agreement between the theory and experimental data is good, especially for the relative phase; however, the theory generally overestimates the amplitude of the response by approximately 3 dB. This indicates that measurement of the amplitude of the source volume velocity, Q_p, may be a source of error. Similar results are found for a

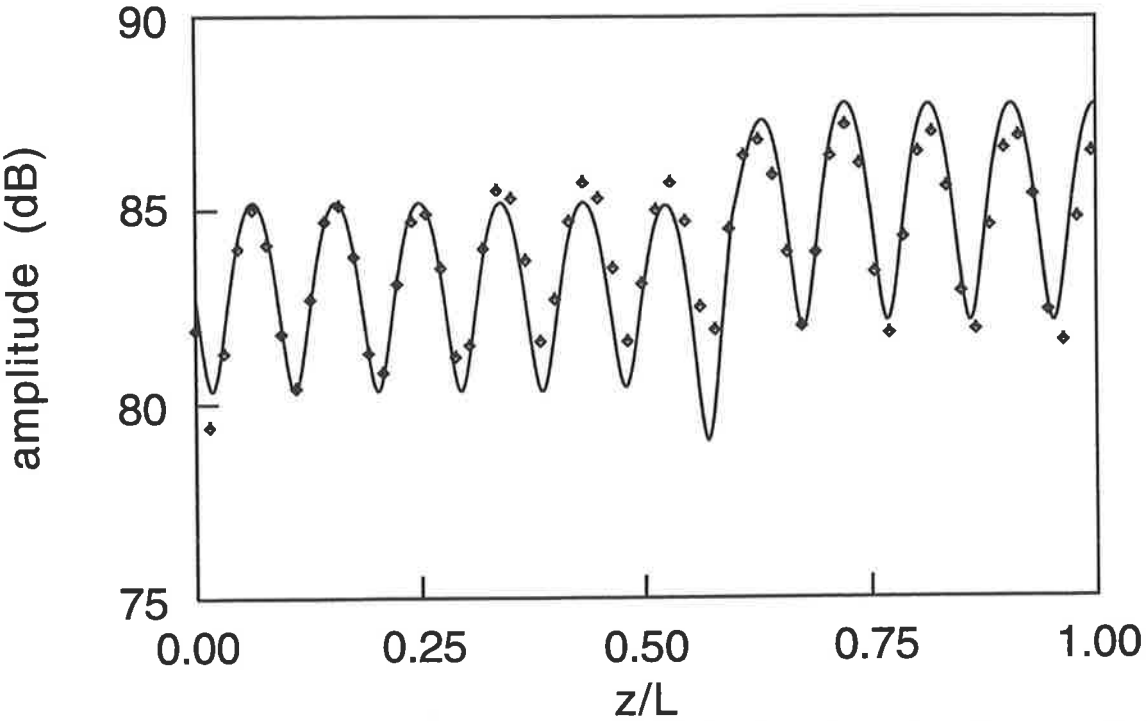

Figure 3.4a Response pressure amplitude for finite impedance-impedance duct at 600 Hz with a source located at $z/L = 0.61$. ♦ = experiment, — = theory.

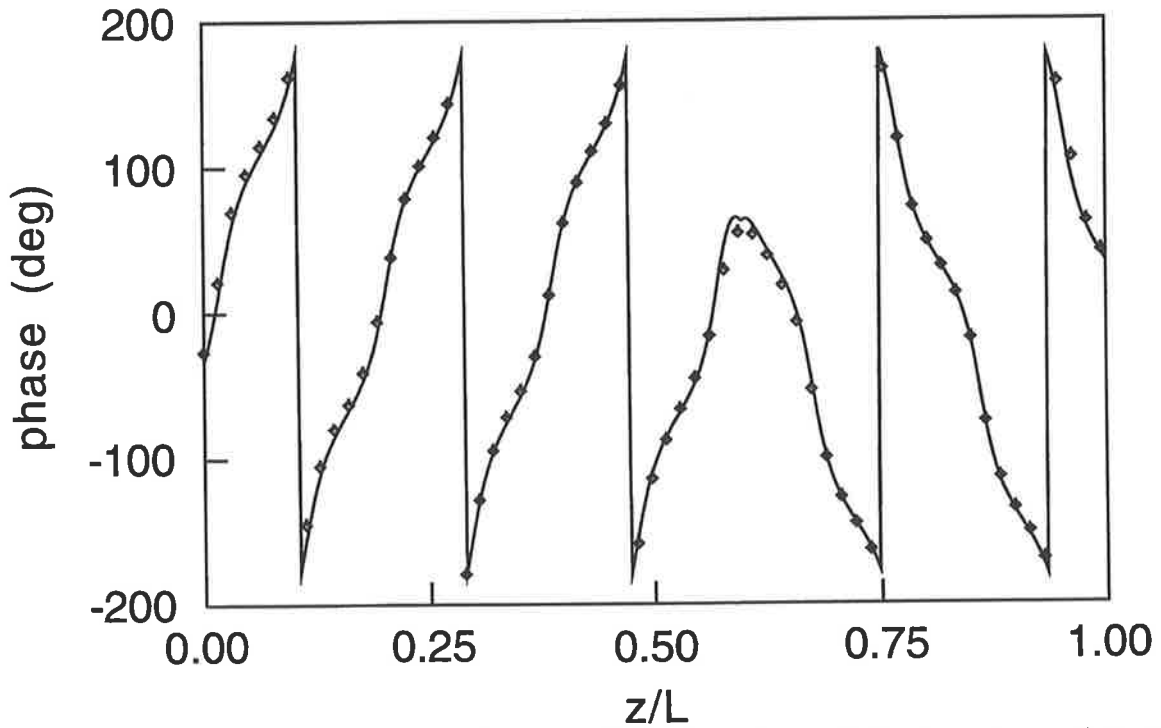

Figure 3.4b Response pressure phase for finite impedance-finite impedance duct at 600 Hz with a source located at $z/L = 0.61$. ♦ = experiment, — = theory.

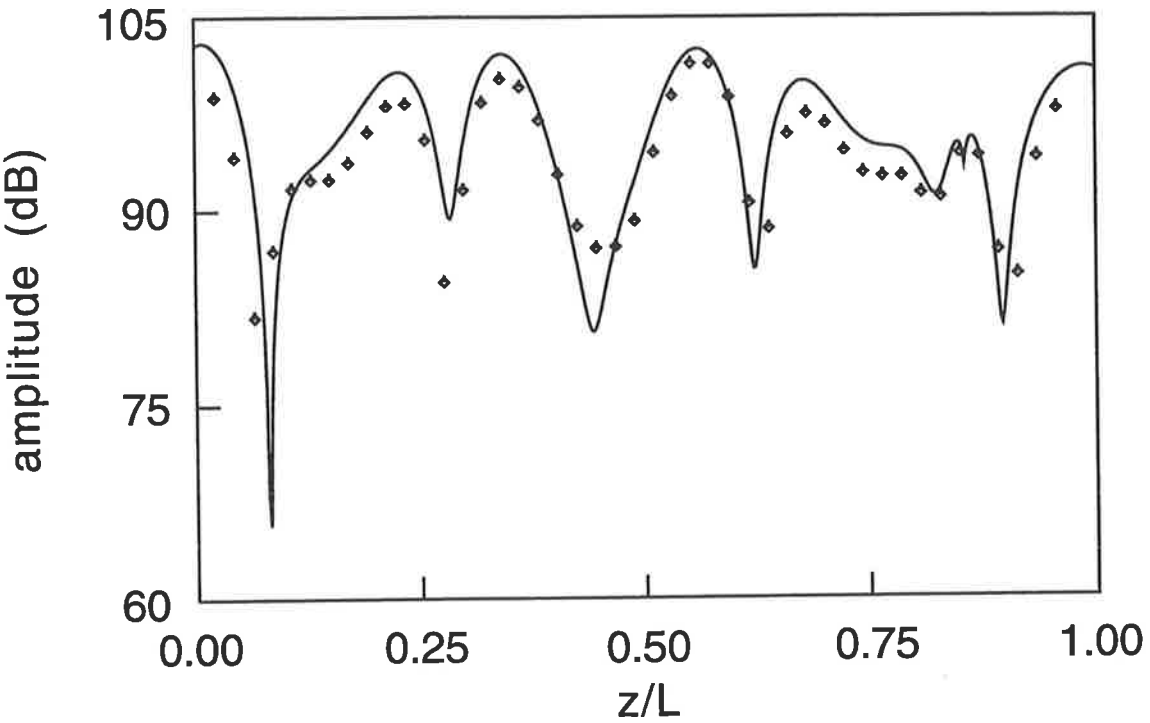

Figure 3.5a Response pressure amplitude for rigid-rigid duct at 900 Hz with a source located at z/L = 0.86. ♦ = experiment, – = theory.

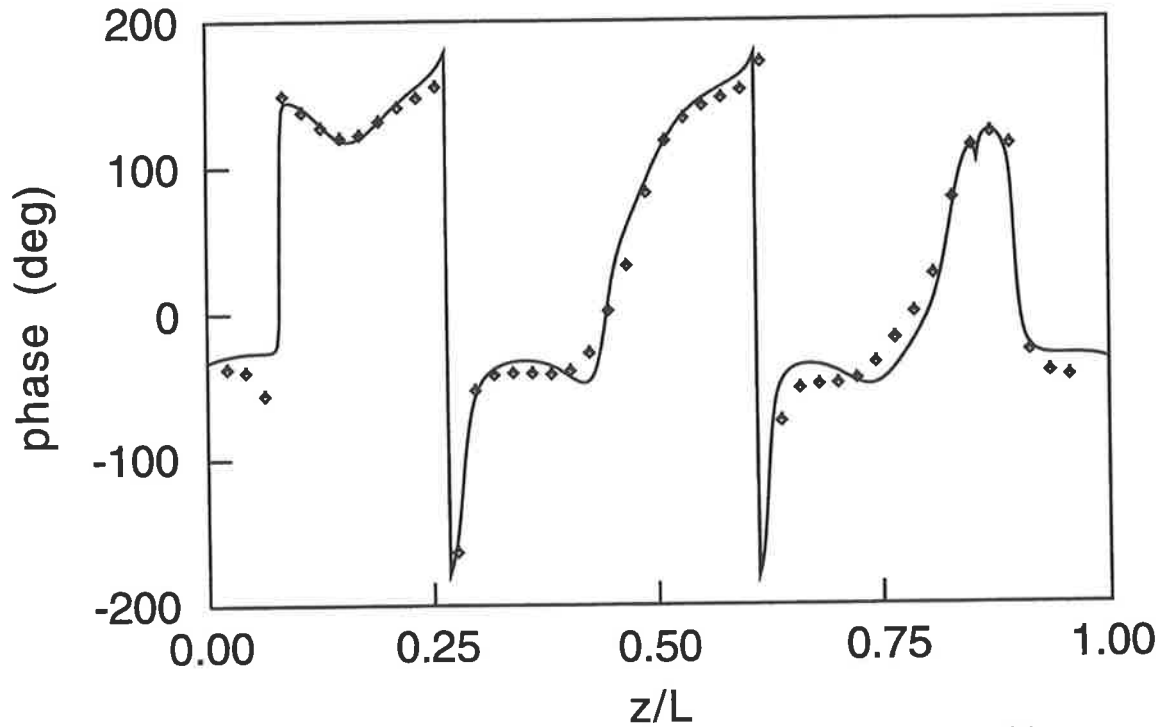

Figure 3.5b Response pressure phase for rigid-rigid duct at 900 Hz with a source located at z/L = 0.86. ♦ = experiment, – = theory.

configuration in which the termination at $z = 0$ is partially absorptive, while a rigid termination exists at $z = L$. Figure 3.6 shows general agreement between theory and experiment for this case; however, the amplitudes of the acoustic response are again overestimated by approximately 3 dB.

Table 3.1

Acoustic Mode Cut-On Frequencies of Experimental Duct

Acoustic Mode	Cut-On Frequency (Hz)
(0,0)	0.0
(1,0)	800.0
(0,1)	800.0
(1,1)	1131.4
(2,0)	1600.0
(0,2)	1600.0

The last of the tests were conducted in an anechoic chamber, the $z = 0$ termination of the duct mounted flush with a large baffle of dimension 2.45 m in width, 2.45 m in height and 18 mm thickness. The baffle and duct were arranged in the anechoic chamber to represent an open, flanged duct radiating into free space. This arrangement was tested by measuring the termination impedances within the duct for a range of excitation frequencies.

Comparison of the experimental data with theoretical values is shown in Figure 3.7, and indicates that the configuration adequately represents the ideal modelled case, in addition to confirming the assumptions made in the model. The acoustic response for such a configuration is shown in Figure 3.8, at an excitation frequency of 600 Hz, for the case of

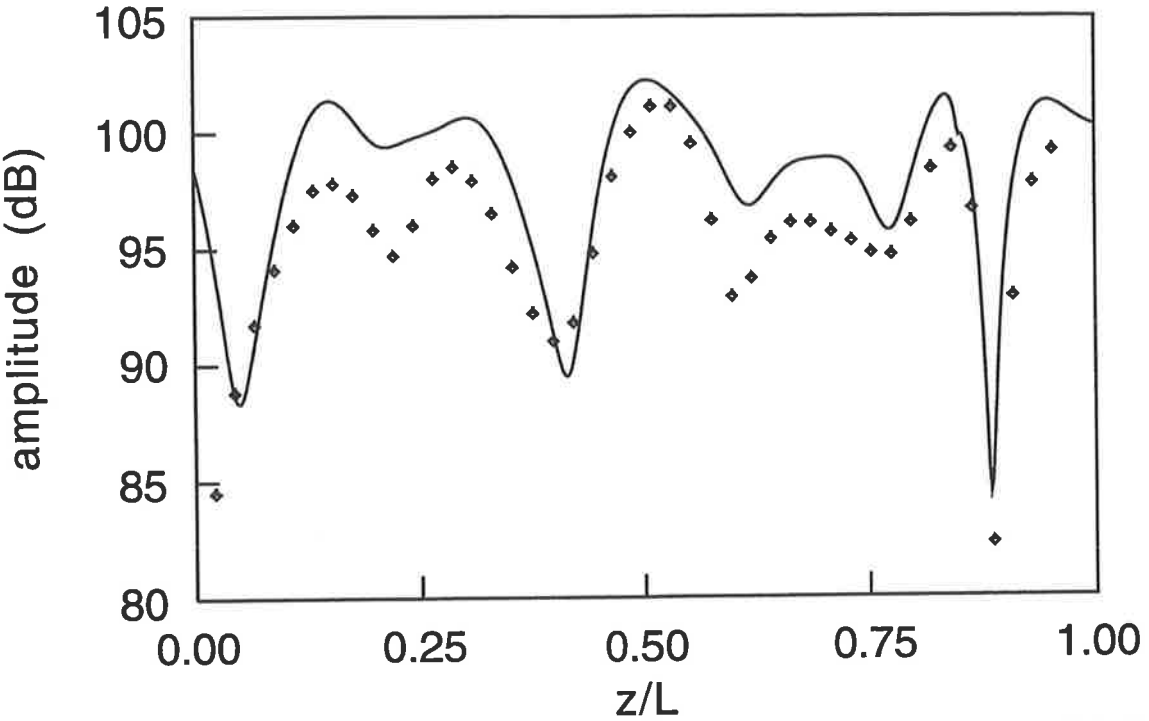

Figure 3.6a Response pressure amplitude for finite impedance-rigid duct at 900 Hz with a source located at $z/L = 0.86$. ♦ = experiment, – = theory.

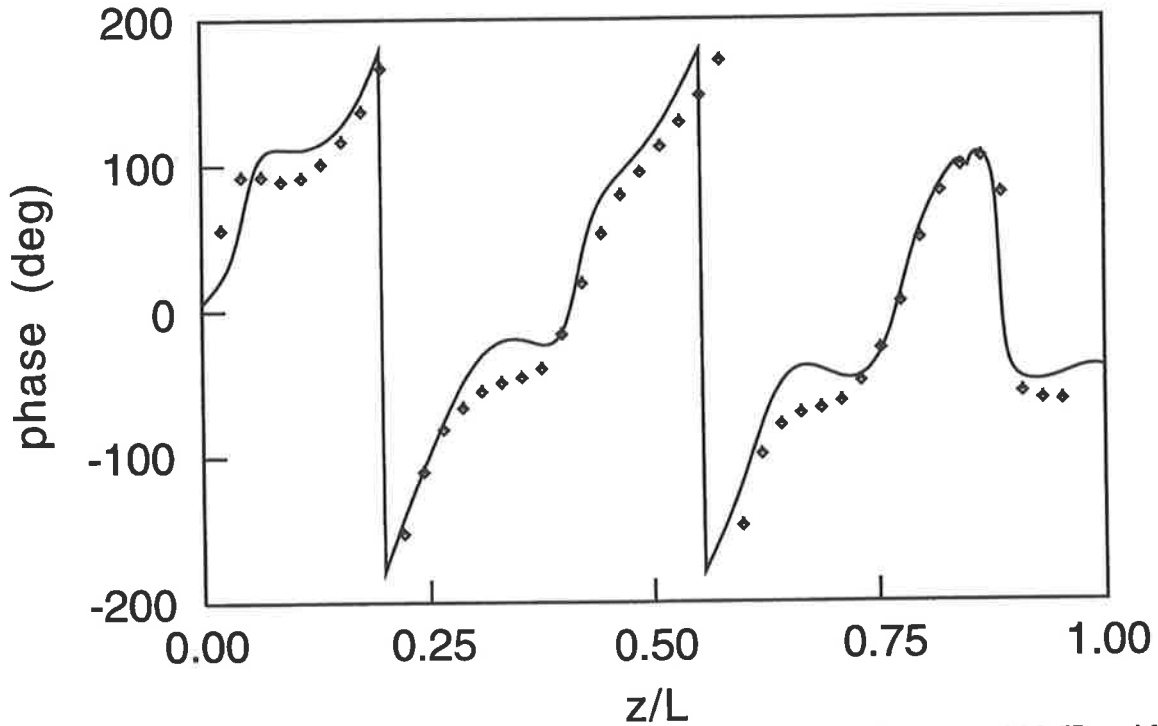

Figure 3.6b Response pressure phase for finite impedance-rigid duct at 900 Hz with a source located at $z/L = 0.86$. ♦ = experiment, – = theory.

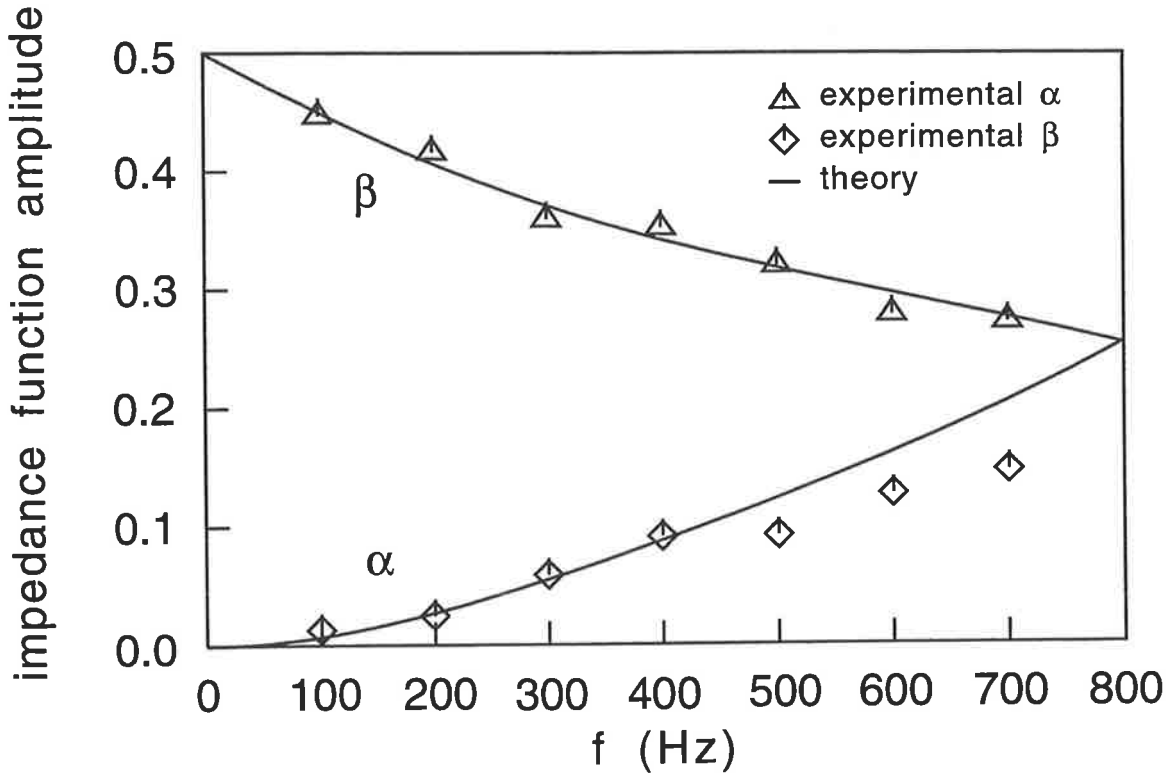

Figure 3.7 Termination impedance functions for experimental baffled duct.

a rigid termination at $z = L$. Good agreement between theory and experiment is realised at this frequency. The acoustic response of the same configuration at an excitation frequency of 900 Hz is shown in Figure 3.9. The general form of the theoretical and experimental values is in agreement, however overestimation of the amplitude is again apparent, and is thought to be due to inaccuracies in measuring the source volume velocity.

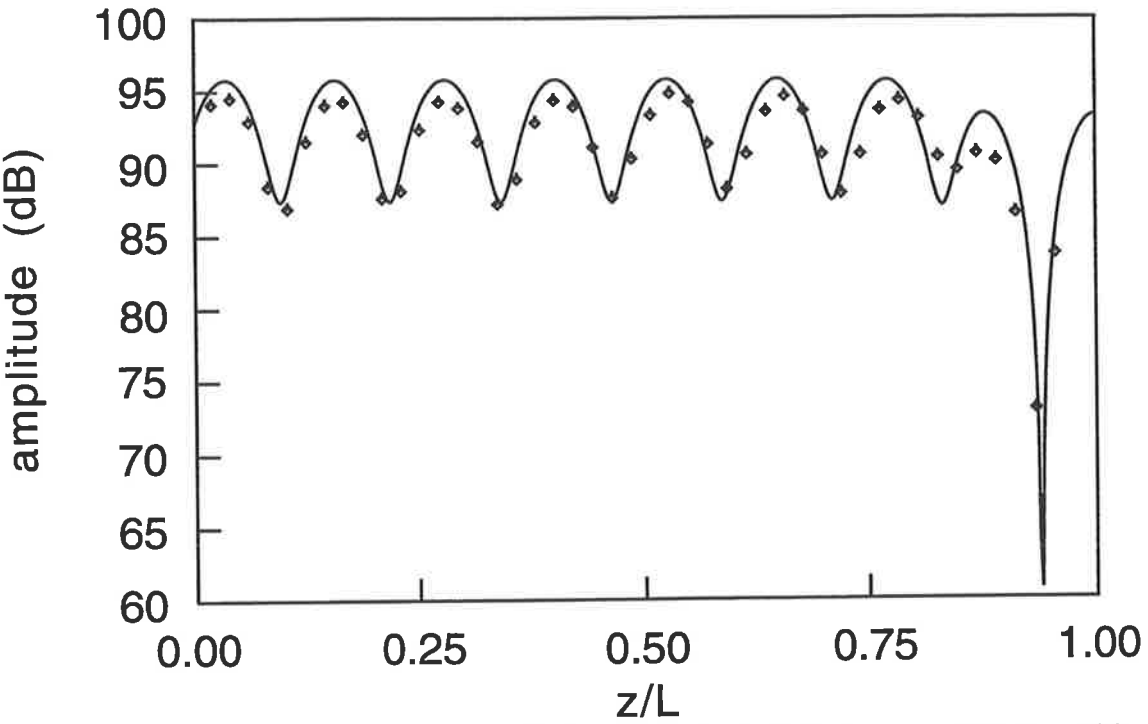

Figure 3.8a Response pressure amplitude for baffled-rigid duct at 600 Hz with a source located at $z/L = 0.86$. ♦ = experiment, – = theory.

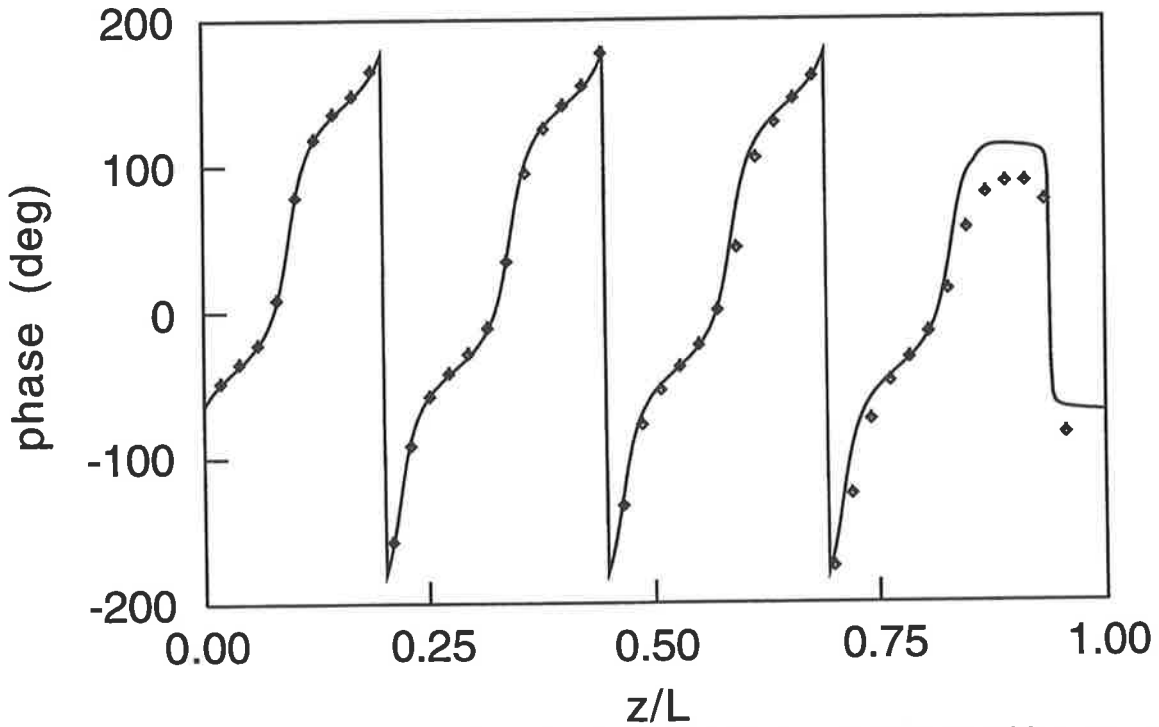

Figure 3.8b Response pressure phase for baffled-rigid duct at 600 Hz with a source located at $z/L = 0.86$. ♦ = experiment, – = theory.

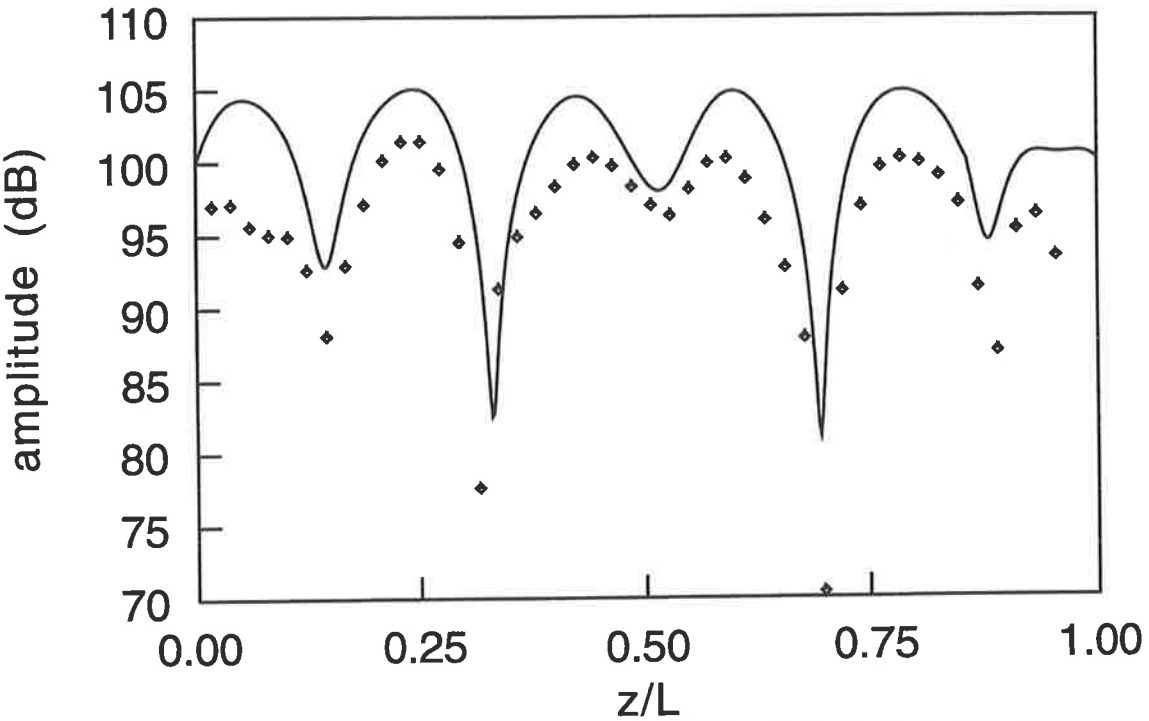

Figure 3.9a Response pressure amplitude for baffled-rigid duct at 900 Hz with a source located at z/L = 0.86. ♦ = experiment, – = theory.

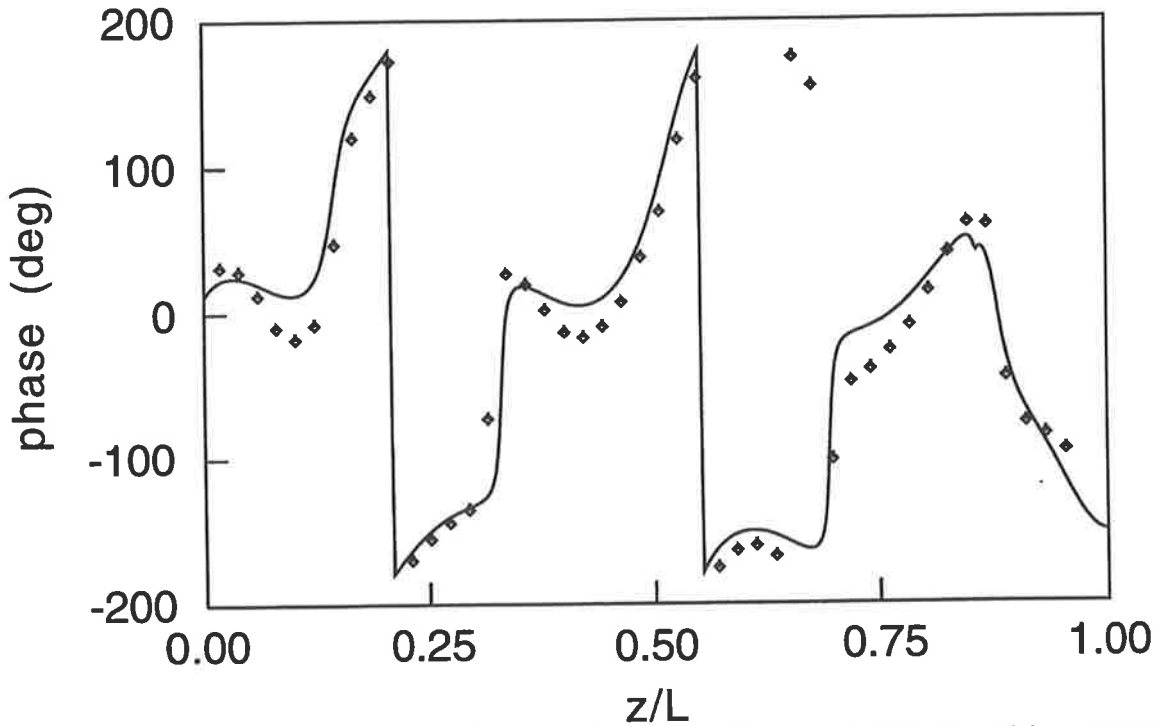

Figure 3.9b Response pressure phase for baffled-rigid duct at 900 Hz with a source located at z/L = 0.86. ♦ = experiment, – = theory.

3.5 CONCLUSIONS

Representation of the acoustic response within an arbitrary length hard-walled duct in terms of the termination impedance conditions has been shown to be appropriate for both plane wave and higher order mode propagation. Agreement between theoretical values and experimental data was demonstrated for terminations ranging from totally reflective through to anechoic. Accurate determination of the source volume velocity using the method employed here was shown to be a problem for frequencies at which higher order modes are propagated. Methods of improving the accuracy of this technique will need to be investigated in future. Accurate prediction of the impedance functions for the case of a flanged duct radiating into free space was verified using a modal decomposition technique based upon the measurement of transfer functions between an appropriate number of locations in the duct.

CHAPTER 4. EFFECT OF ERROR SENSOR AND CONTROL SOURCE CONFIGURATION IN DUCTS

4.1 INTRODUCTION

Having developed a suitable model for describing the acoustic response in ducts of arbitrary length and termination conditions in Chapter 3, comparison of a number of different error sensor strategies for the active control of duct noise is undertaken in this chapter. It is the aim of this chapter to compare a number of error sensor strategies with the objective of determining a strategy, appropriate for both plane wave and higher order mode propagation, for a range of duct termination conditions. The stated objective of minimising the sound field in a region downstream of the control sources implies that the duct may be considered as either an enclosure in which it is required that the sound field need only be minimised downstream of the control sources, or as an acoustical element in a system such as a duct radiating into some external region, where it is required that the acoustic radiation from the duct exit is minimised. Error sensor strategies investigated include minimisation of the acoustic pressure at a point, minimisation of the total real acoustic power output, and minimisation of an estimate of the acoustic potential energy. A new error sensor strategy is also proposed and investigated. The strategy is based upon minimisation of the downstream acoustic power transmission determined by a modal decomposition of the duct sound field. Error sensor strategies are analysed for both plane wave and multi-mode sound fields, and for a range of duct termination conditions. The criterion used to assess the error sensor strategies is the minimisation of the sound field downstream of the control sources. The model is also utilised in this chapter to determine

the influence of various error sensor/control source configurations and duct termination conditions upon the acoustic field, and the resultant effect on the levels of noise reduction achieved using acoustic sources in an active noise control system. Theoretical and experimental results are presented for a range of error sensor, control source and duct configurations, and for both plane wave and higher order mode propagation. A sensor/source strategy is proposed which is applicable to any number of rigid walled duct acoustic modes, and enables the effect of evanescent modes to be eliminated from the error sensor signal.

4.2 GENERAL FORMULATION FOR MINIMISATION FUNCTION

The purpose of this section is to present a general formulation for a quadratic minimisation function, which is then expressed in detail for each particular minimisation criterion in the following section. The duct acoustic response formulation used in the following analysis is derived in the previous chapter. The value of the function, F, to be minimised under the influence of the primary and control sources can be expressed as a quadratic function of the control source volume velocities, $\left[Q_c\right] = \left[Q_{c_1}\ Q_{c_2}\ \cdots\ Q_{c_M}\right]^T$, for M control sources, such that

$$F = \left[Q_c\right]^H \left[a\right] \left[Q_c\right] + \left[b_1\right] \left[Q_c\right] + \left[Q_c\right]^H \left[b_2\right] + c \tag{4.1}$$

The composition of the matrices $\left[a\right]$, $\left[b_1\right]$, $\left[b_2\right]$, and the value of the variable c are all dependent upon F. Note that the matrix form of the preceding equation allows for any number of primary and control sources.

Differentiating Equation (4.1) with respect to the real and imaginary components of the control source volume velocity, $\left[Q_c\right]$, and equating each of these gradients to zero, $\partial F / \partial \left[Q_R\right] = 0$ and $\partial F / \partial \left[Q_I\right] = 0$, yields the optimum control source volume velocity as

$$\left[Q_{c_{opt}}\right] = -\left[a\right]^{-1}\left[b\right] \tag{4.2}$$

where

$$\left[b\right] = \frac{1}{2}\left\{\left[b_1\right]^H + \left[b_2\right]\right\} \tag{4.3}$$

The specific form of the matrices $\left[a\right]$, $\left[b_1\right]$, $\left[b_2\right]$, and the variable c will now be outlined for each error sensor strategy.

4.3 ERROR SENSOR STRATEGIES

The purpose of this section is to present detailed formulations for five different error sensor strategies: minimisation of the squared pressure amplitude at a point; minimisation of the sum of the squared pressure amplitudes at a number of locations throughout the duct; minimisation of the sum of the squared pressure amplitudes at a number of locations downstream of the control source; minimisation of the total real acoustic power output of the primary and control sources; and a newly proposed technique of minimisation of the acoustic power flow downstream of the control source, as determined by modal decomposition of the duct sound field.

For an error criterion of minimisation of the pressure amplitude at a point, $|p(\vec{x})|^2$, such that the error function F in Equation (4.1) is equal to $|p(\vec{x})|^2$, the matrices take the form

$$[a] = [Z_c]^H [Z_c] \tag{4.4}$$

$$[b] = [b_1]^H = [b_2] = [Z_c]^H [Z_p][Q_p] \tag{4.5}$$

$$c = [Q_p]^H [Z_p]^H [Z_p][Q_p] \tag{4.6}$$

where $[Z_p]$ relates the pressure at the point $\vec{x}$ to the primary source volume velocity $[Q_p] = [Q_{p_1} \;\; Q_{p_2} \;\; \cdots \;\; Q_{p_N}]^T$, for N primary sources, by

$$[Z_p] = \left[\frac{p_{p_1}(\vec{x})}{Q_{p_1}}, \;\; \cdots, \;\; \frac{p_{p_N}(\vec{x})}{Q_{p_N}} \right] \tag{4.7}$$

and $[Z_c]$ similarly relates the pressure at $\vec{x}$ to the control source volume velocity $[Q_c]$, such that

$$[Z_c] = \left[\frac{p_{c_1}(\vec{x})}{Q_{c_1}}, \;\; \cdots, \;\; \frac{p_{c_M}(\vec{x})}{Q_{c_M}} \right] \tag{4.8}$$

where $p_{p_N}(\vec{x})$ is the acoustic pressure at $\vec{x}$ due to primary source N, and $p_{c_M}(\vec{x})$ is the acoustic pressure at $\vec{x}$ due to control source M.

A practically achievable estimate of the acoustical potential energy, E_p, in a region of the duct is given by the sum of the squares of the sound pressures at a large number of locations, l, distributed throughout the region (Curtis et al., 1987). The minimisation of the pressure at a single point is a subset of this error strategy for the case of $l = 1$. The quadratic function for the minimisation of the acoustic potential energy estimate, J_p, is

equal to

$$F = J_p = \frac{1}{4\rho c_o^2 l} \sum_{i=1}^{l} |p(\vec{x}_i)|^2 \tag{4.9}$$

where the constant factor $1/4\rho c_o^2 l$ is introduced such that the estimate, J_p, is compatible with the actual acoustic potential energy, E_p (Curtis et al., 1987). The matrices in the quadratic expression take the same form as those in Equations (4.4), (4.5) and (4.6).

Minimisation of the total real acoustic power output of the primary and control sources, W, gives (Nelson et al., 1987) Equation (4.1) where

$$[a] = Re\left\{\left[Z_c(\vec{x}_c)\right]^H\right\} \tag{4.10}$$

$$[b_1] = [Q_p]^H Re\left\{\left[Z_p(\vec{x}_c)\right]^H\right\} \tag{4.11}$$

$$[b_2] = Re\left\{\left[Z_c(\vec{x}_p)\right]^H\right\}[Q_p] \tag{4.12}$$

$$c = [Q_p]^H Re\left\{\left[Z_p(\vec{x}_p)\right]^H\right\}[Q_p] \tag{4.13}$$

where $\left[Z_p(\vec{x}_c)\right]$, an $M \times N$ matrix for M control sources and N primary sources, relates the pressure at the control source location $\vec{x}_c$ due to the primary source volume velocity $[Q_p]$, such that

$$\left[Z_p(\vec{x}_c)\right] = \begin{bmatrix} \dfrac{p_{p_1}(\vec{x}_{c_1})}{Q_{p_1}} & \cdots & \dfrac{p_{p_N}(\vec{x}_{c_1})}{Q_{p_N}} \\ \vdots & \ddots & \vdots \\ \dfrac{p_{p_1}(\vec{x}_{c_M})}{Q_{p_1}} & \cdots & \dfrac{p_{p_N}(\vec{x}_{c_M})}{Q_{p_N}} \end{bmatrix} \tag{4.14}$$

and similarly for $\left[Z_c(\vec{x}_p)\right]$ $(N \times M)$, $\left[Z_c(\vec{x}_c)\right]$ $(M \times M)$, and $\left[Z_p(\vec{x}_p)\right]$ $(N \times N)$. It should be noted that a direct measurement of W is difficult in a practical context, and hence is treated chiefly as a theoretical strategy in this chapter.

To date, the investigations into minimisation of downstream power as an error sensor strategy have expressed the power as the area integral of the acoustic intensity over the duct cross-section, namely

$$W = \frac{1}{2}\int_S Re\left\{p u^*\right\} dS \tag{4.15}$$

which has led other researchers to remark that it is probably impractical to implement such a control strategy due to the difficulty of monitoring power (Stell, 1991).

What is proposed in this chapter is a formulation of the propagating acoustic power in terms of the total pressure at a discrete number of points in the duct. This would allow a realisable measure of the propagating acoustic power, and would hence be suitable for use as an error sensor strategy. Such a formulation would also enable measurement of acoustic power for any number of control sources and any amount of evanescent mode contribution to the acoustic response.

The alternative error strategy proposed here is to use the results from an experimental modal decomposition of the acoustic response as the error criterion. The modal decomposition formulation was outlined in the previous chapter. The total acoustic power flow in each direction of propagation is given by

$$W_i = \sum_g \frac{bdk_g |A_{gi}|^2}{\rho\omega} \tag{4.16}$$

and

$$W_r = \sum_g \frac{bdk_g |A_{gr}|^2}{\rho\omega} \tag{4.17}$$

where W_i and W_r represent the total acoustic power propagating towards, and away from, the termination, respectively. A selection matrix, $[S]$, can be constructed to make the components of the modal amplitude matrix, $[A]$, in a specific direction, equal to the total acoustic power flow in that direction. Hence, multiplication of $[A]$ by the selection matrix $[S]$ enables the calculation of the acoustic power flow in one direction, in this case towards the duct exit, where

$$[S] = \begin{bmatrix} s_0 & & & \\ & 0 & 0 & \\ & & \ddots & \\ & 0 & s_{G-1} & \\ & & & 0 \end{bmatrix} \tag{4.18}$$

and

$$s_g = \sqrt{\frac{bdk_g}{\rho\omega}} \tag{4.19}$$

for propagating acoustic modes, and $s_g = 0$ for evanescent modes, such that the modal amplitudes are compatible with the downstream acoustic power flow, W_d, which is given by

$$W_d = [A]^H [S]^H [S][A] \tag{4.20}$$

Expressing W_d as a quadratic function of the control source volume velocity yields Equation (4.1), where $W_d = F$, and

$$[a] = [Z_c]^H \left([\Omega]^{-1}\right)^H [S]^H [S][\Omega]^{-1}[Z_c] \tag{4.21}$$

$$[b_1] = [Q_p]^H [Z_p]^H \left([\Omega]^{-1}\right)^H [S]^H [S][\Omega]^{-1}[Z_c] \tag{4.22}$$

$$[b_2] = [Z_c]^H \left([\Omega]^{-1}\right)^H [S]^H [S][\Omega]^{-1}[Z_p][Q_p] \tag{4.23}$$

$$c = [Q_p]^H [Z_p]^H \left([\Omega]^{-1}\right)^H [S]^H [S][\Omega]^{-1}[Z_p][Q_p] \tag{4.24}$$

In the preceding equations for any number of primary sources and M control sources, $[a]$ is an $M \times M$ matrix, $[b_1]$ is $1 \times M$, $[b_2]$ is $M \times 1$ and c is a scalar.

4.4 RESULTS

For the results presented here, a black box feed-forward controller has been assumed with a reference signal obtained from the input to the primary source. The control sources are

modelled as constant volume velocity sources, the outputs of which are linearly related to their inputs. The error information is obtained via the strategies outlined in the previous section and input to the controller. In real systems it is unlikely that the exact value of the optimal control source volume velocities will be achieved by the controller, and hence a physical representation of the controller inaccuracies is obtained by multiplying the calculated optimum control source volume velocities by an efficiency factor η. The efficiency value is obtained by considering a controller of precision such that a total rounding error of around 1% is generated in the outputs from the controller. Hence an efficiency factor of 0.99 is obtained. An efficiency factor of 0.99 limits the achievable attenuation to 40 dB, which is the maximum attenuation a practical control system is likely to produce.

4.4.1 Comparison of error sensor strategies

In this section, theoretical calculations are performed for a number of error sensor strategies and various duct configurations and excitation frequencies. A standard configuration has been utilised for a majority of the tests, consisting of a single point primary source located at $\vec{x}_p = (b/4, d/4, 0)$, within a duct of cross-sectional dimension $b \times d = 0.215 \times 0.215$ m, and a single point control source located in the xz plane of the duct at $\vec{x}_c = (0.1, 0, 0.41L)$. Although this configuration may not yield the maximum achievable levels of reduction in the error criterion, F, for particular frequencies and duct termination conditions, it does allow the different error sensor strategies to be compared for the same physical constraints. The ability of each of the error sensor strategies to maximise the levels of reduction in F, for this fixed configuration, is used as a measure of

their effectiveness. The different error sensor criteria were achieved by the following arrangements. For minimisation of the pressure at a point, $|p(\vec{x})|^2$, the pressure was calculated downstream of the control source at $\vec{x} = (0.1, 0.1, 0.84L)$. The number of microphones used for the modal decomposition estimate of power flow, W_d, was dependent upon the number of propagating modes, which is determined by the excitation frequency. For the 600 Hz tests, corresponding to plane wave propagation only, two microphones were located downstream of the control source, with an axial separation of 0.1 m. At 900 Hz, corresponding to three propagating modes, six microphones were arranged such that two planes containing three microphones, at equivalent locations in each plane, were separated by an axial distance of 0.1 m.

An estimate of the acoustic potential energy, J_p, was obtained from the pressure calculated at six microphone locations. J_p was calculated for two cases, the first corresponding to an estimate for the whole duct volume, in which the six microphones were positioned at random locations throughout the entire duct. The second case corresponded to the acoustic potential energy in a region downstream of the control source, and this was achieved by placing the six microphones at random locations within this region. The coordinates of the six locations are given in Appendix D for both cases. The minimisation of the total real acoustic power output of the primary and control sources was calculated using the theory outlined in Equations (4.10), (4.11), (4.12) and (4.13).

The first duct arrangement considered was a semi-infinite duct, excited at 600 Hz allowing

plane wave propagation only, terminated rigidly at $z = 0$ such that $\alpha_1, \beta_1 = (0,0)$, with the other termination being anechoic. The calculated uncontrolled response, corresponding to only the primary source being operational, is shown in Figure 4.1 as a solid line. The calculated controlled response for the error sensor strategy of minimisation of the pressure at a point $\vec{x} = (0.1,0.1,2.678)$ is shown as the dotted line and reveals that good levels of reduction are achievable downstream of the control source. Identical levels of reduction, for an identical control source volume velocity, are achievable for the error sensor strategies of minimisation of real power flow W, minimisation of the acoustic potential energy J_p in a region downstream of the control source, and minimisation of the downstream power flow W_d. This is because minimising the pressure at a single microphone placed downstream of the control source in a semi-infinite duct is equivalent to minimising the above mentioned criteria for plane wave propagation. The controlled response for the error sensor strategy of minimising an estimate of the acoustic potential energy throughout the duct is shown in Figure 4.2, which reveals that the response downstream of the control source is not altered from the uncontrolled case, while the levels at a number of regions located between the primary and control sources have been reduced. Although the sound field has been reduced at a number of locations within the duct, and the total acoustic potential energy has also been reduced, this error sensor strategy does not achieve the previously stated objective of minimising the sound field downstream of the control source.

The difference in the error information provided to the controller by the two different error sensor strategies described above is visualised by comparing the error criterion plots for

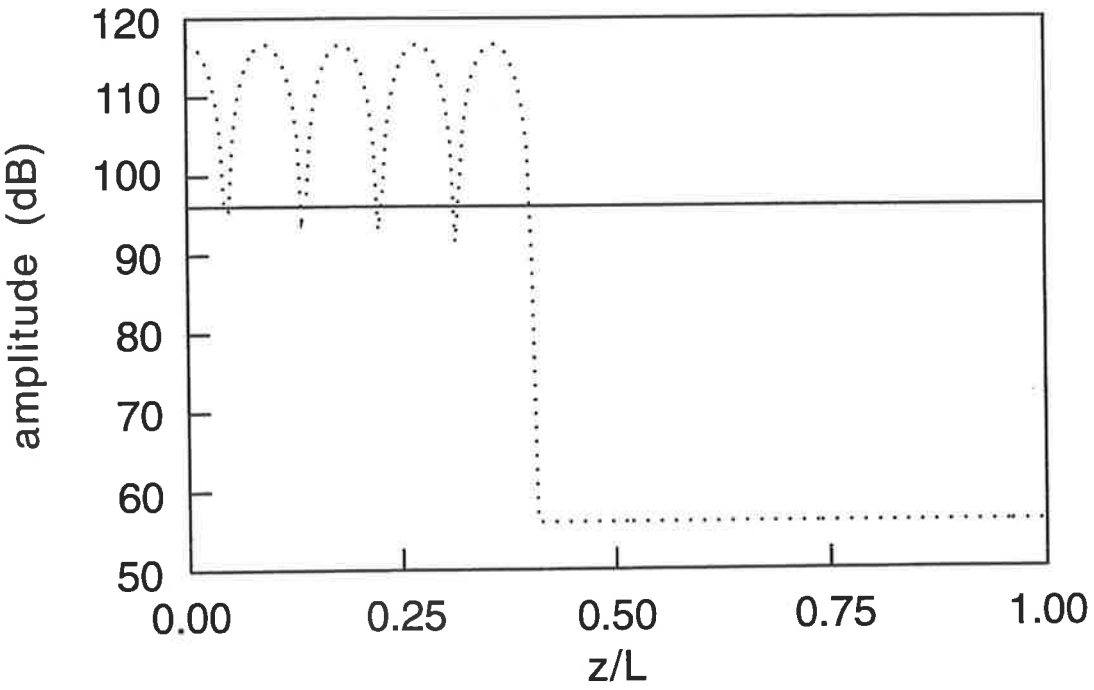

Figure 4.1 Sound pressure amplitude (dB) for a semi-infinite duct at 600 Hz. —— uncontrolled; ····· controlled response for minimisation of pressure at a point (x,y,z) = $(0.1,0.1,0.84L)$. Primary source at $z/L = 0$, control source at $z/L = 0.41$.

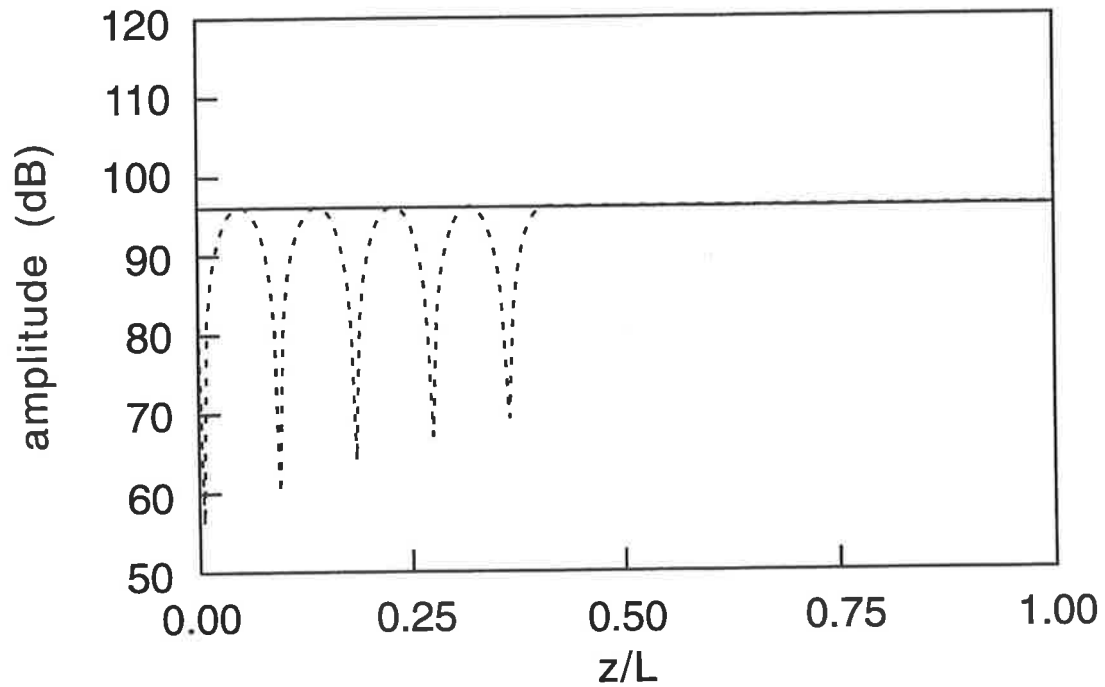

Figure 4.2 Sound pressure amplitude (dB) for a semi-infinite duct at 600 Hz. —— uncontrolled; ····· controlled response for minimisation of J_p throughout the duct. Primary source at $z/L = 0$, control source at $z/L = 0.41$.

the pressure at a point $\vec{x}$ = $(0.1, 0.1, 0.84L)$, shown in Figure 4.3, and the acoustic potential energy throughout the duct, shown in Figure 4.4. The contours in Figure 4.3 are constant levels of the controlled pressure $|p(\vec{x})|^2$, for a range of control source volume velocities, while the contours in Figure 4.4 represent the sum of the squared pressure amplitudes at the six microphones located throughout the duct, for the same range of control source volume velocities. The primary source volume velocity is Q_p = $1.0e{-}4, 1.0e{-}4$ m^3/s. Comparison of the two figures reveals that the information provided to the controller by the two different error sensor strategies differs in that the optimum control source volume velocity for minimisation of the pressure at a point is given by Q_c = $1.08e{-}3, 1.08e{-}3$ m^3/s, while the optimum indicated to the controller by the acoustic potential energy estimate is Q_c = $9.18e{-}5, -1.09e{-}4$ m^3/s. Thus, although the controller may converge to the optimum value as indicated by the error sensor, it may not be the optimum value in terms of the stated objective or desired result.

The second duct arrangement considered was a finite length duct with both terminations almost fully reflective such that α_1, β_1 = $(0.05, 0.05)$ and α_2, β_2 = $(0.05, 0.05)$. The uncontrolled response for an excitation frequency of 600 Hz, allowing plane wave propagation only, is shown as the solid line in Figure 4.5. For an error sensor strategy of minimising the pressure at a point $\vec{x}$ = (0.1,0.1,2.678), the controlled response is shown as the dotted line, and indicates that good levels of reduction are achievable downstream of the control source. Equivalent levels of reduction, for an equivalent control source volume velocity, are realised for the error sensor strategies of minimisation of an estimate of the acoustic potential energy in the region downstream of the control source and also

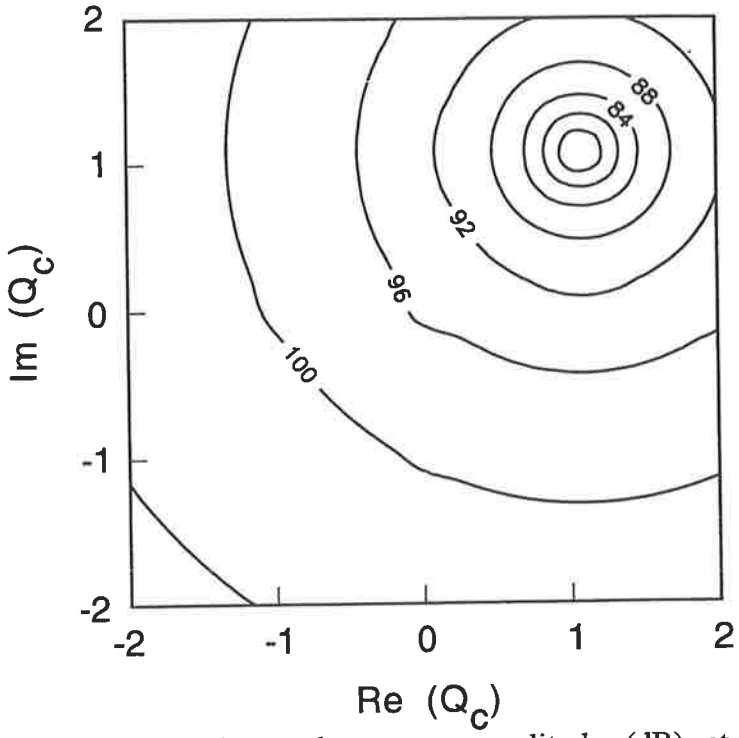

Figure 4.3 Contours of equal sound pressure amplitude (dB) at a point (x,y,z) = (0.1,0.1,0.84L), for a range of control source volume velocities, Q_c (×E-3), for a semi-infinite duct excited at 600 Hz.

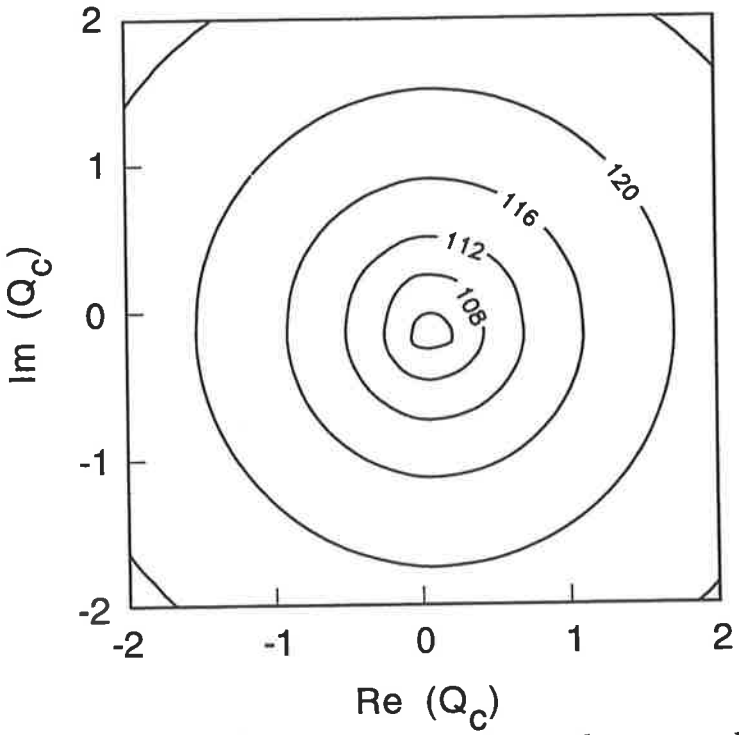

Figure 4.4 Contours of equal J_p (dB) for a range of control source volume velocities, Q_c (×E-3), for a semi-infinite duct excited at 600 Hz.

minimisation of the downstream power flow. Hence these three strategies are equivalent for this duct arrangement and excitation frequency. The strategy of minimising the total real acoustic power output of the primary and control sources, W, results in the controlled acoustic response shown by the dashed line in Figure 4.5. The curve reveals that only relatively small levels of reduction are achievable in comparison to the other strategies. This is because the real power output of the sources is associated with the inherent damping of the system, which in this case is small for α_1,β_1 and $\alpha_2,\beta_2 = (0.05,0.05)$. The majority of the power output is reactive, or imaginary, for this lightly damped case, and hence minimisation of the total real power output of the sources is an inappropriate strategy. Conversely, the first arrangement considered, a semi-infinite duct, is a heavily damped system and hence minimisation of the real power output of the sources is an appropriate strategy for that case.

The third arrangement considered is equivalent to the first test, a semi-infinite duct; however, the excitation frequency of 900 Hz allows three modes to propagate - the plane wave, (0,1) mode and (1,0) mode. The uncontrolled response is shown in Figure 4.6 as a solid line, while the controlled response for minimisation of the downstream power flow is shown as the dotted line. The pressure distribution over the duct cross-section is non-uniform because of the higher order mode propagation. The acoustic response shown in Figure 4.6 is thus the sound pressure calculated at a non-symmetric observer location $\vec{x} = (0.1,0.1)$ along the duct length. Calculated values of total power flow downstream of the control source are presented in Table 4.1 which summarises the results of all of the tests for each of the error sensor strategies. The values calculated for this duct

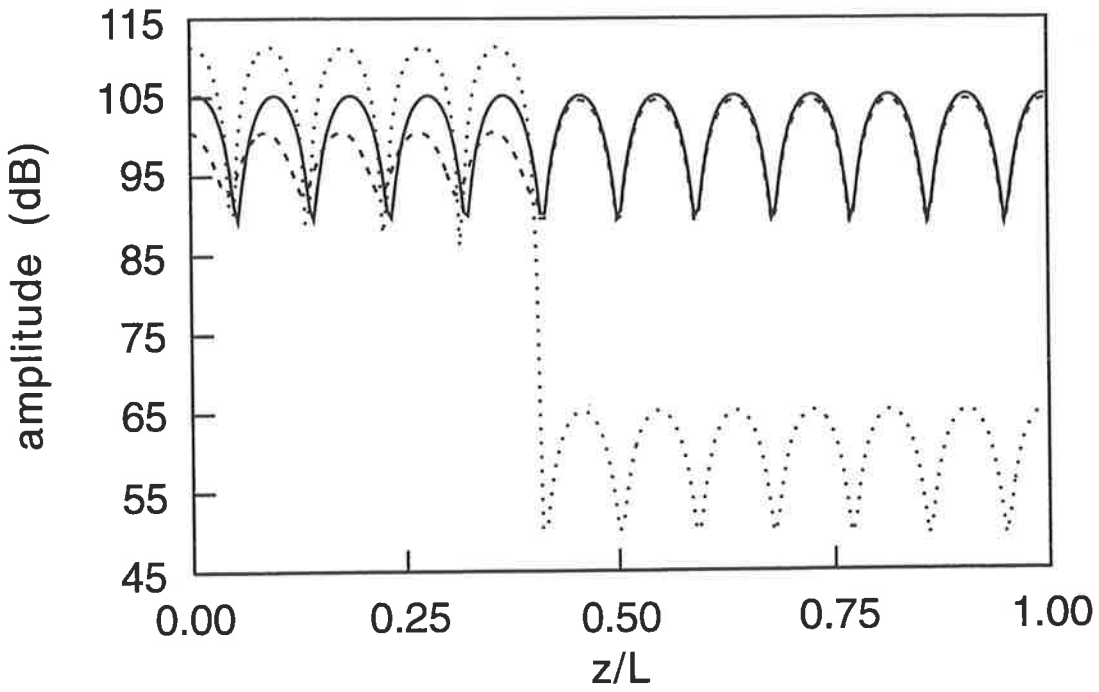

Figure 4.5 Sound pressure amplitude (dB) for a finite length duct at 600 Hz. —— uncontrolled; ····· minimisation of pressure at a point $(x,y,z) = (0.1,0.1,0.84L)$; — — minimisation of W. Primary source at $z/L = 0$, control source at $z/L = 0.41$.

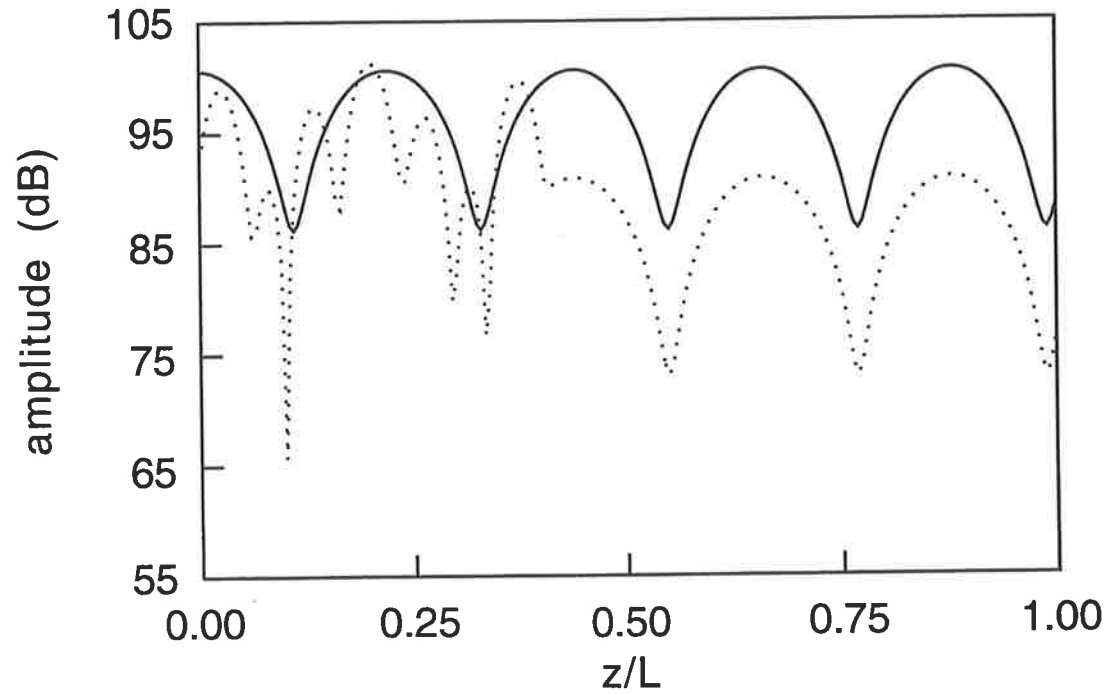

Figure 4.6 Sound pressure amplitude (dB) for a semi-infinite duct at 900 Hz. —— uncontrolled; — — controlled response for minimisation of total downstream acoustic power flow, W_d. Primary source at $z/L = 0$, control source at $z/L = 0.41$.

arrangement reveal that minimisation of the real power output of the sources, W, and the downstream power flow, W_d, give equivalent results for this damped system. The strategy of minimising the pressure at a point yields poorer levels of total power flow reduction for this case because the pressure at a single point is not a good estimate of the total power for higher order mode propagation. This result is indicated by the calculated values of power flow in Table 4.1. Hence, for frequencies at which higher order modes propagate, minimisation of the sound pressure at a point is not an appropriate strategy. The total power flow reduction obtained when the acoustic potential energy in the region downstream of the control source is minimised is less than that obtained by either of the power minimisation strategies. This may be because the six microphones used are insufficient to accurately estimate the acoustic potential energy in the region for higher order mode propagation.

As stated previously, the objective of the investigation was to determine the most effective error sensor strategy, for a fixed arrangement of primary and control sources. Thus the levels of power flow reduction obtained are relatively small for some of the test cases, but introduction of additional control sources can increase these levels. For the last test case examined, which was a semi-infinite duct excited at 900 Hz, introduction of an extra control source at an arbitrary location $\vec{x}_c = (0.05, 0, 0.58L)$ was found to decrease the level of the controlled response to 74.9 dB, a reduction of 15 dB, for the strategy of minimisation of downstream power flow. Addition of another source located at $\vec{x}_c = (0.19, 0, 0.46L)$ resulted in the controlled response being 49.9 dB for the same error strategy, a reduction in downstream power flow of 40 dB. Note that for a number of

Table 4.1

Total downstream acoustic power flow (dB) for uncontrolled and controlled response with each error sensor strategy.

Sensor Criterion	600 Hz semi-infinite	600 Hz finite length	900 Hz semi-infinite
uncontrolled	82.6	86.9	89.9
W	42.5	86.3	85.2
W_d	42.5	46.9	85.2
$\|p\|^2$	42.5	46.9	86.6
J_p (region)	42.5	46.9	86.0
J_p	82.7	85.8	86.0

control sources equal to the number of propagating acoustic modes, it is theoretically possible to completely attenuate the acoustic power flow downstream of the control sources. The maximum reduction achievable is limited to 40 dB here because of the quantisation errors inherent in the controller, which are taken into account in these simulations through the use of the controller efficiency factor. In addition, if the number of control sources is equal to or greater than the number of propagating modes, and if a number of error sensors, equal to or greater than the number of propagating modes, are located in a single cross-sectional plane of the duct, downstream of the control sources, then the minimisation of the sum of the pressures at the error sensors yields a result equivalent to minimisation of downstream power flow, W_d. This is provided that the effect of evanescent modes is negligible at the error sensor locations.

For frequencies at which the contribution of evanescent modes to the acoustic response is significant, the modal decomposition technique can be used to eliminate the effect of the evanescent modes from the error signal. For each dominant evanescent mode, an error sensor is required in both of the two cross-sectional planes used for the modal decomposition, in addition to those used to decompose the propagating acoustic modes.

For the following two simulation cases, the error sensors are located in a cross-sectional plane downstream of the control sources, as shown in Figure 4.7 for the case of multiple error sensors and multiple control sources. A finite size primary source is centred at $\vec{x}_p = (0.067, 0.067, 0)$, within a duct of cross-sectional dimension $b \times d = 0.215 \times 0.215$ m, and length $L = 5.843$ m. For details on the modelling of finite size sources see Chapter 2. The termination impedance parameter at $z = 0$, Φ_1, is given by: $\alpha,\beta = (0.02,0.25)$ for the (0,0) mode; $(0.02,0.30)$ for the (1,0) mode; and $(0.06,0.38)$ for the (0,1) mode. The duct is terminated at $z = L$ by an impedance equivalent to two 25 millimetre thick layers of Rockwool insulation, such that Φ_2 is given by: $\alpha,\beta = (0.11,0.71)$ for the (0,0) mode; $(0.18,0.64)$ for the (1,0) mode; and $(0.16,0.60)$ for the (0,1) mode. At an excitation frequency of 804 Hz only the plane wave propagates, but two evanescent modes, the (1,0) and (0,1) modes, contribute significantly to the acoustic response. A single finite size control source is centred at $\vec{x}_c = (0.075,0,z_c)$, and a single error sensor is located downstream of the control source at $(x,y,z) = (0.043,0.105,0.84L)$. For a strategy of minimisation of the pressure at the single error sensor, the resultant minimisation of the downstream power flow, W_d, is shown in Figure 4.8 as the dashed line, for a range of control source axial locations, z_c. For comparison, the levels of reduction in downstream

power flow achievable using a modal decomposition determination of W_d is shown as the solid line in Figure 4.8. The modal decomposition used three error sensors in each of two duct cross-sectional planes, to decompose the propagating (0,0) mode and the two dominant evanescent modes.

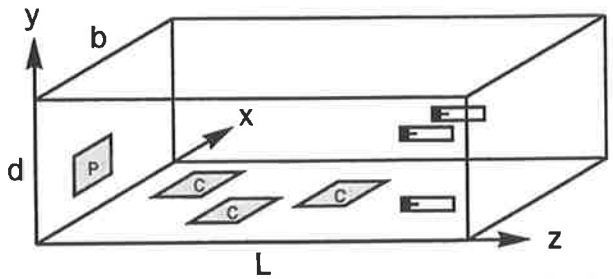

Figure 4.7 Source/sensor arrangement for minimisation of J_p downstream of control sources.

If the number of error sensors located in a single cross-sectional plane is made equivalent to the number of propagating modes plus the number of significantly contributing evanescent modes, namely three in this case, minimisation of the pressure at the error sensors is not equivalent to minimisation of the total downstream power, W_d. The primary and controlled values of J_p at the error sensors and W_d are shown in Table 4.2, for a control source axial location of z_c = 3.0 m. Table 4.2 reveals that for an error criterion of minimising J_p from the three sensors located in the same cross-sectional plane, a reduction in the downstream power flow of 6.3 dB is achievable. For an error criterion of minimising W_d, using the same arrangement of error sensors, but processing the signals to give the required minimisation function, the reduction in W_d increases to approximately 40 dB. Thus, although W_d may be reduced for an error criterion of minimisation of J_p, the level of reduction will not be equivalent to that obtained for the error criterion of minimisation of W_d.

Table 4.2

Values of minimisation functions (dB) for a configuration of three error sensors at 800 Hz

	minimisation of J_p	minimisation of W_d
J_p primary	96.6	96.6
J_p controlled	89.6	95.9
W_d primary	84.0	84.0
W_d controlled	77.7	44.0

At an excitation frequency of 1138 Hz, four acoustic modes contribute significantly to the acoustic response: the propagating (0,0), (1,0) and (0,1) modes; and the dominant (1,1) evanescent mode. Three control sources are located at $\vec{x}_{c_1} = (0.105, 0, 1.718)$, $\vec{x}_{c_2} = (0.140, 0, 2.393)$, and $\vec{x}_{c_3} = (0.075, 0, z_c)$. For minimisation of the sum of the pressures at three error sensors, located in the same cross-sectional plane downstream of the control sources, as shown in Figure 4.7, the resultant minimisation in W_d is shown in Figure 4.9 as the dashed line, for a range of axial locations, z_c, of the third control source. Also shown in Figure 4.9 are the levels of reduction in downstream power flow using a modal decomposition estimate of the downstream power flow. An arrangement incorporating four error sensors in each of two cross-sectional planes was used to decompose the three propagating and single evanescent modes. Thus, eliminating the effect of evanescent modes from the error sensor signal results in much greater levels of reduction in power flow than those achievable using the error sensor strategy of minimisation of the pressure at a number of points, equal to the number of propagating acoustic modes, as shown in Figures 4.8 and 4.9.

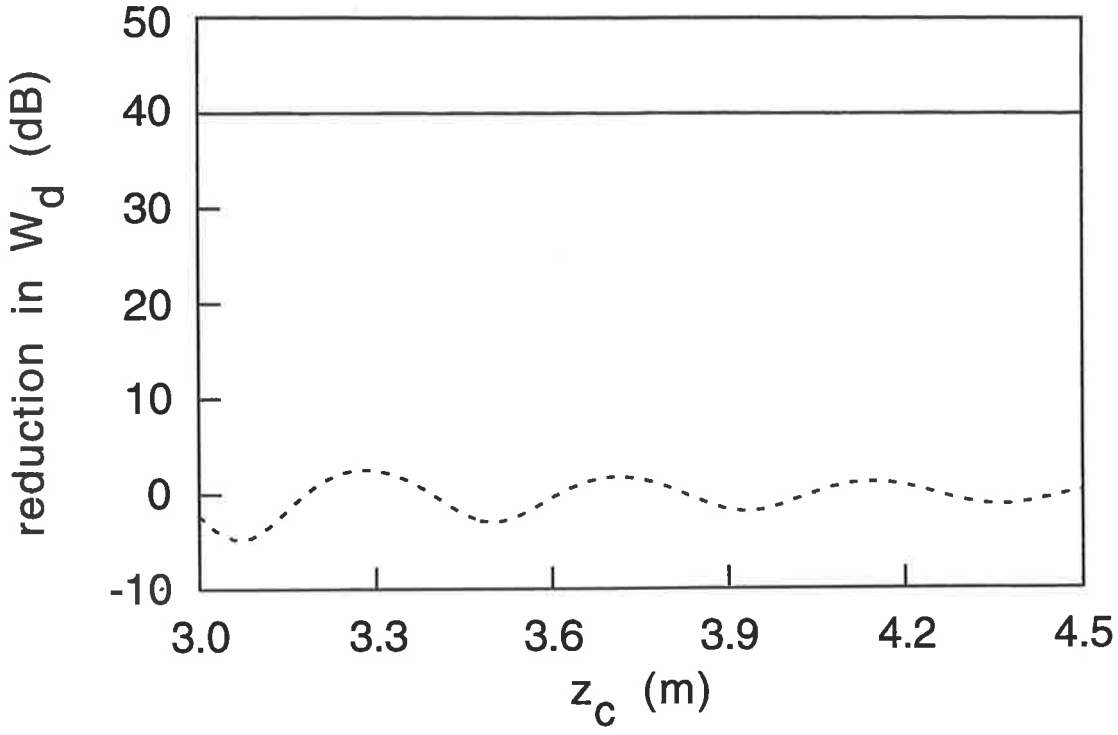

Figure 4.8 Reduction in downstream power flow, W_d, (dB) at 804 Hz using 1 control source. —— minimisation of W_d; – – minimisation of pressure at 1 error sensor located at (x,y,z) = (0.043,0.105,4.925).

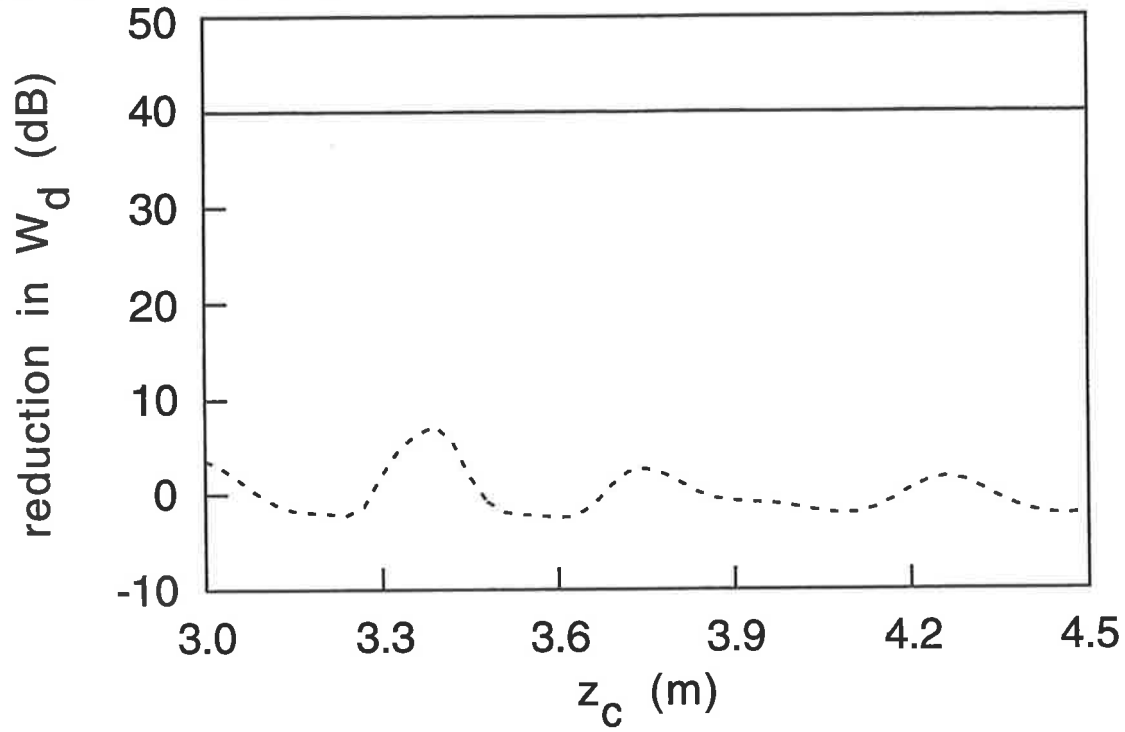

Figure 4.9 Reduction in downstream power flow, W_d, (dB) at 1138 Hz using 3 control sources. —— minimisation of W_d; – – minimisation of pressure at 3 error sensors located at (x,y,z) = (0.043,0.105,4.925), (0.045,0.191,4.925) and (0.170,0.192,4.925).

Table 4.3

Values of minimisation functions (dB) at 1138 Hz

	minimisation of J_p from 4 sensors in a single plane	minimisation of J_p from 4 sensors in each of two planes	minimisation of W_d
J_p primary	100.5	106.3	100.5
J_p controlled	90.0	98.5	104.2
W_d primary	80.5	80.5	80.5
W_d controlled	79.7	75.5	40.5

If the number of error sensors located in a single cross-sectional plane is equal to the number of propagating acoustic modes plus the number of significantly contributing evanescent modes, minimisation of J_p from the error sensors is not equivalent to minimisation of W_d. This is revealed in Table 4.3 which shows the values of the two minimisation functions, J_p and W_d, for the 1138 Hz case. In addition, if the number of error sensors is increased to eight, with four sensors located in one duct cross-sectional plane, and another four in a second cross-sectional plane; minimisation of J_p at the error sensors is not equivalent to minimisation of W_d, even though W_d is obtainable from the same arrangement of error sensors. The calculated results for the eight error sensor configuration are also shown in Table 4.3. The values in Table 4.3 indicate that minimisation of J_p at a number of error sensors equal to that required to perform a modal decomposition of an acoustic response which includes significant evanescent mode contribution, is not equivalent to minimisation of W_d. Thus, further processing of the signals obtained from the error sensors is necessary to provide an error signal proportional

to the downstream power flow, W_d.

4.4.2 Influence of control source location and number

Consideration will now be given to the influence of the location and number of control sources upon the effectiveness of active noise control applied to the rigid walled rectangular duct.

As stated, the objective is to minimise the propagating power, W_d, in the duct downstream of the control sources. The next case considered is for excitation frequencies at which only plane waves propagate and the effect of evanescent modes is negligible. A sensor/source configuration consisting of one control source and one error sensor is able to completely attenuate the sound field downstream of the control source, and the solution obtained by minimising the pressure at the single error sensor is equivalent to minimising the downstream power, W_d. For this configuration, the level of attenuation is independent of the value of the downstream termination impedance parameter, Φ_2, but not the upstream termination impedance parameter, Φ_1. The quadratically optimised control force will be a function of the upstream termination impedance parameter, Φ_1. For a given control source axial location, z_c, a number of values of Φ_1 will produce a nodal line at the control source. In a practical system, for these values of Φ_1, the level of reduction will be dependent on the volume velocity capability of the control source.

For excitation frequencies above the cut-on frequency of the first higher order mode, both the plane wave and higher order acoustic modes are able to propagate. For the duct of

square cross-section considered here, three acoustic modes may propagate: the plane wave, or (0,0) mode, and two higher order modes, the (1,0) and (0,1). From simulations it has been found that the number of control sources and the number of error sensors required for complete attenuation of downstream acoustic power are not independently determined. For a number of control sources equal to the number of propagating acoustic modes, the minimisation of the sum of the pressures at the error sensors, J_p, is equivalent to minimisation of W_d for the same number of error sensors located in a single cross-sectional plane of the duct. Again, this is provided that the effect of evanescent modes is negligible. The minimisation of J_p is also equivalent to minimisation of W_d for a number of error sensors greater than the number of propagating modes, or a number of control sources greater than the number of propagating modes, provided that the number of error sensors and the number of control sources is greater than or equal to the number of propagating modes. Although complete attenuation of downstream acoustic power is theoretically possible when the number of error sensors and control sources is equal to or greater than the number of propagating modes and the effect of evanescent modes is negligible, the maximum reduction achievable practically is limited to around 40 dB, because of quantisation errors inherent in the controller.

For a number of control sources less than the number of propagating acoustic modes, the pressure at the error sensor locations is not completely attenuated, for any number of error sensors greater than or equal to the number of propagating acoustic modes. This is shown in Figure 4.10 which displays the reduction in J_p for the required number of control sources, and for 1 control source only, for a range of axial locations, z_c, of one of the

control sources. Good agreement between the theoretical calculations and the experimental data is shown in the figure.

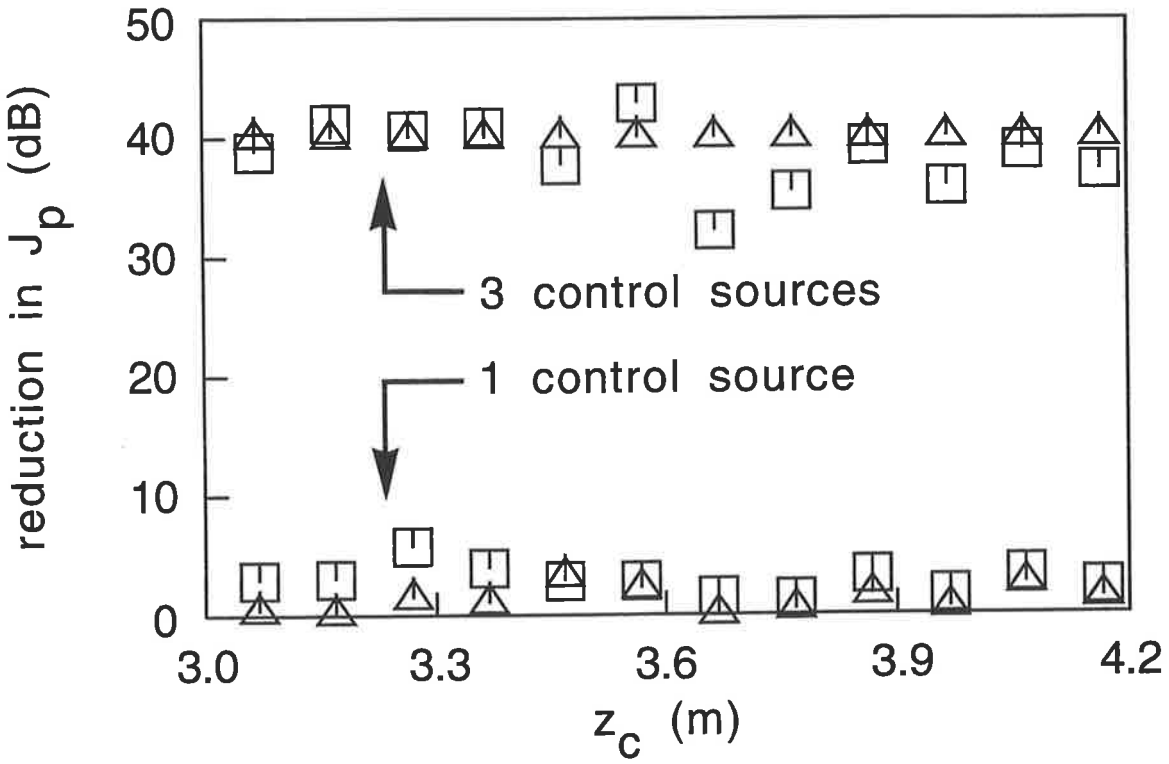

Figure 4.10 Reduction in J_p for 3 error sensors in a finite duct at 900 Hz, for a range of control source locations, z_c : ▵ theory; □ experiment.

As a further example that the number of error sensors and control sources required for attenuation of downstream acoustic power flow are not independently determined, using a number of error sensors less than the number of propagating modes, or not locating them in the same cross-sectional plane, will result in minimisation of J_p not being equivalent to minimisation of W_d, for any number of control sources. This is shown in Figure 4.11 for the case of 1 control source less than the number required, and in Figure 4.12 for the case of 2 control sources less than the number required.

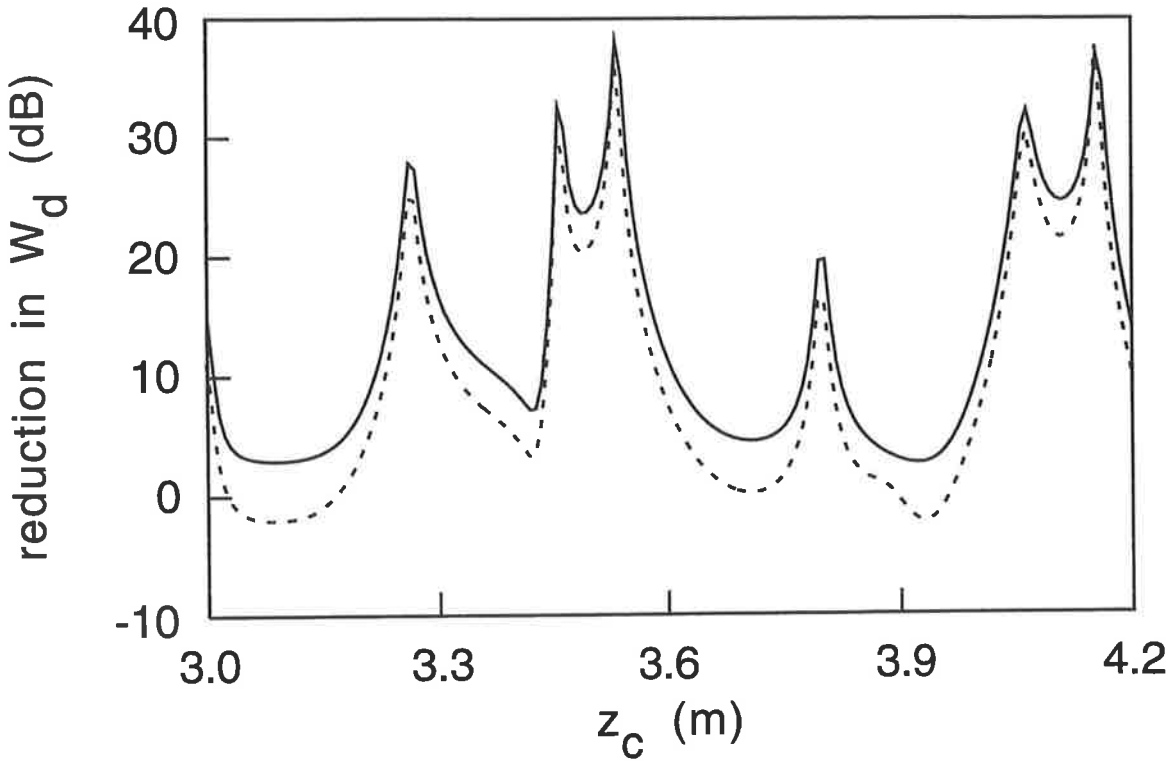

Figure 4.11 Reduction in W_d at 900 Hz for 2 control sources : —— minimisation of W_d ; – – minimisation of J_p.

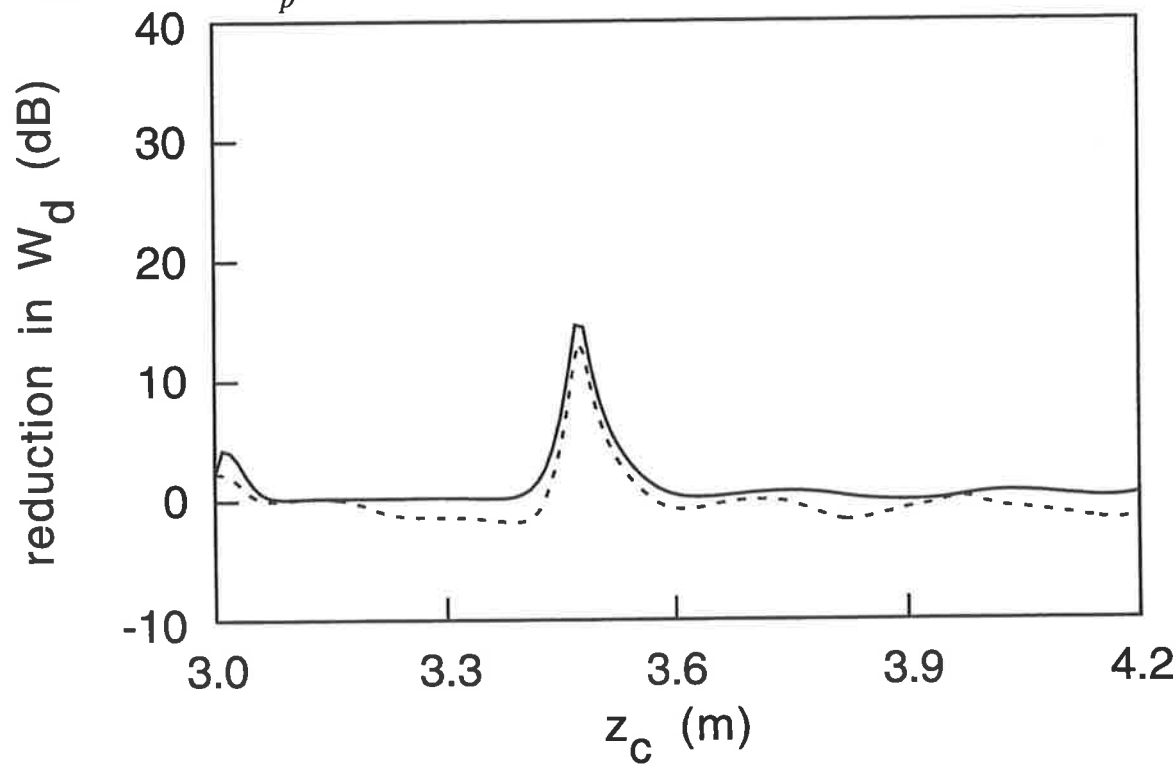

Figure 4.12 Reduction in W_d at 900 Hz for 1 control source : —— minimisation of W_d ; – – minimisation of J_p.

For a number of control sources equal to or greater than the number of propagating acoustic modes, a further simplification to the modal decomposition arrangement can be used as an error strategy to yield equivalent results to minimisation of downstream power flow, W_d. The simplification involves using a number of error sensors equal to the number of acoustic modes, located in a single cross-sectional plane of the duct. The acoustic response is then decomposed to yield the relative amplitudes of the various modes at that cross-section. Hence, the pressure matrix $[p]$ reduces to a $G \times 1$ matrix such that

$$[p]^T = \begin{bmatrix} p_1 & .. & p_G \end{bmatrix} \tag{4.25}$$

and $[\Omega]$, the modal response matrix, reduces to a $G \times G$ matrix, the elements of which represent the modal contributions to the pressure at each measurement location $\vec{x}_m$. Hence, row m of the matrix has the form

$$\begin{bmatrix} \Psi_0(\vec{x}_m) & .. & .. & \Psi_{G-1}(\vec{x}_m) \end{bmatrix} \tag{4.26}$$

and $\Psi_g(\vec{x}_m)$ is the normalised mode shape function of mode g at $\vec{x}_m$. The matrix, $[A]$ $(G \times 1)$, then contains the relative modal amplitude components at the duct cross-section of interest, which are made proportional to the acoustic power through multiplication by the selection matrix, $[S]$, which is given by

$$[S] = \begin{bmatrix} s_0 & & 0 \\ & \ddots & \\ 0 & & s_{G-1} \end{bmatrix} \tag{4.27}$$

Use of the simplified methodology will produce results equivalent to those shown by the solid lines in Figures 4.8 and 4.9.

In a practical system, the signals from the microphone array used for the modal decomposition would need to be processed at some stage to obtain an error signal proportional to the downstream acoustic power flow. This may be performed digitally within the feedforward adaptive controller assumed in this chapter, or prior to the controller input by a separate circuit. The details of such an implementation are beyond the scope of this thesis and hence will not be presented here.

4.5 CONCLUSIONS

The effect of geometric variables on the performance of active noise control systems has been examined. In addition, the structure of the acoustic response has been examined at a number of excitation frequencies, and for a number of error sensor and control source configurations. The particular excitation frequencies were chosen to include a broad range of possible acoustic response scenarios, including propagation of a single acoustic mode; propagation of a single acoustic mode together with dominant evanescent modes; and multiple propagating acoustic modes, with and without dominant evanescent modes.

Previous work (Stell, 1991) has shown significant variation in performance of active noise control systems with respect to frequency, for two fundamental reasons. One reason is the contribution of evanescent modes to the acoustic response measured at the discrete error sensor points. The second reason for variation of the performance with frequency is due to a combination of the excitation frequency and termination impedance values causing a nodal line at either the error sensor or control source locations.

Chapter 4. Effect of sensor/source configuration in ducts

In this chapter, general conclusions have been made based on the results obtained for one frequency in each frequency band of interest. This is possible because a method has been presented for eliminating the effect of evanescent mode contributions from the error sensor signal, thereby removing one of the reasons for frequency dependence of the performance. The second reason for frequency dependence was examined in Section 4.2.2.

The performance of the active noise control system for broadband excitation will be equivalent to the performance of the system at each of the excitation frequencies within the broadband excitation frequency range.

Five different error sensor strategies have been evaluated for the active control of plane wave and higher order mode propagation in a hard-walled rectangular duct with various termination conditions. These strategies were: minimisation of the squared pressure amplitude at a point; minimisation of the sum of the squared pressure amplitudes at a number of locations throughout the duct; minimisation of the sum of the squared pressure amplitudes at a number of locations downstream of the control source; minimisation of the total real acoustic power output of the primary and control sources; and a newly proposed technique of minimisation of the acoustic power flow downstream of the control source, as determined by modal decomposition of the duct sound field. From the results obtained using the five different error sensor strategies, the most appropriate strategy for minimising the sound field downstream of the control source was found to be minimisation of the downstream power flow, because an estimate of downstream power flow obtained from modal decomposition of the duct sound field was the most robust

technique in terms of varying excitation frequency and varying termination conditions. The downstream power flow estimate technique yielded levels of power flow reduction equal to or greater than the other error sensor strategies for all of the tests conducted.

For excitation frequencies at which the contribution of evanescent modes to the overall sound field in a duct is negligible, and for a sensor/source configuration consisting of a number of control sources and error sensors equal to the number of propagating acoustic modes, it has been found that minimising the sum of the pressures at the error sensors is equivalent to minimising the downstream power flow for a duct with any arbitrary termination conditions. This is provided that the error sensors are located in the same cross-sectional plane. If they are not located in the same cross-sectional plane, then minimisation of the sum of the pressures at the error sensors is equivalent to minimisation of an estimate of the acoustic potential energy in a region downstream of the control sources, which is not equivalent to minimisation of the downstream acoustic power flow. For excitation frequencies at which evanescent modes are significant, a modal decomposition can be used to eliminate the effect of evanescent modes from the error signal. For a number of control sources less than the number of propagating modes, a modal decomposition can be used to provide an error signal equal to the downstream power flow.

CHAPTER 5. STRUCTURAL/ACOUSTIC RESPONSE OF A CYLINDER WITH AN INTEGRAL FLOOR

5.1 INTRODUCTION

Various models have been proposed for describing the application of active noise control to the problem of low frequency propeller noise in aircraft (Bullmore et al., 1987; Silcox et al., 1987; Bullmore et al., 1990; Snyder, 1990). The majority of the theoretical models simplify the irregular geometries of a real aircraft fuselage by assuming that the structural response is that of a plain cylinder, and the acoustic response as that of the interior of a plain cylinder (Lester and Fuller, 1986; Bullmore, 1987; Silcox et al., 1987; Silcox et al., 1990; Bullmore et al, 1986). A number also further simplify the axial response of the structure and the acoustic space to be of infinite extent (Lester and Fuller, 1987; Silcox et al., 1989b).

Two main methods have been proposed for actively controlling the interior noise levels in aircraft fuselages, these being - the use of loudspeakers operating within the cabin to directly control the acoustic response, and thus reduce the interior noise levels; and the use of vibrational force inputs to the fuselage structure in a manner such that the resultant vibrational response of the fuselage causes the noise levels in the cabin to be reduced.

Use of control force inputs to a thin cylindrical shell has been theoretically modelled for the cases of minimising the structural vibrational energy (Thomas et al., 1993a), and minimising the acoustic potential energy within the cylinder (Thomas et al., 1993b).

Experimental work has also been undertaken which utilised control force input to plain cylinder structures (Fuller and Jones, 1987a; Thomas et al., 1988; Snyder et al., 1989; Mandic and Jones, 1989a; Mandic and Jones, 1989b), to minimise the acoustic pressure within the cylinder. A large number of publications have been presented which detail the mechanisms of active noise control in a plain cylinder (Lester and Fuller, 1987; Abler and Silcox, 1987; Jones and Fuller, 1987; Silcox and Lester, 1988; Lester, 1988; Jones and Fuller, 1989; Silcox et al., 1989a; Silcox et al., 1989b). The energy flows between the structure and the enclosed acoustic space have been investigated for cylindrical shells (Silcox et al., 1989a) under primary source excitation, and for actively controlled cylindrical shells (Silcox and Lester, 1988). The influence of the sensor and actuator location on the performance of active noise control systems has also been investigated experimentally for a plain cylinder (Fuller and Jones, 1987b). The feasibility of applying active control to an aircraft fuselage has been investigated for cabin sections in the laboratory (Legrain and Gorlain, 1988; Simpson et al., 1989), and by in-flight experiments (Elliott et al., 1989; Dorling et al., 1989; Elliott et al., 1990), using acoustic control sources to minimise the pressure at a head-height plane within the cabin. Demonstration tests of cabin noise reduction using vibration control sources have also been performed on a full-scale aircraft section (Simpson et al., 1991).

Although the use of a plain cylinder model allows a closed form analytical solution for the structural and acoustic modes, the ability of the method to accurately predict the sound pressure levels in a real aircraft fuselage is limited by the selective coupling between the structural and acoustic modes. For a structural/acoustic pair to have non-zero coupling the

circumferential indices of both modes must be equal, and in addition only structural modes with odd axial modal indices will couple with acoustic modes having even axial modal indices, and vice versa. Such selective coupling implies that the response of the acoustic space at a particular frequency would be dominated by relatively few structural/acoustic modal pairs. Comparison of propeller aircraft interior noise models and flight-tests (Pope et al., 1987b) have revealed, however, that for none of the cases examined was there a single highly dominating coupled pair, and that the five highest contributing pairs of modes accounted for only 25 to 50% of the total sound energy in the cabin. This indicates that the propeller tones are being transmitted by a rather large number of modal pairs. Use of a more complex model, which more closely represents an actual aircraft fuselage, having irregular geometry, is thus required.

To overcome the problem of selective coupling between plain cylinder structural and acoustic modes, models have been used which allow only a portion of the plain cylinder to excite the internal acoustic field (Thomas et al., 1993b). Similarly, other models use a modified response of a plain cylinder, which includes the structural effect of the floor as two lines of periodic forces on each side of the shell, located at the floor connections (Fuller, 1987).

The addition of a longitudinal floor partition to a plain cylinder has been shown to significantly alter both the structural response and the acoustic response from that of the plain cylinder (Fuller et al., 1992).

More complex models, describing the interior noise of propeller aircraft, which are based upon the original modal coupling approach used for plain cylinders (Pope, 1971; Pope et al., 1980; Pope and Wilby, 1982), have been presented. These models incorporate structures with stiffened ribbed panels, sidewall trim, and an acoustic response which includes the effect of a floor partition (Pope et al., 1983). Other predictive models for propeller aircraft interior noise also incorporate the structural response for a stiffened shell with a structurally integral stiffened floor partition (Pope et al., 1987a; Pope et al., 1987b). An advanced model for the prediction of propeller tone sound levels in an aeroplane cabin (Pope, 1990) has also been presented. The model is formulated for the case of a trimmed cabin of uniform cross-sectional area, terminating fore and aft with surfaces of finite acoustical impedance. In addition, the axial length of the acoustic region is considered to be different to that of the structure.

A more accurate prediction of the affect of active noise control on an aircraft fuselage may be achieved by incorporating a more complex model of the fuselage, such as those mentioned above, into the active control formulation (Snyder and Hansen, 1991).

A number of finite-element based models of a fuselage structure and an acoustic cabin volume, of various degrees of complexity (Unruh, 1981; Unruh and Dobosz, 1988; Green 1992), have been used to predict the structure-borne noise transmission into light aircraft. The use of such highly detailed finite-element models is generally prohibitive because of the high computational cost required to obtain a solution, with some models having a total number of degrees of freedom in excess of 400,000 (Green, 1992). Problems may also be

encountered at higher frequencies because of the limited resolution of the finite element meshes used in some of the models.

This study is thus confined to a structural model which incorporates a structurally integral longitudinal floor partition in a plain cylindrical shell, such that the influence of the floor upon the structural response is intrinsically accounted for. In addition, the acoustic response is considered to be that of the cabin space which has been modified from a plain cylinder due to the presence of the floor partition. For the model used in this study, the axial dimension of the acoustic space and the structure are taken to be equivalent, and the cabin terminations are assumed to be rigid. Use of such a model eliminates the need to account for the more complex axial acoustic mode shape functions associated with non-rigid cabin terminations, and simplifies the calculations for the correspondingly more complex coupling between the structural and acoustic modes.

It is the aim of the present study to extend the analyses performed for the plain cylinder models, and examine the influence of the error sensor and control source configuration and type upon the performance of active noise control systems applied to structures more representative of aircraft fuselages.

A point force primary excitation has been used in the investigation of the influence of control source and error configuration to simplify the analysis. While a primary excitation more representative of an aircraft propeller would yield results more representative of the actual levels of reduction achievable in a real aircraft for a given control source/error

sensor configuration, much can still be learnt about the mechanism of control and the effect of control source and error sensor arrangement on the achievable levels of reduction by using a simple point force primary input.

This chapter is thus concerned with a physical system consisting of a finite length cylinder with a structurally integral longitudinal floor partition, with the acoustic space enclosed by the structure. A model describing the response of this system to harmonic point force excitation is presented, where the system is modelled theoretically using modal coupling theory between the structure and the interior acoustic field. The structural mode shapes are determined using component mode synthesis, which combines the mode shape basis functions for the plain cylinder and the floor to obtain a mode shape function for the total structure. The two-dimensional acoustic mode shape functions are found using a finite difference implementation of the Helmholtz equation, while the axial acoustic mode shape function is equal to that of a rigid-walled one-dimensional enclosure. Experimental work on a test structure is presented and the results compared with a number of theoretical predictions.

In the latter part of this chapter, a formulation for the optimal control forces required to achieve minimisation of a number of error sensor criteria is given for the modelled structure. Experimental and theoretical results are presented for the application of active noise control to the coupled structural/acoustic system.

The formulation for active control of the cylinder with an integral floor presented in this

chapter is utilised in Chapter 6 to investigate the influence of error sensor and control source configuration and type upon the effectiveness of active noise control applied to the structure via vibrational point forces.

5.2 THEORETICAL FORMULATION FOR STRUCTURAL MODE SHAPES

This section is concerned with presenting formulations for the structural mode shapes, resonance frequencies, and modal mass of a finite length cylinder with a structurally integral longitudinal floor. The structural mode shapes for a cylinder with an integral floor were determined by the method of component mode synthesis (Hurty, 1965; Peterson, 1973; Peterson and Boyd, 1978). Separate displacement functions are assumed for the cylinder and the floor plate. Compatibility of displacement and rotation at the junction of the cylinder and the floor is enforced by constraint equations. The equations of motion for the shell are based on Love's shell theory, and those for the plate are from classical thin plate theory. The geometry and co-ordinate systems are shown in Figure 5.1.

The displacement functions are assumed to be a finite series, each term being a product of the longitudinal mode shape function, the cross-sectional mode shape function, and the modal amplitude. Thus for the shell the displacement in the radial direction is given by

$$w_s = \sum_{m=0}^{m^*} \sum_{n=0}^{n^*} W_{mn}^s X_{wm}(x) \psi_{wn}(\theta) \tag{5.1}$$

and similarly for the axial displacement, u_s, and the transverse displacement, v_s. For a longitudinal modal index m, and a circumferential modal index n, $X_{wm}(x)$ is the longitudinal mode shape function, $\psi_{wn}(\theta)$ is the cylinder circumferential mode shape

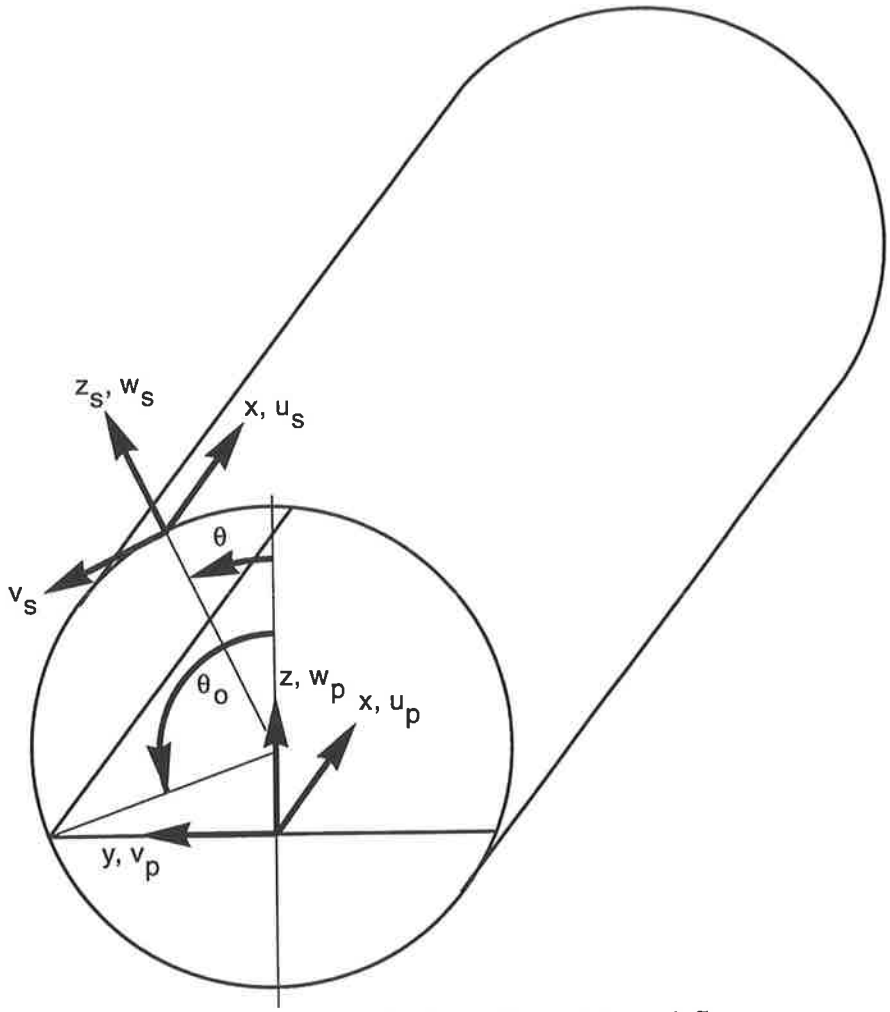

Figure 5.1 Geometry of a circular cylinder with an integral floor.

function, and W_{mn}^{s} the component modal amplitude, or generalised co-ordinate. For the plate, the out of plane displacement is given by

$$w_p = \sum_{m=0}^{m^*} \sum_{n=0}^{n^*} W_{mn}^{p} X_{wm}(x) \xi_{wn}(y) \tag{5.2}$$

and similarly for axial displacement, u_p, and transverse displacement, v_p. $\xi_{wn}(y)$ is the plate transverse mode shape function, and W_{mn}^{p} the component modal amplitude, or generalised co-ordinate. The longitudinal mode shape functions are the same for the plate and the shell, because the support conditions at the terminations are equivalent for the

simply supported case considered here, and are given by

$$X_{um}(x) = \cos\left(\frac{m\pi x}{L}\right) \tag{5.3}$$

$$X_{vm}(x) = \sin\left(\frac{m\pi x}{L}\right) \tag{5.4}$$

$$X_{wm}(x) = \sin\left(\frac{m\pi x}{L}\right) \tag{5.5}$$

where L is the axial length of the cylinder or floor, which are taken to be equivalent in this analysis.

The cylinder circumferential mode shape functions for symmetric modes are

$$\psi_{un} = \cos(n\theta),\ \psi_{vn} = \sin(n\theta),\ \psi_{wn} = \cos(n\theta) \tag{5.6}$$

and, for anti-symmetric modes

$$\psi_{un} = \sin(n\theta),\ \psi_{vn} = -\cos(n\theta),\ \psi_{wn} = \sin(n\theta) \tag{5.7}$$

The plate transverse functions for symmetric modes are

$$\xi_{un} = \cos\left(\frac{n\pi y}{2b}\right),\ \xi_{vn} = \sin\left(\frac{n\pi y}{2b}\right),\ \xi_{wn} = \cos\left(\frac{n\pi y}{2b}\right) \tag{5.8}$$

and, for anti-symmetric modes

$$\xi_{un} = \sin\left(\frac{n\pi y}{2b}\right),\ \xi_{vn} = -\cos\left(\frac{n\pi y}{2b}\right),\ \xi_{wn} = \sin\left(\frac{n\pi y}{2b}\right) \tag{5.9}$$

where b is equal to half the floor width.

Defining a vector of generalised co-ordinates of the shell, $\{q_{sm}\}$, as

$$\{q_{sm}\} = \left[U_{m0} \cdots U_{mn*}, V_{m0} \cdots V_{mn*}, W_{m0} \cdots W_{mn*}\right]^T \tag{5.10}$$

it is possible to express the equation of motion for the shell only, for a particular longitudinal mode m, as

$$[M_{sm}]\{\ddot{q}_{sm}\} + [K_{sm}]\{q_{sm}\} = \{0\} \tag{5.11}$$

where $[M_{sm}]$ is the cylinder mass matrix, and $[K_{sm}]$ the cylinder stiffness matrix, the elements of which are determined using Love's shell theory. Detailed expressions for the elements of $[M_{sm}]$ and $[K_{sm}]$ are given in Appendix A. For harmonic excitation at frequency ω, the equation of motion can be expressed as

$$\left([K_{sm}] - \omega^2[M_{sm}]\right)\{q_{sm}\} = \{0\} \tag{5.12}$$

Solution of this eigenvalue problem yields the eigenvalues, λ_i, which are proportional to the natural frequencies of the cylinder, and the eigenvectors which describe the shell mode shape functions in terms of the generalised co-ordinates.

Similarly the natural frequencies and mode shapes of the floor plate only can be found by solving the eigenvalue problem

$$\left([K_{pm}] - \omega^2[M_{pm}]\right)\{q_{pm}\} = \{0\} \tag{5.13}$$

where $\{q_{pm}\}$ is the vector of generalised co-ordinates for the plate, and $[M_{pm}]$ and $[K_{pm}]$ the plate mass and stiffness matrices for a particular longitudinal mode m. Detailed expressions for the elements of $[M_{pm}]$ and $[K_{pm}]$ are given in Appendix B.

To determine the natural frequencies and mode shapes of the combined shell/plate structure, constraint equations are imposed such that the shell displacements and rotations at the joint are equal to those of the plate at the joint. The constraint equations for a rigid joint between the floor and the shell of radius a are given by

$$u_s - u_p = 0 \tag{5.14}$$

$$v_s \cos(\theta_o) + w_s \sin(\theta_o) - v_p = 0 \tag{5.15}$$

$$-v_s \sin(\theta_o) + w_s \cos(\theta_o) - w_p = 0 \tag{5.16}$$

$$\frac{v_s}{a} - \frac{1}{a}\frac{\partial w_s}{\partial \theta} + \frac{\partial w_p}{\partial y} = 0 \tag{5.17}$$

For the case of a hinged joint between the shell and the floor, rotation compatibility is not enforced, and only the first three, of the above four, constraint equations are used.

It should be noted that the constraint equations presented here differ from those used by Peterson and Boyd, which appear to be inconsistent with the common sign convention, and would have the effect of equating the upwards displacement of the floor to the downwards displacement of the cylinder for floor angles, θ_o, greater than 90°, where the floor angle is measured from the upper vertical.

The constraint equations can be expressed in matrix form as

$$[C]\{q\} = \{0\} \tag{5.18}$$

where $\{q\}$ is the combined vector of generalised co-ordinates for the cylinder and the

plate, and $[C]$ the matrix of constraint terms. The components of $\{q\}$ are not independent because of the introduction of the constraint equations. It is possible to partition $\{q\}$ into a set of independent co-ordinates, $\{q_1\}$, and dependent co-ordinates, $\{q_2\}$, such that

$$[C_1 \vdots C_2]\begin{Bmatrix} q_1 \\ \cdots \\ q_2 \end{Bmatrix} = \{0\} \tag{5.19}$$

provided the subsets are chosen so that $[C_2]$ is non-singular.

The separate eigenvalue problems for the cylinder alone and the plate alone can be transformed to a suitable eigenvalue problem for the combined structure through the transformation

$$[M] = [E]^T[M_{s/p}][E] \tag{5.20}$$

$$[K] = [E]^T[K_{s/p}][E] \tag{5.21}$$

where $[E]$ is the transformation matrix given by

$$[E] = \begin{bmatrix} I \\ \cdots\cdots\cdots \\ C_2^{-1}C_1 \end{bmatrix} \tag{5.22}$$

and $[M_{s/p}]$ and $[K_{s/p}]$ are the combined mass and stiffness matrices formed by the separate shell and plate component partitions. Hence, the eigenvalue problem for the combined structure becomes

$$\left([K]-\omega^2[M]\right)\{q_1\} = \{0\} \tag{5.23}$$

The mode shapes obtained for the combined structure are normalised by the modal mass

constant, M_r. For the combined structure the modal mass includes all energy in both the cylinder and the floor, and is thus defined as

$$M_r = \int_0^L \int_0^{2\pi} \rho_s h_s \left(u_s^2 + v_s^2 + w_s^2 \right) a \, d\theta \, dx + \int_0^L \int_{-b}^{b} \rho_p h_p \left(u_p^2 + v_p^2 + w_p^2 \right) dy \, dx \qquad (5.24)$$

for a shell of density ρ_s and thickness h_s, and a plate of density ρ_p and thickness h_p. The modal generalised co-ordinates of the shell and plate are given by u_s, v_s, w_s, u_p, v_p, and w_p. Thus, if a particular mode of the combined structure is predominantly a floor mode, the modal mass will be dominated by the second term in equation (5.24), and approximately equal to the modal mass of the floor only. Similarly, a mode with predominant shell motion will have a modal mass approximately that of the shell only.

5.2.1 Verification of natural frequencies for components

The natural frequencies for the cylinder only were calculated using equation (5.23), and compared with results calculated using a dynamic stiffness technique (Langley, 1992), and exact results (Webster, 1967). These are shown in Table 5.1 for a simply supported cylinder.

The level of agreement between the results is excellent. The present results were obtained using a finite series approximation of the displacement function, extending from $n = 0$, for both the anti-symmetric and symmetric terms. Hence, the cylinder displacement series used for calculating the mode shapes of the combined structure also include $n = 0$ terms for both the anti-symmetric and symmetric terms.

Table 5.1

Natural frequencies $\Omega = a\omega[\rho(1-\nu^2)/E]^{1/2}$ of a simply supported cylinder with $b/a = 4$, and $h/a = 0.05$

Mode (m,n)	Present Method	Webster	Langley
1 0	0.4647	0.4647	0.4647
1 1	0.2570	0.2570	0.2569
1 2	0.1217	0.1215	0.1211
1 3	0.1308	0.1305	0.1302
2 0	0.9289	0.9284	0.9289
2 1	0.5737	0.5738	0.5735
2 2	0.3348	0.3345	0.3341
2 3	0.2404	0.2398	0.2391

The natural frequencies of the floor plate only were compared with the classical plate theory for a simply supported plate (Leissa, 1969) and agreed exactly. The plate displacement series used for calculating the mode shapes of the combined structure include $n = 0$ terms for both the anti-symmetric and symmetric cases. It should be noted that the plate is simply supported at the ends only, while the edges forming a junction with the cylinder are constrained according to the constraint equations. The $n = 0$ terms in the displacement series for the plate thus correspond to beam mode bending of the plate.

5.2.2 Verification of natural frequencies for combined structure

The natural frequencies for the cylinder with an integral floor were compared with those calculated by Peterson and Boyd, who used the same methodology, and also with those

calculated by the dynamic stiffness technique (Langley, 1992). The results for a combined structure with a rigid joint, having both floor and shell simply supported at the ends, are shown in Table 5.2.

Table 5.2

Natural frequencies $\Omega = a\omega[\rho(1-\nu^2)/E]^{1/2}$ of a simply supported cylinder with an integral floor : a = 0.254 m, $h_s = h_p$ = 0.00508 m, L = 1.27 m, and floor angle, θ_o = 115°

Mode	Present Method	Peterson and Boyd	Langley
symmetric modes			
1	0.0368	0.0367	0.0321
2	0.0712	0.0693	0.0713
3	0.0960	0.0939	0.0949
4	0.1166	0.117	0.116
5	0.1743	0.167	-
6	0.2207	0.219	-
anti-symmetric modes			
1	0.0623	0.0625	-
2	0.0820	0.0828	-
3	0.1061	0.103	-
4	0.1349	0.133	-
5	0.1668	0.163	-
6	0.2104	0.210	-

Detailed plots of the mode shapes were found to be in qualitative agreement with those presented previously. It should be noted that a direct comparison with Peterson and Boyd's

work is not possible because of the afore-mentioned inconsistencies in the constraint equations, and also because they have used only the odd numbered floor basis functions in the displacement series for the symmetric modes, and even numbered floor basis functions only for the anti-symmetric modes. As a result, additional modes to those previously presented have been determined using the present analysis. Allowing for the inconsistencies outlined, the results are seen to be in reasonable agreement with those presented previously. In the present analysis, the displacement series for each of the floor components included a minimum of eight terms, and that for the shell a minimum of 14 terms, yielding an eigenvalue problem for the combined structure of at least 64 degrees of freedom.

5.3 RESULTS FOR TEST STRUCTURE

The method for determining the structural mode shapes of the combined structure, outlined above, was applied to a test structure consisting of a stainless steel cylinder of dimension L = 3 m, a = 0.450 m, and h_s = 0.001 m, into which a floor of equivalent length, thickness and material properties was inserted at a floor angle, θ_o, of 140 degrees. The junction between the shell and floor was modelled as a rigid joint. The material properties of stainless steel used for the calculations were: Young's modulus, E = 205 GPa; density, ρ = 7930 kg/m^3; and Poisson's ratio, ν = 0.30. For the case of axial mode number m = 1, the first six theoretical symmetric modes and their corresponding natural frequencies are shown in Figure 5.2, while the first six theoretical anti-symmetric modes are shown in Figure 5.3.

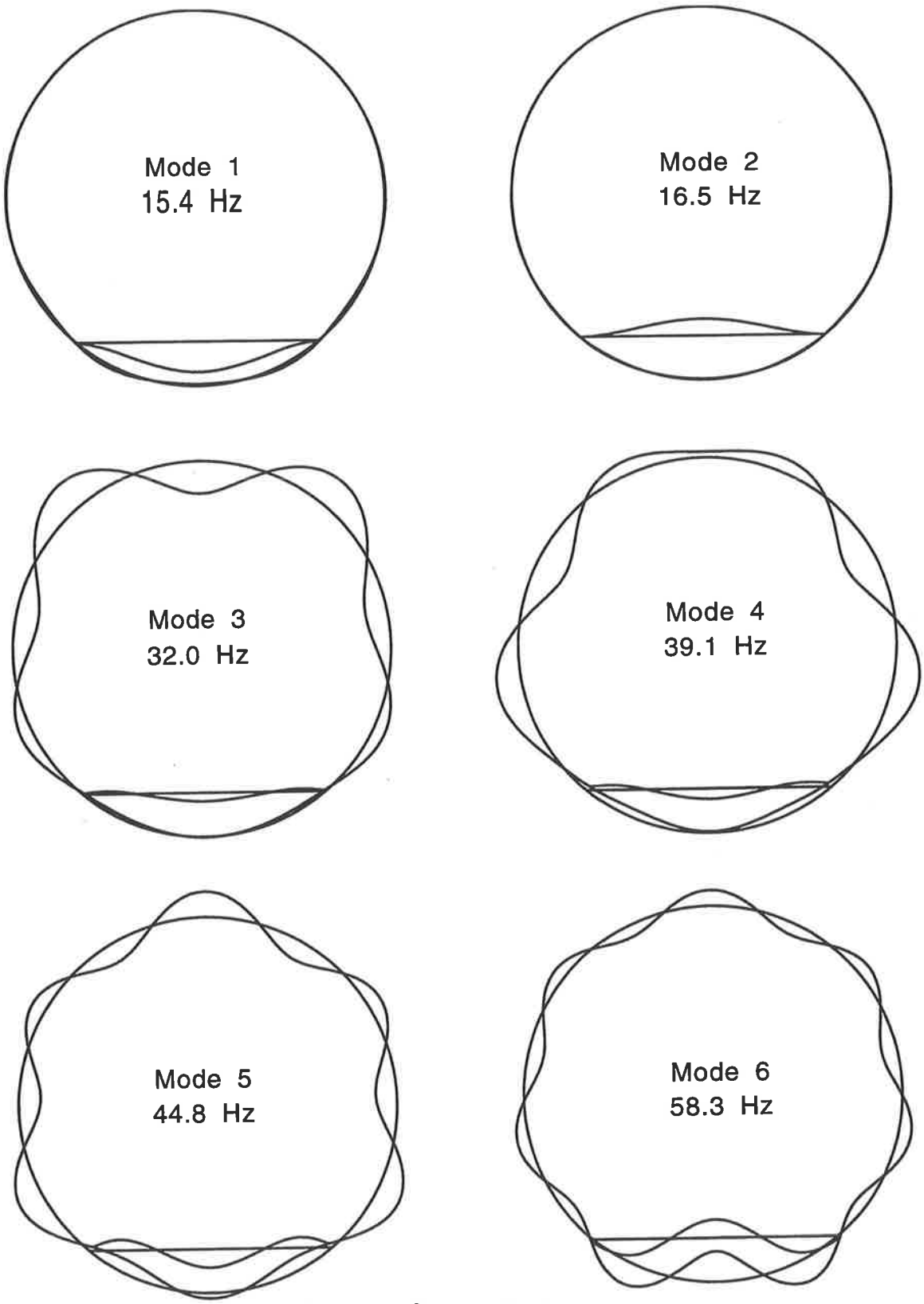

Figure 5.2 Symmetric mode shapes for test structure.

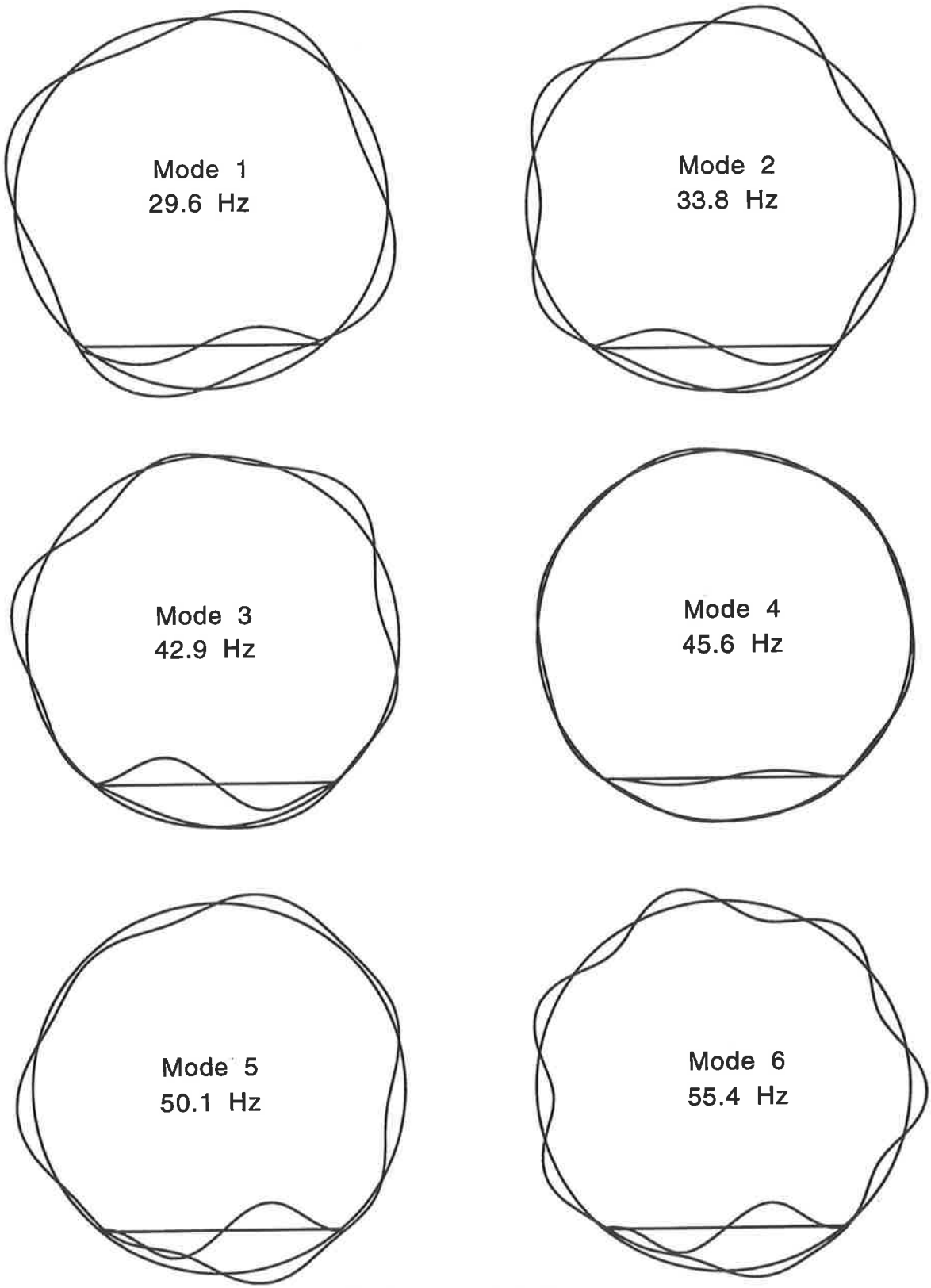

Figure 5.3 Antisymmetric mode shapes for test structure.

The three types of structural modes generated for the combined structure are : modes with predominantly floor motion and negligible shell motion; modes with negligible floor motion and predominant motion of the shell; and modes with a combination of shell and floor motion of varying degrees.

5.3.1 Comparison of theoretical analysis and experimental modal analysis

The junction between the shell and floor was constructed to approximate a rigid joint by joining the two components with an angled steel shim, as shown in Figure 5.4.

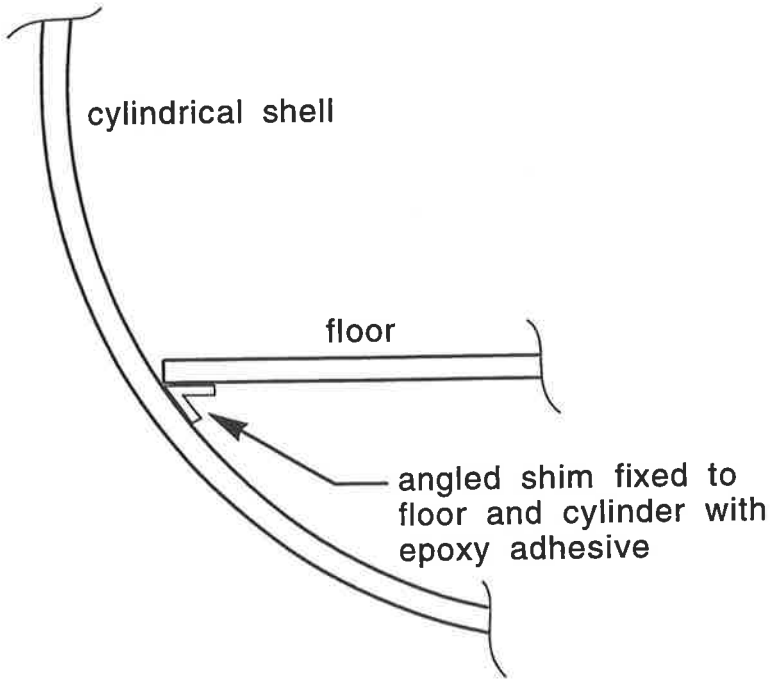

Figure 5.4 Rigid cylinder/floor joint construction.

The test structure is terminated at each end by a rigid end cap, constructed of 28 mm (1.25 in.) thick particle board. A narrow groove, lined with a soft rubber strip, is used to locate the end caps relative to the shell and floor. The shell structure and the end caps are restrained by four tensioned rods connected between the two end caps, as shown in Figure 5.5. This arrangement limits the displacement of the structure at the supports, while

allowing rotational motion of the structure, which is felt to provide a reasonable approximation to simply supported conditions.

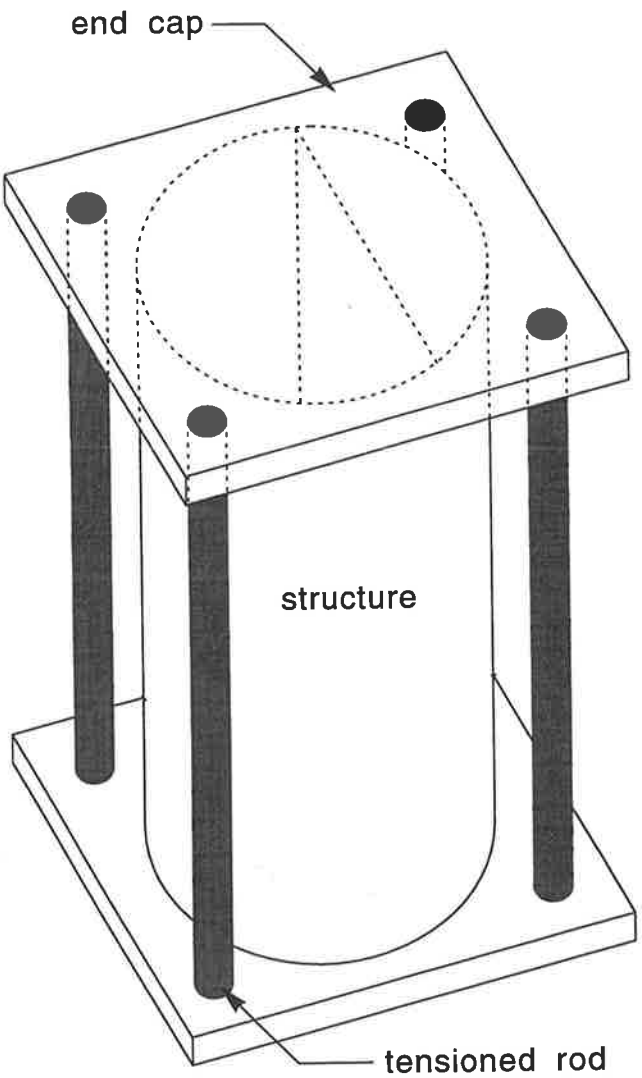

Figure 5.5 Experimental structure support arrangement.

An experimental modal analysis was performed on the combined structure using the line-point model shown in Figure 5.6. The assumed cross-sectional symmetry of the structure, and its assumed uniformity in the axial direction, allowed the use of such a model. This model enabled a considerably smaller number of data points to be used than a complete grid-point model, which would require data to be obtained at points distributed over a grid encompassing the entire surface of the shell and the floor. The use of a full grid-point

model would also present difficulties in obtaining all data points from the floor portion of the enclosed structure. The data for the floor portion of the line-point model was collected by access through a removable portal in one of the end caps.

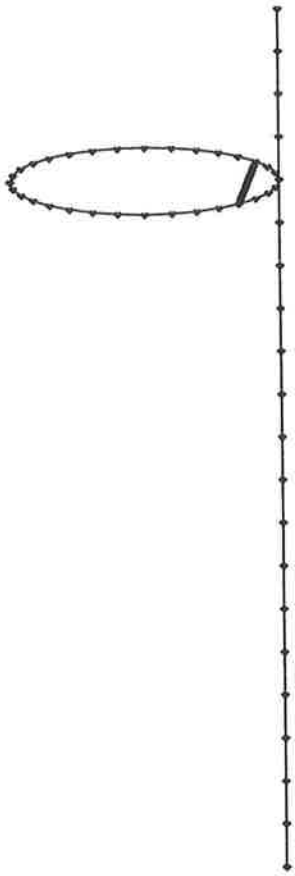

Figure 5.6 Line-point model used for modal analysis of test structure.

A selection of the cross-sectional mode shapes and natural frequencies calculated by the theoretical analysis, and those obtained by experimental modal analysis, are shown in Figure 5.7.

Good qualitative agreement can be seen between the mode shapes produced by the two analyses. The theoretical analysis tends to overestimate the natural frequencies, and this is thought to be due to the joint between the shell and floor not being completely rigid, as

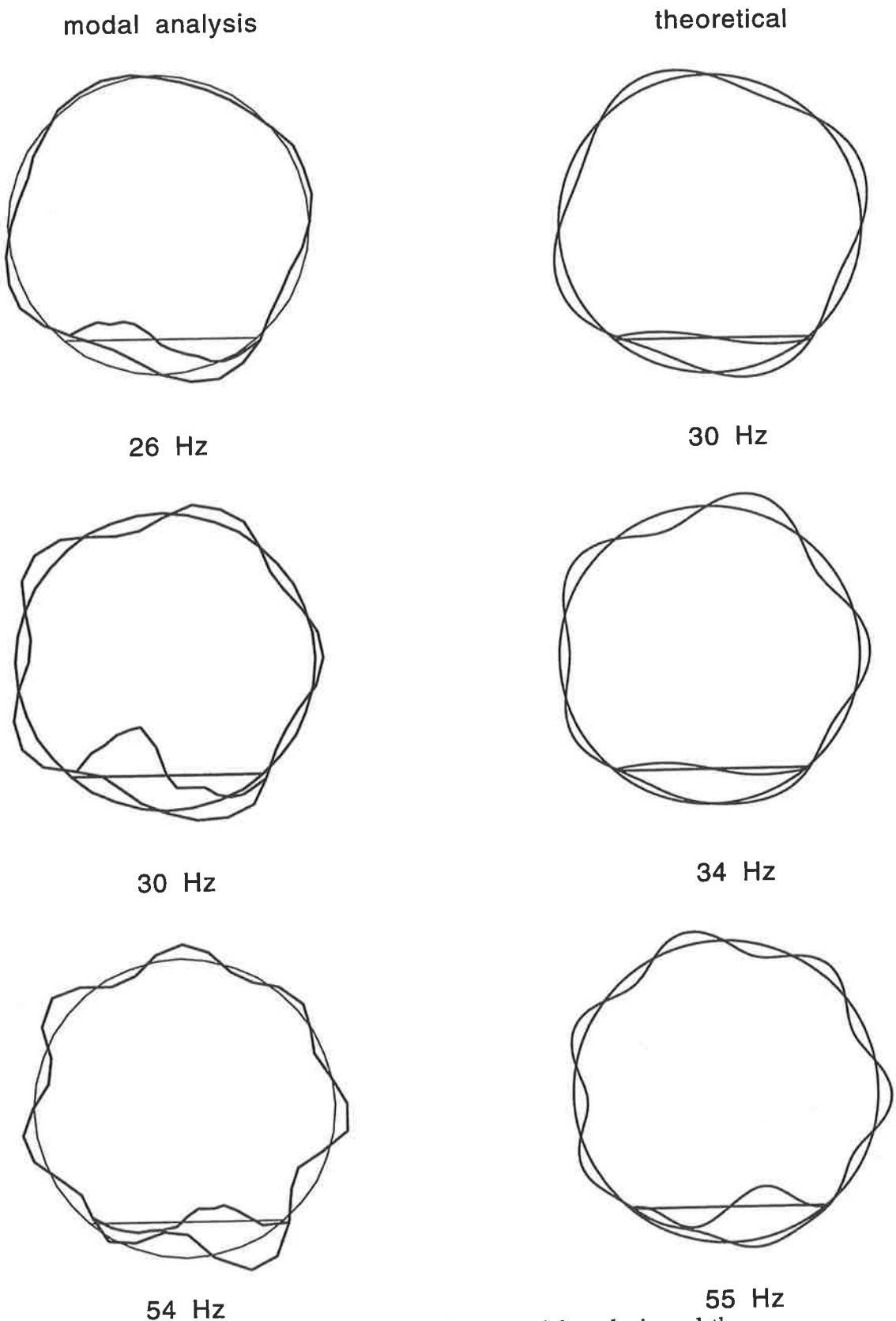

Figure 5.7 Cross-sectional mode shapes from modal analysis and theory.

modelled in the theory. The corresponding axial mode shapes obtained by modal analysis are shown in Figure 5.8. The mode which is resonant at 54 Hz has an axial response which deviates from that predicted theoretically. This is due to inhomogeneities caused by the welding process used for construction of the test structure. These inhomogeneities have not been accounted for in the theoretical model.

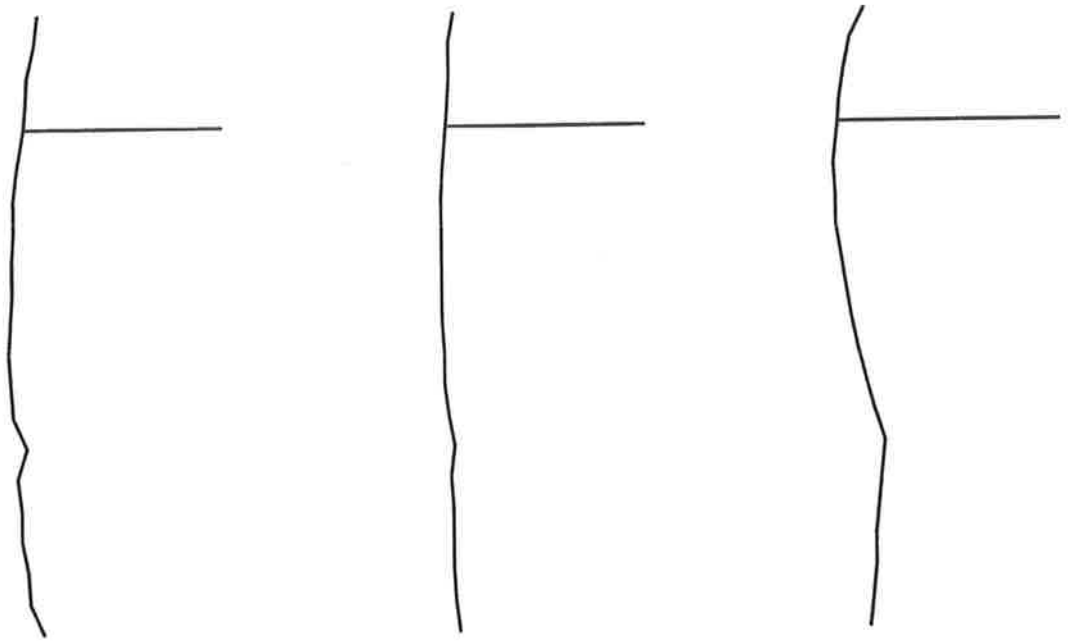

Figure 5.8 Axial mode shapes from experimental modal analysis.

The total structural loss factor, η_r, is the sum of two components, one accounting for dissipation in the structure (*in vacuo*) and the other the radiation losses. Hence (Pope et al., 1987a)

$$\eta_r = \eta_r^{struc} + \eta_r^{rad} \tag{5.25}$$

The total structural loss factor, η_r, was determined by measuring the transfer function between an accelerometer, non-symmetrically located on the structure, and a random point force excitation, provided by a non-symmetrically located electro-dynamic shaker. The loss

factor value was calculated from the quality factor of the resonance peaks. The modally-averaged structural loss factor was found to be $\eta_r = 0.05$. Alternatively, the portion of the structural loss factor due to external radiation losses, η_r^{rad}, which is frequency dependent, can be determined theoretically (Pope et al., 1987a).

5.4 THEORETICAL FORMULATION FOR ACOUSTIC MODE SHAPES

This section is concerned with presenting a theoretical formulation for the acoustic mode shapes, resonance frequencies and acoustic mode normalisations for the acoustic space enclosed by a finite length cylinder with a structurally integral longitudinal floor, which is terminated by rigid end caps. The acoustic response of the three-dimensional space enclosed by the cylinder, floor and end caps was modelled using the finite-difference implementation of the Helmholtz equation (Pope, 1987a). Only the portion of the acoustic space above the floor was modelled, because the acoustic space below the floor would only have a significant response at higher frequencies, and because of the weak modal coupling assumed between the structure and the acoustic space, this second acoustic space would contribute little to the response of the cabin region considered in the analysis. A closed form analytical solution of the wave equation is not possible for the volume bounded by the cylinder with floor structure because of the irregular geometry of the boundary conditions. A finite difference approach was taken because the acoustic mode function in the axial direction is known, being that of a one dimensional enclosure for an axially uniform acoustic space. The finite-difference method was also chosen as it is simpler to implement than the finite element method for this case.

The two-dimensional Helmholtz equation for the acoustic space can be expressed, with central differences, as (Pope, 1983)

$$4P_{m,n} - P_{m+1,n} - P_{m-1,n} - P_{m,n+1} - P_{m,n-1} = k^2 h^2 P_{m,n} \tag{5.26}$$

where $P_{m,n}$ is the pressure at each grid point, h the grid spacing, and k the acoustic wavenumber in the enclosure. The grid co-ordinate specification is shown in Figure 5.9.

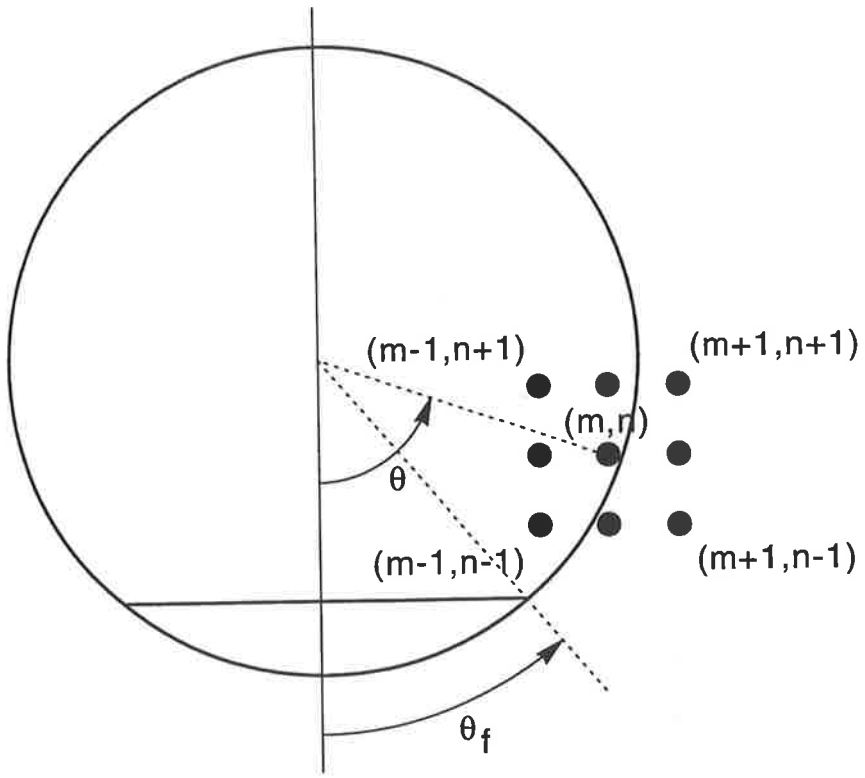

Figure 5.9 Grid co-ordinate specification.

The boundary condition for the surrounding structure is that the outward normal gradient is zero. The wall admittance, β, is thus considered sufficiently small to allow this assumption. This boundary condition can be expressed as

$$\left(P_{m,n+1} - P_{m,n-1}\right)\cos(\theta_{mn}) = \left(P_{m+1,n} - P_{m-1,n}\right)\sin(\theta_{mn}) \tag{5.27}$$

for $\theta_f < \theta < 2\pi - \theta_f$, and

$$P_{m,n+1} - P_{m,n-1} = 0 \tag{5.28}$$

for $-\theta_f < \theta < \theta_f$. θ_{mn} describes the angular location of grid point (m,n). In contrast to the angular convention used in the expressions describing the structural response, where θ is measured from the upper vertical, the acoustic formulation uses a convention where θ is measured from the lower vertical. Hence a structure with floor angle θ_o, measured from the upper vertical, will enclose an acoustic space with floor angle θ_f relative to the lower vertical. The matrix formulation of the problem, and the associated solution methodology is detailed in Pope et al. (1983). Eigenvectors, ϕ_i, and natural frequencies, f_i, are obtained from the two-dimensional finite-difference formulation for an enclosure of radius $a = 1$, and combined with the axial mode shape functions to obtain the eigenvectors, $\phi_{qi}(\vec{y})$, and natural frequencies, f_{qi}, of the three-dimensional enclosure. The resonance frequencies for arbitrary radius, a, are given by

$$f_{qi} = \frac{c_o}{2\pi}\left[\left(\frac{q\pi}{L}\right)^2 + \left(\frac{2\pi f_i}{c_o a}\right)^2\right]^{\frac{1}{2}} \tag{5.29}$$

where f_i is the result obtained for the 1 metre radius case, q the axial mode number, L the axial length of the acoustic space, and c_o the speed of sound in the cabin fluid. The acoustic modes for the three-dimensional cabin are given by

$$\phi_{qi}(\vec{y}) = \phi_{qi}(x,y,z) = \cos\left(\frac{q\pi z}{L}\right)\phi_i(x,y) \tag{5.30}$$

where $\phi_i(x,y)$ is the two-dimensional eigenvector, and $\cos\left(\frac{q\pi z}{L}\right)$ the axial mode shape function for the rigid end cap termination condition considered here.

The acoustic mode normalisation, Λ_{qi}, is defined as

$$\Lambda_{qi} = \int_V \phi_{qi}^2(y)d\vec{y} \tag{5.31}$$

where $\phi_{qi}(\vec{y})$ is the three-dimensional acoustic mode shape at a point, $\vec{y}$, in the enclosure of volume V. For the finite-difference solution of the acoustic modes, the mode normalisation, Λ_{qi}, for radius, $a = 1$ can be expressed as (Pope et al., 1983)

$$\Lambda_{qi} = \frac{L}{2}\varepsilon_q \sum_{j=1}^{n_j} \phi_i^2(j)h^2C(j) \tag{5.32}$$

where n_j is the number of interior and boundary points used in the finite difference formulation to determine the two-dimensional acoustic mode shape at point j, $\phi_i(j)$. $C(j) = 1$ for boundary points and centreline locations, and $C(j) = 2$ for interior points. Also

$$\varepsilon_q = \begin{cases} 2 & q = 0 \\ 1 & q > 0 \end{cases} \tag{5.33}$$

The general radius acoustic mode normalisation, Λ_q, is thus

$$\Lambda_q = a^2\frac{L}{2}\varepsilon_q \sum_{j=1}^{n_j} \phi_i^2(j)h^2C(j) \tag{5.34}$$

5.4.1 Verification of acoustic space natural frequencies

The natural frequencies obtained by the present analysis were compared with those calculated previously (Pope et al., 1983), and the two sets of results are shown in Table 5.3.

Table 5.3

Acoustic mode natural frequencies (Hz) for $\theta_f = 49°$, $q = 0$, and $a = 1$ m

Mode	Present Implementation	Pope et al.
0	0	0
1	96.679	96.416
2	113.906	113.002
3	168.261	166.997
4	179.336	178.748
5	214.111	212.718

The agreement between the two sets of results is excellent, with only minor differences in the natural frequencies, these being because of the variation in the number and location of the grid points used in each formulation. The acoustic mode shapes determined by the two formulations were found to be in qualitative agreement.

5.5 RESULTS FOR TEST STRUCTURE ACOUSTIC SPACE

The theoretical results obtained for an acoustic space of dimension $\theta_f = 40°$, measured from the lower vertical, and $a = 0.450$ m, are shown in Figure 5.10. The first cross-sectional mode, which is not shown, is designated (s1) and has uniform pressure distribution over the cross-section. The symmetric modes are notated by an (s), while the anti-symmetric acoustic modes are notated as (a). The numeric corresponds to the ascending resonance frequency order of the $q = 0$ modes.

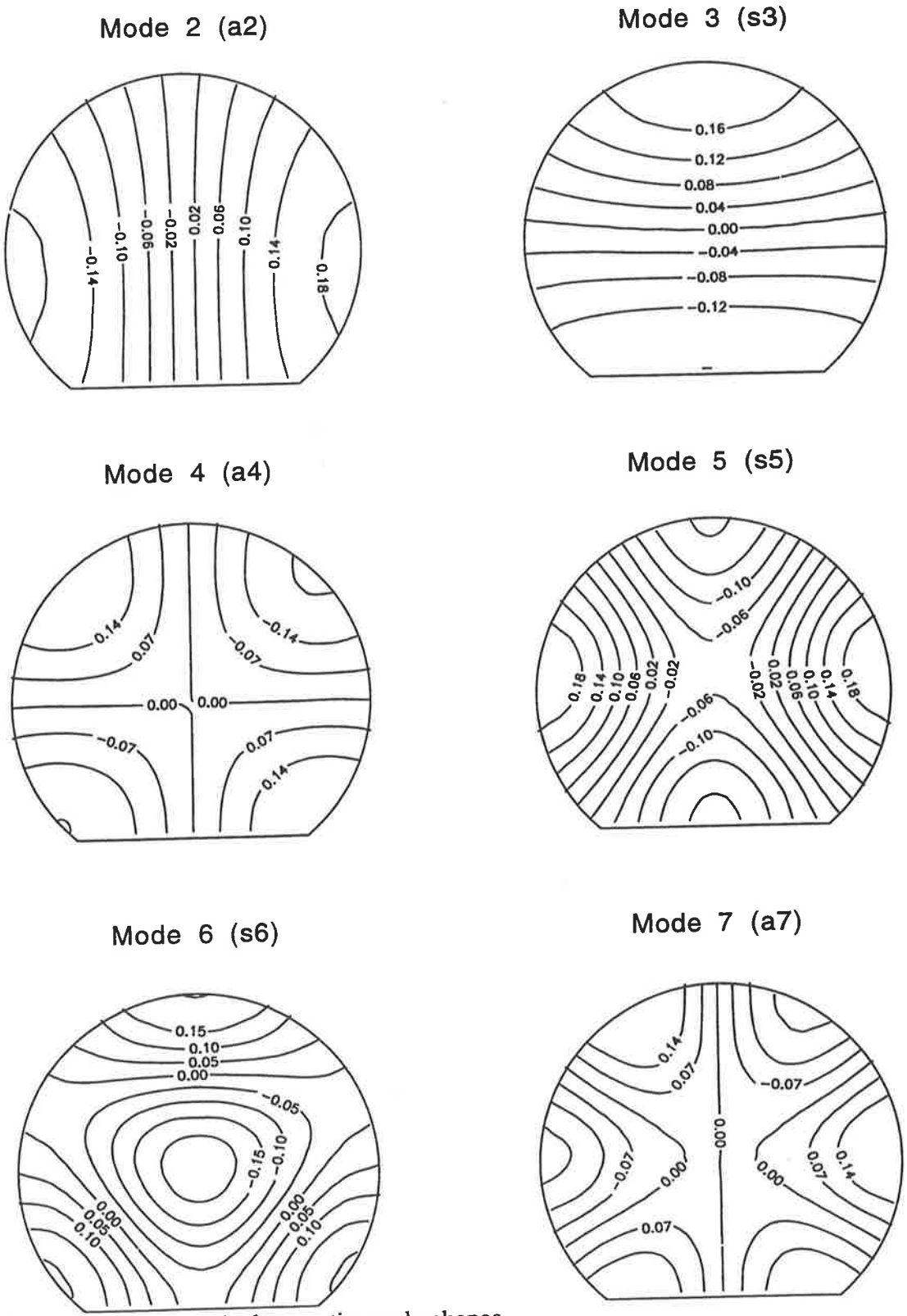

Figure 5.10 Theoretical acoustic mode shapes.

5.5.1 Experimental verification of acoustic mode shapes and natural frequencies

The natural frequencies of the acoustic space bounded by the upper region of the cylinder and the longitudinal floor partition of the test structure were determined experimentally using swept sine excitation of an acoustic source. The transfer function was measured between the inputs to a 145 mm (5.75 in.) diameter loudspeaker, non-symmetrically mounted over a portal in one of the rigid end caps, and a microphone, non-symmetrically located in the acoustic space. The spectrum obtained is shown in Figure 5.11, and a number of the natural frequencies, corresponding to the selection of peaks designated in Figure 5.11, are given in Table 5.4.

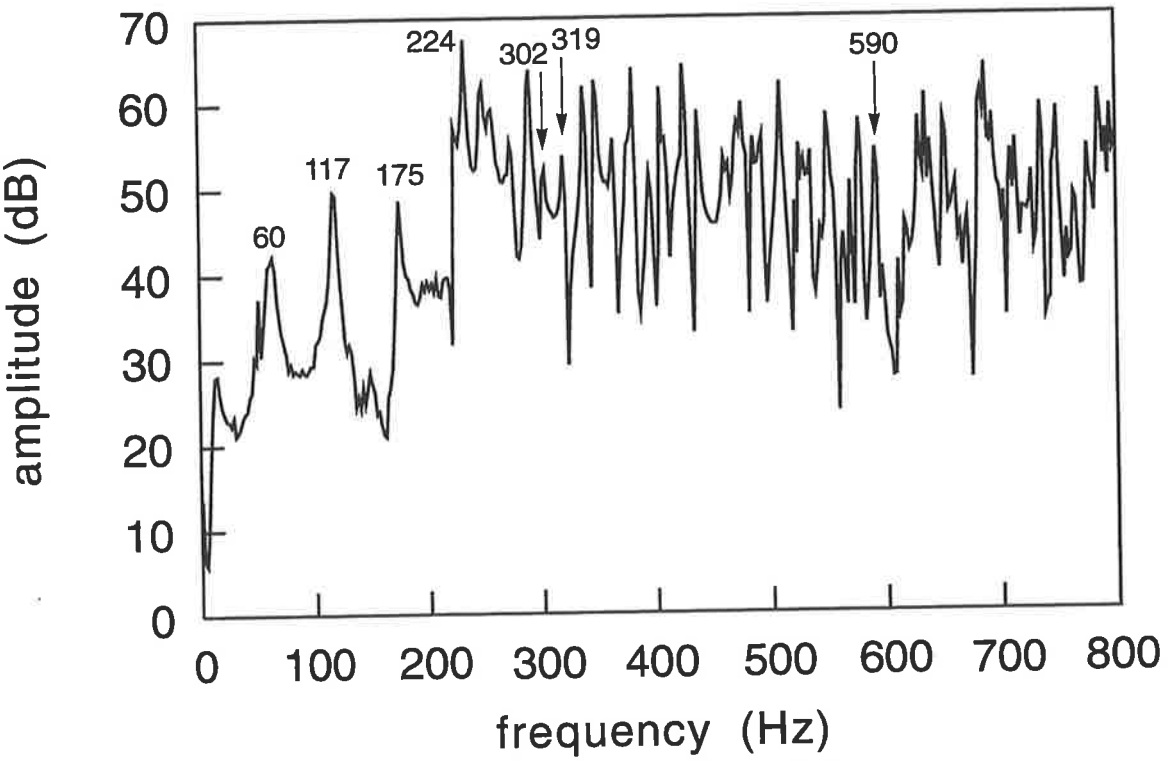

Figure 5.11 Acoustic response to swept-sine acoustic excitation.

The frequencies of all the resonant peaks have not been indicated in Figure 5.11 for clarity; however, good agreement between the theoretical and experimental results was evident for all of the peaks in the spectrum, as shown by the selection of resonance

Table 5.4

Acoustic mode natural frequencies for $\theta_f = 40°$, $L = 3$ m, and $a = 0.450$ m

Mode (cross-sectional,q)	Experimental (Hz)	Theoretical (Hz)
s1, 1	60	57
s1, 2	117	114
s1, 3	175	172
a2, 0	224	219
s3, 3	302	295
a2, 4	319	317
s6, 6	590	579

frequencies in Table 5.4. It should be noted that the theoretical results are calculated using the properties of air at ambient conditions, and that no correction has been applied for alternate conditions. The acoustic loss factor, η_q, was also determined experimentally from the obtained spectrum. The value used for the subsequent calculations, $\eta_q = 0.05$, is the average of a number of acoustic modes. This measured acoustic loss factor represents the combined loss due to conductance of the sidewalls and the conductance of the end caps, which terminate each end of the acoustic space.

Having experimentally determined the natural frequencies of the acoustic space enclosed by the test structure, the acoustic response at a number of excitation frequencies was measured, using an automated microphone traverse having three degrees of freedom. The cross-sectional responses for harmonic excitation at the indicated frequencies are shown in Figures 5.12 to 5.17. For comparison, the corresponding theoretical modal responses are

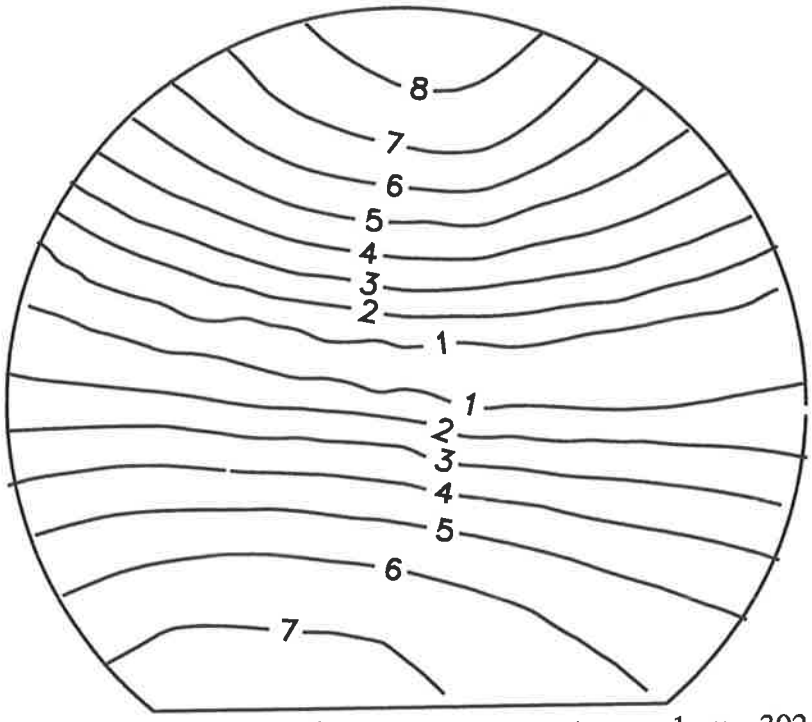

Figure 5.12 Experimental acoustic pressure scan at z = 1 m, 302 Hz acoustic excitation. Contour values are linear acoustic pressure.

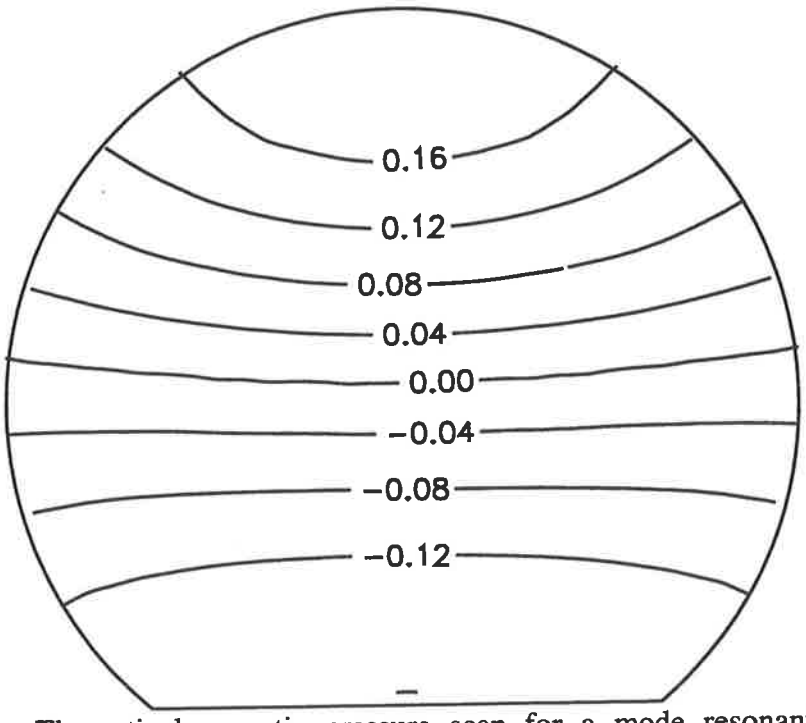

Figure 5.13 Theoretical acoustic pressure scan for a mode resonant at 295 Hz. Contour values are non-normalised acoustic mode shape function.

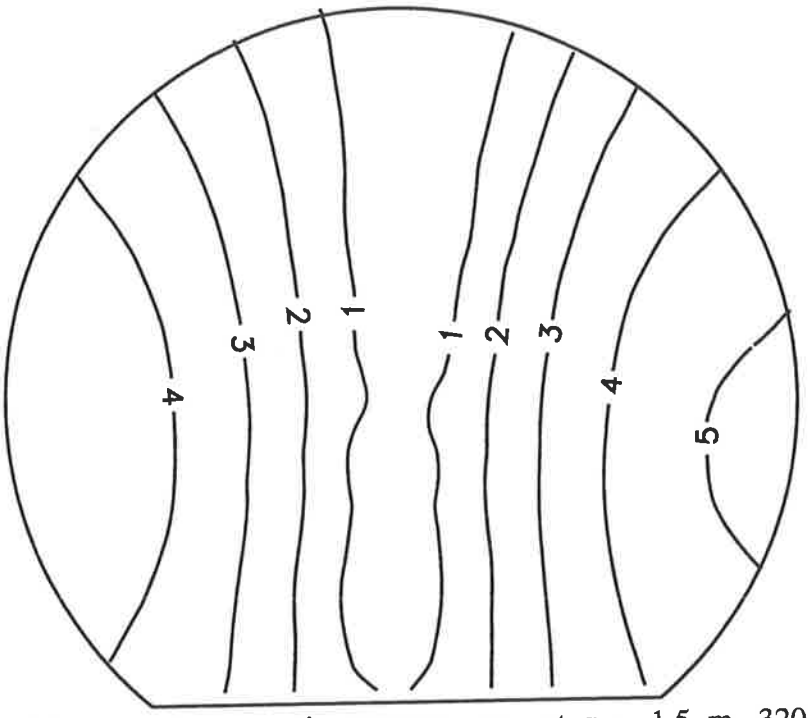

Figure 5.14 Experimental acoustic pressure scan at z = 1.5 m, 320 Hz acoustic excitation. Contour values are linear acoustic pressure.

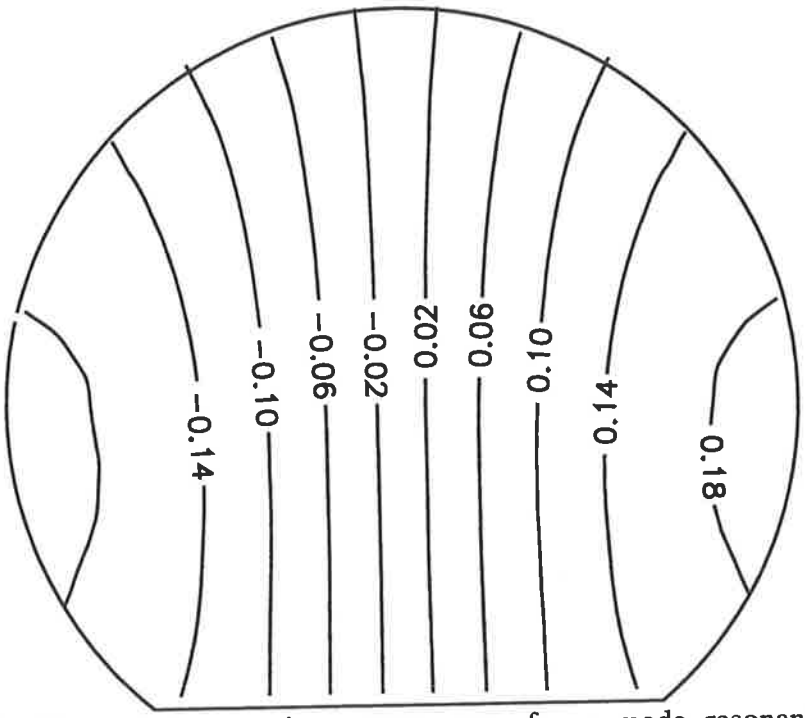

Figure 5.15 Theoretical acoustic pressure scan for a mode resonant at 317 Hz. Contour values are non-normalised acoustic mode shape function.

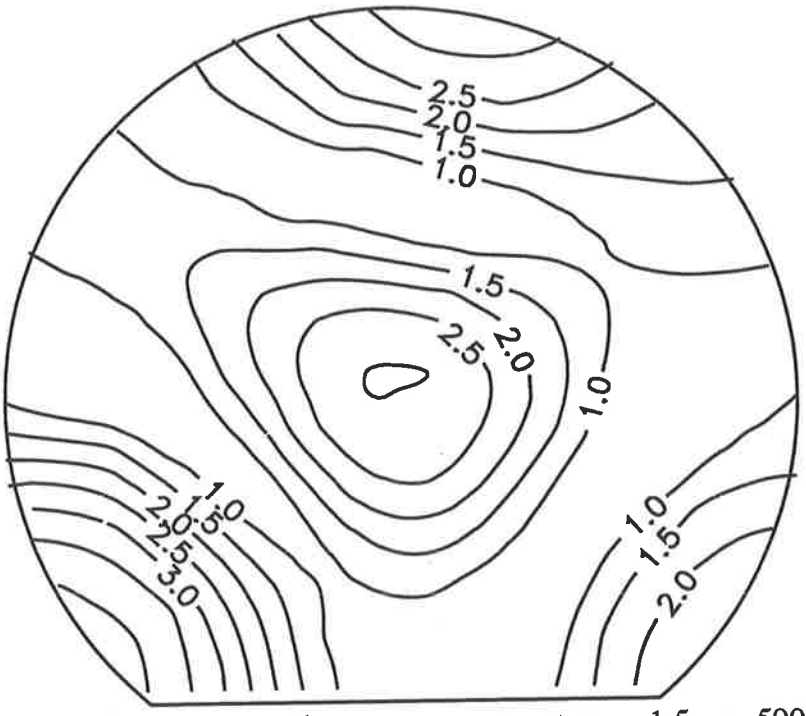

Figure 5.16 Experimental acoustic pressure scan at z = 1.5 m, 590 Hz acoustic excitation. Contour values are linear acoustic pressure.

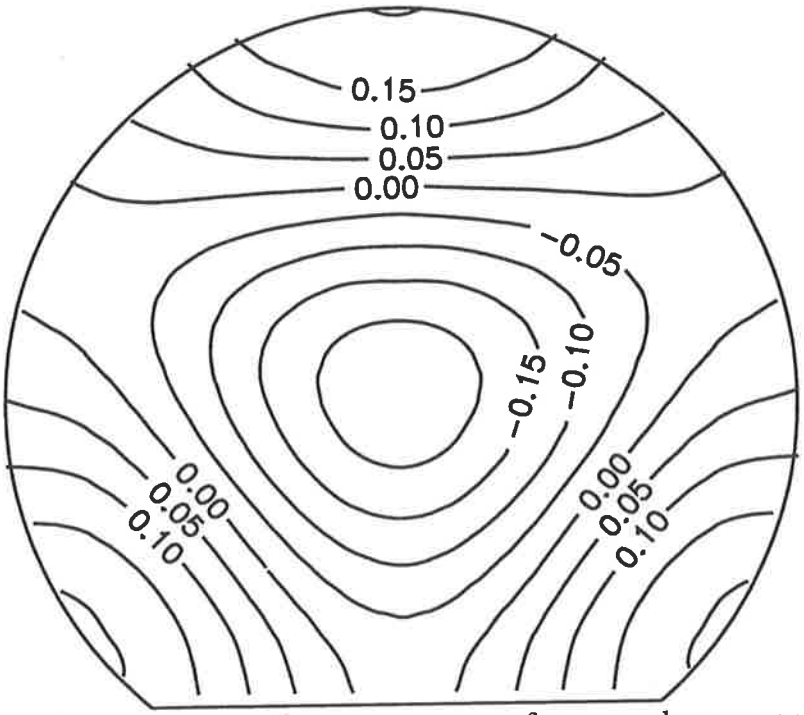

Figure 5.17 Theoretical acoustic pressure scan for a mode resonant at 579 Hz. Contour values are non-normalised acoustic mode shape function.

also shown. The experimental values used for the mapping are linear pressures, because decibel values would distort the response from that shown for the linear theoretical mode shapes. A cross-sectional scan was also performed at 117 Hz, corresponding to a resonance of the first acoustic mode which has a uniform pressure distribution over the cross-section. The mapping for this case is not shown because the range of values obtained experimentally was smaller than the contour interval used for the mappings of the other acoustic responses.

The general agreement between the theoretical and experimental values is good. It should be noted that slight deviations in the measured values for a point tend to have a significant affect upon the mapping of the mode shape. The data shown for the theoretical cases corresponds to the response of a single resonant mode, while the data for the experimental cases is the total acoustic response, assumed to be dominated by the single resonant mode, and hence no attempt has been made to decompose the acoustic response into its modal components.

The longitudinal response of the cabin acoustic space was also measured using the microphone traverse. The longitudinal response of the first cross-sectional mode (s1) is shown in Figure 5.18 for an excitation frequency of 62 Hz, corresponding to the first axial resonance of this mode, and in Figure 5.19 for an excitation frequency of 119 Hz, which is equal to the second axial resonance. Figure 5.20 shows the longitudinal response of the sixth cross-sectional mode (s6) at an excitation frequency of 590 Hz, equal to the sixth longitudinal resonance of this mode. Excellent agreement exists between the theoretical

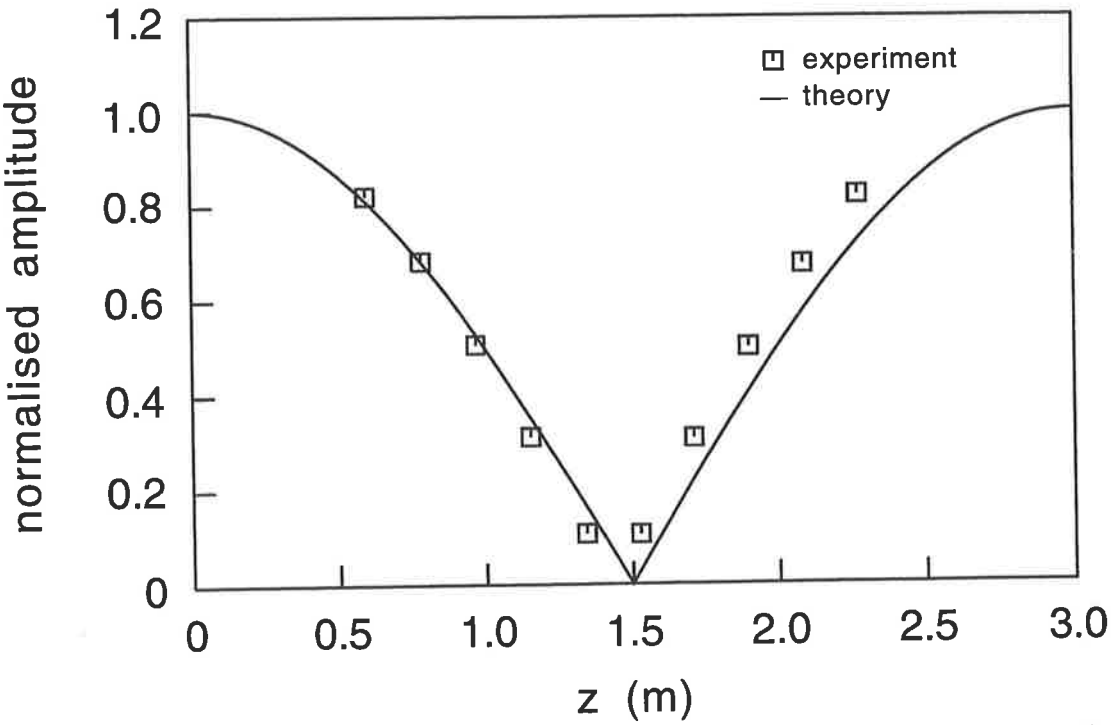

Figure 5.18 Longitudinal acoustic pressure response for the test structure excited acoustically at 62 Hz.

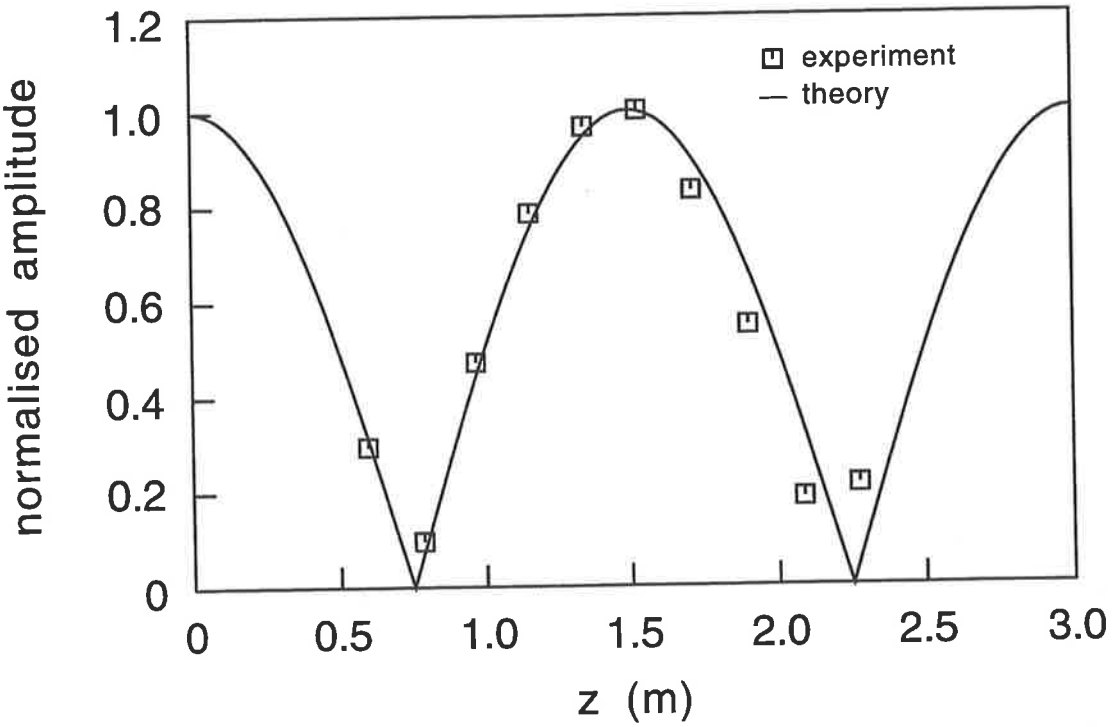

Figure 5.19 Longitudinal acoustic pressure response for the test structure excited acoustically at 119 Hz.

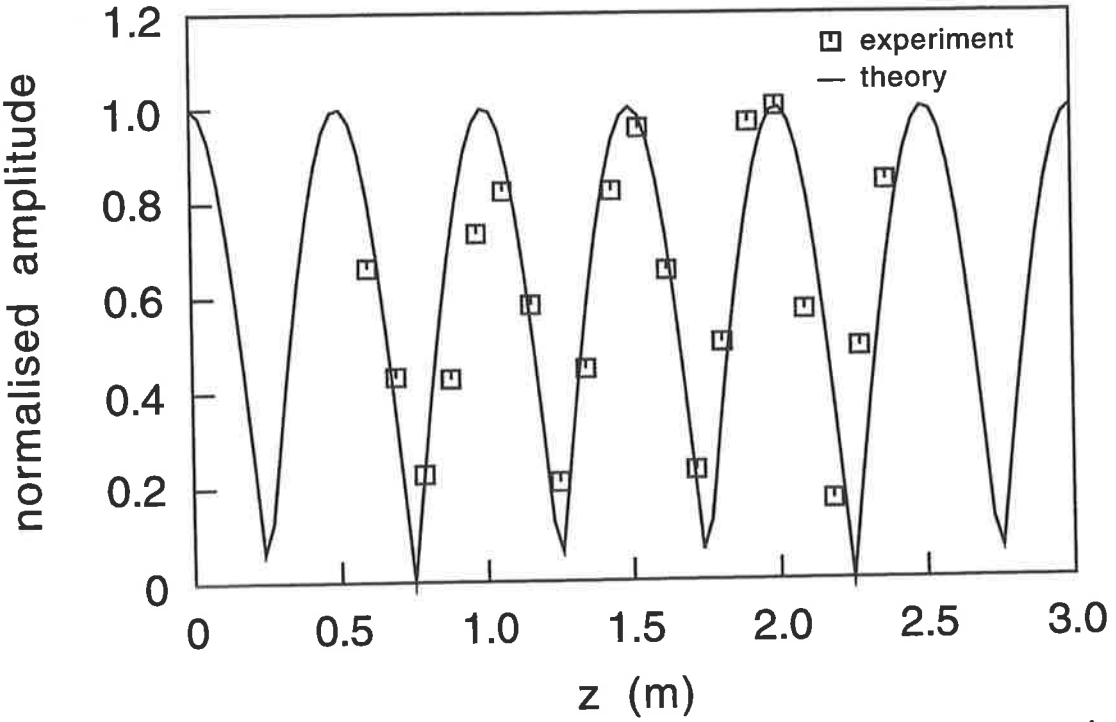

Figure 5.20 Longitudinal acoustic pressure response for test structure excited acoustically at 590 Hz.

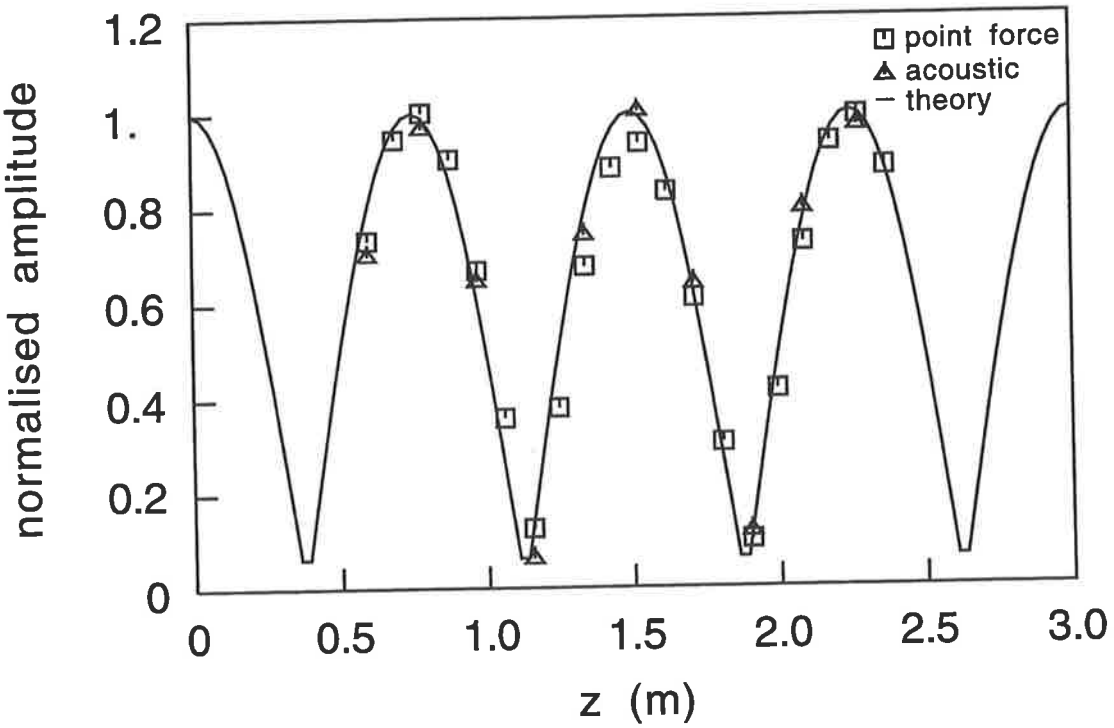

Figure 5.21 Longitudinal acoustic pressure response for test structure at resonance frequency of the (a2,4) acoustic mode.

modal response and the experimentally measured response. This confirms that the theory is accurately predicting the acoustic response of the cabin, and that the assumption of rigid end caps holds reasonably well.

As a preliminary test that the motion of the structure does not significantly distort the shape of the acoustic modes from that of the rigid-walled modes, an electro-dynamic shaker was non-symmetrically located on the structure. The response within the acoustic space due to the point force harmonic excitation of the structure was measured by the traversing microphone at the experimentally determined acoustic natural frequencies. The longitudinal response of the acoustic space, at an excitation frequency corresponding to the fourth longitudinal resonance of the second cross-sectional mode (a2), is shown in Figure 5.21. The values obtained for point force excitation of the structure are in excellent agreement with those for acoustic excitation, and the theoretical prediction. This indicates that the assumed rigid-walled acoustic modes are not significantly altered by the motion of the structure, and that the modal-coupling approach used in the following theory is appropriate.

The total cross-sectional response, obtained for point force excitation of the structure, is shown in Figures 5.22 to 5.28, together with the theoretical modal responses, for a number of excitation frequencies. The resonant frequencies shown for the experimental and theoretical cases differ slightly because the theoretical values are calculated for ambient conditions of air at 20 degrees Celsius, whereas the experimental values were obtained for a range of air temperatures ranging from 18 to 28 degrees.

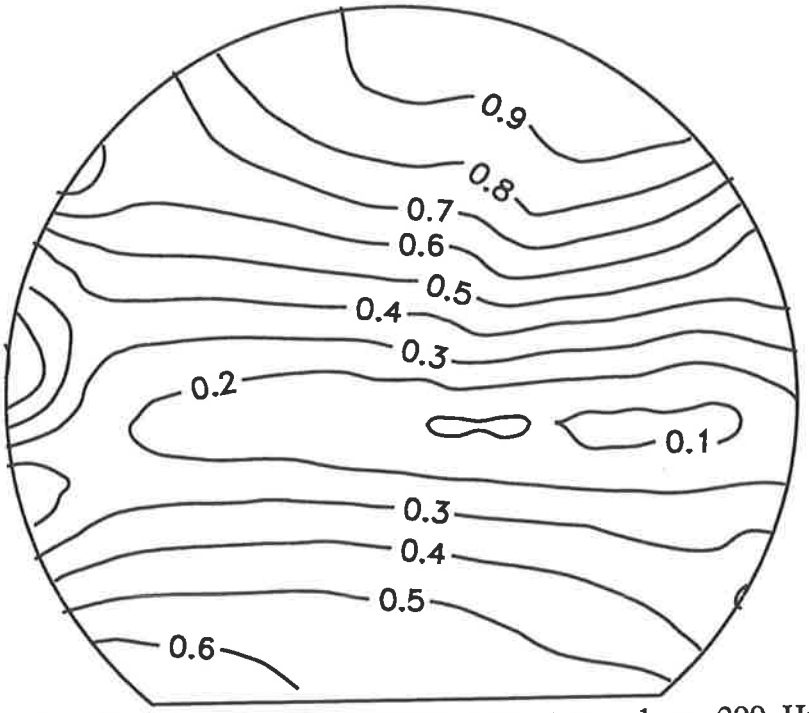

Figure 5.22 Experimental acoustic pressure scan at z = 1 m, 299 Hz point force excitation. Contour values are linear acoustic pressure.

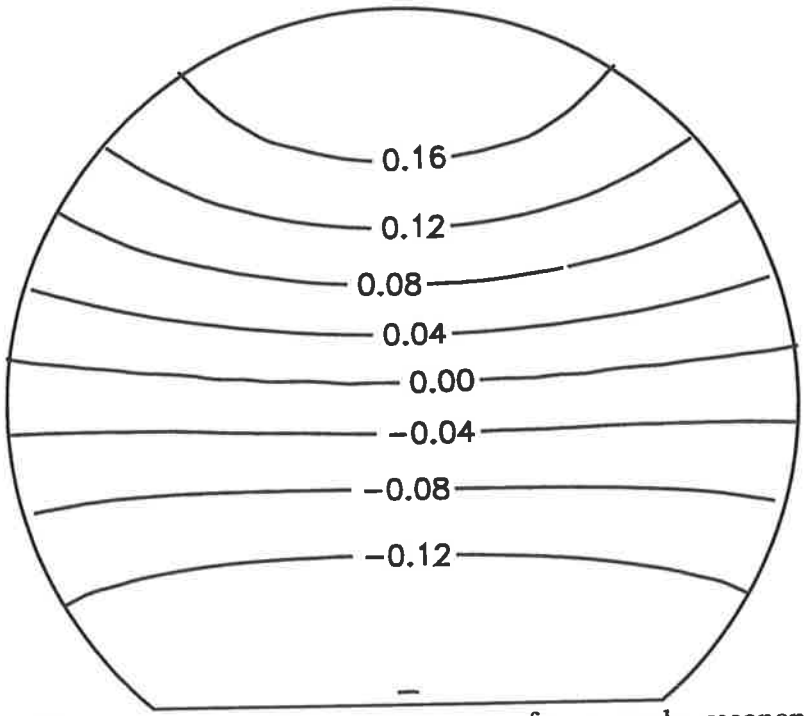

Figure 5.23 Theoretical acoustic pressure scan for a mode resonant at 295 Hz. Contour values are non-normalised acoustic mode shape function.

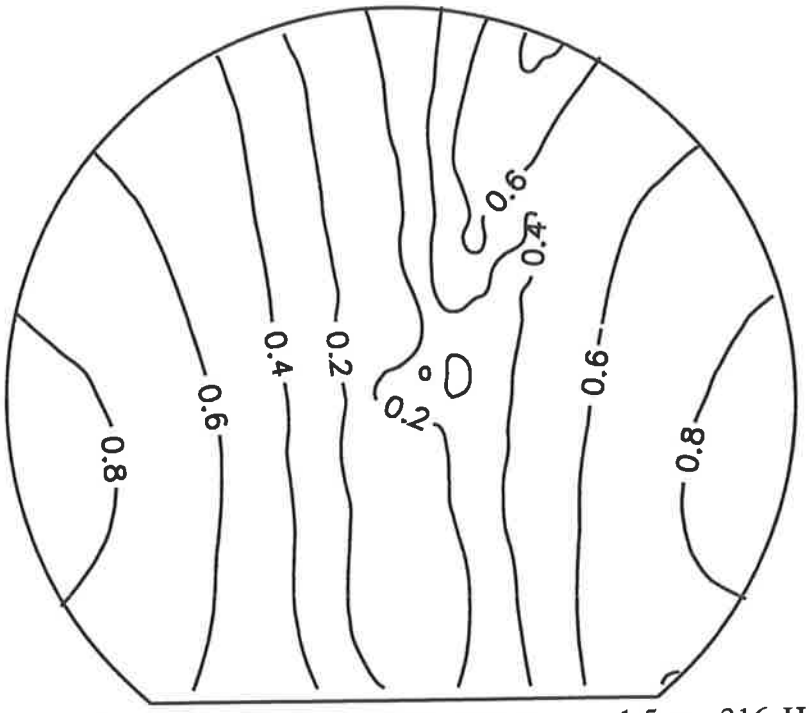

Figure 5.24 Experimental acoustic pressure scan at z = 1.5 m, 316 Hz point force excitation. Contour values are linear acoustic pressure.

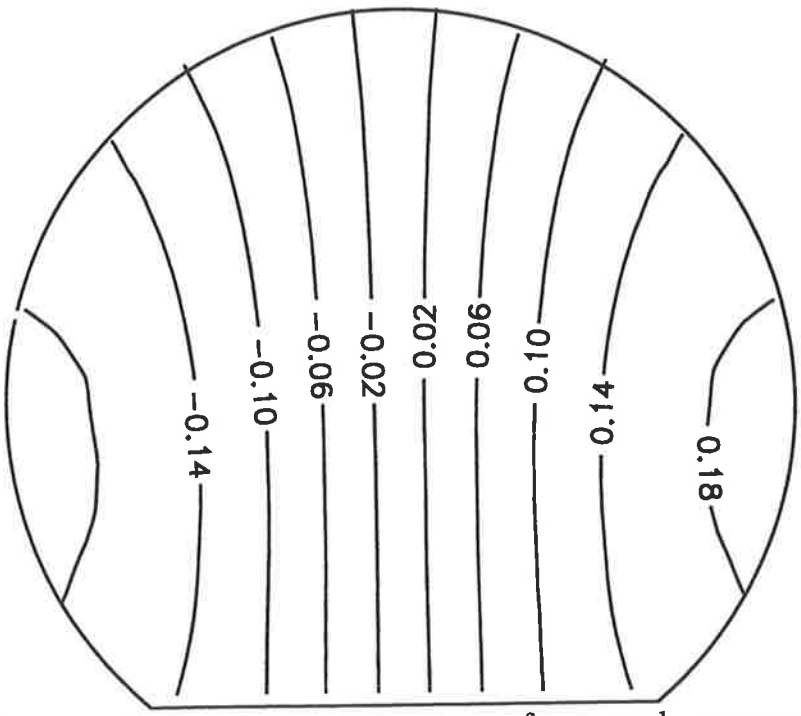

Figure 5.25 Theoretical acoustic pressure scan for a mode resonant at 317 Hz. Contour values are non-normalised acoustic mode shape function.

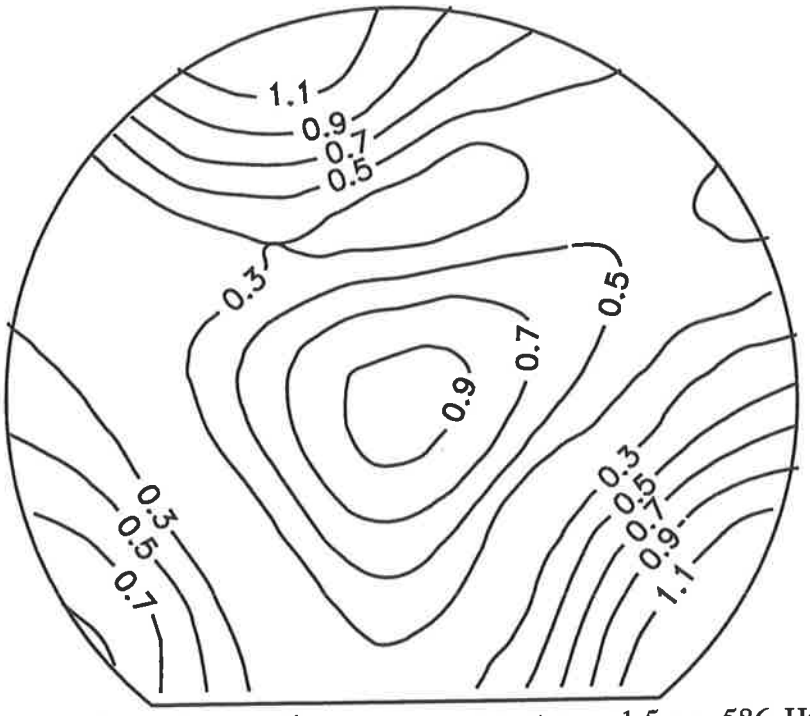

Figure 5.26 Experimental acoustic pressure scan at z = 1.5 m, 586 Hz point force excitation. Contour values are linear acoustic pressure.

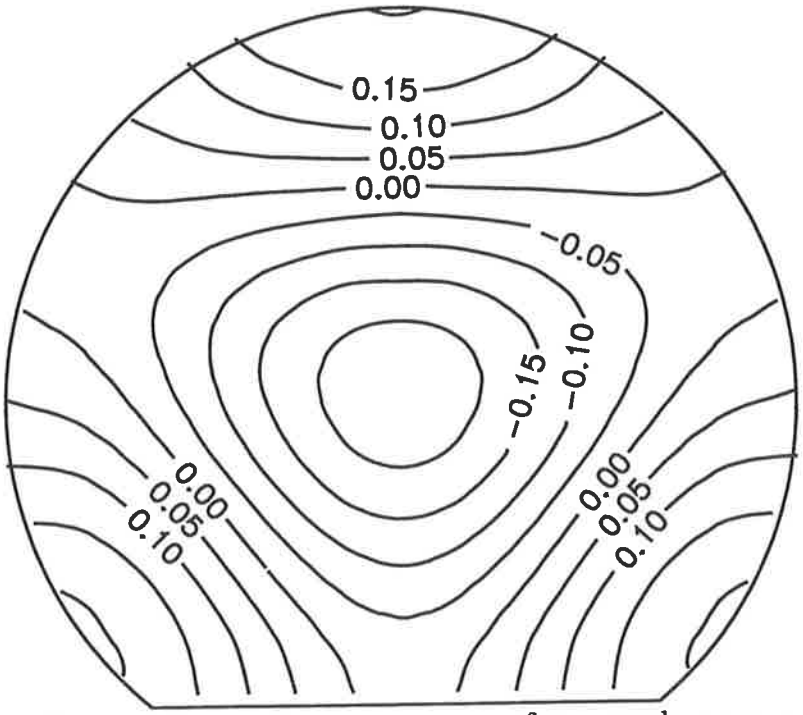

Figure 5.27 Theoretical acoustic pressure scan for a mode resonant at 579 Hz. Contour values are non-normalised acoustic mode shape function.

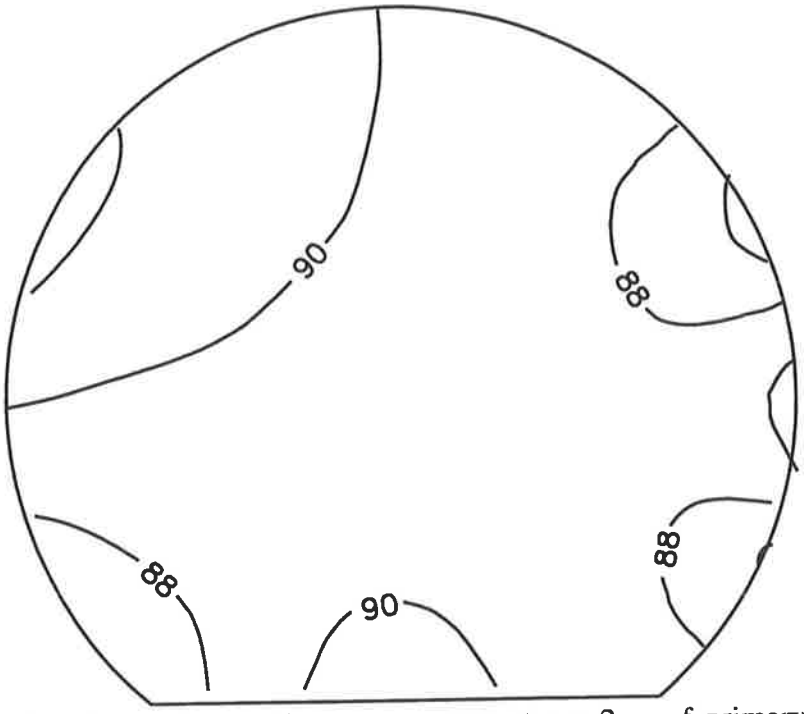

Figure 5.28 Experimental acoustic pressure scan at z = 2 m of primary response for point force excitation at 59 Hz. Contour values are acoustic pressure in dB.

The general level of agreement between the two cases is good. For the acoustic mode with the lowest natural frequency, (s1, 1), found from experiment to be resonant at 60 Hz, the theoretical and experimental cross-sectional mode shapes show only limited agreement. The theoretical analysis yields a mode shape with uniform values over the cross-section, while the experimental response indicates regions of spatially varying pressure near the perimeter of the acoustic space. The poor agreement may by caused by a number of factors mentioned previously in the literature.

Reference has been made (Pope et al., 1983) to the discrepancies between theoretical and experimental values below the first resonance frequency of the acoustic space; that is, in the frequency range where the noise level depends on the net volume displacement of the shell structure, and on the compliance of the cavity, which effectively acts as an air

spring. Although end cap transmission and leaks can be significant transmitters, and thus alter the acoustic response, relief of membrane stress over limited regions of the shell is also a significant factor (Pope et al., 1983). Hence slight manufacturing imperfections, wrinkles and depressions are highly detrimental to the noise levels transmitted into a perfect cylinder in the volume stiffness controlled region. The influence of slight manufacturing imperfections appears to be evident for the experiments detailed here because the results for acoustic excitation and structural excitation only differ significantly for excitation frequencies within the volume stiffness controlled region. the addition of other imperfections to the test structure such as ring frames and stringers will not produce profoundly different noise levels (Pope et al., 1983). Thus, for more realistic aircraft structures with added structural stiffening, the influence of slight manufacturing imperfections should not be a problem.

5.6 THEORETICAL FORMULATION FOR ACOUSTIC PRESSURE IN THE COUPLED STRUCTURAL/ACOUSTIC SYSTEM

Having determined the structural and acoustic mode shapes for the finite cylinder with an integral floor, it is possible to use modal coupling theory (Pope, 1970) to determine the acoustic pressure within the enclosure. This is provided that the assumption of weak coupling between the *in vacuo* structural modes and the rigid-walled acoustic modes is applicable.

Modal coupling theory has been used previously to predict the total response of cylinder models of aircraft fuselages (Pope et al., 1983, Pope et al., 1987a), and has been shown to

be accurate in determining the interior space-average sound pressure for such models. The formulation for the interior sound pressure used here follows that outlined in previous studies of aircraft interior noise using modal coupling theory (Snyder, 1990; Snyder and Hansen, 1991).

Truncating the infinite modal sums for the structural and acoustic response to m structural modes and n acoustic modes, the response at ε points in the acoustic space, located at $\vec{y}_\varepsilon$, caused by i forces input to the structure, can be estimated by (Snyder, 1990)

$$\left[p(\vec{y}_\varepsilon)\right] = [\Phi][Z_a]\left[Z_I\right]^{-1}[\Psi][F] \tag{5.35}$$

where $[F]$ is a $(i\times 1)$ vector of input forces, the $(m\times i)$ matrix $[\Psi]$ is the structural mode shape matrix, $\left[Z_I\right]$ is the $(m\times m)$ modal structural impedance matrix, $\left[Z_a\right]$ is the $(n\times m)$ matrix of acoustic modal radiation transfer functions and $[\Phi]$ the $(\varepsilon\times n)$ matrix of acoustic mode shape functions at the ε points of interest. The force and structural mode shape matrices can be combined to yield a $(m\times 1)$ vector of modal generalised forces, $[\Gamma]$, where

$$[\Gamma] = [\Psi][F] \tag{5.36}$$

to accommodate types of excitation other than point forces. For an external pressure field excitation the elements of $[\Gamma]$ are given by

$$\Gamma_r = \int_{S_e} \psi_r(\vec{x}) p_e(\vec{x}) d\vec{x} \tag{5.37}$$

where $p_e(\vec{x})$ is the external pressure excitation applied to the external surface area of the

structure, $S_e = 2\pi aL$.

The elements of $[Z_a]$, for acoustic mode q and structural mode r, are given by

$$Z_{a_{qr}} = \frac{j\rho_o \omega S c_o^2}{\Lambda_q Y_q} B_{qr} \tag{5.38}$$

where ρ_o is the air density, ω the angular frequency of excitation, S the contacting area between the structure and the enclosed acoustic space, given by

$$S = 2aL\left[\sin(\theta_f) + \pi - \theta_f\right] \tag{5.39}$$

and the floor angle θ_f is measured in radians. Y_q is the acoustic impedance of the q^{th} mode, given by

$$Y_q = \omega_q^2 - \omega^2 + j\eta_q \omega \omega_q \tag{5.40}$$

where ω_q is the natural frequency, and η_q is the acoustic loss factor, of acoustic mode q. The coupling factor, B_{qr}, between the q^{th} acoustic mode, ϕ_q, and the r^{th} structural mode, ψ_r, is defined as

$$B_{qr} = \frac{1}{S}\int_S \phi_q(\vec{x})\psi_r(\vec{x})d\vec{x} \tag{5.41}$$

The elements of the structural modal input transfer function matrix, $[Z_I]$, can be expressed as the sum of the modal impedance presented by the structure, $[Z_{IS}]$, and that presented by the impedance of the enclosed space acoustic modes, $[Z_{IA}]$, such that

$$[Z_I] = [Z_{IS}] + [Z_{IA}] \tag{5.42}$$

where $[Z_{IS}]$ is a diagonal matrix with elements

$$Z_{IS_{rr}} = \frac{jM_r Z_r}{\omega} \tag{5.43}$$

Z_r being the input impedance of the r^{th} structural mode, having modal mass M_r, natural frequency ω_r, and structural loss factor η_r, such that

$$Z_r = \omega_r^2 - \omega^2 + j\eta_r \omega \omega_r \tag{5.44}$$

The matrix $\left[Z_{IA}\right]$ is $(m \times m)$, with elements given by (Snyder, 1990)

$$Z_{IA_{\hat{m}\hat{n}}} = j\rho_o S^2 \omega \sum_{q=1}^{n} \frac{B_{q\hat{m}} B_{q\hat{n}}}{\Lambda_q Y_q} \tag{5.45}$$

5.7 COMPARISON OF THEORETICAL AND EXPERIMENTAL ACOUSTIC RESPONSE OF COUPLED STRUCTURAL/ACOUSTIC SYSTEM

This section presents a formulation for the acoustic pressure within the finite length cylinder with a structurally integral longitudinal floor, caused by harmonic point force excitation of the structure. The computer program implementation of the present theoretical formulation was verified, for a simplified scenario, against hand calculations, and also against previously presented theory (Pope et al., 1987a). The agreement between the program implementation and the two theoretical formulations was confirmed, for the simplified case examined.

A number of experiments were undertaken for comparison with the predicted response. The force input by an electro-dynamic shaker, located non-symmetrically on the structure, was measured using a force transducer, positioned in series between the point of

attachment to the structure and a stinger connected to the shaker. The acoustic response caused by the harmonic point force was determined from measurements made by a microphone traverse in the enclosure.

5.7.1 Experimental results for primary excitation case

A series of experiments were conducted on the test structure to investigate the ability of the theoretical model to predict the acoustic response within the cabin space due to excitation of the structure by a point force. For the theoretical predictions, the first 100 acoustic modes, and the first 144 structural modes were used in the calculations. An electro-dynamic shaker was non-symmetrically located on the external surface of the structure at (θ, z) = (165.3°, 1.323 m), relative to the coordinate axes shown in Figure 5.29.

An axial scan of pressure values was taken along the length of the enclosed acoustic space at a non-symmetric cross-sectional location of $(\theta, r/a)$ = (63.0°, 0.4466), to yield the axial sound pressure response within the test structure, at the given cross-sectional location.

For an excitation frequency corresponding to resonance of the first acoustic mode, (s1, 1), at 57 Hz, the experimental values obtained are shown in Figure 5.30. Also shown in Figure 5.30 are the theoretical predictions obtained using the input force measured using the force transducer. The general agreement between the gradient values for the experimental and theoretical cases is good, however, the amplitudes differ by approximately 30 dB. The difference in amplitudes between the two sets of data occurs

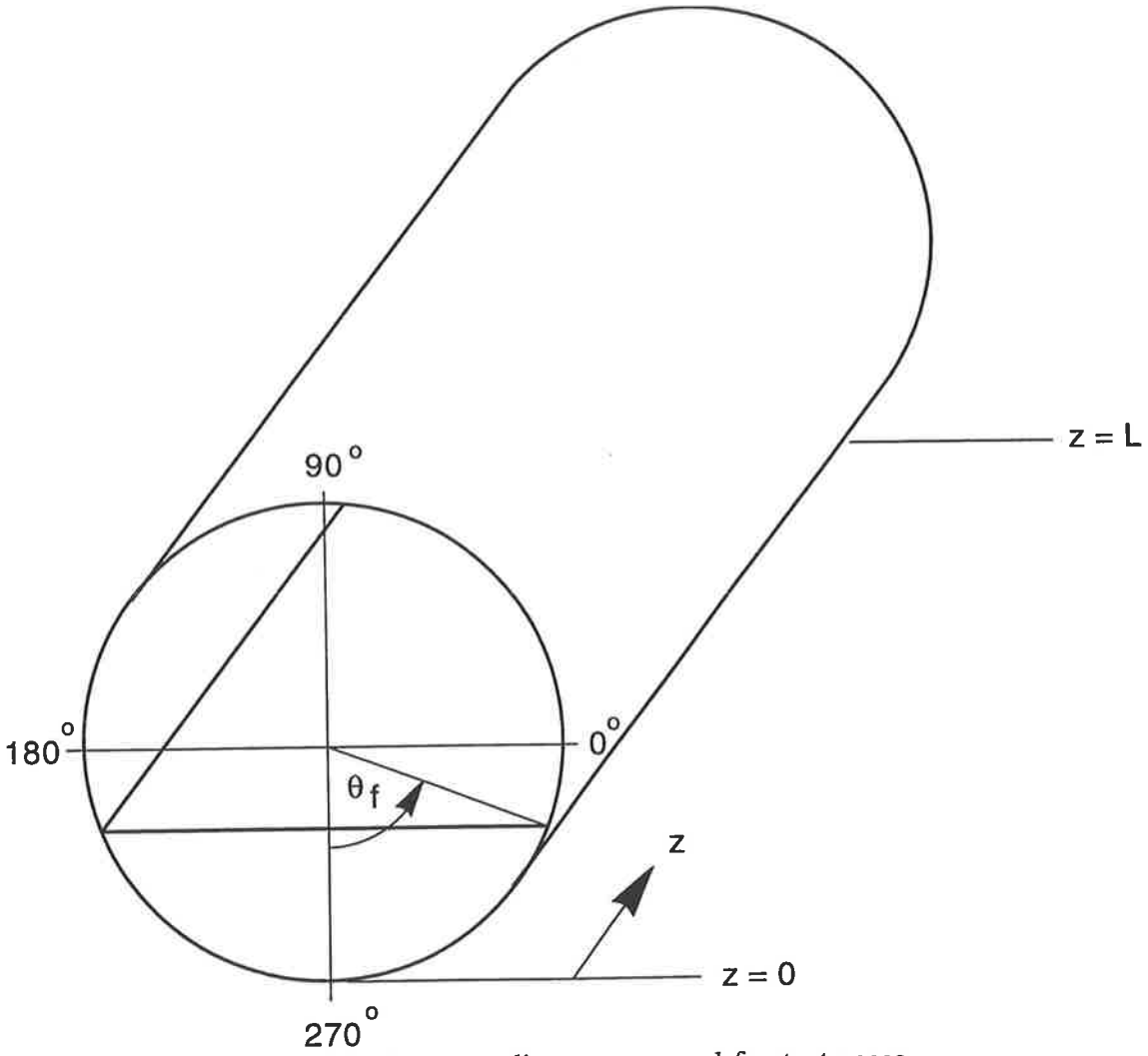

Figure 5.29 Cylinder with floor coordinate axes used for test cases.

because the theoretical prediction does not consider the (0,0,0) acoustic mode, and hence has not taken into account the low frequency contribution to the acoustic response which is dependent on the net volume displacement of the structure and the compliance of the cavity, which acts as an air-spring. Pope et al. (1983) cites a number of references (Pope, 1971; Plotkin et al., 1978; Lyon et al., 1966) which have found, without exception, that the measured noise reductions differ from the theoretical predictions by between 25 to 30 dB in the low frequency volume stiffness controlled region. Normalising the theoretical prediction produces the curve shown in Figure 5.30 as a dotted line. These normalised

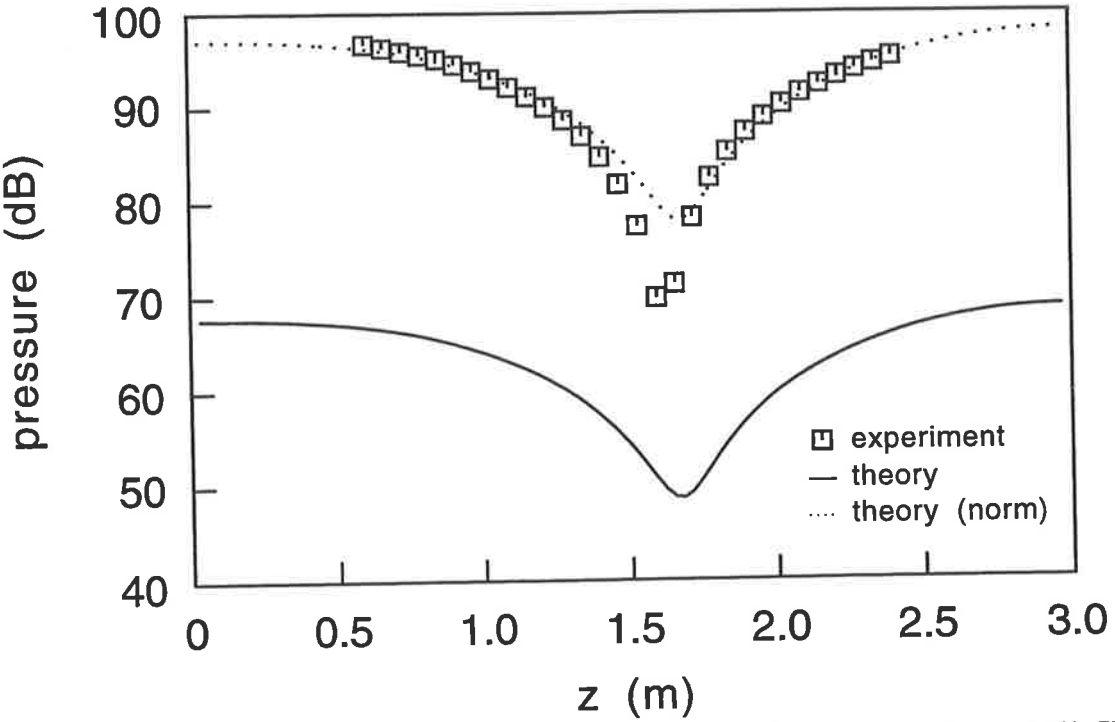

Figure 5.30 Longitudinal acoustic pressure response of the test structure at 59 Hz from point force excitation.

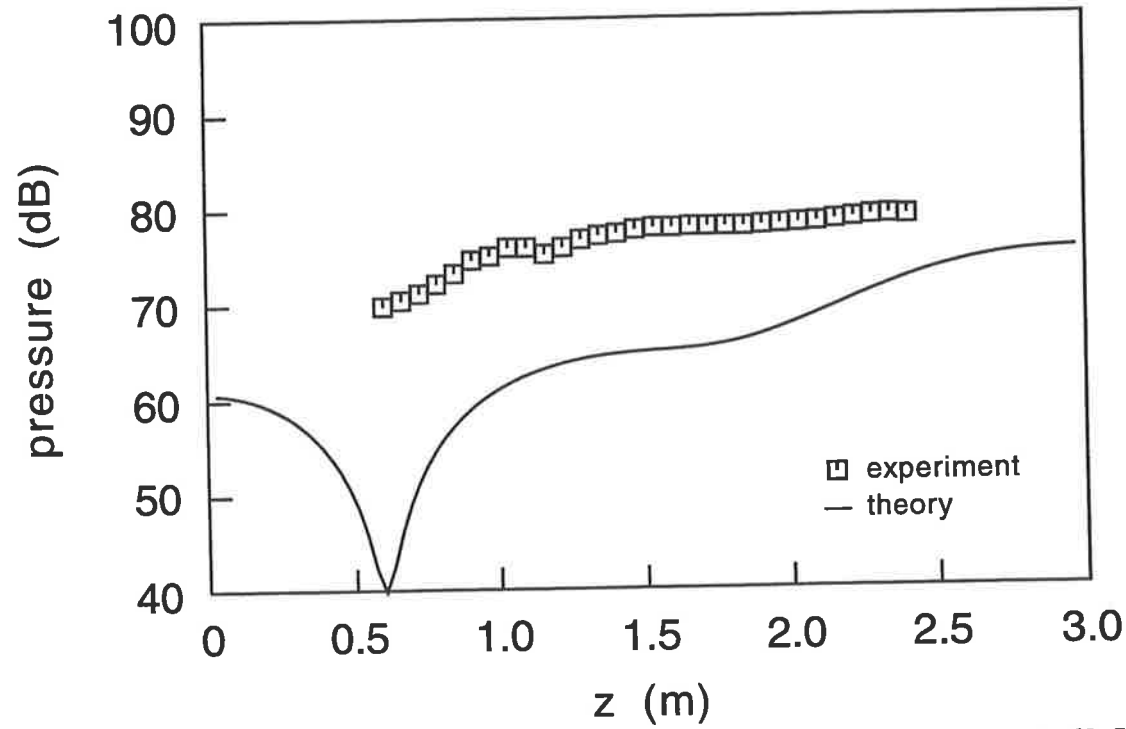

Figure 5.31 Longitudinal acoustic pressure response of the test structure at 69 Hz from point force excitation.

theoretical values agree well with the experimental values. The theory can also be seen to predict the slight asymmetry of the pressure values about the cylinder mid-point.

The results obtained for an excitation frequency of 69 Hz, which corresponds to resonant structural excitation and off-resonance acoustic excitation, are shown in Figure 5.31. The agreement between the theoretical and experimental gradients is reasonable, but the amplitudes are again seen to differ. For an excitation at 83 Hz, which is approximately mid-way between the first two acoustic resonant frequencies, the pressure scan values are shown in Figure 5.32. The gradients and amplitudes of the two sets of data are seen to differ for this excitation frequency. The differences in the two sets of data for the 69 Hz and 83 Hz excitations are considered to be due to variation between the actual structural mode resonant frequencies and those calculated in the model. Even at low frequencies the unstiffened test structure used in the experiments has a high modal density (approximately 1 mode/Hz), and hence errors in estimating the resonance frequencies of the structural modes will result in the amplitude and phase of the structural response being incorrectly estimated at a particular frequency. This problem would be alleviated for a stiffer test structure, which would also be more representative of a real aircraft fuselage. In particular, stiffening of the floor portion of the composite structure would decrease the modal density in the low frequency range, and is hence recommended for any future work.

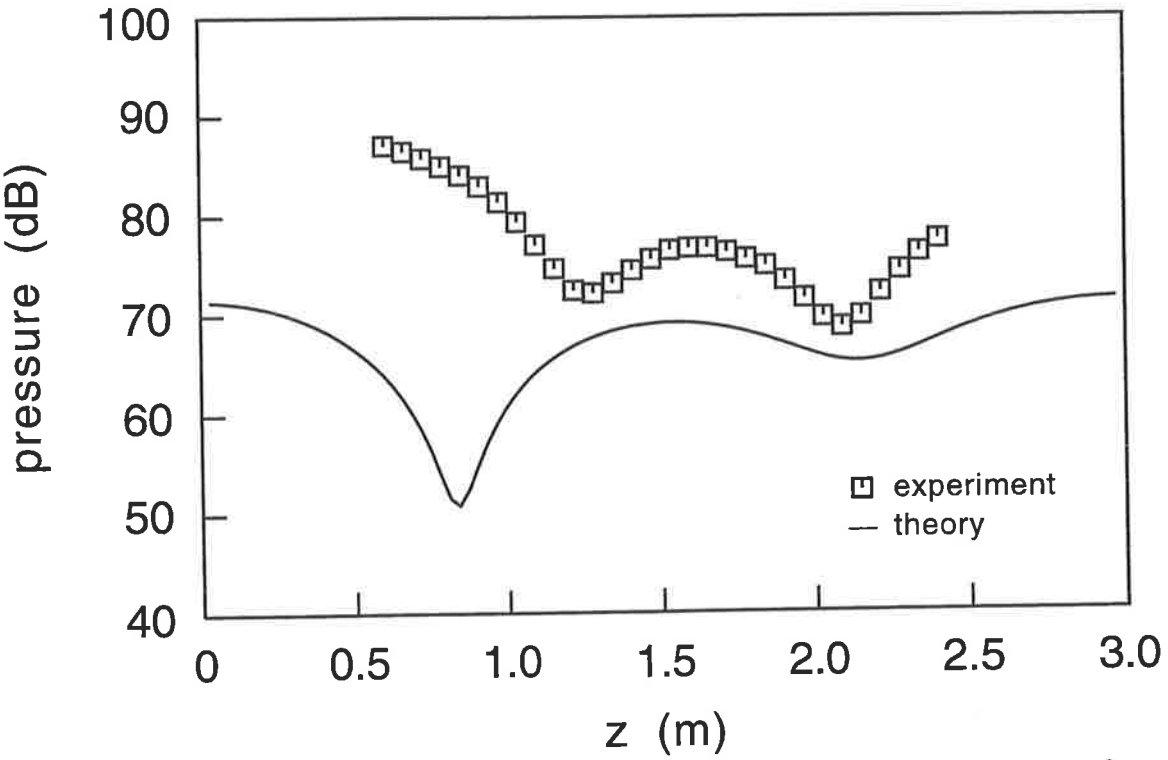

Figure 5.32 Longitudinal acoustic pressure response of test structure at 83 Hz from point force excitation.

5.7.2 Experimental results for controlled case

The ability of the theoretical model to predict the response of the coupled structural/acoustic system, under the influence of active control, applied via control forces input to the structure, was investigated through a number of experimental tests. A point force primary source was again located at (θ_p, z_p) = (165.3°, 1.323 m), and a single point force control source was located on the shell portion of the test structure at (θ_c, z_c) = (237.0°, 0.913 m). The pressure was minimised at a microphone located within the enclosure at $(\theta_e, r_e/a, z_e)$ = (63.0°, 0.4466, 1.718 m). An excitation frequency of 83 Hz, corresponding to off-resonant acoustic excitation, was used. The primary longitudinal response is shown in Figure 5.32 and the controlled longitudinal response is shown in Figure 5.33. Reasonable agreement between the predicted and experimentally measured

response is shown in Figure 5.33, which suggests that the model is capable of predicting the response of the entire acoustic field, or a global function, for minimisation of the pressure at a point, which is a local or point criterion.

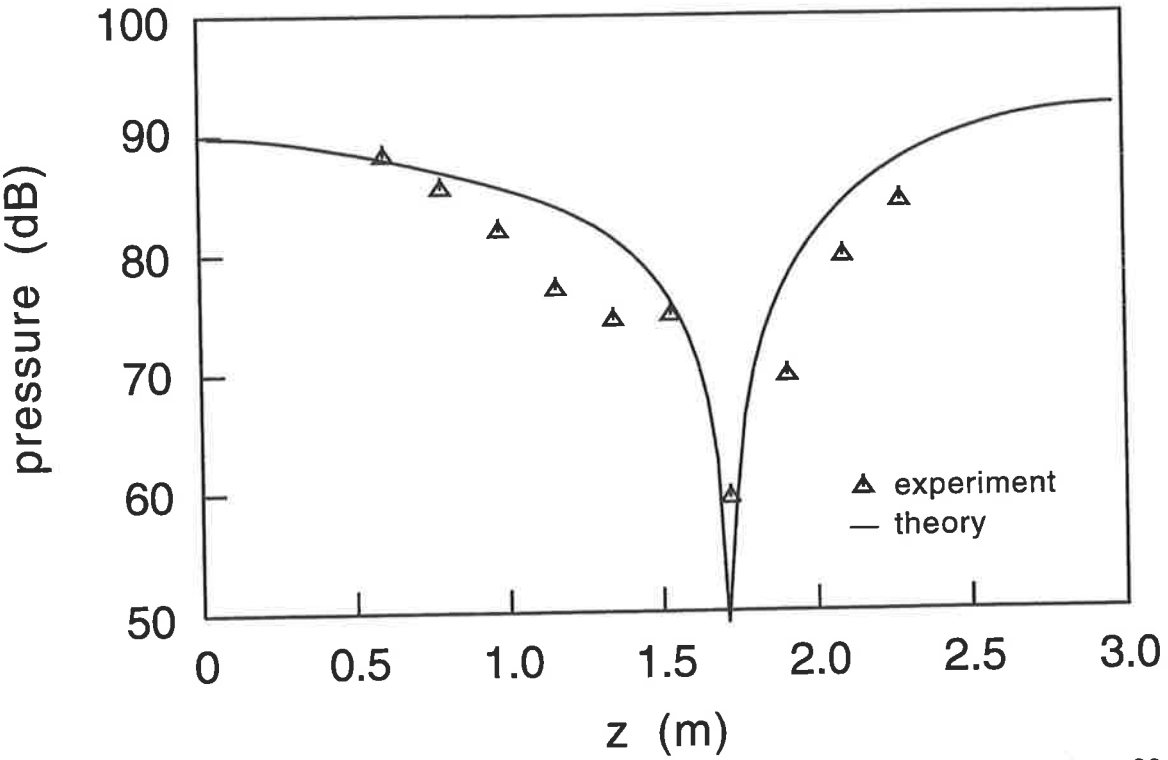

Figure 5.33 Controlled longitudinal acoustic pressure response of test structure at 83 Hz for a single error sensor located at (θ_e, r_e/a, z_e) = (63.0°, 0.4466, 1.718 m).

The theoretical primary response for a cross-sectional plane at z = 1.718 m, which corresponds to the error sensor axial location, is shown in Figure 5.34. The theoretical controlled response is shown in Figure 5.35, which shows the local reduction in pressure at the error sensor location, (θ_e,r_e/a,z_e) = (63.0°, 0.4466, 1.718 m). The corresponding experimental primary response is shown in Figure 5.36, while the experimental controlled response is shown in Figure 5.37.

Comparison of these experimental and theoretical pressure scans reveals that the predicted

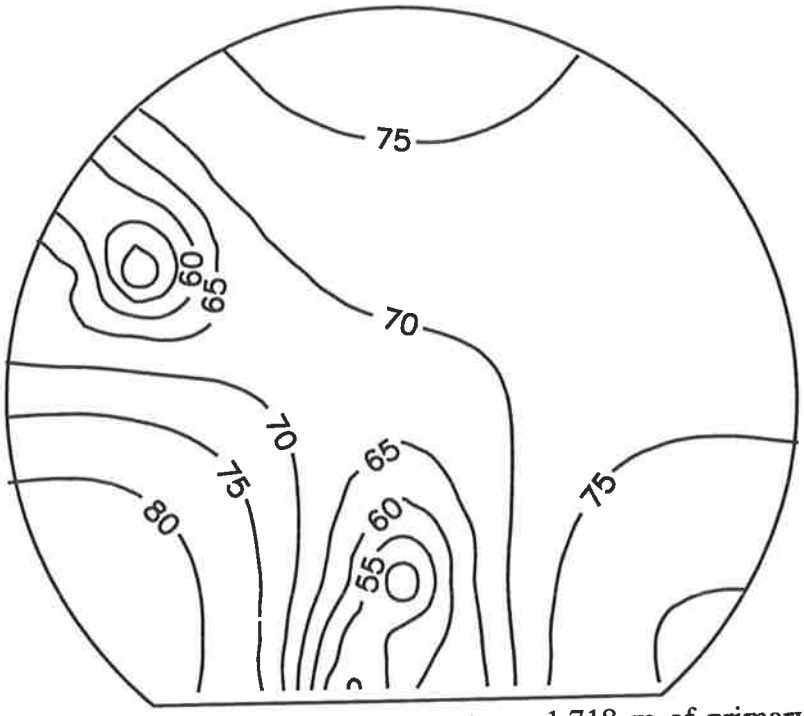

Figure 5.34 Theoretical acoustic pressure scan at z = 1.718 m of primary response at 83 Hz.

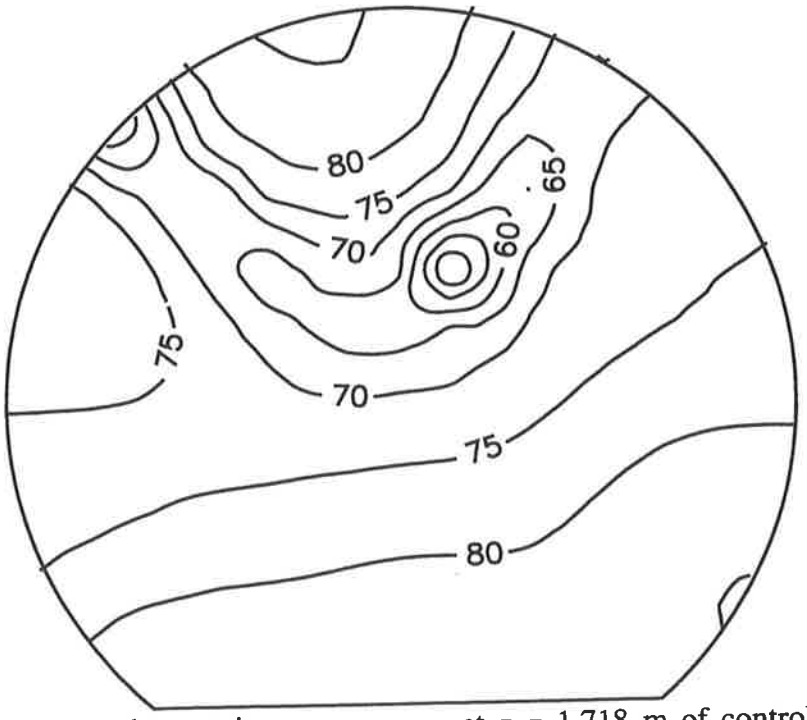

Figure 5.35 Theoretical acoustic pressure scan at z = 1.718 m of controlled response at 83 Hz.

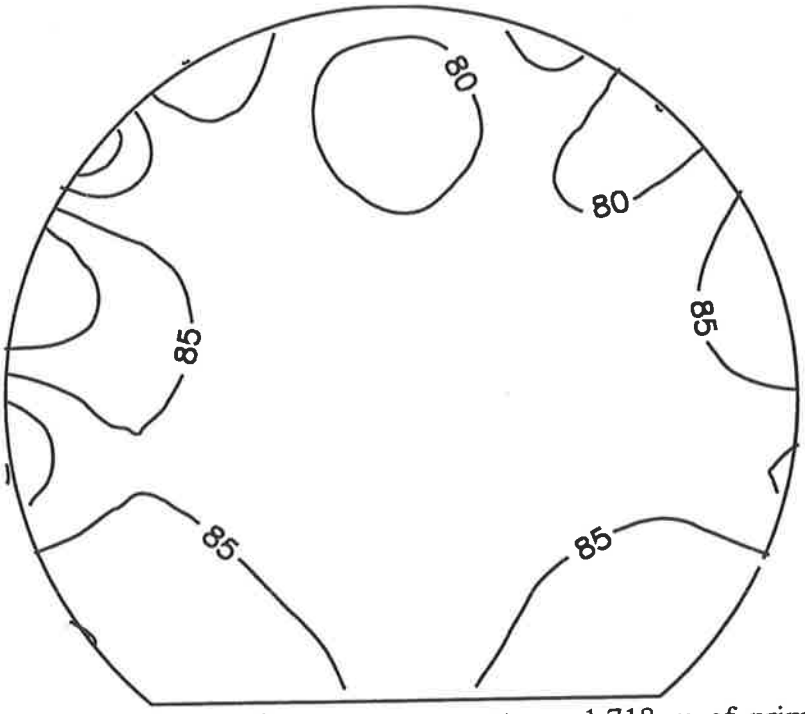

Figure 5.36 Experimental acoustic pressure scan at z = 1.718 m of primary response at 83 Hz.

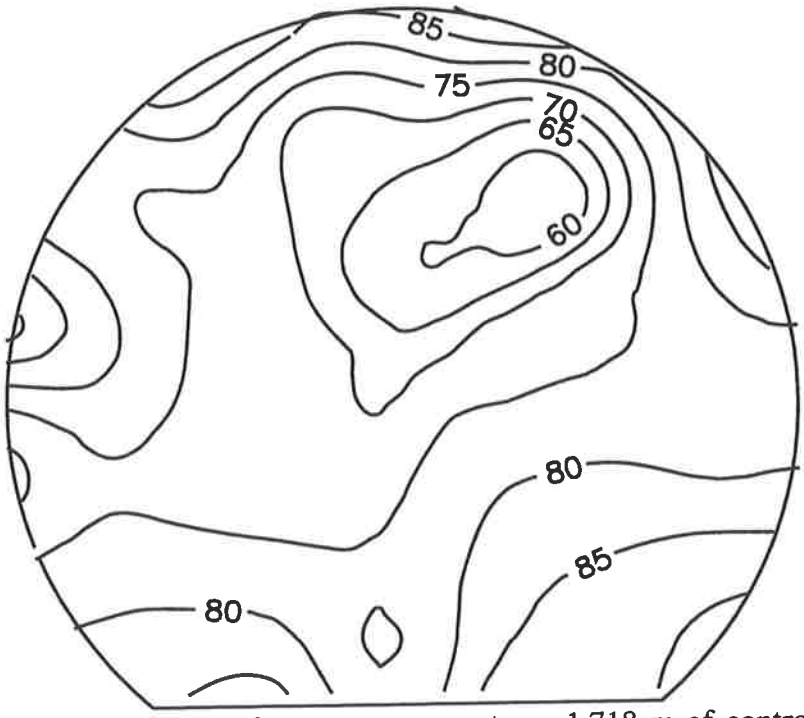

Figure 5.37 Experimental acoustic pressure scan at z = 1.718 m of controlled response at 83 Hz.

and measured pressure fields are reasonably similar, apart from the regions of smaller pressure amplitudes which are predicted for the primary response, but do not appear in the experimental case. The absence of these small regions from the experimental scan may be due to the limited spacing of the grid of points at which the experimental response was measured, and the consequent smoothing which occurs as part of the interpolation process involved in generation of the contour maps from this measurement grid.

The ability of the theoretical model to predict the effect of various source/sensor configurations was tested by scanning the axial location of the error sensor, at a fixed cross-sectional location of $(\theta_e, r_e/a)$ = (63.0°, 0.4466). The primary pressure at each error microphone location was recorded, in addition to the controlled response for minimisation of the acoustic pressure at that particular location. The acoustic pressure was minimised using the filtered-X version of the LMS algorithm, implemented on a digital signal processor. Figure 5.38 shows predicted and experimental values for both the primary and controlled response at the error sensor, for a range of error sensor axial locations, for an excitation frequency of 83 Hz. The figure reveals that for most of the error sensor locations, a pressure reduction of 27 dB was achieved at the error sensor. The controlled longitudinal response for minimisation of the acoustic pressure at an error sensor located at $(\theta_e, r_e/a, z_e)$ = (63.0°, 0.4466, 1.718 m), was shown previously in Figure 5.33. Generally the response of the system to active control has been reasonably predicted, apart from a region around z = 1 m. The discrepancy in the two values may be related to the inhomogeneity in the structure located around this axial length, which was detailed previously. Although the amplitudes of both the primary and controlled response are

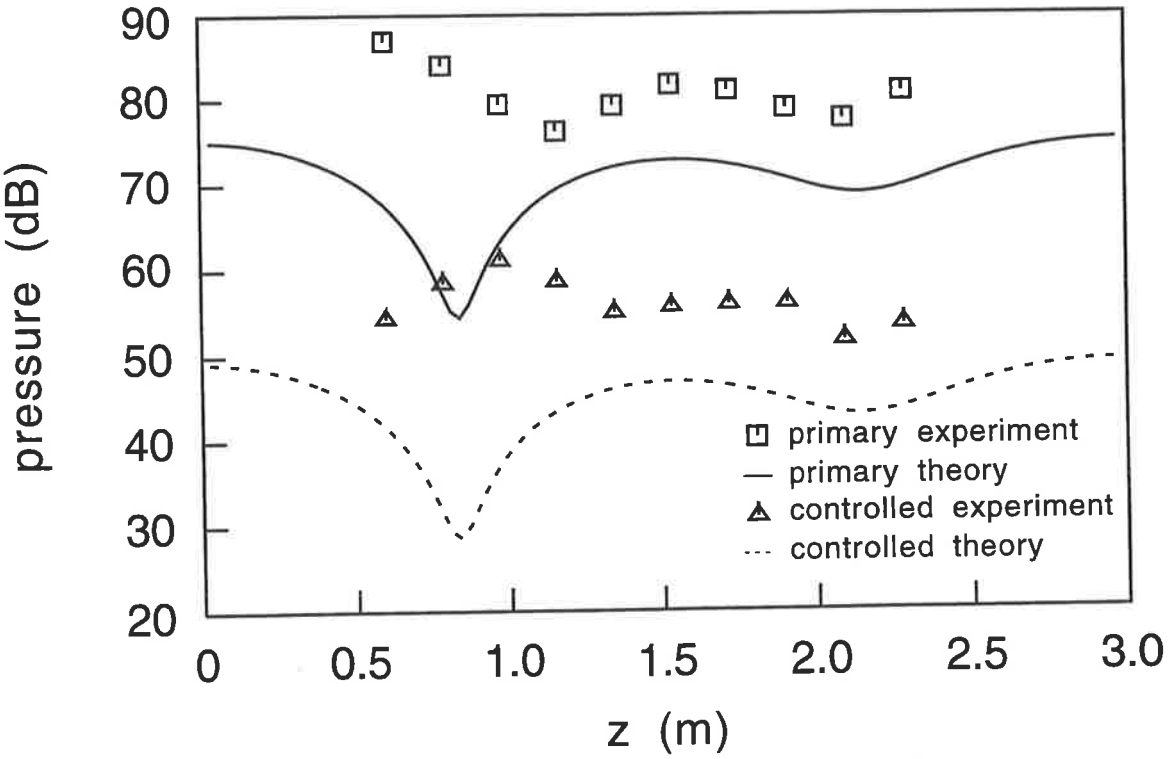

Figure 5.38 Theoretical and experimental primary and controlled acoustic pressure response at the error sensor as a function of error sensor axial location for 83 Hz excitation.

underestimated by the theory, the model is able to predict the relative levels of reduction and the general trends for the effect of each source/sensor configuration on these levels. The theoretical results and those obtained experimentally are thus in total seen to be reasonably consistent. The attenuation achieved for the theoretical case is limited by the efficiency factor which is applied to the controller, and not by the physics of the system examined.

Previous work has used the theory to predict trends and generalised results, rather than absolute point-by-point values. Previously, only values for the space-averaged acoustic pressure within models of aircraft cabins (Pope, 1971; Pope et al., 1983), or the axial variation (or gradient) of the average mean-square acoustic pressure in cross-section within

aircraft (Pope, 1990), have been presented. Snyder (1990) predicted the residual sound fields in a plain finite-length cylinder under the action of active vibration sources, and presented mappings of the acoustic pressure at various cylinder cross-sections. However, the theoretical results presented were normalised to best fit the experimental data for ease of comparison. Pope et al. (1983) emphasised that although the acoustic pressure at every interior point in the enclosure can be obtained theoretically, a good point-by-point prediction may require better input data than can ever be generated. Pope does, however, conclude that the point-by-point prediction might be quite informative nevertheless. In light of these comments, and considering the tests conducted, it is felt that the theoretical model can be utilised to predict the interior noise reduction due to active control with reasonable confidence.

5.8 OPTIMAL CONTROL FORCES FOR MINIMISATION OF ACOUSTIC PRESSURE

In this section a formulation for the optimal control force required for minimisation of the acoustic pressure within the finite length cylinder with a structurally integral longitudinal floor is presented. The sum of the sound pressure squared at the ε discrete interior points can be expressed by

$$\sum_{\varepsilon} |p(\vec{y}_{\varepsilon})|^2 = \left[p(\vec{y}_{\varepsilon})\right]^H \left[p(\vec{y}_{\varepsilon})\right] \tag{5.46}$$

where the superscript H represents the Hermetian of the matrix. The total pressure, $p(\vec{y}_{\varepsilon})$, at an arbitrary point within the enclosure, $\vec{y}_{\varepsilon}$, is equal to the sum of the pressure field due to the action of the primary excitation, $p_p(\vec{y}_{\varepsilon})$, and that due to the influence of

the applied control forces, $p_c(\vec{y}_\varepsilon)$, such that

$$p(\vec{y}_\varepsilon) = p_p(\vec{y}_\varepsilon) + p_c(\vec{y}_\varepsilon) \tag{5.47}$$

For i complex control forces, modelled as point forces, equation (5.46) can be re-expressed as (Nelson et al., 1987a)

$$\sum_\varepsilon |p(\vec{y}_\varepsilon)|^2 = \left[F_c\right]^H [a] \left[F_c\right] + \left[F_c\right]^H [b] + [b]^H \left[F_c\right] + c \tag{5.48}$$

where $\left[F_c\right]$ is the $(i \times 1)$ vector of complex control forces, and

$$[a] = \left[\Psi_c\right]^H \left(\left[Z_I\right]^{-1}\right)^H \left[Z_a\right]^H \left[\Phi_\varepsilon\right]^H \left[\Phi_\varepsilon\right] \left[Z_a\right] \left[Z_I\right]^{-1} \left[\Psi_c\right] \tag{5.49}$$

$$[b] = \left[\Psi_c\right]^H \left(\left[Z_I\right]^{-1}\right)^H \left[Z_a\right]^H \left[\Phi_\varepsilon\right]^H \left[\Phi_\varepsilon\right] \left[Z_a\right] \left[Z_I\right]^{-1} \left[\Gamma_p\right] \tag{5.50}$$

$$c = \left[\Gamma_p\right]^H \left(\left[Z_I\right]^{-1}\right)^H \left[Z_a\right]^H \left[\Phi_\varepsilon\right]^H \left[\Phi_\varepsilon\right] \left[Z_a\right] \left[Z_I\right]^{-1} \left[\Gamma_p\right] \tag{5.51}$$

where the subscripts p and c refer to primary and control respectively. Differentiating equation (5.48) with respect to the real and imaginary components of the complex control force, F_c, and equating the result to zero, yields the optimum control force as (Nelson et al., 1987b)

$$\left[F_c\right]_{opt} = -[a]^{-1}[b] \tag{5.52}$$

5.9 OPTIMAL CONTROL FORCES FOR MINIMISATION OF ACOUSTIC POTENTIAL ENERGY

In this section a formulation for the optimal control force required for minimisation of the acoustic potential energy within the finite length cylinder with a structurally integral

longitudinal floor is presented. The acoustic potential energy within a bounded enclosure is defined as (Bullmore et al., 1986)

$$E_p = \frac{1}{4\rho_o c_o^2}\int_V |p(\vec{y})|^2 d\vec{y} \tag{5.53}$$

which can expressed as

$$E_p = \frac{1}{4\rho_o c_o^2}\int_V [p(\vec{y})]^H [p(\vec{y})] d\vec{y} \tag{5.54}$$

Utilising the orthogonal properties of the rigid-walled acoustic modes used in the present model, allows equation (5.54) to be expressed as (Thomas et al., 1993b)

$$E_p = \frac{V}{4\rho_o c_o^2}[P]^H[P] \tag{5.55}$$

where $[P]$ is the $(n\times 1)$ vector of acoustic modal amplitudes given by

$$[P] = [Z_a][Z_I]^{-1}[\Gamma] \tag{5.56}$$

In a similar manner to that used for determining the optimum control force for minimisation of acoustic pressure at a point, the acoustic potential energy in the enclosure, under the action of primary and control forces, can be expressed as

$$E_p = [F_c]^H[\hat{a}][F_c] + [F_c]^H[\hat{b}] + [\hat{b}]^H[F_c] + \hat{c} \tag{5.57}$$

where

$$[\hat{a}] = [\Psi_c]^H \left([Z_I]^{-1}\right)^H [Z_a]^H [Z_a][Z_I]^{-1}[\Psi_c] \tag{5.58}$$

$$[\hat{b}] = [\Psi_c]^H \left([Z_I]^{-1}\right)^H [Z_a]^H [Z_a][Z_I]^{-1}[\Gamma_p] \tag{5.59}$$

$$\hat{c} = [\Gamma_p]^H \left([Z_I]^{-1}\right)^H [Z_a]^H [Z_a][Z_I]^{-1}[\Gamma_p] \tag{5.60}$$

The optimal complex control force vector, $[\hat{F}_c]_{opt}$, to minimise the acoustic potential energy in the enclosure, is found from quadratic optimisation to be

$$[\hat{F}_c]_{opt} = -[\hat{a}]^{-1}[\hat{b}] \tag{5.61}$$

5.10 FORMULATION FOR VIBRATIONAL KINETIC ENERGY OF THE STRUCTURE

The purpose of this section is to present a formulation for vibrational kinetic energy associated with the out-of-plane displacement of the finite length cylinder and the structurally integral floor. The vibrational kinetic energy, V_p, associated with the out-of-plane displacement of the test structure, is given by the integral of the outward velocity over the area of the shell and floor. Hence

$$V_p = \frac{1}{2}\int_{S_s} \rho_s h_s |\dot{w}(\vec{x})|^2 d\vec{x} \tag{5.62}$$

where $w(\vec{x})$ is the out of plane displacement of the structure of area S_s, material density ρ_s, and thickness h_s. Equation (5.59) can be re-expressed as

$$V_p = \frac{1}{2}\rho_s h_s \int_{S_s} [\dot{w}(\vec{x})]^H [\dot{w}(\vec{x})] d\vec{x} \tag{5.63}$$

Utilising the orthogonal properties of the structural modes yields

$$V_p = \frac{1}{2} M_s [V]^H [V] \tag{5.64}$$

where $[V]$ is the $(m \times 1)$ vector of structural mode amplitudes given by

$$[V] = [Z_I]^{-1} [\Gamma] \tag{5.65}$$

and M_s is the combined mass of the shell and the floor.

Although V_p is not used in this study as an error criterion, it is used in the next chapter as a measure of the response of the structure to the application of active control.

5.11 CONCLUSIONS

A physical system consisting of a finite length cylinder with a structurally integral longitudinal floor partition, and the acoustic space enclosed by the structure was examined. A model describing the response of this system to harmonic point force excitation was presented. The system was modelled theoretically using modal coupling theory between the structure and the interior acoustic field. The structural mode shapes have been determined using component mode synthesis, which combines the mode shape basis functions for the plain cylinder and the floor to obtain a mode shape function for the total structure. Good qualitative agreement was found between the theoretical structural mode shapes and those found experimentally by modal analysis. The theoretical resonance

frequencies of the structural modes were found to differ slightly from those obtained experimentally, with the theoretical analysis tending to overestimate the frequencies. This is thought to be due to the joint between the shell and floor not being completely rigid, as modelled in the theory. Inhomogeneities in the test structure, introduced by the welding process used for construction, caused the theoretical and experimental axial structural mode shape functions to differ slightly. The structural imperfections also appeared to have an effect upon the acoustic response for point force excitation of the structure.

The two-dimensional acoustic mode shape functions were found using a finite difference implementation of the Helmholtz equation, while the axial acoustic mode shape function was made equal to that of a rigid-walled one-dimensional enclosure. Experimental work on a test structure was presented and the results compared with a number of theoretical predictions. The agreement between the theoretical and experimental acoustic mode resonance frequencies was excellent. The acoustic mode shapes determined by experiment and theory were found to be in qualitative agreement, for excitation of the acoustic space by an acoustic source, and for point force excitation of the structure.

Formulations for the optimal control forces required to achieve minimisation of acoustic pressure and acoustic potential energy were given for the structure modelled. Experimental and theoretical results are presented for the application of active noise control to the coupled structural/acoustic system. Comparison of the theoretical and experimental results for point force excitation of the structure revealed that the theory underestimated the amplitude of the acoustic response for both the primary and controlled cases. The theory

was able to predict the relative levels of reduction and the general trends for the effect of each of the source/sensor configurations examined.

CHAPTER 6. EFFECT OF ERROR SENSOR AND CONTROL SOURCE CONFIGURATION ON A CYLINDER WITH AN INTEGRAL FLOOR

6.1 INTRODUCTION

The formulation for active control of the cylinder with an integral floor presented in Chapter 5 is utilised in this chapter to investigate the influence of error sensor and control source configuration and type upon the effectiveness of active noise control applied to the structure via vibrational point forces. Simulations are performed for various numbers of control sources and error sensors, and different locations of each of these active control system elements. Two different frequencies are examined: one corresponding to resonant acoustic excitation; and the other to non-resonant excitation. The distinction between resonant and non-resonant structural excitation has not been made in this thesis because of the high modal density of the structural modes for the test structure examined. A summary of the major factors influencing the performance of the active control system, applied to the simple aircraft fuselage model, is presented.

The test structure under consideration is the same as that used in the previous chapter and has the following dimensions: Length L = 3 m; radius a = 0.45 m; and floor angle θ_f = 40°. The thickness of the shell and the floor are equivalent, being $h_f = h_s$ = 0.001 m, and each has the same material properties: Young's Modulus E = 209 GPa; Poisson's ratioν = 0.3; and material density ρ = 7930 kg/m^3. The fluid within the enclosure is modelled with density ρ_o = 1.19 kg/m^3, and speed of sound c_o = 343 m/s. The co-ordinate axis

notation used in this chapter reverts to that used in Chapter 5 for derivation of the structural mode shapes of the cylinder with an integral floor, where y is the floor transverse location, x the floor or shell axial location, and θ the circumferential location on the shell, relative to the rotational axis shown in Figure 5.29.

The theoretical infinite acoustic mode summation and infinite structural mode summation were both truncated to a finite number of modes, such that the model is applicable over a finite frequency band. In all the calculations performed, the first 100 acoustic modes and 144 structural modes were used to model the response of the coupled system. The structural impedance component contributed by the acoustic enclosure is considered to be negligible, and hence only the structural component has been used to determine the total structural impedance.

For the following simulations the measure used to determine the effectiveness of the application of active control, for various control source and error sensor configurations, is the acoustic potential energy, E_p, in the cabin region enclosed by the shell and the longitudinal floor partition. The acoustic potential energy has been chosen as a performance gauge because it is a global quantity, and is felt to best represent the effect that applying active control has upon the whole of the acoustic space, and not just a localised region, as would be the case for the pressure measured at a point in the cabin. Throughout this chapter the term error sensor denotes a sensor which measures the acoustic pressure at a point. The primary excitation is provided by a point force mounted on the shell at location $\vec{x}_p = (x_p, \theta_p)$ = (1.323 m, 165.3°). The complex primary force

used in all of the simulations is -6.0 + j1.9 N.

For the results presented here, a black box feed-forward controller has been assumed with a reference signal obtained from the input to the primary source. The control sources are modelled as constant force sources, the outputs of which are linearly related to their inputs. In real systems it is unlikely that the exact value of the optimal control source forces will be achieved by the controller, and hence a physical representation of the controller inaccuracies is obtained by multiplying the calculated optimum control source forces by an efficiency factor η. The efficiency value is obtained by considering a controller of precision such that a total rounding error of around 1% is generated in the outputs from the controller. Hence an efficiency factor of 0.99 is obtained.

6.2 SIMULATIONS FOR OFF-RESONANCE ACOUSTIC SPACE EXCITATION FREQUENCY

The first set of simulations were conducted at a frequency of 83 Hz, which corresponds to off-resonance excitation for the acoustic modes. For the first case modelled, a single error sensor was located within the enclosure at $\vec{x}_e = (x_e, \theta_e, r_e/a)$ = (1.7178 m, 63.0°, 0.4466). A single point force control source was applied to the shell at an axial height x_c = 1.323 m, and is thus in the same cross-sectional plane as the primary source. The circumferential location of the control source, θ_c, was varied over the entire circumference. From the simulations performed for this case, the reduction in pressure at the error sensor location was approximately 40 dB for all control source positions. The acoustic potential energy estimate, J_p, provided by the single error sensor, was thus also

reduced by approximately 40 dB. The actual acoustic potential energy within the enclosure, E_p, was, however, not reduced for all control source locations, as shown in Figure 6.1. The theoretical reduction in acoustic potential energy using this quantity as the error criterion is also shown in Figure 6.1. It can be seen from the figure that if the control source is well matched to the primary acoustic field, and can produce an equivalent acoustic response, then minimisation of the acoustic potential energy estimate, J_p, will result in minimisation of the actual potential energy, E_p. For control source locations which are not well matched to the primary excitation, minimisation of J_p can result in an increase in E_p. Hence, for a well matched control source location, a single error sensor, detecting the acoustic pressure at a point, is capable of providing suitable information to the controller so that the actual acoustic potential energy in the enclosure is minimised. As the number of error sensors is increased the acoustic potential energy estimate, J_p, more accurately models the actual acoustic potential energy, E_p, for all control source circumferential locations. This can be seen in Figure 6.2, which displays the acoustic potential energy reduction achievable for 2, 3 and 10 error sensors randomly located within the enclosure. The error sensor locations are shown in Appendix C. Comparison of Figures 6.1 and 6.2 reveals that the reduction achievable with the 10 error sensor configuration is almost equivalent to the maximum theoretically achievable for one control source. In addition the estimate J_p, provided by as few as three error sensors, is adequate to minimise E_p for this configuration and excitation frequency.

Increasing the number of randomly located control sources, positioned on either the shell or the floor, results in increased levels of reduction in acoustic potential energy for all

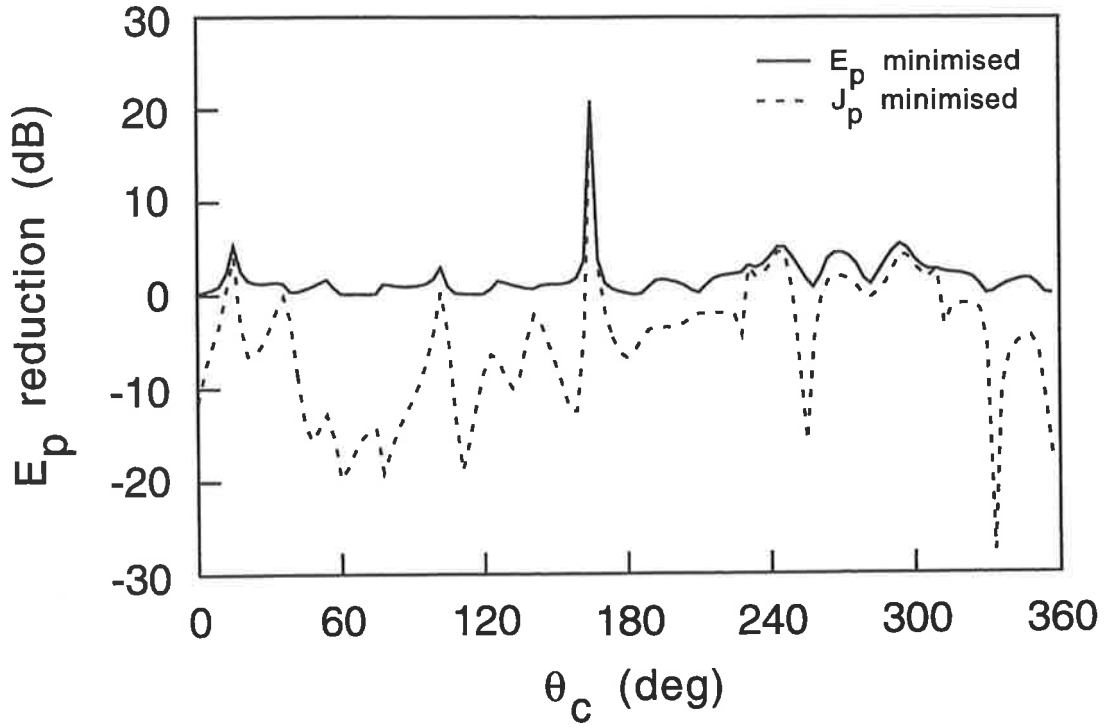

Figure 6.1 E_p reduction as a function of θ_c at 83 Hz for two error criteria with 1 control source and 1 error sensor.

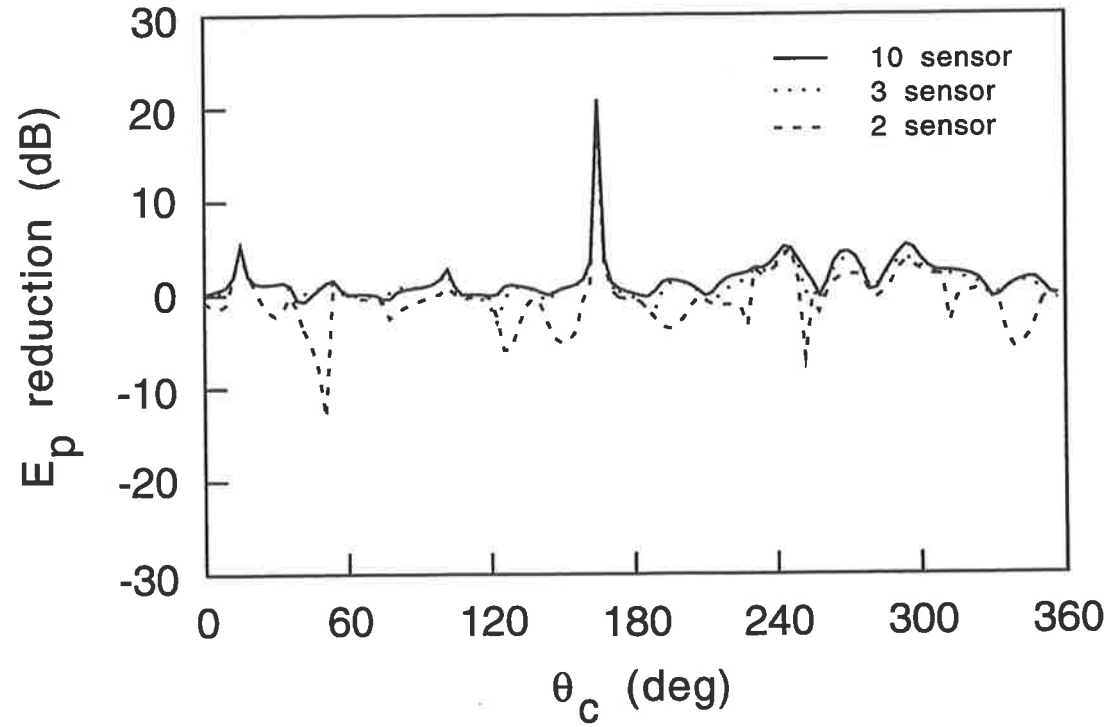

Figure 6.2 E_p reduction as a function of θ_c at 83 Hz for various numbers of error sensors with 1 control source.

circumferential locations of the control source under consideration. This is shown in Figure 6.3 which displays the theoretical reduction achievable with E_p as the error criterion, for different numbers of control sources.

Examination of the pressure at each of the error sensors, for a configuration consisting of three sensors and one control source reveals that, for minimisation of J_p, the pressure is not necessarily reduced at all of the error sensors. This can be seen in Figure 6.4 which shows the pressure reduction at the 3 error sensors for a range of circumferential locations of the single control source. In particular, for a control source circumferential location of θ_c = 245°, the pressure at sensor 2 has increased by approximately 7 dB, even though both J_p and E_p have decreased by approximately 4 dB, as shown in Figure 6.2. This indicates that although the acoustic potential energy in the enclosure may be minimised, the pressure at each location in the enclosure is not necessarily also minimised. In a practical context, this may mean that not every passenger is able to perceive the benefits of the reduced levels of acoustic potential energy throughout the cabin, and may in fact experience increased sound pressure levels in their vicinity.

As shown in Figure 6.1, the actual reduction in E_p due to minimisation of J_p at a single error sensor varies with the location of the control source. For those control source locations which produced a reduction in E_p, a reduction in the amplitudes of the predominant acoustic modes was found to be the mechanism whereby the reduction in pressure at the error sensor was achieved. Conversely, locations of the control source which were characterised by a rearrangement of the relative amplitudes and phases of the

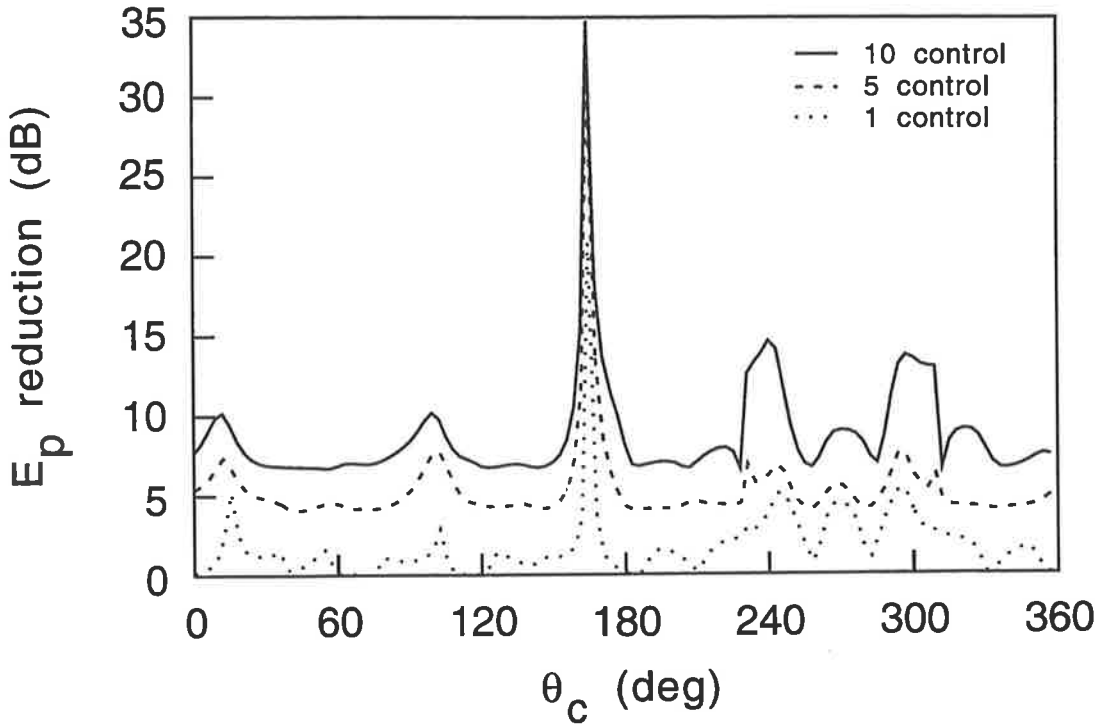

Figure 6.3 E_p reduction as a function of θ_c for control source #1, at 83 Hz for various numbers of control sources.

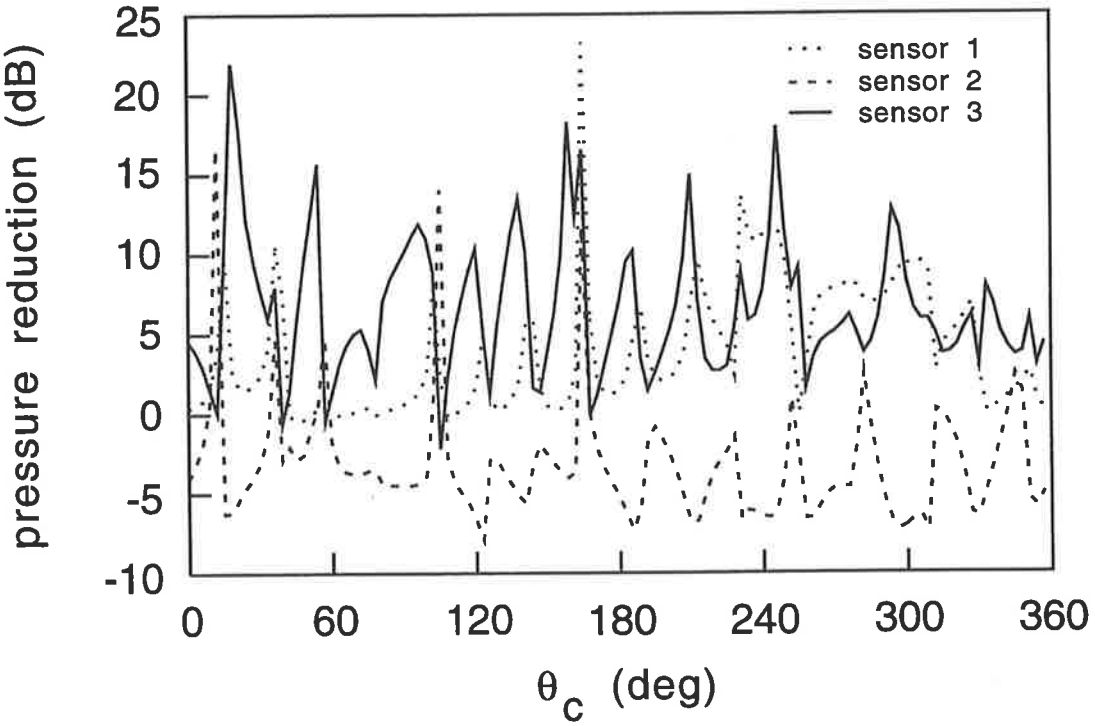

Figure 6.4 Acoustic pressure reduction at each error sensor as a function of θ_c at 83 Hz with 1 control source.

acoustic modes as the mechanism to achieve control at the error sensor, produced an increase in the acoustic energy, E_p. Figure 6.5 shows the relative amplitudes and phases of the first eight acoustic modes for control applied at a circumferential location $\theta_c = 15°$. The figure reveals that the three predominant acoustic modes under primary excitation (modes 1, 2 and 7) have been reduced in amplitude by the action of the control force applied to the structure. The acoustical potential energy has thus been reduced by approximately 4 dB. In contrast, Figure 6.6 reveals that, for control applied at $\theta_c = 0°$, most of the acoustic modes displayed are increased in amplitude under the action of control. Minimisation of pressure at the error sensor has been achieved by rearrangement of the relative phase of the acoustic modes, in particular modes 1 and 3. Due to the increased amplitudes of the acoustic modes the acoustic potential energy has increased by 11.6 dB for this control source location.

Increasing the number of error sensors to 10, for the single control source located at $\theta_c = 15°$, produces the acoustic modal response shown in Figure 6.7. In a similar manner to the single error sensor case, modal reduction is the mechanism by which J_p has been minimised, and correspondingly a reduction in E_p of 5.3 dB is realised. For a single control source located at $\theta_c = 0°$ the mechanism by which J_p has been minimised for the ten error sensor configuration is modal reduction. The relative modal amplitudes and phases for this case are shown in Figure 6.8. The amplitudes and relative phase of the first and third acoustic modes have been altered, while the other modes displayed have remained almost unchanged by the influence of the control source. The resultant modal response only reduces the acoustic potential energy, E_p, by 0.1 dB.

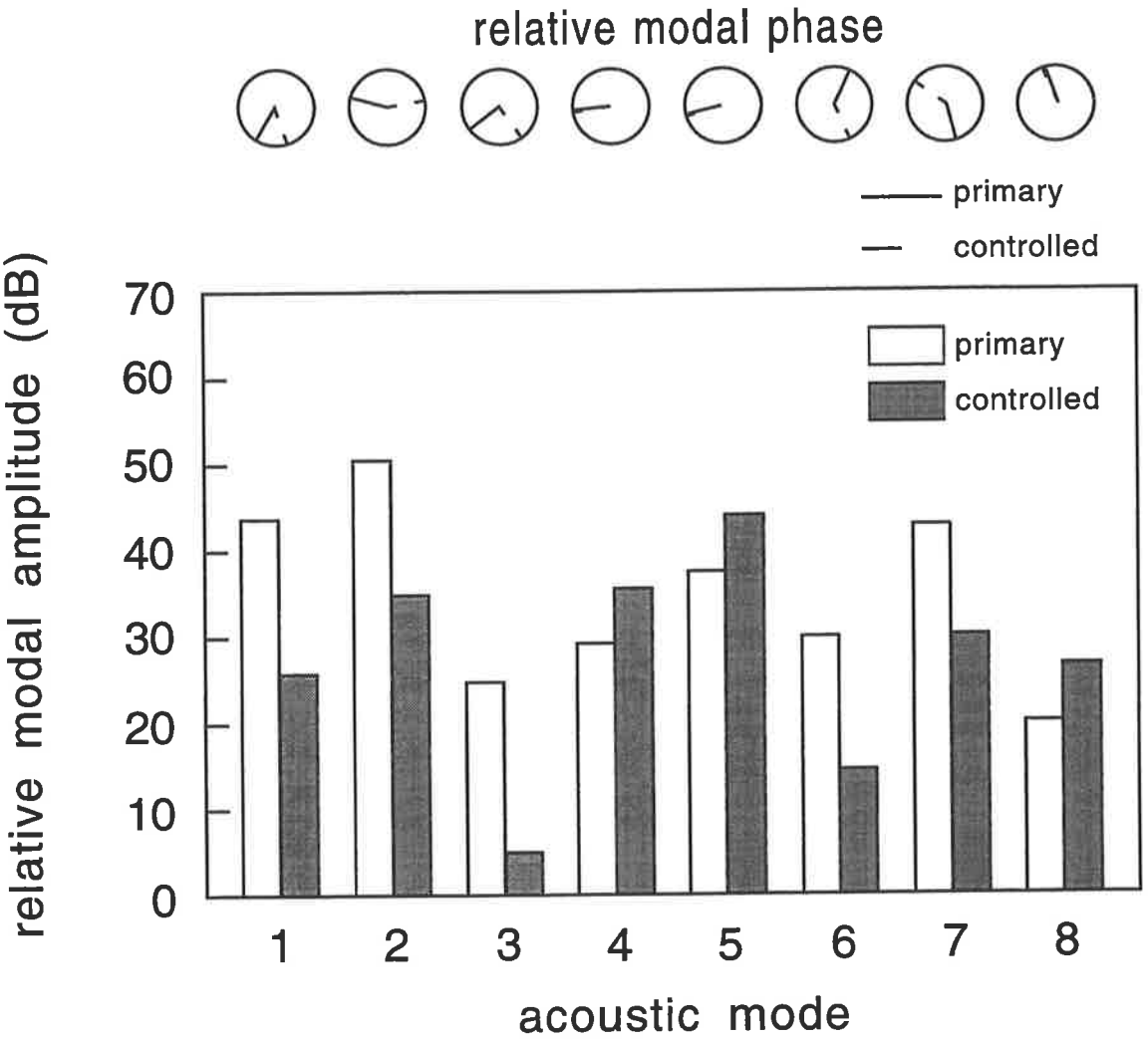

Figure 6.5 Acoustic mode response at 83 Hz for 1 control source at θ_c = 15° and minimisation of J_p from 1 error sensor.

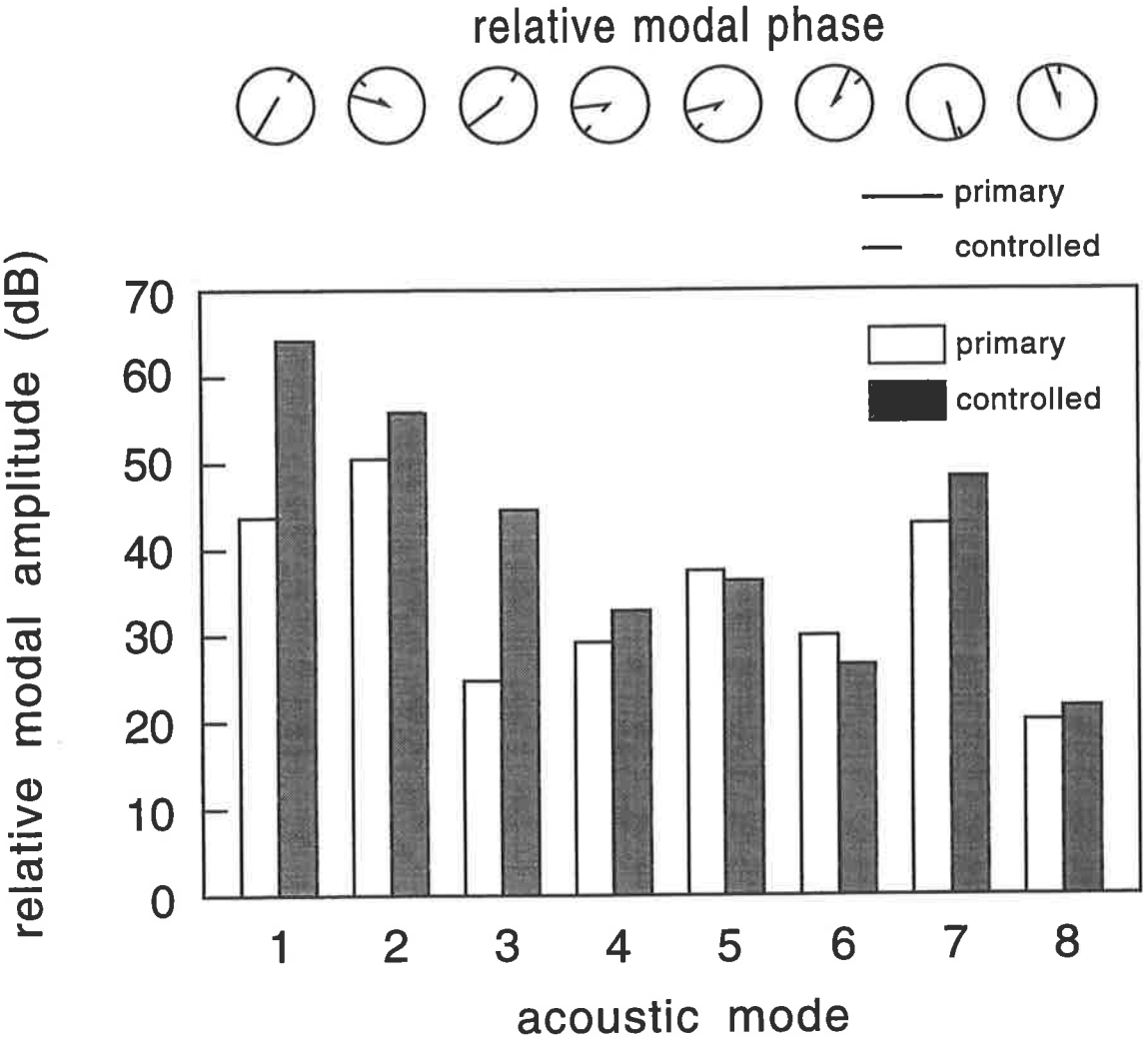

Figure 6.6 Acoustic mode response at 83 Hz for 1 control source at $\theta_c = 0°$ and minimisation of J_p from 1 error sensor.

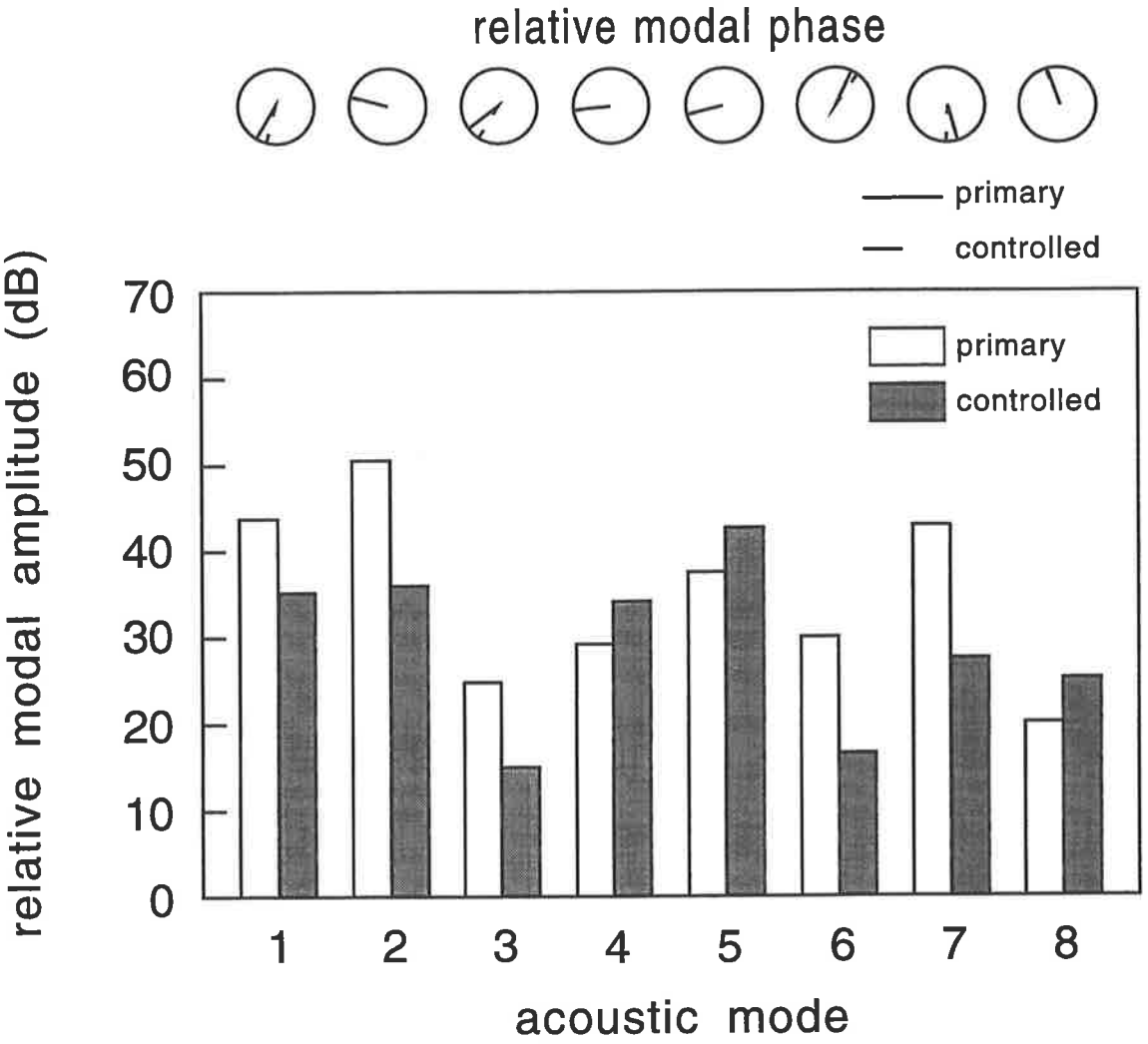

Figure 6.7 Acoustic mode response at 83 Hz for 1 control source at θ_c = 15° and minimisation of J_p from 10 error sensors.

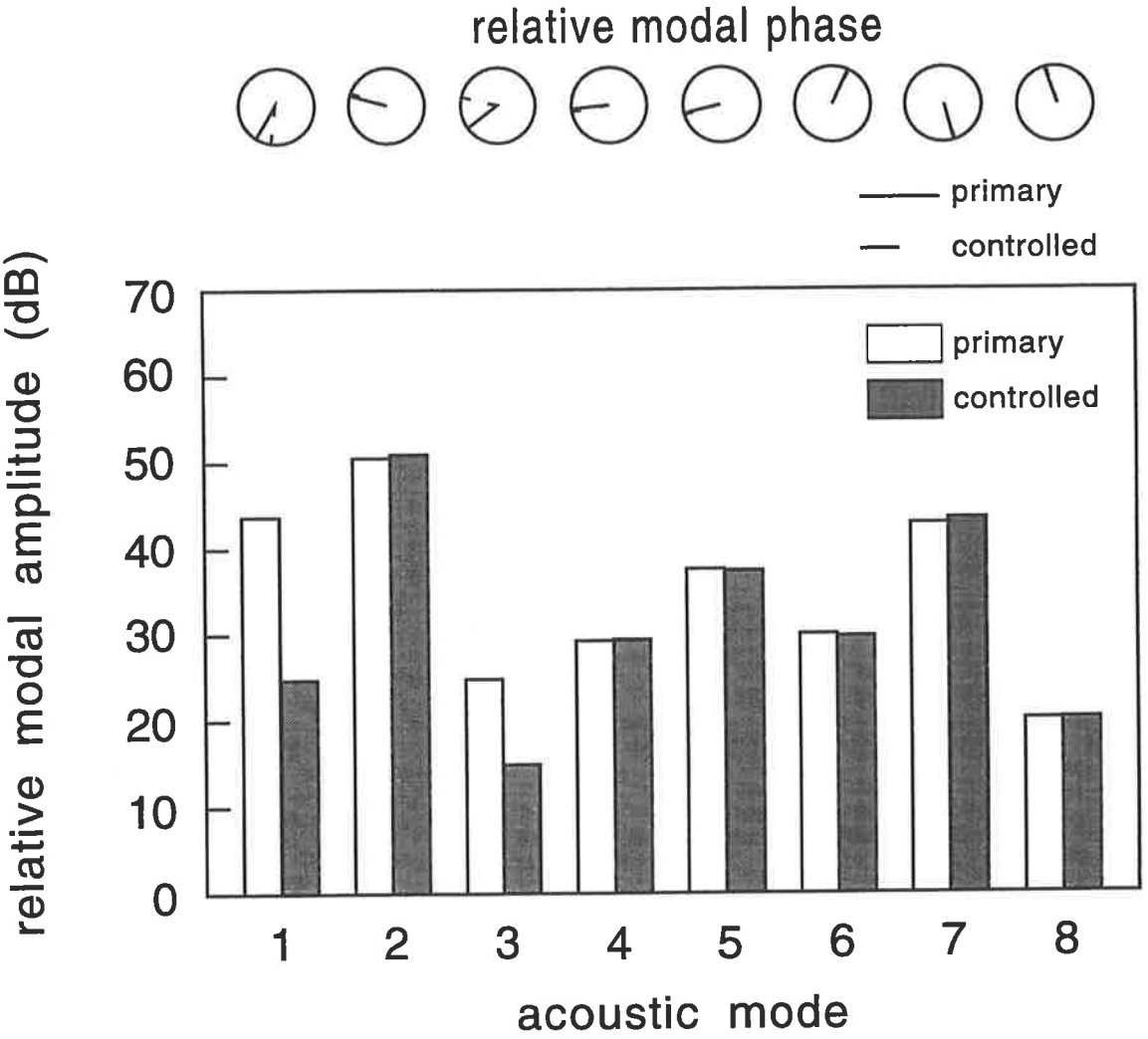

Figure 6.8 Acoustic mode response at 83 Hz for 1 control source θ_c = 0° and minimisation of J_p from 10 error sensors.

The mechanism of control thus appears to be predominantly a function of the control source location with relation to the primary excitation. The number of error sensors does not appear to affect the mechanism but an accurate estimate of the acoustic potential energy, J_p, will prevent the actual acoustic potential energy, E_p, being increased under the action of control.

Consider now the relationship between the minimisation of J_p and the consequent level of vibrational kinetic energy in the structure, V_p, for a single control source. The increase in V_p upon application of active control to the structure is shown in Figure 6.9 for 1, 3 and 10 error sensor configurations. It can be seen from the figure that for the single sensor configuration, the level of vibrational kinetic energy rises to a level which would be unacceptable in practice. This is due to the poor estimate of E_p provided by the single error sensor for most of the control source circumferential locations, θ_c. For example, at $\theta_c = 60°$, a 16 dB increase in vibrational kinetic energy has occurred to provide the 40 dB reduction in pressure at the single error sensor. The actual acoustic potential energy, E_p , has also risen by 20 dB. Thus, the minimisation of the pressure at a single error sensor has deleterious effects upon both the acoustic potential energy within the enclosure, and the vibrational kinetic energy within the structure, for this particular control source location.

As mentioned earlier, increasing the number of error sensors provides an improved estimate of E_p for all control source circumferential locations, and in addition ensures that local minimisations in pressure do not result in increases in the overall acoustic potential

and vibrational kinetic energies. From Figure 6.9 it can be seen that for the 10 sensor configuration, the maximum increase in vibrational kinetic energy is only 2 dB, a level which is likely to be acceptable in practice.

From the simulations conducted for a range of control source circumferential locations, the results of which are shown in Figures 6.1, 6.2, 6.3, and 6.4, it is evident that, although the control and primary source are in the same cross-sectional plane, and would thus have equivalent axial structural mode shape function values, there are relatively few circumferential locations where a single control source is well matched to the primary source. Consequently, the levels of E_p are generally reduced by less than 5 dB. This gives an indication of the large number of structural modes which contribute significantly to the response. If the structural response was dominated by a small number of modes, the control and primary source would be well matched at an increased number of circumferential control source locations. Thus for a more realistic aircraft structure which would include stiffening of both the shell and the floor, the resultant decreased structural modal density would cause less modes to contribute significantly to the acoustic response at a given frequency, and thus the control and primary source would be more likely to be well matched at a greater number of circumferential control source locations.

For the next configuration examined, the point force control source is applied to the floor portion of the test structure, at the same axial location of x_c = 1.323 m, such that the primary and control sources are in the same cross-sectional plane.

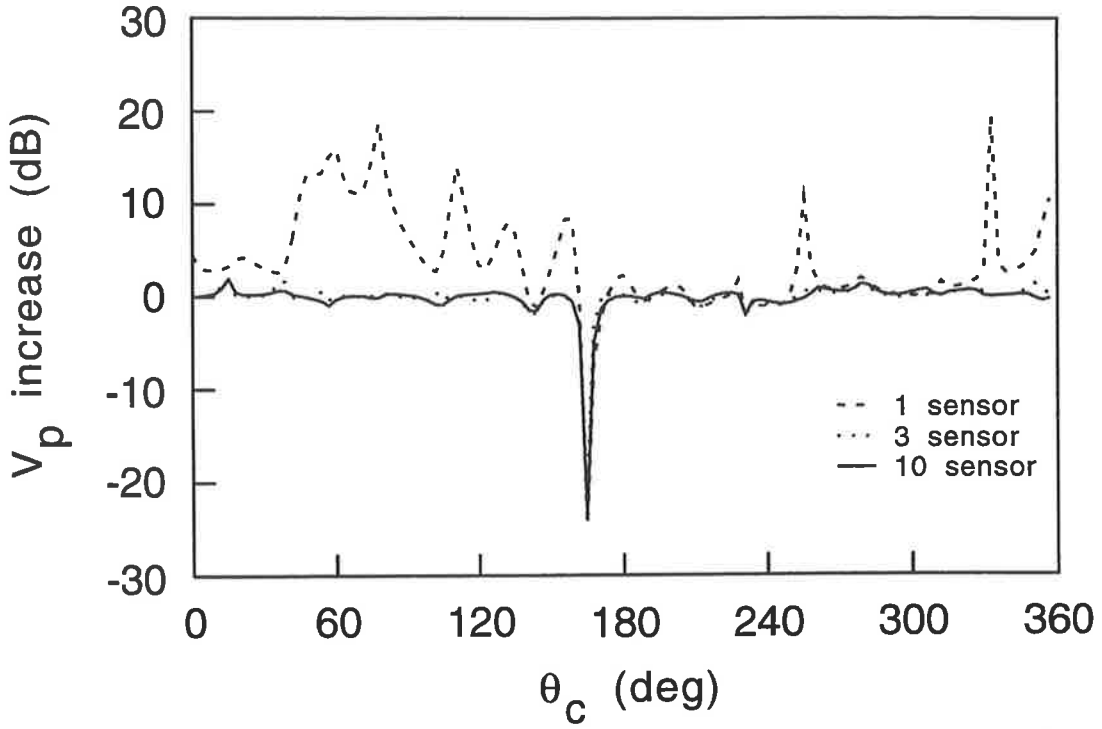

Figure 6.9 V_p increase as a function of θ_c at 83 Hz for various numbers of error sensors with 1 control source.

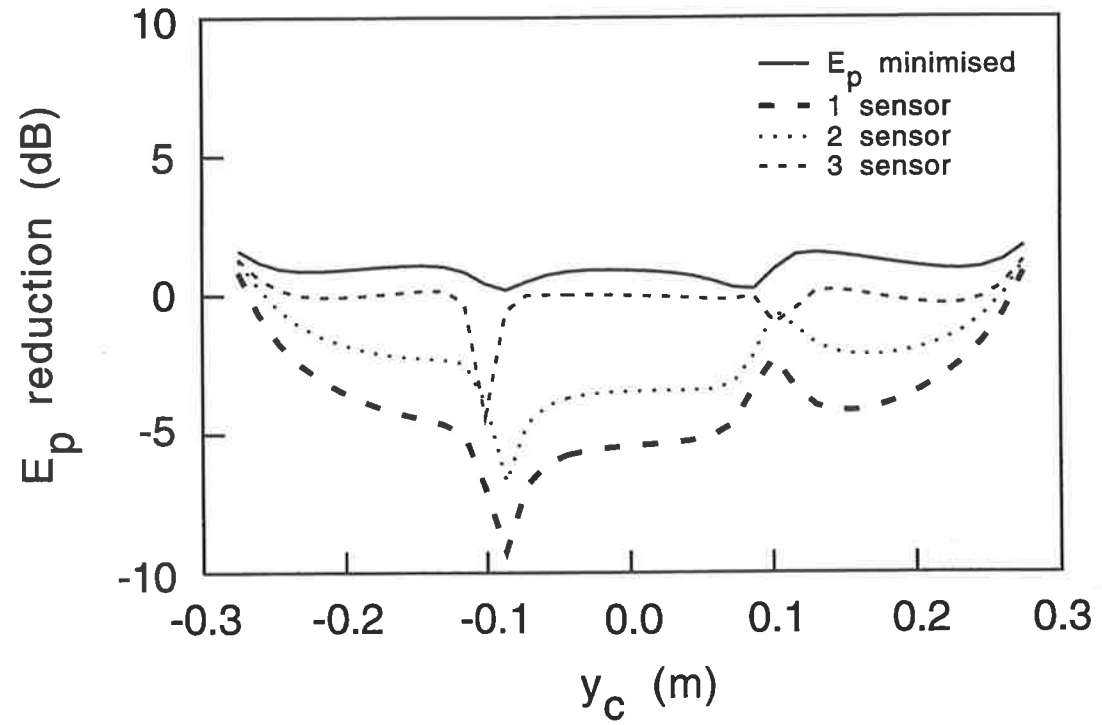

Figure 6.10 E_p reduction as a function of y_c at 83 Hz for various numbers of error sensors with 1 control source.

Again, the level of pressure reduction at a single error sensor is approximately 40 dB for all transverse locations of the control force, y_c, however, at almost all transverse control source locations the actual acoustic potential energy E_p rises because the control source is not well matched to the primary source at any of these locations. Figure 6.10 shows the reduction in E_p achievable for minimisation of J_p with 1, 2, and 3 sensor configurations, and the theoretical minimum acoustic potential energy E_p for the single control source applied at the transverse locations, y_c. In contrast to the previous case examined, where the 3 sensor configuration gave an estimate of acoustic potential energy, J_p, close to the actual value E_p, the estimate is not as accurate for this case. This indicates that the accuracy of the estimate J_p is not only a function of the number of error sensors but also the relative location of the control and primary sources. Thus the influence of the error sensor configuration and the control source configuration upon the behaviour of the system cannot be examined independently. The dependence of the estimate of E_p on the error sensor locations is investigated later in this chapter.

Comparison of the values for minimisation of E_p, shown in Figures 6.10 and 6.1, reveals that the theoretical minimisation for a control source located in the floor is generally less than that for a control source located on the shell, for this particular primary source location and excitation frequency. Again this can be explained by the relative matching of the mode shape functions at the primary and control source locations.

Examination of the control force amplitude required to achieve control reveals that the amplitude needed to reduce the pressure at three error sensors is generally less for a force

applied to the floor portion of the test structure than for a force located on the shell portion of the structure. The control force amplitude for a range of transverse control source locations is shown in Figure 6.11, and for a range of circumferential locations in Figure 6.12. Although the control source positioned on the floor can be seen to achieve reduction at the error sensors more easily, in that the control force required is generally less than that required for a control source located on the shell, the actual reduction in acoustic potential energy is not as great as that for a source located on the shell because the control source is not as well matched to the primary source.

For the next case examined the control source was located on the shell portion of the structure at the same circumferential location as the primary source, such that $\theta_p = \theta_c = 165.3°$. The axial location of the control source, x_c, was varied over the length of the test structure. For a single error sensor, single control source configuration, approximately 40 dB reduction in pressure at the error sensor is achievable for all control source axial locations. The actual reduction in acoustic potential energy is shown in Figure 6.13, which reveals that for the single sensor case the acoustic potential energy is only decreased for control source locations, x_c, between 1.2 m and 1.7 m, and is increased at other locations. For increased numbers of error sensors the estimate of E_p provided by J_p is more accurate, and the actual minimisation in E_p is closer to that theoretically achievable. Figure 6.14 displays the control force amplitude required for control, while Figure 6.15 shows the corresponding control force phase. These figures illustrate the effect that the estimate of E_p has upon the control force produced by the controller and its subsequent effect upon the levels of E_p. In particular, Figure 6.15 reveals that minimisation of E_p is

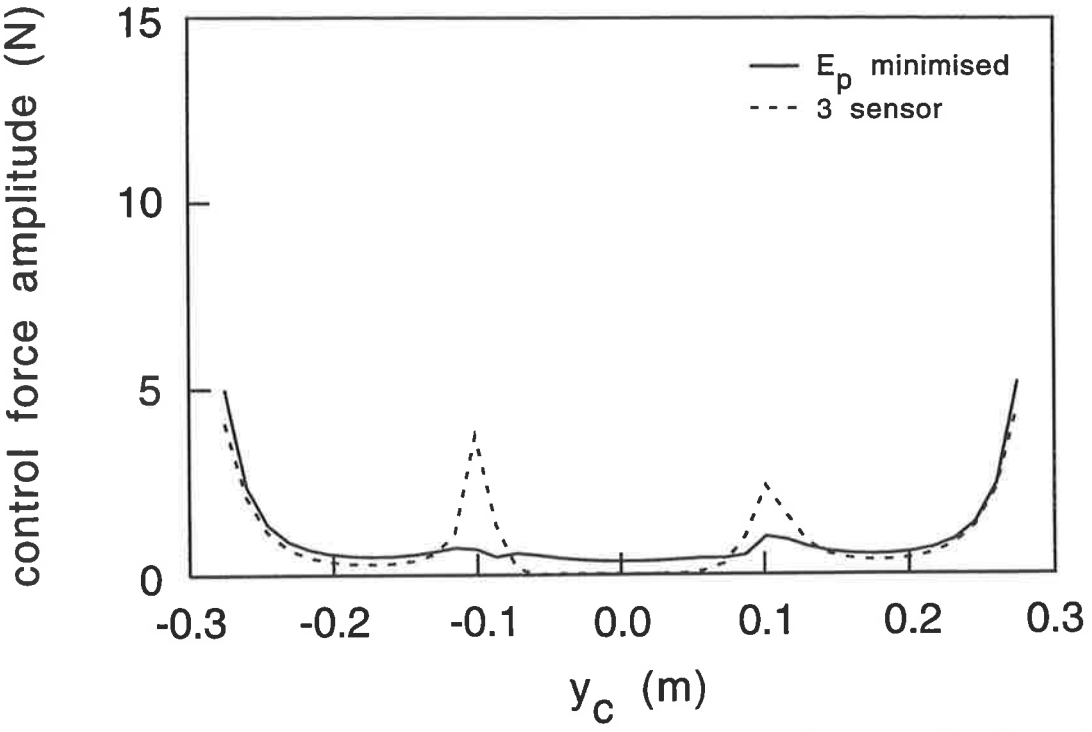

Figure 6.11 Required control force amplitude applied to the floor as a function of y_c at 83 Hz for two error criteria with 1 control source.

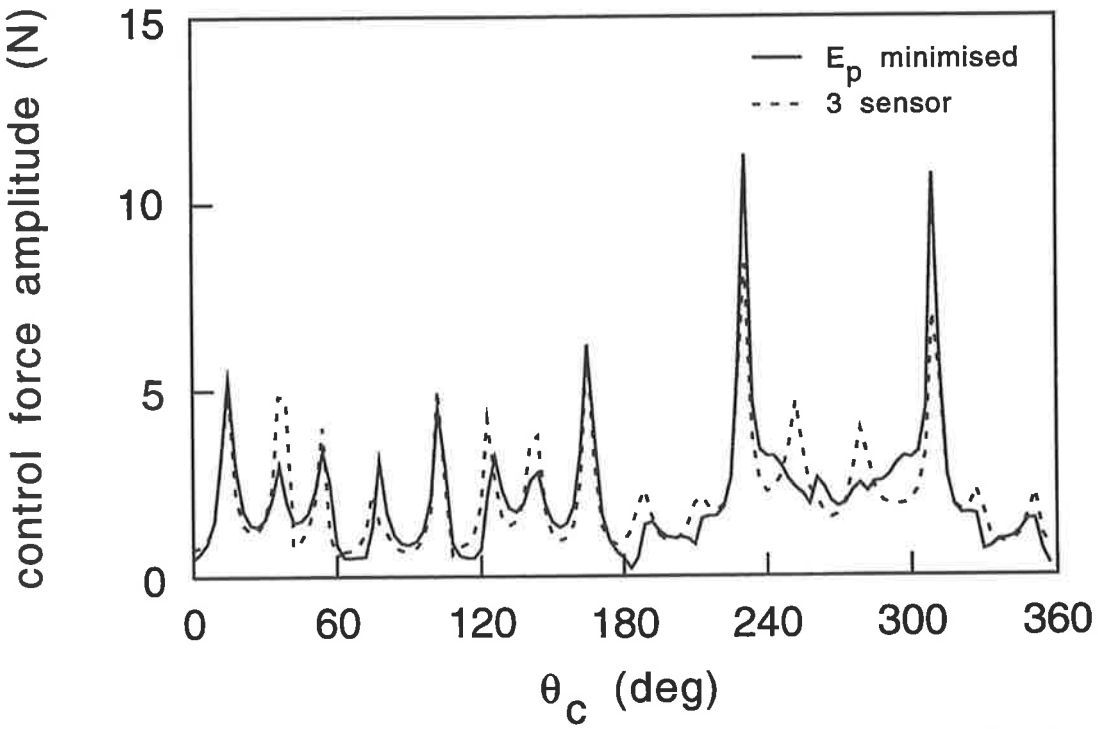

Figure 6.12 Required control force amplitude applied to the cylinder as a function of θ_c at 83 Hz for two error criteria with 1 control source.

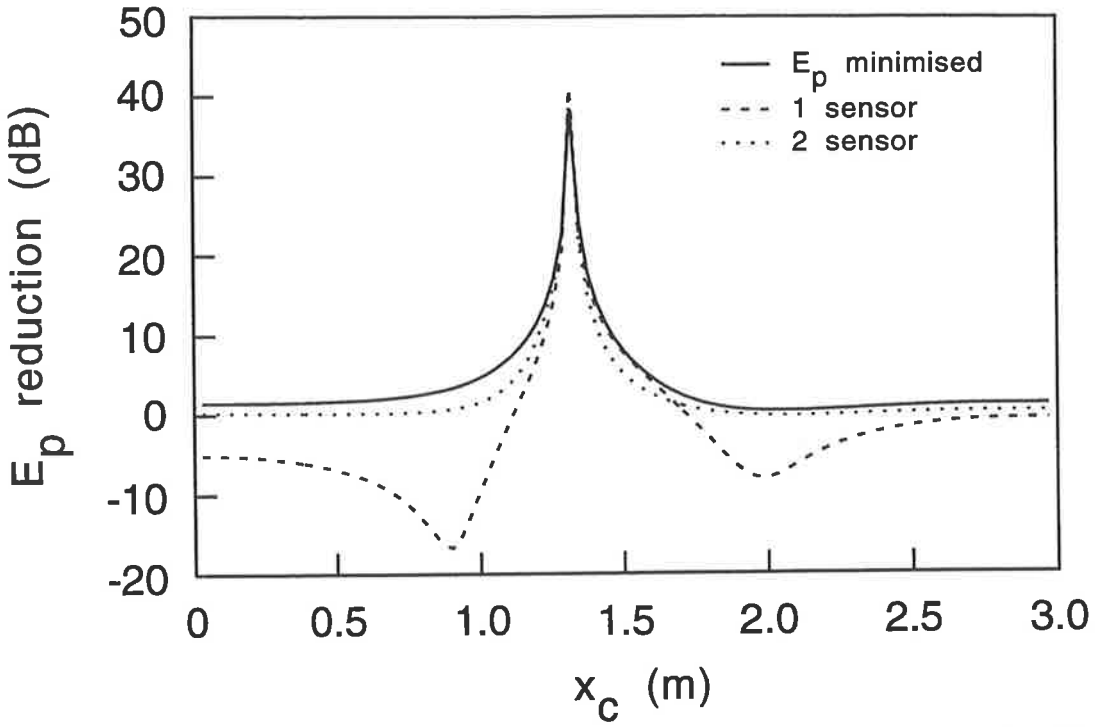

Figure 6.13 E_p reduction as a function of x_c at 83 Hz for two error criteria with 1 control source.

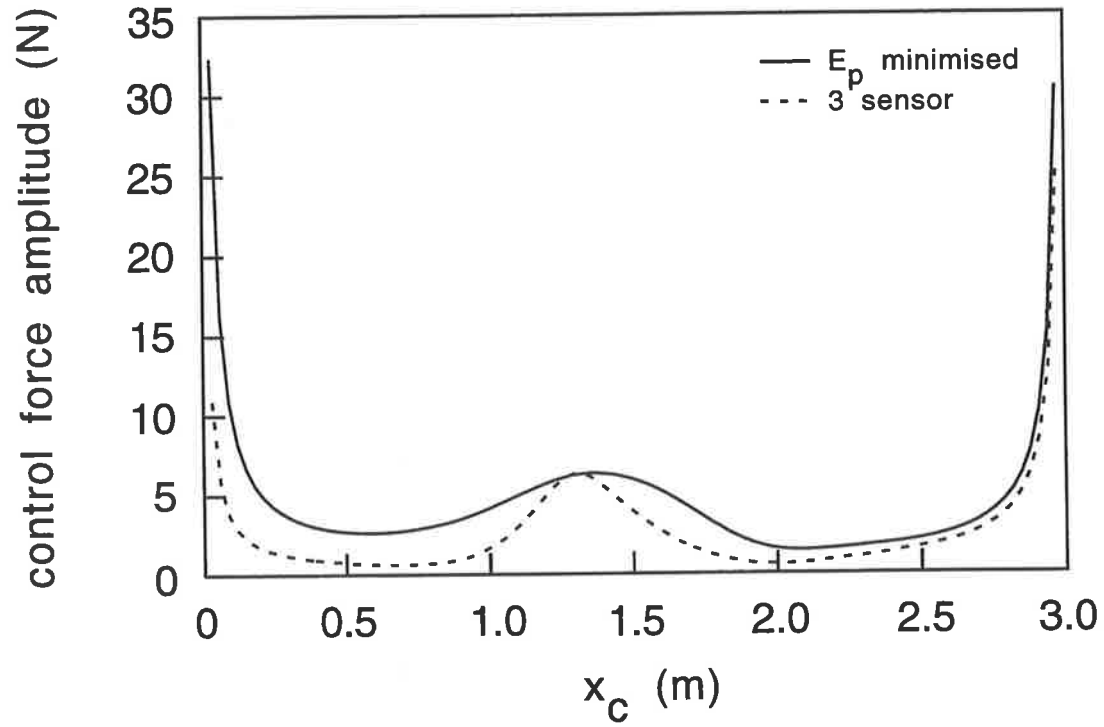

Figure 6.14 Control force amplitude as a function of x_c at 83 Hz for two error criteria with 1 control source.

only achievable when the control force phase calculated from the acoustic potential energy estimate J_p is very close to that theoretically required to minimise E_p. Also it can be seen that the control source is well matched to the primary source only within a relatively small region around the primary source. This again indicates that there are a high number of structural modes contributing to the response of the system. In comparison, considering the extreme case of only one mode dominating the structural response, all control source axial locations, x_c, would result in equivalent actual reductions in acoustic potential energy, E_p, for any number of error sensors.

The influence of error sensor location upon the performance of active control applied to the test structure was investigated for the case of a single control source located at the same axial height, x_c, as the primary source such that $x_p = x_c = 1.323$ m. The control source circumferential location was set to $\theta_c = 237.0°$. For the first case the axial location of the error sensor, x_e, was varied over the length of the acoustic space for a fixed cross-sectional location of $\theta_e = 63°$ and $r_e/a = 0.4466$. A pressure reduction of 40 dB was encountered for all x_e. Figure 6.16 shows the influence of the sensor location upon the level of acoustic potential energy reduction for 1, 2 and 3 sensor configurations. The theoretical maximum reduction in E_p for the primary and control source configuration used is 3.3 dB. Figure 6.16 reveals that for the one sensor case the level of reduction in E_p is dependent on the error sensor location, and that for x_e between 0 and 1.5 m, the level of reduction is close to that theoretically achievable for minimisation of E_p. Increasing the number of error sensors reduces the influence of any particular error sensor upon the levels of reduction, and the 3 sensor configuration produces levels of reduction

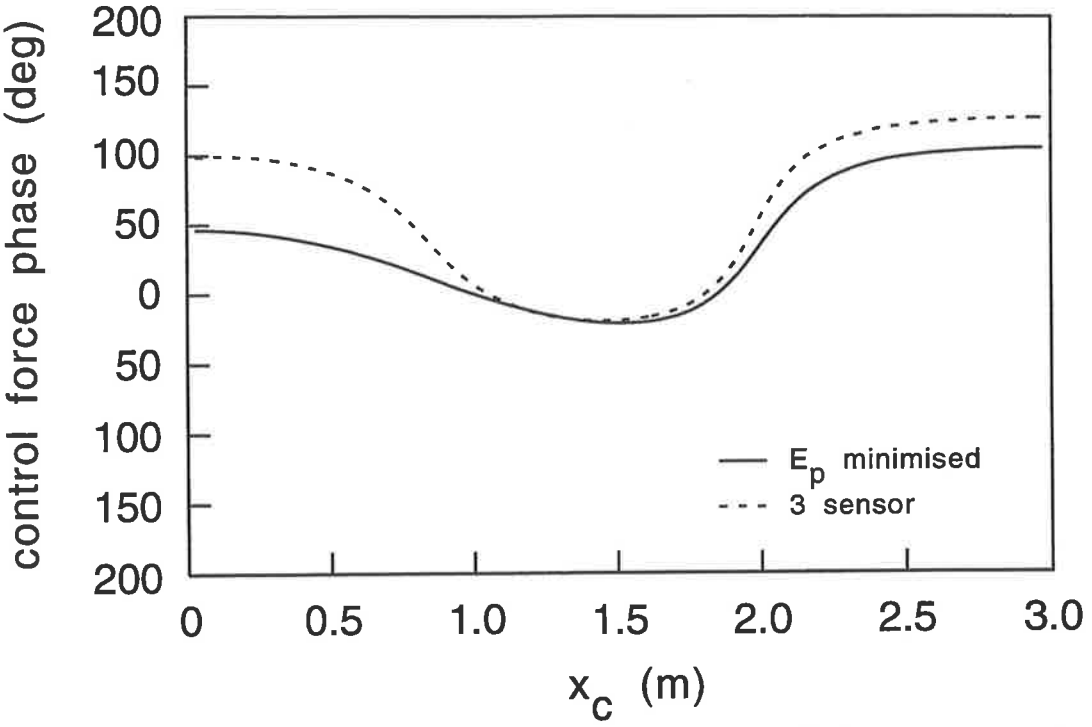

Figure 6.15 Control force phase as a function of x_c at 83 Hz for two error criteria with 1 control source.

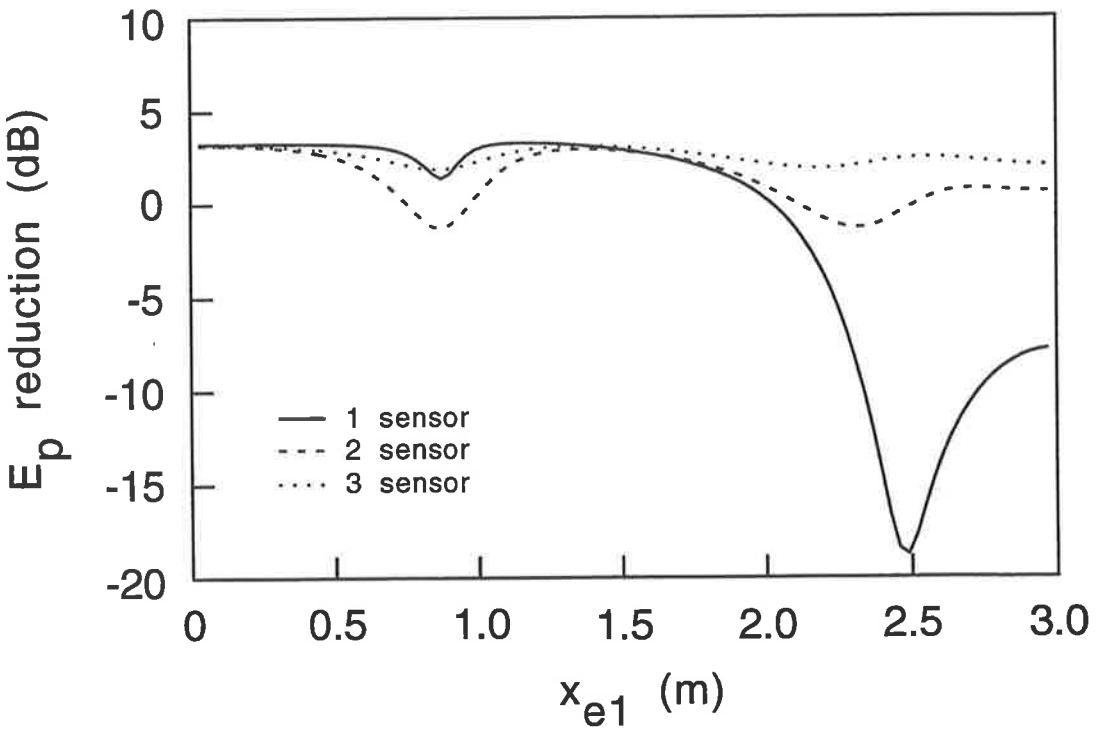

Figure 6.16 E_p reduction as a function of x_{e1} at 83 Hz for various numbers of error sensors with 1 control source.

close to those theoretically achievable for all axial locations of error sensor 1. The results presented in Figure 6.16 indicate that having the error sensor, control source and primary source in the same cross-sectional plane, at $x_p = x_c = x_e = 1.323$ m, does not give the greatest level of reduction in E_p, and that it is also not important that the error sensor be near the region of the primary or control source to achieve levels of reduction close to those theoretically possible.

For the following case the cross-sectional location of the error sensor was varied over a fixed plane at $x_e = 1.323$ m. Figures 6.17, 6.18 and 6.19 show the level of reduction in E_p achievable for cross-sectional variation of this sensor for the 1, 2 and 3 sensor configurations. These figures indicate the level of reduction in E_p is dependent upon the error sensor location, and that reduction levels approaching the theoretical maximum reduction in E_p of 3.3 dB are only realised in a small band for the single error sensor case. Increasing the number of error sensors increases the size of the area for which the particular error sensor location produces a reduction in E_p. Thus, in a practical situation wherein the locations of the error sensors and the control sources are likely to be fixed, increasing the number of error sensors increases the likelihood of achieving a reduction in the acoustic potential energy within the cabin.

Figure 6.20 displays the relationship between the number of control sources applied to the structure and the level of reduction in E_p, for the error criterion of minimisation of E_p. The control source locations are given in Appendix C. The figure illustrates that the level of reduction in E_p increases with the number of control sources in an approximately

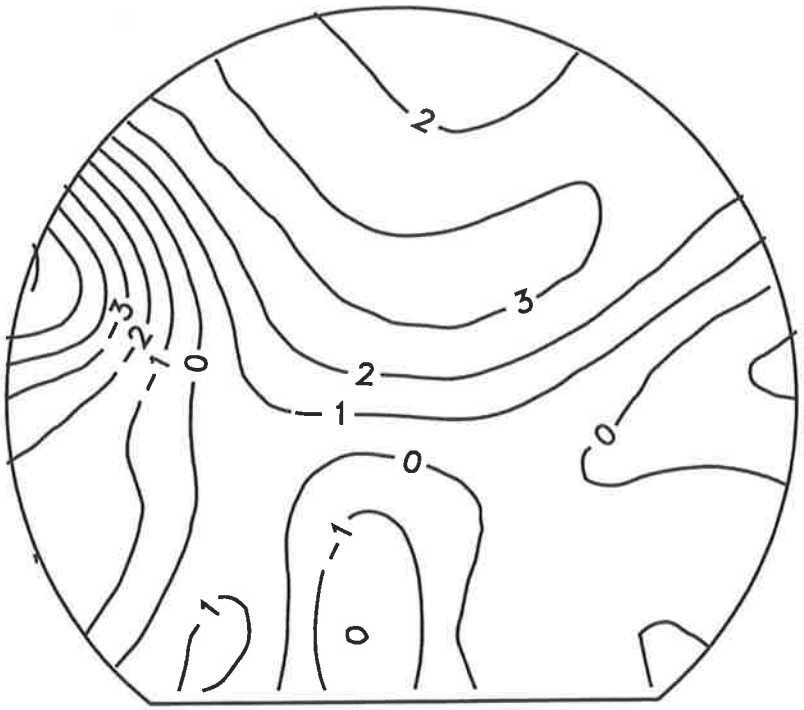

Figure 6.17 E_p reduction for 1 error sensor at 83 Hz as a function of sensor location.

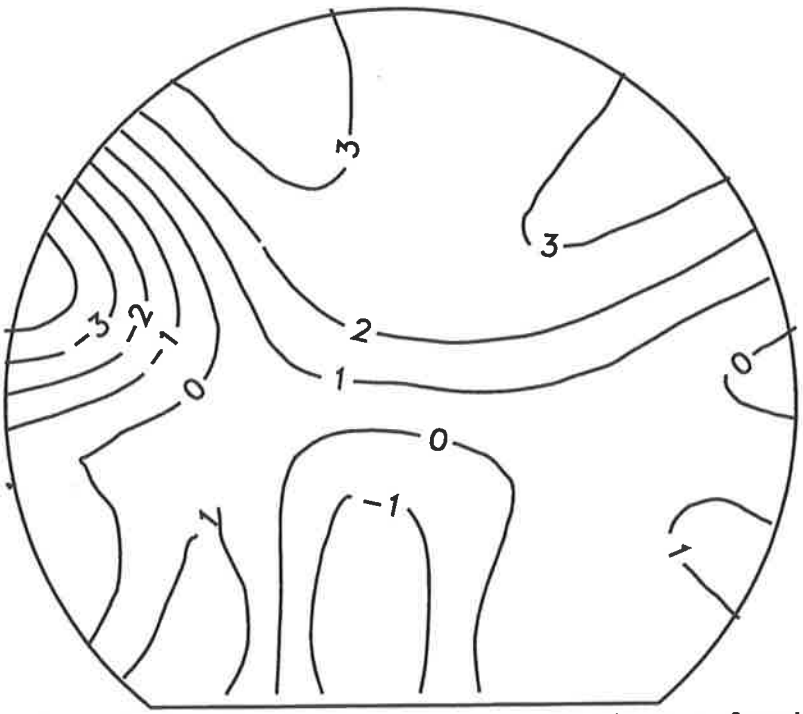

Figure 6.18 E_p reduction for 2 error sensors at 83 Hz as a function of sensor location, with the other sensor fixed at (x_e, θ_e, r_e/a) = (2.430 m, 249.0°, 0.7728).

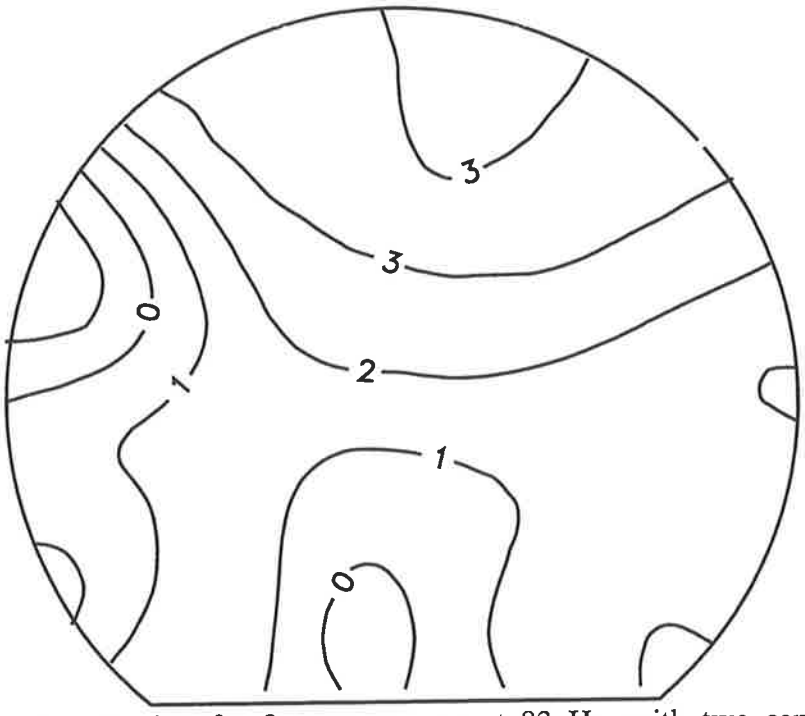

Figure 6.19 E_p reduction for 3 error sensors at 83 Hz, with two sensors fixed at $(x_e, \theta_e, r_e/a)$ = (2.430 m, 249.0°, 0.7728) and (0.649 m, 112.0°, 0.5069).

linear manner. Also shown in Figure 6.20 is the relationship between the number of control sources and the sum of the control force amplitudes required to achieve the corresponding reduction in acoustic potential energy, E_p. The figure reveals that the total force amplitude input to the structure increases with the number of control forces. In addition, the sum of quadratically optimised control force amplitudes, in Newtons, is closely related to the reduction in acoustic potential energy, E_p, expressed in dB, upon application of the quadratically optimised control forces. The individual force amplitude components are shown in Figure 6.21, which indicates a general trend for the quadratically optimised amplitude of each control force to decrease for an increasing total number of control sources. As shown in the figure, there are exceptions to the trend; for example, in the instance when the number of control sources increases from 3 to 4, the control force amplitude for control source 2 rises from 0.2 N to 1.2 N. Thus in a practical context,

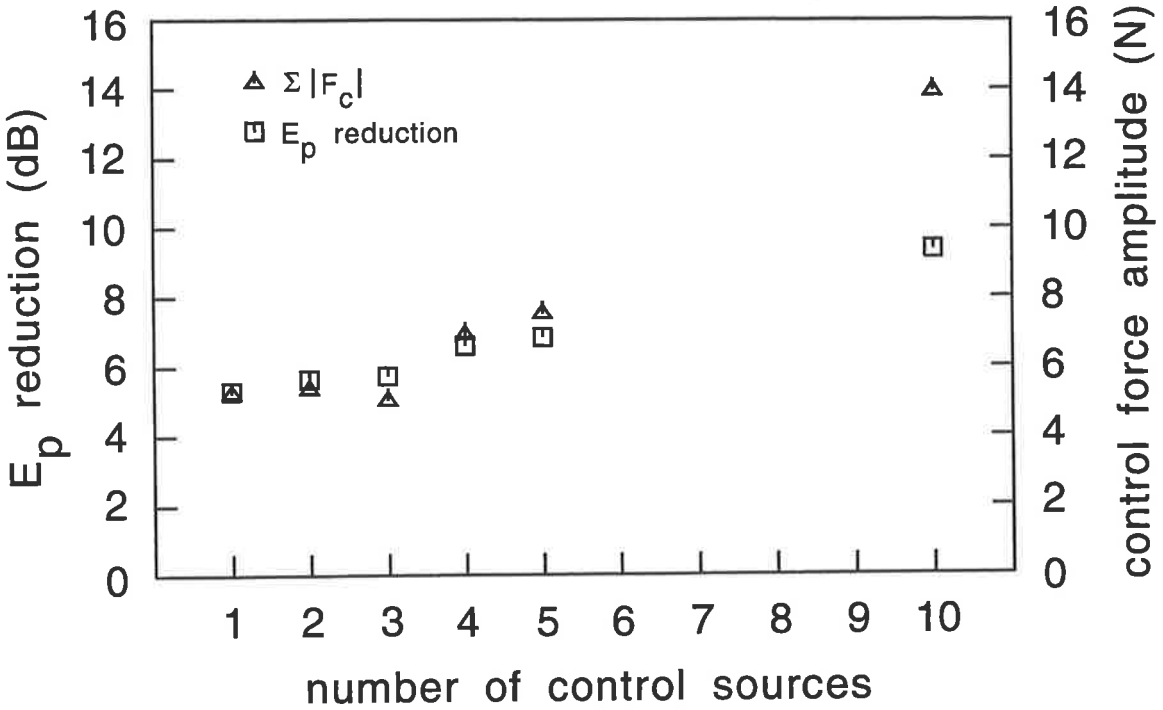

Figure 6.20 E_p reduction and total required control force amplitude as a function of the number of control sources at 83 Hz.

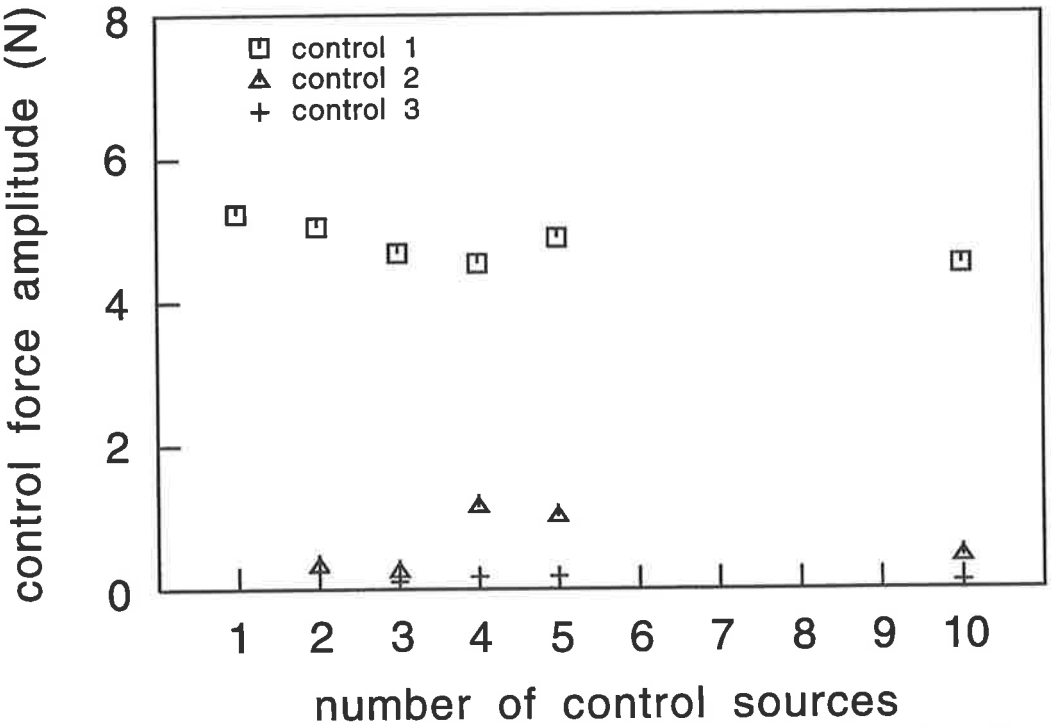

Figure 6.21 Required control force amplitude as a function of the number of control sources at 83 Hz.

increasing the number of control sources does not necessarily reduce the control force amplitude required from a particular control source.

6.3 SIMULATIONS FOR RESONANT ACOUSTIC SPACE EXCITATION FREQUENCY

For the remainder of the simulations performed, an excitation frequency of 57 Hz was used, which corresponds to resonant excitation of the (s1, 1) acoustic mode. For the primary source located as in the previous tests, and of equivalent complex force, and a single error sensor located at $\vec{x}_e = (x_e, \theta_e, r_e/a)$ = (1.7178 m, 63.0°, 0.4466), a single control source was utilised over a range of circumferential locations, θ_c, for a fixed control source axial location, x_c = 1.323 m. Figure 6.22 shows the resultant reduction in E_p, for the minimisation of J_p, obtained from the single error sensor. For this single error sensor case, the pressure reduction at the error sensor is approximately 40 dB for all θ_c. At the control source location, θ_c, which yields the greatest level of reduction in E_p for the 57 Hz case, the level of reduction is less than that for the corresponding 83 Hz case. At other control source locations the levels of reduction in E_p are generally greater for an excitation frequency of 57 Hz than for an excitation frequency of 83 Hz. Also, for an excitation frequency of 57 Hz, there are far fewer control source locations for which minimisation of J_p results in an increase in E_p. This indicates that for resonant excitation of an acoustic mode, the estimate of E_p provided by a single error sensor is more accurate than the estimate provided for off-resonant excitation. Thus, the accuracy of J_p as an estimate of E_p is also a function of the excitation frequency. Figure 6.22 also shows the levels of reduction in E_p with minimisation of E_p as the error criterion, for different

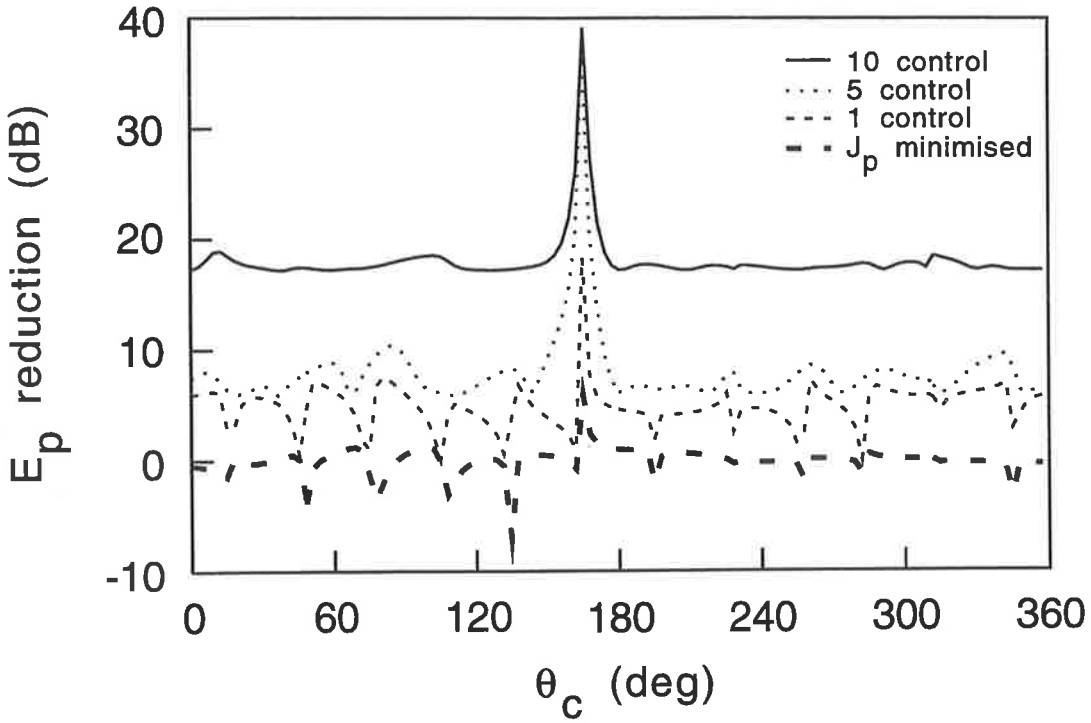

Figure 6.22 E_p reduction as a function of θ_c at 57 Hz for various numbers of control sources.

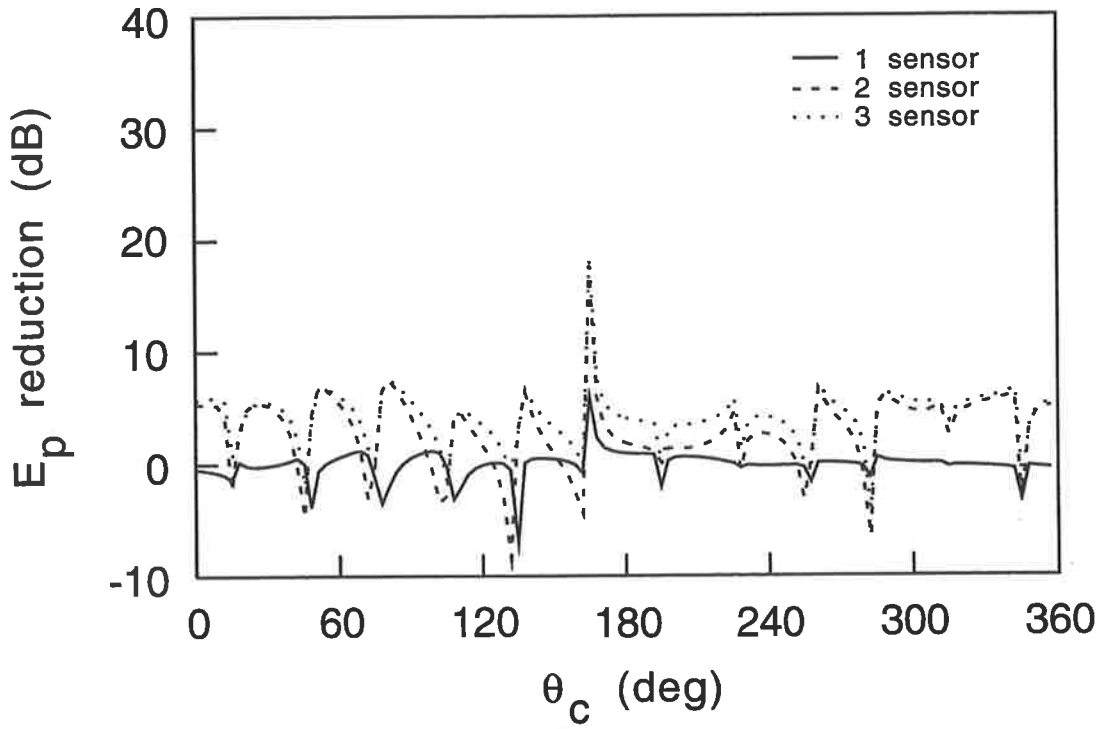

Figure 6.23 E_p reduction as a function of θ_c at 57 Hz for various numbers of error sensors with 1 control source.

numbers of control sources. Again, as the number of control sources is increased the levels of reduction in E_p rise for all circumferential locations of control source 1.

Using the 10 control source case as an example, the minimum level of reduction in E_p over the range of circumferential control source locations examined is around 17 dB. In comparison, the same configuration of control sources produces a minimum reduction of 7 dB for the 83 Hz excitation case. Thus it appears from the cases examined that greater levels of reduction in acoustic potential energy are achievable at frequencies corresponding to resonant acoustic excitation. Figure 6.23 shows the levels of reduction in E_p for minimisation of J_p obtained for different numbers of error sensors, with a single control source. With comparison to Figure 6.22, as the number of error sensors is increased, the acoustic potential energy estimate, J_p, increases in accuracy, with 3 error sensors providing an estimate which produces almost equivalent levels of reduction in E_p to those theoretically achievable.

Figure 6.24 displays the increase in vibrational kinetic energy within the structure, V_p, for the 1, 2 and 3 sensor configurations. The figure indicates that for the resonant excitation case examined, a control source location for which the mode shape function is poorly matched to the mode shape function at the primary source will not greatly increase the vibrational kinetic energy in the structure. Also, an increased number of error sensors does not significantly reduce the levels of V_p produced due to the application of active control. Figure 6.24 also reveals that for a reduction in acoustic potential energy within the acoustic space, the vibrational kinetic energy within the structure may rise. Hence, an error

criterion based upon minimisation of the vibrational kinetic energy, V_p, would not reduce the acoustic potential energy, E_p, for all circumferential control source locations, θ_c.

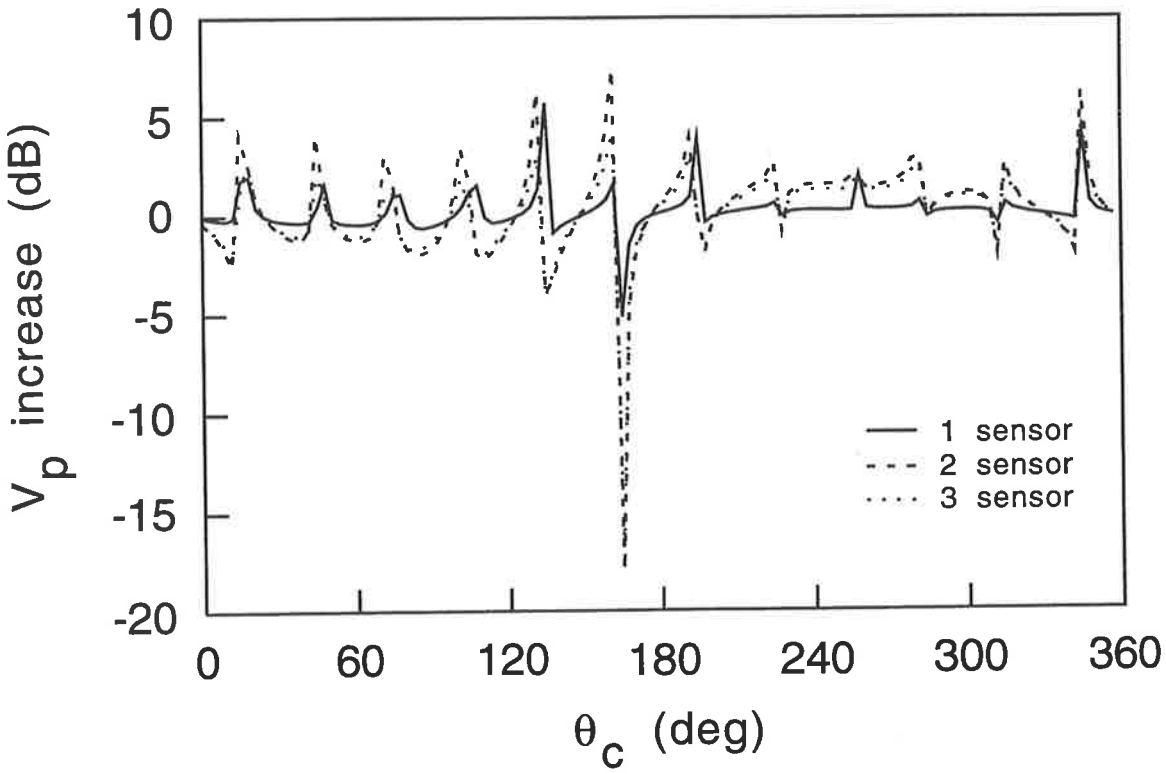

Figure 6.24 V_p increase as a function of θ_c at 57 Hz for various numbers of error sensors with 1 control source.

Comparing the acoustic modal response for a single error sensor and a single control source located at θ_c = 42°, shown in Figure 6.25, with that for a control source located at θ_c = 48°, shown in Figure 6.26, it can be seen that, for a 6° change in the control source circumferential location, the mechanism by which a reduction of pressure at the error sensor is achieved has altered. In addition, the ability of the single error sensor to estimate E_p has also altered. Figure 6.25 shows that the amplitude of the first acoustic mode has been reduced to provide the reduction at the error sensor, whereas Figure 6.26 shows an increase in the amplitudes of all of the modes displayed, because modal rearrangement is the mechanism by which a reduction has been achieved at the error sensor. Thus for an

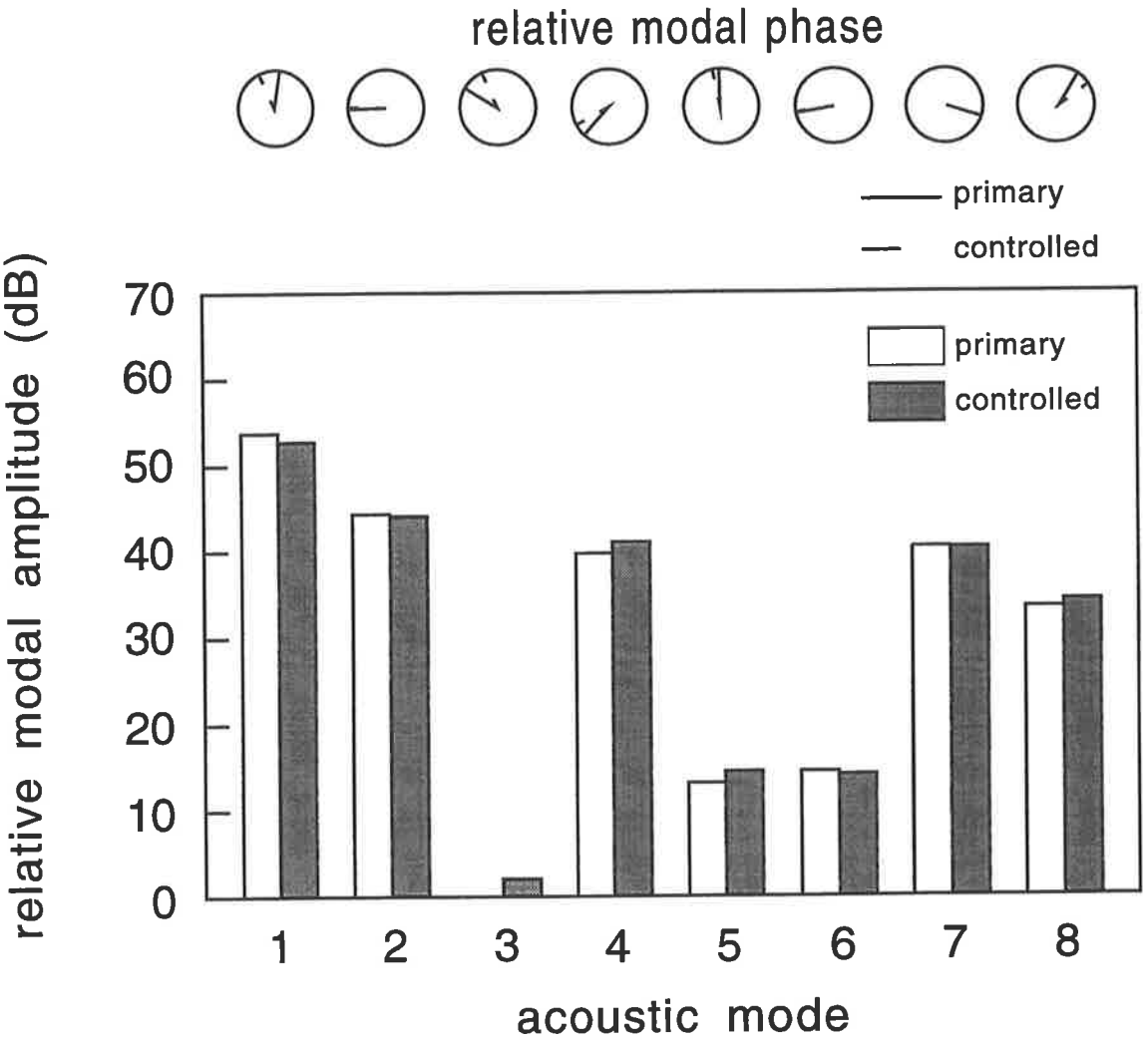

Figure 6.25 Acoustic mode response at 57 Hz for 1 control source at θ_c = 42° and minimisation of J_p from 1 error sensor.

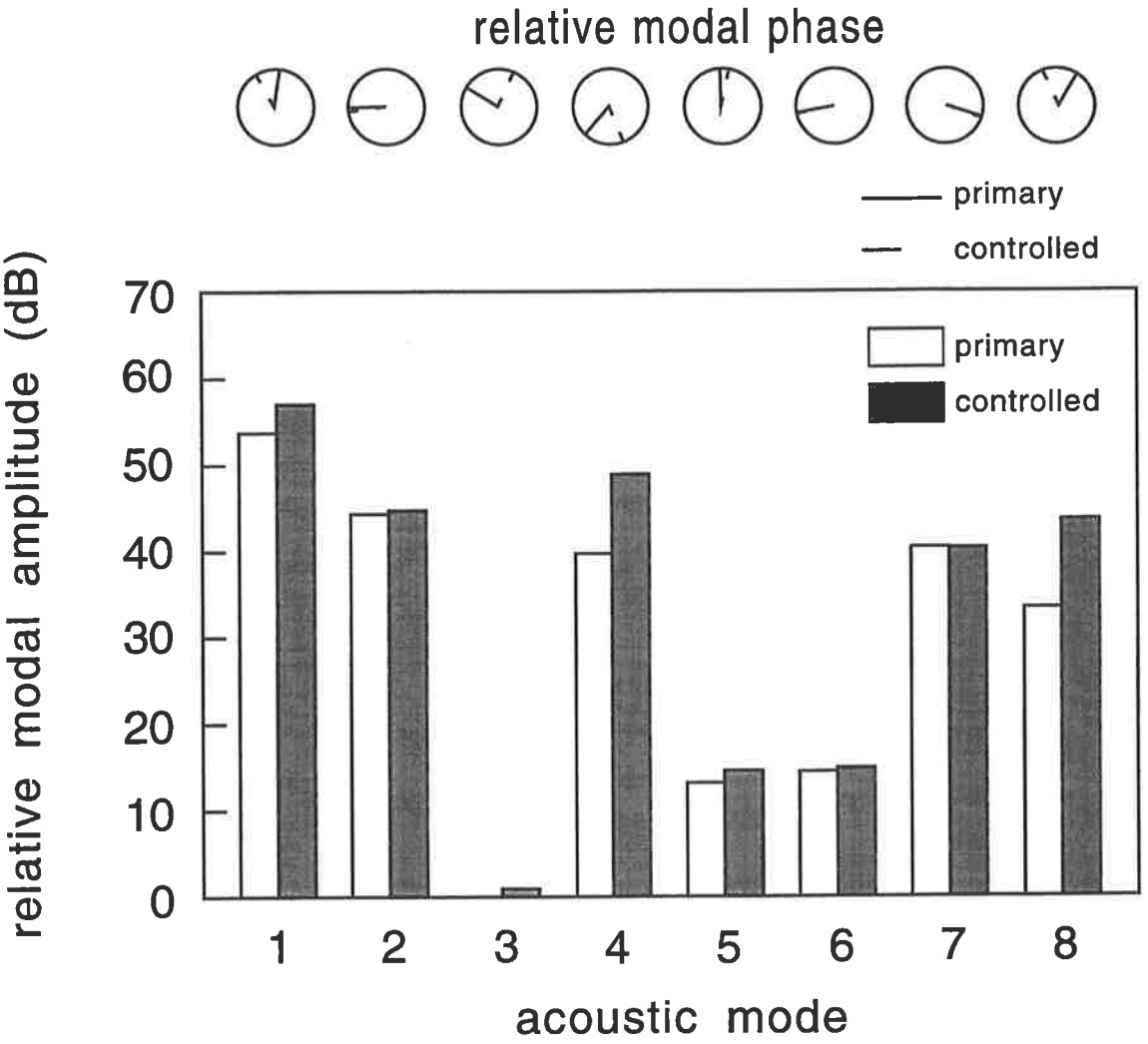

Figure 6.26 Acoustic mode response at 57 Hz for 1 control source θ_c = 48° and minimisation of J_p from 1 error sensor.

excitation frequency corresponding to acoustic resonance, modal rearrangement may still be the control mechanism by which the pressure at the error sensors is minimised, leading to increased levels of acoustic potential energy in the enclosure. This is because the coupling between the structural modes and the acoustic modes is not highly selective for the test structure examined here, which directly incorporates the influence of the cabin floor. This non-selective coupling results in a large number of acoustic modes contributing to the acoustic response, even at a frequency corresponding to an acoustic mode resonance, hence allowing the possibility of modal rearrangement as a control mechanism.

Examination of the modal responses for the same control source locations for an error criterion of minimising E_p, shown in Figures 6.27 and 6.28, reveals that modal amplitude reduction is the control mechanism for both control source circumferential locations. This indicates that if an accurate estimate of E_p is provided to the controller, the mechanism by which a reduction in E_p is achieved will generally be modal reduction, however, not all acoustic modes will be reduced in amplitude. Figures 6.27 and 6.28 reveal that even though modal amplitude reduction is the control mechanism, only the amplitude of the dominant acoustic mode has been significantly reduced and other acoustic modes have actually increased in amplitude, to produce a resultant decrease in the acoustic potential energy. This indicates that an error criterion based upon reducing the acoustic modal amplitudes would not necessarily reduce the acoustic potential energy in the cabin.

Figure 6.29 shows the control force required of a single control source to achieve 40 dB reduction in pressure at a single error sensor located in the acoustic space. The figure

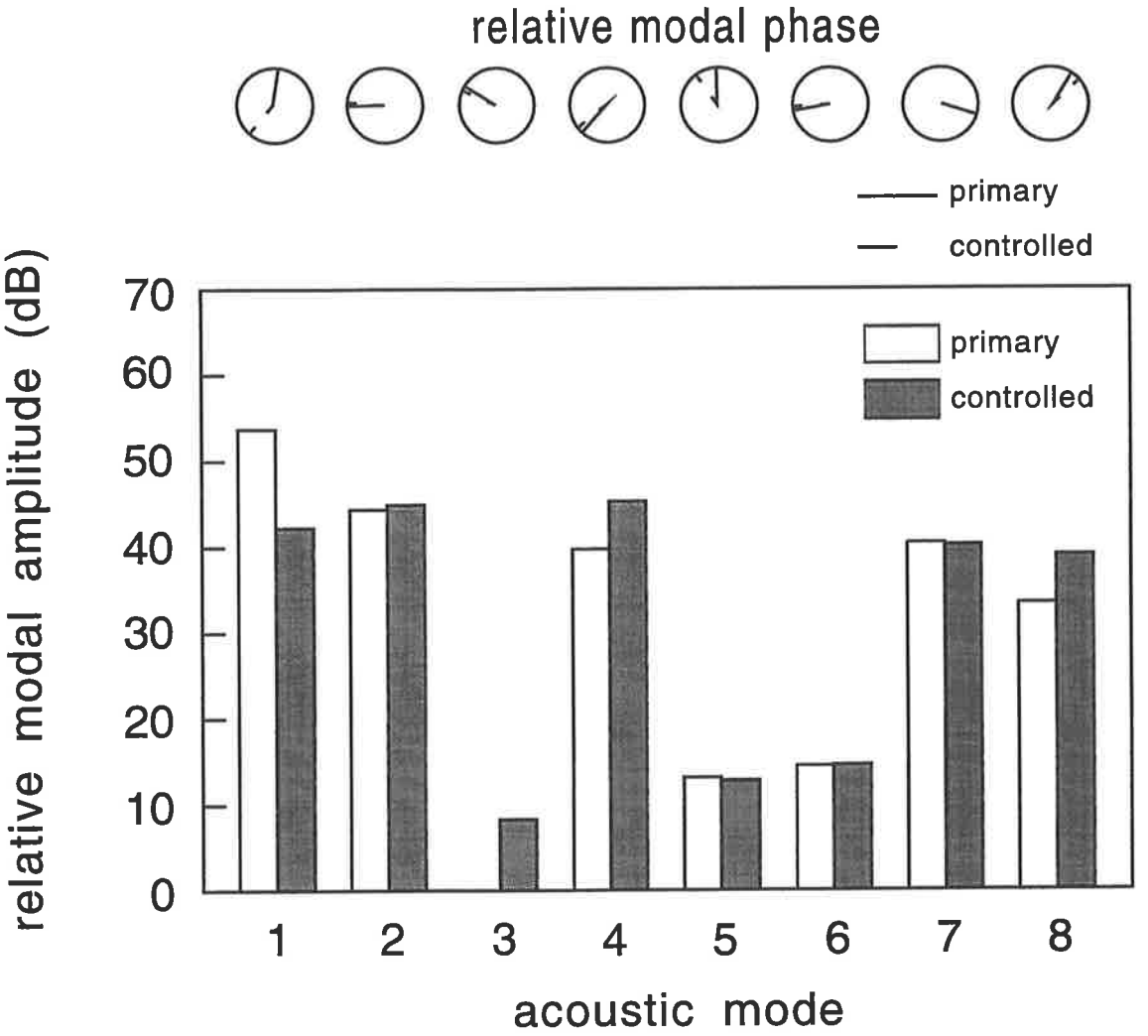

Figure 6.27 Acoustic mode response at 57 Hz for 1 control source at θ_c = 42° and minimisation of E_p.

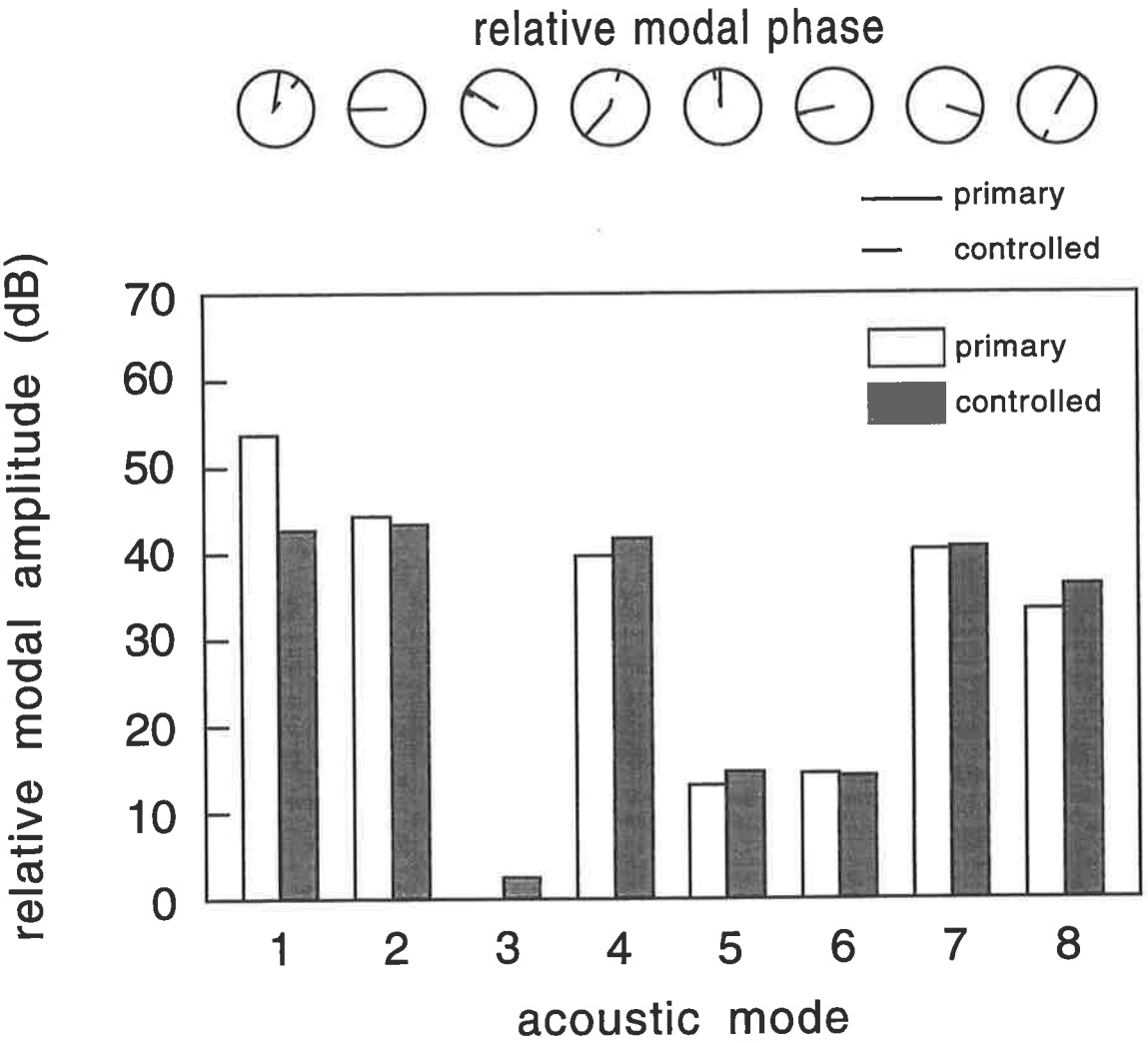

Figure 6.28 Acoustic mode response at 57 Hz for 1 control source θ_c = 48° and minimisation of E_p.

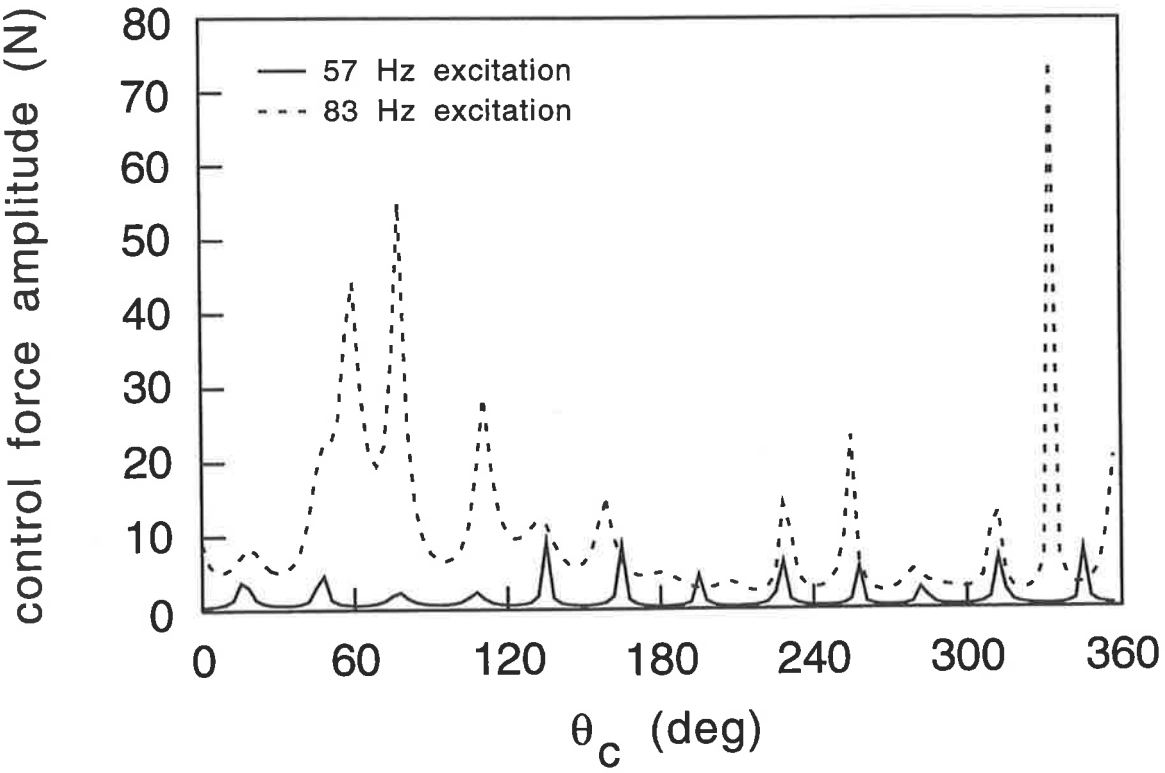

Figure 6.29 Required control force amplitude as a function of θ_c for 57 Hz and 83 Hz excitation with 1 control source.

reveals that for the circumferential control source locations examined, the control force required is generally much less for the resonant acoustic excitation case than for non-resonant acoustic excitation. This again confirms that the control source location and force required to achieve a level of control are a function of frequency.

6.4 CONCLUSIONS

A number of simulations were conducted to determine the influence of a number of different error sensor and control source configurations upon the effectiveness of active control applied to a test structure consisting of a finite length cylinder with a structurally integral longitudinal floor partition. The measure used to determine the effectiveness of the source/sensor configurations was the acoustic potential energy, E_p, in the region enclosed

by the structure. The vibrational kinetic energy, V_p, associated with out-of-plane displacement of the structure was also monitored. The error sensors used in the simulations measured acoustic pressure at a point. Control was applied via point forces input to the structure and the primary excitation was a harmonic point force input. The simulations were performed at two frequencies: 83 Hz, corresponding to off-resonant excitation of the acoustic space; and 57 Hz, corresponding to an acoustic mode resonance.

The simulations performed indicate that the accuracy of the estimate of the acoustic potential energy, provided by the sum of the acoustic pressure amplitudes at a number of error sensors, is not only a function of the number of error sensors but also the location of the control sources relative to the primary source, and also the excitation frequency.

The level of reduction in acoustic potential energy was seen to be proportional to the number of control sources, and it was also found that the sum of the quadratically optimised control force amplitudes, in Newtons, is linearly related to the reduction in acoustic potential energy, expressed in dB. The level of reduction in acoustic potential energy was also dependent on the control source location. The level of reduction was greatest for control source locations which were well matched to the primary source, in that the control source could generate a structural/acoustic response closely approximating that produced by the primary source acting alone. Thus, the degree to which the mode shape functions at the control source location can match those at the primary source location determines the level of control achievable. For control source locations which were not well matched with the primary source, use of multiple error sensors, generally

three or more, improved the accuracy of the estimate of the acoustic potential energy, and thus increased the likelihood that the acoustic potential energy would be decreased under the application of active control. Multiple error sensors also reduced the amount by which the vibrational kinetic energy would rise, as a consequence of minimising the acoustically sensed error criterion.

The control mechanism by which minimisation at the error sensors was achieved, either modal reduction or modal rearrangement, was found to be a function of the control source location and number, and also the error sensor location and number.

The level of reduction in acoustic potential energy, for a given configuration of control sources and error sensors, was found to be greater for an excitation frequency corresponding to resonant excitation of the acoustic space, than for off-resonance excitation. Also, the control force amplitude required to achieve an equivalent level of reduction in the error criterion is generally less for resonant acoustic excitation than off-resonance excitation.

In summary, for the type of structural/acoustic system examined, in which a large number of non-selectively coupled structural and acoustic modes contribute to the response, the factor of major importance is characterisation of the primary excitation. Accurate characterisation of the primary excitation would enable a suitable arrangement of control sources, well matched to the primary excitation, to be configured such that the control sources could produce an equivalent structural/acoustic response to the primary excitation

acting alone. Use of multiple error sensors, generally three or more, located within the acoustic space, would ensure that the acoustic potential energy is minimised under the application of active control, and would also limit the amount by which the vibrational kinetic energy of the structure increases.

Increasing the number of control sources increases the level of reduction in acoustic potential energy in the cabin, provided a sufficient number of error sensors are used to estimate the acoustic potential energy error criterion.

CHAPTER 7. CONCLUSIONS

The application of active control, and in particular the effect of the control source and error sensor configuration, has been examined for two physical systems; one a modally discrete system and another a modally continuous system.

The first physical system examined, a rigid walled duct of rectangular cross-section, is a discrete modal system because the number of propagating acoustic modes is determined by the duct geometry and the excitation frequency. Hence, for a given frequency, a finite number of modes are able to propagate, and the system is thus modally discrete. The second physical system examined, a simplified model of a light aircraft fuselage, consisting of a finite length cylinder with a structurally integral longitudinal floor partition, and the acoustic space enclosed by the structure, forms a system which is modally continuous because all structural and acoustic modes contribute to the interior sound field to varying degrees, with a finite number of dominant modes contributing most to the enclosed sound field at any particular frequency.

A model was developed for the acoustic response within an arbitrary length hard-walled duct in terms of the termination impedance conditions, and was shown to be appropriate for both plane wave and higher order mode propagation. Agreement between the theoretical values and experimental data was demonstrated for terminations ranging from totally reflective through to anechoic. Accurate determination of the source volume velocity using the method employed here was shown to be a problem for frequencies at

which higher order modes propagate. Methods of improving the accuracy of this technique will need to be investigated in future. Accurate prediction of the impedance functions for the case of a flanged duct radiating into free space was verified using a modal decomposition technique based upon the measurement of transfer functions between an appropriate number of locations in the duct.

The duct analytical model was used to evaluate five different error sensor strategies for the active control of plane wave and higher order mode propagation in a hard-walled rectangular duct with various termination conditions. These strategies were: minimisation of the squared pressure amplitude at a point; minimisation of the sum of the squared pressure amplitudes at a number of locations throughout the duct; minimisation of the sum of the squared pressure amplitudes at a number of locations downstream of the control source; minimisation of the total real acoustic power output of the primary and control sources; and a newly proposed technique of minimisation of the acoustic power flow downstream of the control source, as determined by modal decomposition of the duct sound field. From the results obtained using the five different error sensor strategies, the most appropriate strategy for minimising the sound field downstream of the control source was found to be minimisation of the downstream power flow, because an estimate of downstream power flow obtained from modal decomposition of the duct sound field was the most robust technique in terms of varying excitation frequency and varying termination conditions. The downstream power flow estimate technique yielded levels of power flow reduction equal to or greater than the other error sensor strategies for all of the tests conducted.

For excitation frequencies at which the contribution of evanescent modes to the overall sound field in a duct was negligible, and for a sensor/source configuration consisting of a number of control sources and a number of error sensors equal to the number of propagating acoustic modes, it was found that minimising the sum of the pressures at the error sensors was equivalent to minimising the downstream power flow for a duct with any arbitrary termination conditions. This is provided that the error sensors are located in the same cross-sectional plane. If they are not located in the same cross-sectional plane, then minimisation of the sum of the pressures at the error sensors is equivalent to minimisation of an estimate of the acoustic potential energy in a region downstream of the control sources, which is not equivalent to minimisation of the downstream acoustic power flow. For excitation frequencies at which evanescent modes are significant, a modal decomposition can be used to eliminate the effect of evanescent modes from the error signal.

The modally continuous physical system consisting of a finite length cylinder with a structurally integral longitudinal floor partition, and the acoustic space enclosed by the structure, was also examined. A model describing the response of this system to harmonic point force excitation was presented. The system was modelled theoretically using modal coupling theory between the structure and the interior acoustic field. The structural mode shapes were determined using component mode synthesis, which combines the mode shape basis functions for the plain cylinder and the floor to obtain a mode shape function for the total structure. Good qualitative agreement was found between the theoretical structural mode shapes and those found experimentally by modal analysis. The theoretical resonance

frequencies of the structural modes were found to differ slightly from those obtained experimentally, with the theoretical analysis tending to overestimate the frequencies. This is thought to be due to the joint between the shell and floor not being completely rigid, as modelled in the theory. Inhomogeneities in the test structure, introduced by the welding process used for construction, caused the theoretical and experimental axial structural mode shape functions to differ slightly. The structural imperfections also appeared to have an effect upon the acoustic response for point force excitation of the structure.

The two-dimensional acoustic mode shape functions were found using a finite difference implementation of the Helmholtz equation, while the axial acoustic mode shape function was made equal to that of a rigid-walled one-dimensional enclosure. Experimental work on a test structure was presented and the results compared with a number of theoretical predictions. The agreement between the theoretical and experimental acoustic mode resonance frequencies was excellent. The acoustic mode shapes determined by experiment and theory were found to be in qualitative agreement, for excitation of the acoustic space by an acoustic source, and for point force excitation of the structure.

Experimental and theoretical results were presented for the application of active noise control to the coupled structural/acoustic system. Comparison of the theoretical and experimental results for point force excitation of the structure revealed that the theory underestimated the amplitude of the acoustic response for both the primary and controlled cases. The theory was able to predict the relative levels of reduction and the general trends for the effect of each of the source/sensor configurations examined.

The error sensor criteria used in this study for the two physical systems were different. For the duct case the objective was to minimise the acoustic power propagating downstream of the control sources. This reduction downstream of the control sources may result in increased levels of acoustic pressure in the region between the primary source and the control source; however, this was not included in consideration of the effectiveness of the error criterion. Thus, as the whole of the acoustic field is not minimised, but only the portion of interest, the error criterion can be considered a local criterion. For the cylinder with an integral floor the objective was to minimise the acoustic potential energy in the enclosure, and thus the whole of the acoustic field was given consideration when determining the effectiveness of the application of active noise control.

Examination of the results from the study of error sensor strategies for the modally discrete duct case revealed that it was possible to sense all acoustic modes, with a suitable arrangement of error sensors and processing of the sensor signals, for any number of control sources and control source locations. For the modally continuous cylinder with floor case it generally was not practical to sense all of the acoustic modes. An estimate of the total response was determined from a finite number of error sensors rather than a modal criterion. In contrast to the duct case, the estimate provided by the error sensors was found to be a function of the number and location of the error sensors, the location of the control sources relative to the primary source, and the excitation frequency.

The work on the modally discrete physical system indicates that there is a particular number of control sources, equal to the number of propagating acoustic modes, for which

the amount of attenuation in downstream acoustic power flow is constant for all control source locations. The amount of attenuation for this particular number of control sources is greater than that for a lesser number of control sources, and the system is also more robust in terms of placement of the control sources. Having a number of control sources greater than the number of propagating acoustic modes does not yield greater levels of reduction. For the modally continuous physical system, the level of reduction in the error criterion is much more a function of the control source location relative to the primary source. In addition, as the number of control sources is increased, the level of reduction in the minimisation criterion is also increased.

For the modally discrete system, with the number of control sources less than the number of propagating acoustic modes, the results obtained for semi-infinite ducts revealed that the reduction in total acoustic power is dependent upon the relative location of the primary and control sources, both laterally across the wall of the duct and axially along the duct. The reduction in total acoustic power was found to be a maximum at axial source separation distances corresponding to multiples of half-wavelengths of the propagating modes, and at relative lateral locations such that the primary and control source mode shape function values were equivalent. Thus, the degree to which the mode shape functions at the control source location can match those at the primary source location determines the level of control achievable. Similarly, for the modally continuous system, the degree to which the mode shape functions at the control source location match those at the primary source location will determine the level of control, especially for a small number of control sources. For multiple control sources, the level of matching between the

mode shape functions at the primary and control source locations is determined by the degree to which the configuration of control sources can excite the system to produce a response equivalent to that for single control source, located such that the mode shape function is equal to that at the primary source location.

The nature of the duct system examined, which has a finite number of propagating acoustic modes with a repetitive axial structure, implies that generally there are a number of control source locations which have mode shape functions equal to those at the primary source location. In the modally continuous physical system, the large number of structural and acoustic modes, and the non-selective coupling between them which causes the majority of the acoustic modes to be coupled with the majority of the structural modes to some degree, generally results in there being relatively few control source locations which have mode shape functions equal to those at the primary source location. Thus, for the modally discrete case, with a number of control sources less than the number of propagating acoustic modes, characterisation of the primary source is an important consideration, as the locations of the control sources relative to the primary source will determine the levels of reduction. Similarly, for the modally continuous system characterisation of the primary source is of major importance for determining the optimal control source locations, as the degree to which the mode shape functions at control source locations are matched to those at the primary source location determines the level of reduction achievable, and may also affect the accuracy of the estimate of the error criterion obtained from the error sensors.

If the number of control sources used in the modally discrete duct case is equivalent to the number of propagating acoustic modes, characterisation of the primary source is no longer important, as the number of control sources ensures that the control configuration is effectively well matched with the primary source for all control source locations. The control sources and primary source are well matched because the control source configuration having a number of sources equal to the number of propagating acoustic modes is able to provide a response which is equivalent to that for a single control source, located such that the mode shape function of each propagating mode is equal to that at the primary source location. As it is generally not feasible to have a number of control sources equal to the number of structural modes for the modally continuous case, the level of reduction achievable is generally limited by the number of control sources used in the error sensor and control source configuration.

It is recommended that future work on the active control of higher order modes in ducts be concentrated upon implementing the modal decomposition determination of downstream power flow error strategy. In a practical system, the signals from the microphones used for the modal decomposition would need to be processed at some stage to obtain an error signal proportional to the downstream power flow. This may be performed digitally within a feedforward adaptive controller, or prior to the controller input by a separate circuit.

For the finite length cylinder with a structurally integral longitudinal floor, a number of simulations were conducted to determine the influence of a number of different error sensor and control source configurations upon the effectiveness of active control applied to

such a test structure. The measure used to determine the effectiveness of the source/sensor configurations was the acoustic potential energy in the region enclosed by the structure. The vibrational kinetic energy associated with out-of-plane displacement of the structure was also monitored. The error sensors used in the simulations measured acoustic pressure at a point. Control was applied via point forces input to the structure and the primary excitation was a harmonic point force input. The simulations were performed at two frequencies: 83 Hz, corresponding to off-resonant excitation of the acoustic space; and 57 Hz, corresponding to an acoustic mode resonance.

The simulations performed indicate that the accuracy of the estimate of the acoustic potential energy, provided by the sum of the acoustic pressure amplitudes at a number of error sensors, is not only a function of the number and location of the error sensors but also the location of the control sources relative to the primary source, and also the excitation frequency.

The level of reduction in acoustic potential energy was seen to be proportional to the number of control sources, and it was also found that the sum of the quadratically optimised control force amplitudes, in Newtons, is linearly related to the reduction in acoustic potential energy, expressed in dB. The level of reduction in acoustic potential energy was also dependent on the control source location. The level of reduction was greatest for control source locations which were well matched to the primary source, in that the control source could generate a structural/acoustic response closely approximating that produced by the primary source acting alone. Thus, the degree to which the mode

shape functions at the control source location can match those at the primary source location determines the level of control achievable. For control source locations which were not well matched with the primary source, use of multiple error sensors, generally three or more, improved the accuracy of the estimate of the acoustic potential energy, and thus increased the likelihood that the acoustic potential energy would be decreased under the application of active control. Multiple error sensors also reduced the amount by which the vibrational kinetic energy would rise, as a consequence of minimising the acoustically sensed error criterion.

The control mechanism by which minimisation at the error sensors was achieved, either modal reduction or modal rearrangement, was found to be a function of the control source location and number, and also the error sensor location and number.

The level of reduction in acoustic potential energy, for a given configuration of control sources and error sensors, was found to be greater for an excitation frequency corresponding to resonant excitation of the acoustic space, than for off-resonance excitation. Also, the control force amplitude required to achieve an equivalent level of reduction in the error criterion was generally less for resonant acoustic excitation than off-resonance excitation.

For the type of modally continuous structural/acoustic system examined, in which a large number of non-selectively coupled structural and acoustic modes contribute to the response, the factor of major importance is characterisation of the primary excitation.

Accurate characterisation of the primary excitation would enable a suitable arrangement of control sources, well matched to the primary excitation, to be configured such that the control sources could produce an equivalent structural/acoustic response to the primary excitation acting alone. Use of multiple error sensors, generally three or more, located within the acoustic space, would ensure that the acoustic potential energy is minimised under the application of active control, and would also limit the amount by which the vibrational kinetic energy of the structure increases.

Increasing the number of control sources increases the level of reduction in acoustic potential energy in the cabin, provided a sufficient number of error sensors are used to estimate the acoustic potential energy error criterion.

For the finite length cylinder with a structurally integral longitudinal floor, it is recommended that stiffening in the form of ring frames and stringers be incorporated into the theoretical model, and the effect of the stiffening on the application of active control be investigated, both by simulations and experimental work. The addition of stiffening would make the model more representative of a real aircraft fuselage. The inclusion of stiffening would also decrease the modal density of the structural modes, allowing the effect of resonant and non-resonant structural excitation on the performance of active control to be examined more easily than for the unstiffened structure examined in this thesis.

Incorporation of a propeller noise excitation model into the theoretical analysis would

enable examination of the effectiveness of the application of active control to an aircraft fuselage, and is also recommended for future work. The reduction in acoustic potential energy in the cabin region enclosed by the finite length cylinder and the floor was used in this thesis as a measure of the effectiveness of active control applied to the simple aircraft fuselage model. It is recommended that future work be directed toward investigation of other error sensor criteria, such as minimisation of the acoustic pressure in a region of the cabin, for example, around the pilot and passengers seated position, and also applying some small weighting to minimisation of fuselage vibration levels so that these do not unduly increase as a consequence of the application of active control.

APPENDIX A

The stiffness matrix for the shell, for a particular axial mode number m, $\left[K_{sm}\right]$, is determined from Love's shell theory. This stiffness matrix can be partitioned as

$$\left[K_{sm}\right] = \begin{bmatrix} KSUU & KSUV & KSUW \\ (KSUV)^T & KSVV & KSVW \\ (KSUW)^T & (KSVW)^T & KSWW \end{bmatrix} \tag{A1}$$

For a shell of radius a, length L, and thickness h_s, with material properties characterised by Young's modulus E_s, density ρ_s, and Poisson's ratio ν, the constants

$$K_s = \frac{E_s h_s}{(1-\nu^2)} \tag{A2}$$

$$G_s = \frac{E_s}{2(1+\nu)} \tag{A3}$$

and

$$D_s = \frac{E_s h_s^3}{12(1-\nu^2)} \tag{A4}$$

can be defined. The sub-matrices of $\left[K_{sm}\right]$ are given by

$$KSUU = a\int_0^{2\pi}\int_0^{L} K_s\left(\frac{\partial u}{\partial x}\right)^2 + \frac{G_s h_s}{a^2}\left(\frac{\partial u}{\partial \theta}\right)^2 d\theta\, dx \tag{A5}$$

Appendix A.

$$KSUV = a\int_0^{2\pi}\int_0^{L}\frac{\nu K_s}{a}\frac{\partial v}{\partial\theta}\frac{\partial u}{\partial x}+\frac{G_s h_s}{a}\frac{\partial u}{\partial\theta}\frac{\partial v}{\partial x}d\theta dx \tag{A6}$$

$$KSUW = a\int_0^{2\pi}\int_0^{L}\frac{\nu K_s w}{a}\frac{\partial u}{\partial x}d\theta dx \tag{A7}$$

$$KSVV = a\int_0^{2\pi}\int_0^{L}\left[\frac{K_s}{a^2}+\frac{D_s}{a^4}\right]\left(\frac{\partial v}{\partial\theta}\right)^2+\left[G_s h_s+\frac{G_s h_s^3}{12a^2}\right]\left(\frac{\partial v}{\partial x}\right)^2 d\theta dx \tag{A8}$$

$$KSVW = a\int_0^{2\pi}\int_0^{L}\frac{1}{a^2}\frac{\partial v}{\partial\theta}\left[K_s w-\nu D_s\frac{\partial^2 w}{\partial x^2}-\frac{D_s}{a^2}\frac{\partial^2 w}{\partial\theta^2}\right] -\frac{G_s h_s^3}{6a^2}\frac{\partial v}{\partial x}\frac{\partial^2 w}{\partial x\partial\theta}d\theta dx \tag{A9}$$

$$KSWW = a\int_0^{2\pi}\int_0^{L}\frac{K_s w^2}{a^2}+\frac{\partial^2 w}{\partial x^2}\left(D_s\frac{\partial^2 w}{\partial x^2}+\frac{\nu D_s}{a^2}\frac{\partial^2 w}{\partial\theta^2}\right) +\frac{1}{a^2}\frac{\partial^2 w}{\partial\theta^2}\left(\nu D_s\frac{\partial^2 w}{\partial x^2}+\frac{D_s}{a^2}\frac{\partial^2 w}{\partial\theta^2}\right)+\frac{G_s h_s^3}{3a^2}\left(\frac{\partial^2 w}{\partial x\partial\theta}\right)^2 d\theta dx \tag{A10}$$

The mass matrix for the shell, $\left[M_{sm}\right]$, is a diagonal matrix with non-zero elements given by

$$M_{sm_{ii}} = \rho_s h_s a\int_0^{2\pi}\int_0^{L}\psi_i^2 d\theta dx \tag{A11}$$

APPENDIX B

The stiffness matrix for the plate, for a particular axial mode number m, $\left[K_{pm}\right]$, is determined from classical plate theory. This stiffness matrix can be partitioned such that

$$\left[K_{pm}\right] = \begin{bmatrix} KPUU & KPUV & 0 \\ (KPUV)^T & KPVV & 0 \\ 0 & 0 & KPWW \end{bmatrix} \tag{B1}$$

The constants K_p, G_p and D_p are defined similarly to those of the shell, for plate thickness h_p, length L, Young's modulus E_p, density ρ_p, and Poisson's ratio ν. The sub-matrices of $\left[K_{pm}\right]$ are given by

$$KPUU = \int_{-b}^{b}\int_{0}^{L} K_p\left(\frac{\partial u}{\partial x}\right)^2 + G_p h_p\left(\frac{\partial u}{\partial y}\right)^2 dxdy \tag{B2}$$

$$KPUV = \int_{-b}^{b}\int_{0}^{L} \nu K_p \frac{\partial v}{\partial y}\frac{\partial u}{\partial x} + G_p h_p \frac{\partial u}{\partial y}\frac{\partial v}{\partial x} dxdy \tag{B3}$$

$$KPVV = \int_{-b}^{b}\int_{0}^{L} K_p\left(\frac{\partial v}{\partial y}\right)^2 + G_p h_p\left(\frac{\partial v}{\partial x}\right)^2 dxdy \tag{B4}$$

$$KPWW = \int_{-b}^{b}\int_{0}^{L} D_p\left(\frac{\partial^2 w}{\partial x^2}\right)^2 + D_p\left(\frac{\partial^2 w}{\partial y^2}\right)^2 + 2\nu D_p \frac{\partial^2 w}{\partial x^2}\frac{\partial^2 w}{\partial y^2} + \frac{G_p h_p^3}{3}\left(\frac{\partial^2 w}{\partial x \partial y}\right)^2 dxdy \tag{B5}$$

The mass matrix for the plate, $\left[M_{pm}\right]$, is a diagonal matrix with non-zero elements given by

$$M_{pm_{ii}} = \rho_p h_p \int_{-b}^{b} \int_{0}^{L} \psi_i^2 \, dx dy \tag{B6}$$

APPENDIX C

Table C.1

Control source locations used for multiple control source simulations

Control Source	Location	y_c / θ_c	x_c
1	shell	15.0°	1.323 m
2	shell	107.2°	2.103 m
3	floor	0.154 m	2.711 m
4	shell	69.2°	0.384 m
5	floor	-0.163 m	0.814 m
6	shell	297.7°	0.841 m
7	shell	283.7°	1.953 m
8	floor	0.150 m	2.271 m
9	shell	168.1°	0.508 m
10	shell	56.5°	1.779 m

Table C.2

Error sensor locations used for multiple error sensor simulations

Error Sensor	θ_e	r_e / a	x_e
1	63.0°	0.4466	1.718 m
2	249.0°	0.7728	2.430 m
3	112.0°	0.5069	0.649 m
4	14.3°	0.7822	1.461 m
5	155.9°	0.0378	0.851 m
6	20.7°	0.6336	2.894 m
7	159.6°	0.8601	0.632 m
8	116.9°	0.2245	0.572 m
9	191.1°	0.2309	2.030 m
10	151.1°	0.8651	1.018 m

APPENDIX D

Table D.1

Microphone locations used for estimate of J_p throughout duct

x	y	z	z/L
0.171	0.028	1.977	0.62
0.090	0.031	2.932	0.92
0.078	0.102	2.840	0.89
0.055	0.151	0.654	0.20
0.120	0.198	1.108	0.35
0.055	0.158	1.113	0.35

Table D.2

Microphone locations used for estimate of J_p in the region downstream of the control source located at $z/L = 0.41$

x	y	z	z/L
0.171	0.028	2.607	0.82
0.090	0.031	2.454	0.77
0.078	0.102	1.981	0.62
0.055	0.151	1.501	0.47
0.120	0.198	1.796	0.56
0.055	0.158	1.766	0.55

REFERENCES

Åbom, M. (1989) "Modal decomposition in ducts based on transfer function measurements between microphone pairs," Journal of Sound and Vibration, 135(1), 95-114.

Abler, S.B. and Silcox, R.J. (1987) "Experimental evaluation of active noise control in a thin cylindrical shell", *Proceedings of Noise-Con 1987*, 341-346.

Banks, H.T., Propst, G., and Silcox, R.J. (1990) "Groups generated by wave-duct acoustics with impedance boundary conditions," USC CAMS #90-10.

Baumann, D.C. and Greiner, R.A. (1992a) "Number of error microphones for multi-modal cancellation," *Proceedings of Inter-Noise 92*, 345-348.

Baumann, D.C. and Greiner, R.A. (1992b) "Modal identification approach to multi-modal cancellation," Proceedings of Inter-Noise 92, 341-344.

Berengier, M. and Roure, A. (1980) "Radiation impedance of one or several real sources mounted in a hard-walled rectangular waveguide," Journal of Sound and Vibration, 71, 389-398.

Bullmore, A.J., Nelson, P.A. and Elliott, S.J. (1986) "Active minimisation of acoustic potential energy in harmonically excited cylindrical enclosed sound fields", AIAA Paper, 86-1958.

References.

Bullmore, A.J. (1987) "The active minimisation of harmonic enclosed sound fields with particular application to propeller induced cabin noise", Ph.D Thesis, University of Southampton.

Bullmore, A.J., Nelson, P.A., Elliott, S.J., Evers, J.F. and Chidley, B. (1987) "Models for evaluating the performance of propeller aircraft active noise control systems", AIAA Paper, 87-2704.

Bullmore, A.J., Nelson, P.A. and Elliott, S.J. (1990) "Theoretical studies of the active control of propeller-induced cabin noise", Journal of Sound and Vibration, 140, 191-217.

Curtis, A.R.D, Nelson, P.A., Elliott S.J. and Bullmore, A.J. (1987) "Active suppression of acoustic resonance," Journal of the Acoustical Society of America, 81(3), 624-631.

Davies, P.O.A.L., Bento Coelho, J.L., and Bhattacharya, M. (1980) "Reflection coefficients for an unflanged pipe with flow," Journal of Sound and Vibration, 72(4), 543-546.

Doak, P.E. (1973a) "Excitation, transmission and radiation of sound from source distributions in hard-walled ducts of finite length (I): The effects of duct cross-section geometry and source distribution space-time pattern," Journal of Sound and Vibration, 31, 1-72.

Doak, P.E. (1973b) "Excitation, transmission and radiation of sound from source

distributions in hard-walled ducts of finite length (II): The effects of duct length," Journal of Sound and Vibration, 31, 137-174.

Dorling, C.M., Eatwell, B.P., Hutchins, S.M., Ross, C.F. and Sutcliffe, S.G.C. (1989) "A demonstration of active noise reduction in an aircraft cabin", Journal of Sound and Vibration, 128, 358-360.

Elliott, S.J., and Nelson, P.A. (1984) "Models for describing active noise control in ducts," ISVR Technical Report 127.

Elliott, S.J., Nelson, P.A., Stothers, I.M. and Boucher, C.C. (1989) "Preliminary results of in-flight experiments on the active control of propeller-induced cabin noise", Journal of Sound and Vibration, 128, 355-357.

Elliott, S.J., Nelson, P.A., Stothers, I.M. and Boucher, C.C. (1990) "In-flight experiments on the active control of propeller-induced cabin noise", Journal of Sound and Vibration, 140, 219-238.

Eriksson, L.J., Allie, M.C., Hoops, R.H. and Warner, J.V. (1989) "Higher order mode cancellation in ducts using active noise control," *Proceedings of Inter-Noise 89*, 495-500.

Fahy, F.J. (1985) *Sound and Structural Vibration: Radiation, Transmission and Response* (Academic Press, London).

References.

Fedoryuk, M.V. (1975) "The suppression of sound in acoustic waveguides," Akust. Zh. 21, 281 [English transl.: Sov. Phys. Acoust. 21(2), 174-176 (1975)].

Ffowcs-Williams, J.E. (1984) "Anti-sound," Proceedings of Royal Society of London Ser A 395, 63-88.

Fuller, C.R. (1987) "Structural influence of the cabin floor on sound transmission into aircraft - analytical investigations", AIAA Journal of Aircraft, 24, 731-736.

Fuller, C.R. and Jones, J.D. (1987a) "Experiments on reduction of propeller induced interior noise by active control of cylinder vibration", Journal of Sound and Vibration, 112, 389-395.

Fuller, C.R. and Jones, J.D. (1987b) "Influence of sensor and actuator location on the performance of active control systems", *Proceedings of ASME Conference 1987*, Paper 87-WA/NCA-9.

Fuller, C.R., Snyder, S.D., Hansen, C.H. and Silcox, R.J. (1992) "Active control of interior noise in model aircraft fuselages using piezoceramic actuators", AIAA Journal, 30, 2613-2617.

Green, I.S. (1992) "Vibro-acoustic analyses of the SAAB 2000 aircraft", *Proceedings of 4th NASA/SAE/DLR Aircraft Interior Noise Workshop.*

References.

Guicking, D., and Karcher, K. (1984) "Active impedance control for one-dimensional sound," Journal of Vibration, Acoustics, Stress and Reliability in Design, 106, 393-396.

Hansen, C.H., and Bies, D.A. (1979) "Near field determination of the complex radiation efficiency and acoustic intensity distribution for a resonantly vibrating surface," Journal of Sound and Vibration, 62(1), 93-110.

Hansen, C.H. and Snyder, S.D. (1990) "Influence of source size, location and number upon power flow attenuation achieved with duct active noise control systems," *Proceedings of Australian Vibration and Noise Conference*, 179-182.

Hull, A.J., Radcliffe, C.J., Miklavcic, M., and MacCluer, C.R. (1990) "State space representation of the nonself-adjoint acoustic duct system," Journal of Vibration and Acoustics, 112, 483-488.

Hurty, W.C. (1965) "Dynamic analysis of structural systems using component modes", AIAA Journal, 3, 678-685.

Jessel, M.J.M and Mangiante, G.A. (1972) "Active sound absorber in an air conditioning duct," Journal of Sound and Vibration, 27(3), 383-390.

Jones, J.D. and Fuller, C.R. (1987) "Active control of sound fields in elastic cylinders by vibrational inputs", *Proceedings of Noise-Con 1987*, 413-418.

Jones, J.D. and Fuller, C.R. (1989) "Active control of sound fields in elastic cylinders by multicontrol forces", AIAA Journal, 27, 845-852.

Koopmann, G.H., Fox, D.J. and Neise, W. (1988) "Active noise cancellation of the blade tone fundamental and harmonics in centrifugal fans," Journal of Sound and Vibration, 126, 209-220.

La Fontaine, R.F. and Shepherd, I.C. (1985) "The influence of waveguide reflections and system configuration on the performance of an active noise attenuator," Journal of Sound and Vibration, 100(4), 569-579.

Langley, R.S. (1992) "A dynamic stiffness technique for the vibration analysis of stiffened shell structures", Journal of Sound and Vibration, 156, 521-540.

Legrain, I. and Goulain, M. (1988) "Active noise reduction in a transport aircraft cabin", *Proceedings of Inter-Noise 88*, 1009-1012.

Leissa, A.W. (1969) "Vibration of plates", NASA SP-160.

Leitch, R.R., and Tokhi, M.O. (1987) "Active noise control systems," IEE Proceedings A 134, 525-546.

Lester, H.C. (1988) "Mechanisms of noise control inside a finite cylinder", *Proceedings*

of Noise-Con 1988, 217-222.

Lester, H.C. and Fuller, C.R. (1986) "Active control of propeller induced noise fields inside a flexible cylinder", AIAA Paper, 86-1957.

Lester, H.C. and Fuller, C.R. (1987) "Mechanisms of active control for noise inside a vibrating cylinder", *Proceedings of Noise-Con 1987*, 371-376.

Levine, H., and Schwinger, J. (1948) "On the radiation of sound from an unflanged circular pipe," Physical Review, 73, 383-406.

Lyon, R.H., Dietrich, C.W., Ungar, E.E., Pyle Jr., R.W. and Apfel, R.E. (1966) "Low frequency noise reduction of spacecraft structures", NASA CR-589.

Mandic, D.S. and Jones, J.D. (1989a) "Active noise control in damped elastic cylinders using vibrational force inputs", *Proceedings of Inter-Noise 89*, 441-446.

Mandic, D.S. and Jones, J.D. (1989b) "Adaptive active control of enclosed sound fields in elastic cylinders via vibrational inputs", AIAA Paper, 89-1075.

Mazanikov, A.A. and Tyutekin, V.V. (1976) "Autonomous active systems for the suppression of sound fields in single-mode waveguides," Akust. Zh. 22, 729-734. [English transl.: Sov. Phys. Acoust. 22(5), 409-412 (1976)].

References.

Mazanikov, A.A., Tyutekin, V.V. and Ukolov, A.T. (1977) "An active system for the suppression of sound fields in a multimode waveguide," Akust. Zh. 23, 485-487 [English transl.: Sov. Phys. Acoust. 23(3), 276-277 (1977)].

Morfey, C.L. (1969) "A note on the radiation efficiency of acoustic duct modes," Journal of Sound and Vibration, 9(3), 367-372.

Morse, P.M. (1948) Vibration and Sound, 2nd edition, *Vibration and Sound*, McGraw-Hill, New York.

Morse, P.M. and Ingard, K.U. (1968) *Theoretical Acoustics* (McGraw-Hill, New York), Chap. 9.

Nashif, P.J. and Sommerfeldt, S.D. (1992) "An active control strategy for minimizing the energy density in enclosures," *Proceedings of Inter-Noise 92*, 357-362.

Neise, W. and Koopmann, G.H. (1991) "Active sources in the cutoff of centrifugal fans to reduce the blade tones at higher-order duct mode frequencies," Journal of Vibration and Acoustics, 113, 123-131.

Nelson, P.A., Curtis, A.R.D., and Elliott, S.J. (1985) "Quadratic optimization problems in the active control of free and enclosed sound fields," Proc. Inst. Acoust. 7, 45-54.

References.

Nelson, P.A., Curtis, A.R.D., Elliott, S.J. and Bullmore, A.J. (1987a) "The active minimization of harmonic enclosed sound fields, part I: theory", Journal of Sound and Vibration, 117, 1-13.

Nelson, P.A., Curtis, A.R.D., Elliott, S.J. and Bullmore, A.J. (1987b) "The minimum power output of free field point sources and the active control of sound", Journal of Sound and Vibration, 116, 397-414.

Norris, A.N., and Sheng, I.C. (1989) "Acoustic radiation from a circular pipe with an infinite flange," Journal of Sound and Vibration, 135(1), 85-93.

Orduña-Bustamante, F. and Nelson, P.A. (1992) "An adaptive controller for the active absorption of sound," Journal of the Acoustical Society of America, 91(5), 2740-2747.

Pan, J. and Hansen, C.H. (1990) "Active control of total power flow along a beam," *Proceedings of International Congress on Recent Developments in Air- and Structure-Borne Sound and Vibration*, 229-236.

Peterson, M.R. and Boyd, D.E. (1978) "Free vibrations of circular cylinders with longitudinal, interior partitions", Journal of Sound and Vibration, 60, 45-62.

Peterson, M.R. (1973) "A study of the effects of a longitudinal, interior plate on the free vibrations of circular cylindrical shells", Ph.D Thesis, Oklahoma State University.

References.

Plotkin, K.J., Kasper, P.K. and Glenn, P.K. (1978) "Prediction of low frequency sound transmission through aerospace structures, with application to space shuttle", Wyle Laboratories Report WR 78-5.

Pope, L.D. (1970) "On the transmission of sound through finite closed shells: statistical energy analysis, modal coupling, and nonresonant transmission", Journal of the Acoustical Society of America, 50, 1004-1018.

Pope, L.D., Rennison, D.C. and Wilby, E.G. (1980) "Analytical prediction of the interior noise for cylinder models of aircraft fuselages for prescribed exterior noise fields, Phase I", NASA CR-159363.

Pope, L.D. and Wilby, E.G. (1982) "Analytical prediction of the interior noise for cylinder models of aircraft fuselages for prescribed exterior noise fields, Phase II", NASA CR-165869.

Pope, L.D., Wilby, E.G., Willis, C.M. and Mayes, W.H. (1983) "Aircraft interior noise models: Sidewall trim, stiffened structures, and cabin acoustics with floor partition", Journal of Sound and Vibration, 89, 371-417.

Pope, L.D., Wilby, E.G. and Wilby, J.F. (1987a) "Propeller aircraft interior noise model, part I: analytical model", Journal of Sound and Vibration, 118, 449-467.

References.

Pope, L.D., Willis, C.M. and Mayes, W.H. (1987b) "Propeller aircraft interior noise model, part II: scale-model and flight-test comparisons", Journal of Sound and Vibration, 118, 469-493.

Pope, L.D. (1990) "On the prediction of propeller tone sound levels and gradients in an airplane cabin", Journal of the Acoustical Society of America, 88, 2755-2765.

Rubenstein, S.P., Popovich, S.R., Melton, D.E. and Allie, M.C. (1992) "Active cancellation of higher order modes in a duct using recursively-coupled multi-channel adaptive control system," *Proceedings of Inter-Noise 92*, 337-340.

Silcox, R.J. and Elliott, S.J. (1990) "Active control of multi-dimensional sound in ducts," NASA TM #102653.

Silcox, R.J., Fuller, C.R. and Lester, H.C. (1987) "Mechanisms of active control in cylindrical fuselage structures", AIAA Paper, 87-2703.

Silcox, R.J., and Lester, H.C. (1988) "Energy flows for active control systems in a cylindrical shell", *Proceedings of Inter-Noise 88*, 1003-1008.

Silcox, R.J., Fuller, C.R. and Lester, H.C. (1989a) "Modal coupling and acoustic intensity measurements", Journal of Sound and Vibration, 130, 171-176.

References.

Silcox, R.J., Lester, H.C. and Abler, S.B. (1989b) "An evaluation of active noise control in a cylindrical shell", Journal of Vibration, Acoustics, Stress, and Reliability in Design, 111, 337-342.

Silcox, R.J., Fuller, C.R. and Lester, H.C. (1990) "Mechanisms of active control in cylindrical fuselage structures", AIAA, 28, 1397-1404.

Simpson, M.A., Luong, T.M., Swinbanks, M.A., Russell, M.A. and Leventhall, H.G. (1989) "Full scale demonstration tests of cabin noise reduction using active noise control", *Proceedings of Inter-Noise 89*, 459-462.

Simpson, M.A., Luong, T.M., Fuller, C.R. and Jones, J.D. (1991) "Full-scale demonstration tests of cabin noise reduction using active vibration control", AIAA Journal of Aircraft, 28(3), 208-215.

Snyder, S.D. and Hansen, C.H. (1989) "Active noise control in ducts: some physical insights," Journal of the Acoustical Society of America, 86(1), 184-194.

Snyder, S.D., Hansen, C.H. and Fuller, C.R. (1989) "An experimental investigation of the active control of sound transmission into a cylindrical enclosure", *Proceedings of Inter-Noise 89*, 501-504.

Snyder, S.D. (1990) "A fundamental study of active noise control system design", Ph.D

Thesis, University of Adelaide.

Snyder, S.D. and Hansen, C.H. (1991) "The effect of modal coupling characteristics on one mechanism of active noise control", *Proceedings of Conference on Recent Advances in Active Control of Sound and Vibration*, 708-727.

Stell, J.D. (1991) Ph.D Thesis, Purdue University.

Stell, J.D. and Bernhard, R.J. (1991) "Active control of sound in waveguides," *Proceedings of Recent Advances in Active Control of Sound and Vibration*, 258-270.

Stell, J.D. and Bernhard, R.J. (1990a) "The effect of evanescent modes on the performance of active noise control in a finite waveguide," 119th Meeting of the Acoustical Society of America, Y2, May.

Stell, J.D. and Bernhard, R.J. (1990b) "Active control of high order acoustical modes in a semi-infinite waveguide," ASME 1990 Winter Meeting NCA-8, 131-142.

Swinbanks, M.A. (1973) "The active control of sound propagation in long ducts," Journal of Sound and Vibration, 27, 411-436.

Thomas, D.R., Nelson, P.A. and Elliott, S.J. (1988) "Active control of the acoustic field in a vibrating cylindrical shell by the application of secondary force inputs", *Proceedings*

of Inter-Noise 88, 1013-1016.

Thomas, D.R., Nelson, P.A. and Elliott, S.J. (1993a) "Active control of the transmission of sound through a thin cylindrical shell, Part I : The minimisation of vibrational energy", Journal of Sound and Vibration, 167(1), 91-111.

Thomas, D.R., Nelson, P.A. and Elliott, S.J. (1993b) "Active control of the transmission of sound through a thin cylindrical shell, Part II : The minimisation of acoustic potential energy", Journal of Sound and Vibration, 167(1), 113-128.

Tichy, J., Warnaka, G.E. and Poole, L.A. (1984) "A study of active control of noise in ducts," Journal of Vibration, Acoustics, Stress, and Reliability in Design, 106, 399-404.

Trinder, M.C.J., and Nelson, P.A. (1983) "Active noise control in finite length ducts," Journal of Sound and Vibration, 89, 95-105.

Unruh, J.F. (1981) "Structure-borne noise prediction for a single-engine general aviation aircraft", AIAA Journal of Aircraft, 18, 687-694.

Unruh, J.F. and Dobosz, S.A. (1988) "Fuselage structural-acoustic modeling for structure-borne interior noise transmission", Journal of Vibration, Acoustics, Stress, and Reliability in Design, 110, 226-233.

References.

Webster, J.J. (1967) "Free vibrations of shells of revolution using ring finite elements", International Journal of Mechanical Science, 9, 559-570.